



P H D
T H E
S I S

MODELLING OF HEAT PUMPS

WORKING WITH
VARIABLE-SPEED
COMPRESSORS

January 2024

Rubén Josep Ossorio Santiago

Supervisor

Emilio Navarro Peris



UNIVERSITAT
POLITÈCNICA
DE VALÈNCIA



Instituto
Ingeniería
Energética



UNIVERSITAT
POLITÈCNICA
DE VALÈNCIA



Instituto
Ingeniería
Energética

Modeling of heat-pumps working with variable-speed compressors

PhD Thesis

Rubén Josep Ossorio Santiago

Supervisor

Dr. D. Emilio Navarro Peris

"AD ASTRA PER ASPERA"

Acknowledgements

Completing this doctoral thesis has been an incredible journey, and I am deeply grateful to the many individuals and institutions who have contributed to its realization. Their unwavering support, guidance, and encouragement have been instrumental throughout this endeavor.

First, I express my gratitude to my thesis advisor, Emilio Navarro-Peris, whose expertise and guidance have been the cornerstone of this research.

My heartfelt thanks also go to my colleagues and friends whose camaraderie, intellectual exchange, and encouragement provided a supportive academic environment. Their diverse perspectives and collaborative spirit have greatly enriched this journey. In particular, I would like to thank Pepe for believing in me and recruiting me to the group; Javier for being my mentor and kindly sharing all his knowledge with me with infinite patience; the lab team for the technical maintenance and construction of the prototypes and especially their lovely humor; Luis for integrating me in the group and showing me the way to the force and to the Ph.D.; Paloma, for introducing me to compressor testing. And finally, I can't forget Professor Corberán, who, although no longer with us, keeps inspiring the team with his legacy.

I am profoundly grateful to my family for their unwavering love, understanding, and encouragement throughout this academic pursuit. Their support and belief in my abilities have been a constant source of motivation since elementary school.

All my love to Sandra, my eternal friend and beloved wife. Thank you for your unwavering belief in me, bearing with me in all my pursuits, and helping me focus when I feel lost.

I am indebted to the Spanish and European governments for their financial support with the grant PRE2018-083535, which made this research possible. Their commitment to academic excellence and research advancement has been crucial in successfully completing this thesis.

Lastly, I acknowledge the countless researchers, scholars, and authors whose work laid the foundation for this thesis. Their contributions to the field have been invaluable in shaping my understanding and informing this research.

To all those mentioned and the many others who have contributed in ways both seen and unseen, your support and encouragement have been indispensable in this academic endeavor. Thank you for being an integral part of this journey.

Abstract

Heat pump technology has become strategic in Europe, it is rapidly spreading, and it is planned to replace gas boilers in the near future. However, they still have challenges to solve, such as finding new viable and highly efficient refrigerants and further increasing their system performance. For this latter issue, variable-speed heat pumps arise, which claim to decrease annual consumption and increase comfort by adapting the delivered capacity to the changing loads. This technology is being implemented but lacks a standardized methodology to design and select its components.

This thesis aims to establish comprehensive design guidelines for selecting and designing variable-speed heat pump components and give insights that can translate into valuable information and tools for engineers to assist them in the pump simulation, design, selection and fault detection. The content of the study can be divided into three thematic areas:

In the first part, variable-speed **compressors** are studied. The compressor is the first selected heat pump component; it modulates the capacity and is the primary energy consumer. However, there are no well-established methodologies to model their behavior. In this part, extensive testing of variable-speed compressors and their inverters was carried out to understand their behavior and to provide compact correlations to model their performance.

The second part proposes a **methodology to size heat exchangers** for variable-speed heat pumps. Typically, they are designed for a fixed capacity and constant working temperatures. However, the capacity and working temperatures fluctuate significantly overtime in variable-speed pumps. In this part, the

performance evolution of heat exchangers with capacity is studied, and a methodological selection/sizing technique is proposed that considers the evolution of external climatic conditions and loads over the year.

Lastly, the **oil circulation** in variable-speed heat pumps is assessed. Managing lubrication in variable-speed compressors is a typical issue, as a design valid for sufficient lubrication at low compressor speeds will end up pumping excess oil at high speeds. In this final part, the evolution of oil circulation rates with speed is studied, and its effect on heat pump performance is theoretically analyzed.

Resumen

La tecnología de bombas de calor se ha vuelto estratégica en Europa, está extendiéndose rápidamente y se planea que reemplace las calderas de gas en un futuro cercano. Sin embargo, aún enfrenta desafíos, como encontrar refrigerantes nuevos viables y altamente eficientes, y mejorar aún más el rendimiento del sistema. Para abordar este último problema, han surgido las bombas de calor de velocidad variable que prometen reducir el consumo anual e incrementar el confort adaptando la potencia suministrada a las necesidades cambiantes. Esta tecnología se está implementando ya, pero carece de una metodología estandarizada para diseñar y seleccionar sus componentes.

Esta tesis tiene como objetivo establecer pautas de diseño generales para la selección y diseño de componentes de bombas de calor de velocidad variable, y ofrecer información valiosa que se pueda traducir en herramientas para asistir en la simulación, diseño, selección y detección de fallas en estos dispositivos. El contenido del estudio se puede dividir en tres áreas temáticas:

En una primera parte, se estudian los **compresores** de velocidad variable. El compresor es el primer componente que se selecciona en una bomba de calor, modula la capacidad y es el principal consumidor de energía. Sin embargo, no existen metodologías bien establecidas para modelar su comportamiento. En esta parte, se realizan ensayos de caracterización de compresores de velocidad variable y sus inversores para comprender su comportamiento y proporcionar correlaciones compactas para modelar su rendimiento.

En la segunda parte, se propone una metodología para **dimensionar los intercambiadores de calor** en bombas de calor de velocidad variable. Normalmente, se diseñan para una potencia fija y temperaturas de trabajo constantes, sin embargo, en las bombas de velocidad variable, la capacidad y las temperaturas de trabajo fluctúan significativamente con el tiempo. En esta parte, se estudia la evolución del rendimiento de los intercambiadores de calor con la capacidad (velocidad del compresor) y se propone una metodología de selección/dimensionamiento que considera la evolución de la capacidad requerida y de las condiciones climáticas externas a lo largo del año.

Por último, se evalúa la **circulación del aceite** en las bombas de calor de velocidad variable. Gestionar la lubricación en los compresores de velocidad variable es un problema típico ya que, para tener suficiente lubricación a bajas velocidades, el compresor termina bombeando un exceso de aceite a altas velocidades. En esta parte se estudia la evolución de las tasas de circulación de aceite con la velocidad y se analiza teóricamente su efecto en el rendimiento de la bomba de calor.

Resum

La tecnologia de les bombes de calor s'ha tornat estratègica a Europa, s'està estenent ràpidament i es preveu que substituisca les calderes de gas en un futur pròxim. Tanmateix, encara s'enfronta a desafiaments com trobar refrigerants nous viables i altament eficients, i millorar encara més el rendiment del sistema. Per abordar aquest darrer problema, han sorgit les bombes de calor de velocitat variable que prometen reduir el consum anual i incrementar el confort adaptant la potència subministrada a les necessitats variables. Aquesta tecnologia ja s'està implementant, però manca d'una metodologia estandarditzada per dissenyar i seleccionar els seus components.

Aquesta tesi té com a objectiu establir pautes de disseny generals per a la selecció i disseny de components de bombes de calor de velocitat variable, i oferir informació valuosa que es pugui traduir en eines per ajudar en la simulació, disseny, selecció i detecció de fallades d'aquests dispositius. El contingut de l'estudi es pot dividir en tres àrees temàtiques:

En una primera part, s'estudien els **compressors de velocitat variable**. El compressor és el primer component seleccionat d'una bomba de calor, modula la capacitat i és el principal consumidor d'energia. Tanmateix, no hi ha metodologies ben establides per modelar el seu comportament. En aquesta part, es realitzen assajos de caracterització de compressors de velocitat variable i els seus inversors per comprendre el seu comportament i proporcionar correlacions compactes per modelar el seu rendiment.

En la segona part, es proposa una **metodologia per dimensionar els intercanviadors de calor** en bombes de calor de velocitat variable. Normalment, es dissenyen per a una potència fixa i temperatures de treball constants, no obstant això, en les bombes de velocitat variable, la capacitat i les temperatures de treball fluctuen significativament amb el temps. En aquesta part, s'estudia l'evolució del rendiment dels intercanviadors de calor amb la capacitat (velocitat del compressor) i es suggereix una metodologia de selecció/dimensionament que considera l'evolució de les càrregues i de les condicions climàtiques externes al llarg de l'any.

Finalment, s'avalua la **circulació de l'oli** a les bombes de calor de velocitat variable. Gestionar la lubricació als compressors de velocitat variable és un problema típic, ja que per tenir suficient lubricació a baixes velocitats, el compressor acaba bombejant un excés d'oli a altes velocitats. En aquesta part s'estudia l'evolució de les taxes de circulació d'oli amb la velocitat i s'analitza teòricament el seu efecte en el rendiment de la bomba de calor.

Contents

<i>Acknowledgements</i>	<i>i</i>
<i>Abstract</i>	<i>iii</i>
<i>Resumen</i>	<i>v</i>
<i>Resum</i>	<i>vii</i>
<i>Contents</i>	<i>ix</i>
<i>List of figures</i>	<i>xv</i>
<i>List of tables</i>	<i>xxi</i>
Chapter 1: INTRODUCTION	1
1.1. Context	2
1.1.1. Energy sector in Europe	2
1.1.2. Heat pump technology	4
1.2.3. Refrigerant regulations	5
1.1.3. Part-load	6
1.1.4. Inverter technology	9
1.1.5. Compressor modeling	10
1.1.6. Oil Management	14
1.1.7. Heat pump design and sizing	14
1.1.8. Thesis Framework	15
	ix

1.2. Identified gaps	17
1.3. Aims of the thesis	18
1.4. Structure	19
1.4.1. Compressor Modeling.....	19
1.4.2. Heat Exchanger design for variable-speed heat pumps.....	19
1.4.3. Effect of oil in heat pump.....	20
1.5. Chronology	21
Chapter 2: FIRST PUBLICATION	23
<i>Testing of Variable-Speed Scroll Compressors and their inverters for the evaluation of compact energy consumption models</i>	24
2.1. Abstract	24
2.2. Introduction	25
2.3. Methodology	29
2.3.1. Test bench description.....	29
2.3.2. Experimental data	30
2.4. Compressor performance	33
2.4.1. Analysis of the experimental results	33
2.4.2. Characterization models.....	37
2.4.3. Design of Experiments.....	40
2.5. Inverter Performance	44
2.5.1. Inverter Model.....	44
2.5.2. Effect of the carrier frequency.....	47
2.6. Conclusion	49
2.7. Nomenclature	51
Chapter 3: SECOND PUBLICATION	53
<i>Development of compact empirical models for variable-speed compressors for the prediction of energy consumption, mass flow and discharge temperature</i>	54
3.1. Abstract	54

3.2. Introduction:	55
3.3. Methodology	58
3.4. Mass flow Results	62
3.4.1. Experimental results	62
3.4.2. Model.....	64
3.5. Energy Consumption results	71
3.5.1. Experimental results	71
3.5.2. Model.....	76
3.6. Discharge temperatures	83
3.6.1. Experimental results	83
3.6.2. Model.....	88
3.7. Effect of suction conditions	92
3.8. Robustness Analysis	95
3.9. Conclusions	100
3.10. Appendix 1: Electro-mechanical losses	102
3.11. Nomenclature	104
Chapter 4: THIRD PUBLICATION	105
<i>Heat Exchanger sizing for Variable-Speed Heat Pumps based on part load conditions and economic assessment</i>	106
4.1. Abstract	106
4.2. Introduction	107
4.3. Methodology	110
4.3.1. Bäckström.....	110
4.3.2. Evaporator model.....	113
4.3.3. Condenser Model.....	115
4.3.4. Compressor model	118
4.3.5. Optimum temperature difference.....	120

4.4. Results	123
4.4.1. Optimization of HX size	123
4.4.2. Influence of the economic parameters on the optimization.....	127
4.5. Discussion and limitations of results	130
4.6. Conclusion	132
4.7. Nomenclature	133
Chapter 5: FORTH PUBLICATION	135
<i>Study of Oil Circulation Rate in Variable-Speed Scroll Compressors Working with Propane</i>	<i>136</i>
5.1. Abstract	136
5.2. Introduction	137
5.3. Methodology	141
5.3.1. Test bench.....	141
5.3.2. Description of the methodology to estimate the oil mass flow rate (Discrepancy Method).....	143
5.3.3. Experimental campaign.....	144
5.4. Experimental results.....	146
5.4.1. Validation of the methodology.....	146
5.4.2. Oil circulation results.....	146
5.4.3. Oil mass flow correlation.....	150
5.5. Discussion.....	152
5.6. Conclusions	156
5.7. Nomenclature	158
Chapter 6: FIFTH PUBLICATION.....	159
<i>A Novel and Compact Correlation for the Prediction of Oil-Refrigerant Miscibility.....</i>	<i>160</i>
6.1. Introduction	160
6.2. Experimental data.....	163
6.3. Results	164

6.4. Conclusions	167
Chapter 7: SIXTH PUBLICATION	169
<i>Impact of Lubricant in the Performance of Variable Speed Heat Pumps.....</i>	<i>170</i>
7.1. Abstract	170
7.2. Introduction	171
7.3. Methodology.....	173
7.3.1. Impact of lubricant on HTC	173
7.3.2. Impact of lubricant solubility on the evaporator	177
7.3.3. Impact of lubricant in compressor.....	179
7.4. Results.....	180
7.4.1. Impact of lubricant on HTC	180
7.4.2. Impact of solubility on performance	184
7.4.3. Impact of oil in compressor consumption.....	187
7.5. Conclusions	190
7.6. Nomenclature	191
Chapter 8: THESIS CONCLUSIONS.....	193
8.1. Conclusions	194
8.1.1. Variable-speed compressor modeling.....	194
8.1.2. Heat Exchanger design for variable-speed heat pumps.....	195
8.1.3. Oil impact	195
8.2. Future Work	197
8.3. Science Production	198
8.3.1. Journal Contribution	198
8.3.2. International Congress Contributions.....	199
Chapter 9: References.....	201

Appendixes:

Appendix 1 : Compressor Data “scroll-R290”

Appendix 2 : Compressor Data “scroll-R410A”

Appendix 3 : Compressor Data “scroll-R454C”

Appendix 4 : Inverter Data “Inverter A”

Appendix 5 : Inverter Data “Inverter B”

Appendix 6 : Inverter Data “Inverter C”

Appendix 7 : OCR measurements

List of figures

Figure 1.1: Pathway to achieve a net-zero emissions in EU for 2050	3
Figure 1.2: Climate profiles according to the standard (European Commission, 2018a)6	
Figure 1.3: Capacity control techniques (Inspired from Bitzer, 2016)	7
Figure 1.4: Comparison of various capacity control techniques at half load (Qureshi & Tassou, 1996)	8
Figure 1.5: Internal schematic of a Variable Frequency Drive (VFD)	9
Figure 1.6: Compressor + Inverter scheme	13
Figure 1.7: Areas of the research institute.....	16
Figure 2.1: Variable-Speed Compressor Test Bench	29
Figure 2.2: Test Matrix of Compressor A	31
Figure 2.3: Experimental Mass Flow evolution with compression condition and speed [Compressor A]	33
Figure 2.4: Consumption results of Compressor A and its evolution with the compression condition and speed	34
Figure 2.5: Compressor A efficiency and its evolution with the working variables	35
Figure 2.6: Performance of the different models fitted to various compressor datasets	39

Figure 2.7: Robustness of the different models when adjusted with 21 tests selected randomly (Left) or with a clustering methodology (right)	40
Figure 2.8: Train set selection using Optimal Design for AHRI-20 model	42
Figure 2.9: Train set selection using Optimal Design for Shao	43
Figure 2.10: Experimental results and predicted performance of inverter A	45
Figure 2.11: Performance of the inverter model applied to Inverter A	46
Figure 2.12: Evolution of Drive Efficiency and Inverter Power Flows with Switching Frequency	48
Figure 3.1: Test matrix and compressor envelope	58
Figure 3.2: Evolution of mass flow with compression conditions at nominal speed (Up). Evolution of mass flow as a function of evaporating temperatures (Down-left) and pressures (Down-right)	62
Figure 3.3: Evolution of volumetric efficiency with pressure ratio and speed	63
Figure 3.4: <i>km</i> and <i>kv</i> evolution with speed for two different compressors	65
Figure 3.5: Correlation plot of mass flow model applied to reference compressor	67
Figure 3.6: Goodness of fit of mass flow models applied to different data sets	68
Figure 3.7: Evolution of energy consumption with compression conditions at nominal speed (Up). Evolution of energy consumption as a function of evaporating temperatures and speed (Down)	71
Figure 3.8: Evolution of compressor efficiency	73
Figure 3.9: Specific consumption evolution with operating pressures (UP). Evolution of specific consumption with pressure ratio and speed (DOWN)	75
Figure 3.10: <i>kp</i> and <i>kc</i> evolution with speed for two different compressors	78
Figure 3.11: Correlation plot of energy consumption model applied to reference compressor	79

Figure 3.12: Goodness of fit of energy consumption models applied to different data sets	80
Figure 3.13: Discharge temperature as a function of working pressures for nominal speed (UP). Discharge temperatures as a function of pressure ratio, compressor speed and condensing temperature (DOWN)	83
Figure 3.14: Isentropic efficiency as a function of RP, compressor speed and condensing temperatures.....	85
Figure 3.15: Evolution of Electro-Mechanical efficiency with pressure ratio, condensing temperature and speed. Lines represent proposed model predictions.	87
Figure 3.16: Correlation plot of discharge temperature model applied to reference compressor	89
Figure 3.17: Goodness of fit of discharge temperature models applied to different data sets	90
Figure 3.18: Discharge temperature correlation graphs. Without correction (LEFT). Using the correction term with $F = 0.75$	93
Figure 3.19: Train-Test methodology to evaluate the robustness of the studied mass flow models.....	96
Figure 3.20: Train-Test methodology to evaluate the robustness of the studied consumption models.....	98
Figure 3.21: Evolution of specific losses as a function of pressure ratio and speed...	103
Figure 3.22: Evolution of k_1 as a function of pressure ratio and speed	103
Figure 4.1: Climate profiles according to the standard (European Commission, 2018a)	107

Figure 4.2: Operating hours and heat capacity required as a function of external temperature for a HP with a rated capacity of 6.5kW working in an intermediate climate	112
Figure 4.3: Dependence of ΔT in the evaporator as a function of heating capacity and coil width and prediction of the used model	114
Figure 4.4: Dependence of ΔT as a function of heating capacity and number of plates and prediction of the used models	116
Figure 4.5: Heat pump operational zones	118
Figure 4.6: Compressor model performance	119
Figure 4.7: Calculation flow for sizing HXs	121
Figure 4.8: Compressor zones in the optimum condition and working hours for each bin	124
Figure 4.9: Optimization of temperature differences in heat exchangers using (4.6)	125
Figure 4.10: Optimization of temperature differences in heat exchangers with Bäckström method	126
Figure 4.11: Study of the influence of the different economic parameters in the optimization of HXs	128
Figure 4.12: Operating hours and cooling capacity required as a function of external temperature for a HP with a rated capacity of 10 kW	131
Figure 5.1: Calorimetric Test Bench	141
Figure 5.2: Envelope of the compressor and tested conditions	145
Figure 5.3: Comparison between OCR against speed for both methodologies ASRHARE and Discrepancies	146
Figure 5.4: Evolution of \dot{m}_{oil} and OCR against total massflow with and without oil separator a) Results of \dot{m}_{oil} with oil separator b) Results of \dot{m}_{oil} without oil	

separator c) Results of OCR with oil separator d) Results of OCR without oil separator	147
Figure 5.5: Effect of the Evaporating Temperature and Speed in OCR.....	149
Figure 5.6: Evaluation of the model estimation of oil mass flow as a function of speed compared with the experimentally estimated values of oil mass flow.	151
Figure 5.7: Compressor Efficiency calculated for different Evaporating Temperatures at 110Hz with different approaches	153
Figure 5.8: Compressor Efficiency calculated with different approaches for different Evaporating Temperatures at 110 Hz.	155
Figure 6.1: Miscibility test bench	163
Figure 6.2: Test results and model predictions.....	164
Figure 6.3: New model predictions of low miscibility mixtures (k=0.11) [Left] and high miscibility mixtures (k=0.25)[Right]	167
Figure 7.1: Diagram of the iterative procedure to obtain the Heat Transfer Coefficient and <i>T_{evap}</i>	175
Figure 7.2: Liquid-Vapor-Equilibrium diagram of R290 and POE68.....	177
Figure 7.3: Evolution of heat transfer as a function of vapor quality	180
Figure 7.4: HTC ratio evolution with: OCR and <i>T_{air, in}</i> (up), HTC ratio evolution with OCR, assuming <i>T_{air, in}</i> = 0°C (down)	181
Figure 7.5: Evolution of the drop in <i>T_{evap}</i> with OCR and <i>T_{air, in}</i> (up). Dependence of the drop in <i>T_{evap}</i> and the decrease of COP with of OCR <i>T_{air, in}</i> = 0°C (down).....	182
Figure 7.6: Evolution of COP with OCR and <i>T_{air, in}</i> (up). Dependence of COP reduction with OCR assuming <i>T_{air, in}</i> = 0°C (down).....	183
Figure 7.7: P-h-X diagram of R290 and POE68 (OCR=5%).....	184

Figure 7.8: Relation between vapor quality, oil concentration in the liquid and
apparent SH.....185

Figure 7.9: Evolution of Rh (up) and NEQ (down) with apparent SH for different OCR
values.....186

Figure 7.10: COP reduction due to refrigerant solved in oil as a function of OCR and
the methodology used.187

Figure 7.11: Contribution to the total compressor consumption of the different terms
of Eq.(7.20)188

Figure 7.12: Evolution of the COP reduction due to the heating of oil during
compression for different OCR values.189

List of tables

Table 2.1 Sensors used and their uncertainty.....	30
Table 2.2: Experimental Data set used for the evaluation of the consumption models	32
Table 2.3: Experimental Inverter data	32
Table 2.4: List of models fitted with the experimental data.....	38
Table 2.5: Model summary for the tested inverters.....	47
Table 3.1: Summary of variable-speed compressor datasets	59
Table 3.2: Summary of multiple SH dataset.....	61
Table 3.3: Model coefficients and goodness of fit of the mass flow model applied to the different compressors.....	70
Table 3.4: Model coefficients and goodness of fit of the energy consumption model applied to the different compressor data sets	82
Table 3.5: Model coefficients and goodness of fit of the proposed discharge temperature model applied to the different compressor data sets.....	91
Table 3.6: Improvement of prediction errors when Dabiri correction is implemented	94
Table 4.1: Model coefficients of the HXs and Compressor	123
Table 5.1: Uncertainty of Sensors	142
Table 6.1 Equations for the characterization of Oil-Refrigerant Miscibility.....	162

Table 6.2 Fitting coefficients of the different models.....166
Table 7.1: Fitting parameters and R^2 of the compressor models.....176



Chapter 1:

INTRODUCTION

This thesis comprises a compendium of published articles related to the modeling of variable-speed heat pumps. This first chapter establishes a common framework and it is designed to give the reader a holistic perspective of the thesis, introduce its general objectives and highlight the relations existing among the different publications.

1.1. Context

1.1.1. Energy sector in Europe

Throughout history, industrialization has consistently been perceived as the gateway to prosperity and an enhanced quality of life. The ascendancy of the telecommunications and transportation sectors, the shift towards globalized societies, and advancements in various fields of production represent only a few of the benefits and outcomes resulting from technological innovations. Nevertheless, the rapid societal transformation of the past century has also brought forth its share of drawbacks.

As it is well-known, contemporary society is grappling with an energy crisis triggered by the future scarcity of fossil fuels and the environmental impact of global energy consumption. This impact is evident in environmental pollution and factors such as the greenhouse effect on the atmosphere, which tends to raise the planet's overall temperature (the last two decades included 18 of the warmest years on record).

The presented framework urged the European Union to start the transition to renewable energies and reduce CO₂ emissions by establishing a plan to reach carbon neutrality by 2050 (Energy Roadmap 2050, 2011). Figure 1.1 shows a graphical representation of the planned reduction in greenhouse gas emissions, achieving net-zero emissions by 2050.

In this line, the European Union established in 2010 its energy strategy for 2020, which included targets for a 20% reduction in greenhouse gas emissions compared to 1990 levels, achieving 20% of energy generation from renewable sources, and reducing energy consumption by 20% through the use of more efficient processes and equipment (Energy 2020 A Strategy for Competitive, Sustainable and Secure Energy, 2010).

In 2014, the European Union agreed to set the energy strategy for 2030, which includes a 40% reduction in greenhouse gas emissions compared to 1990 levels, increasing the share of renewable energy to 27% in the total energy consumption, and a 27% reduction in energy consumption (EUCO 169/14, 2014).

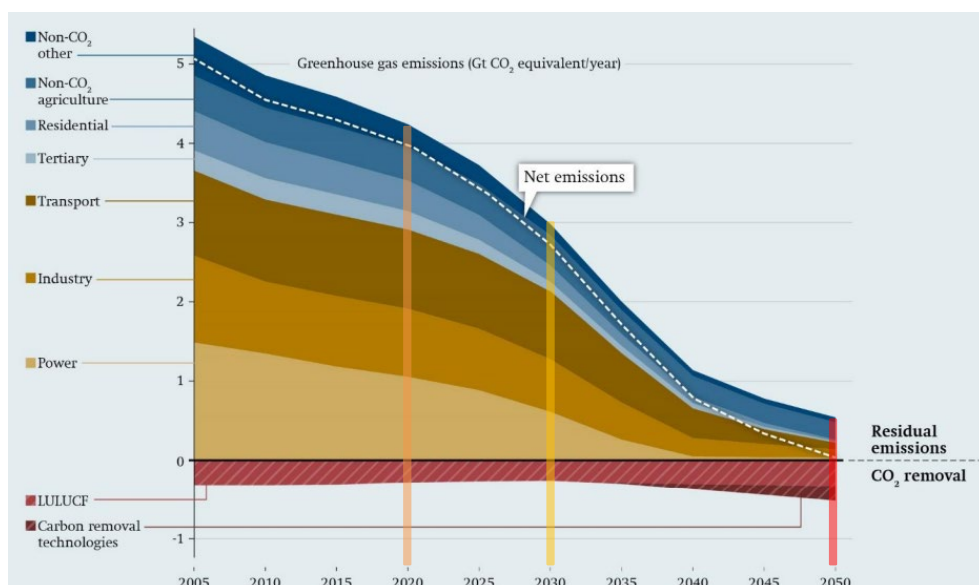


Figure 1.1: Pathway to achieve net-zero emissions in EU for 2050

(Original: European Commission, 2018)

In Europe, the energy crisis is even more critical due to its dependence on external fossil fuel imports and scarce energy resources which historically has made Europe very vulnerable to price volatility. In 2021, the European Union sourced over 40% of its overall gas consumption, 27% of its oil imports, and 46% of its coal imports from Russia (62% of the EU's total imports – 77% in 2011).

This over-dependence on gas, coal and oil imports has been explicitly manifested after the Ukrainian crisis and could be further enhanced by the present conflicts in the Middle East. In this line, the European Commission approved the REPowerEU plan in May 2022 (REPowerEU Plan, 2022), whose main objective is to terminate the EU's dependence on Russian fossil fuels.

This plan includes many strategies, among which the following stand out:

- Enhance the objectives for 2030: From 40% reduction in net emissions to 45%.
- Accelerate the rollout of renewables.
- Double solar photovoltaic capacity by 2025 and reach 600GW by 2030.
- **Speed up the deployment of heat pumps.** (10M additional units by 2027)

1.1.2. Heat pump technology

As explained in the previous section, there is an urgency to reduce energy consumption by increasing overall efficiency and decreasing the usage of fossil fuels in favor of renewable energies. For this matter, Europe considers that the general deployment of heat pumps is necessary to meet all the proposed climate objectives (Progress on Competitiveness of Clean Energy Technologies, 2022).

According to Eurostat data, 50% of all consumed energy in the EU is used for heating and cooling (Eurostat, 2023) and 70% of that energy is still being derived from fossil fuels, primarily natural gas. Additionally, around 80% of the total energy consumption in the residential sector is used for space and water heating by using gas boilers.

Compared to gas boilers, heat pumps do not use fossil fuels and represent a well-established technology known for their superior energy efficiency. Heat pumps facilitate the utilization of renewable energy sources, ambient energy and waste heat and can be used for heating, domestic hot water (DHW) and also space cooling. Rather than producing heat, these devices pump and upgrade existing energy in the ambient or in the ground, which allows to obtain coefficients of performance of 4-5 compared to boilers that are limited to 1.

As reported by the International Energy Agency (IEA), heat pumps are predicted to decrease Europe's gas consumption for building heating by at least 21 billion cubic meters in 2030 (International Energy Agency, 2022). In this line, the European Commission has declared heat pumps to be a critical factor in the energetic transformation to reach net-zero emissions and energy independence. Consequently, Europe is financing instruments to support the roll-out of heat pumps and is planning a *de facto* ban on fossil fuel boilers for the next decade (EHPA, 2023).

1.2.3. Refrigerant regulations

The most widespread heat pump technology utilizes a vapor compression cycle in which a working fluid is compressed and circulated through a condenser, an expansion valve, and an evaporator. This working fluid is typically called refrigerant and must comply with some thermodynamic requirements, such as high latent heat or suitable phase change pressures, as well as technical compatibility with materials, safety and availability among others.

The initial working fluids used during the early years of the development of this technology were not capable of meeting the desirable requirements effectively. This fact was either because their use posed dangers related to toxicity or the risk of explosion, or it was technically challenging due to the high working pressures required.

In the 1930s, a series of compounds known as CFCs were developed, which seemed to meet all the desirable requirements. They were harmless to humans, non-flammable, and exhibited outstanding thermodynamic properties. Due to these properties, CFCs appeared to be also the ideal compounds for propellants in aerosol sprays.

However, in 1974, Mario Molina and Sherwood Rowland published an article in the journal *Nature*, in which they explained that the degradation of CFCs in the stratosphere initiated a cycle leading to the destruction of the ozone layer (Molina & Rowland, 1974). These predictions were confirmed in 1985 when the appearance of an ozone hole over Antarctica was discovered. This led to Rowland and Molina being awarded the Nobel Prize in Chemistry in 1995 and the implementation of the Montreal Protocol (1987) and the Copenhagen Amendment (1992), which mandated the reduction and eventual discontinuation of the production and use of CFCs.

In order to find an alternative to CFCs, the molecular structure of refrigerant compounds was modified, leading to the creation of HCFCs with a lower potential for ozone layer destruction and, later, HFCs, which replaced chlorine with hydrogen in their composition and did not harm the ozone layer. However, their high chemical stability and relatively high opacity in the infrared spectrum mean that when released into the atmosphere, they have a significant potential to contribute to global warming.

The Kyoto Protocol of 1997 and the subsequent Kigali Amendment, which took effect in January 2019, seek to reduce the anticipated impact of global warming by limiting the use of HFCs and imposing a schedule for phasing out compounds based on their contribution to global warming.

As a result, one of the major challenges facing the heat pump industry today is the search for working fluids that meet all the necessary requirements for refrigerants. Recent studies, however, demonstrate that the only compounds capable of meeting thermodynamic needs and not contributing to global warming or ozone layer destruction are toxic or flammable (McLinden et al., 2017).

1.1.3. Part-load

Another challenge that heat pumps have to overcome is working at part-load conditions. Heating and cooling loads change continuously in most applications as external temperatures cycle between seasons and day/night. Figure 1.2 shows the yearly temperature distribution expected for Europe according to three different climate profiles.

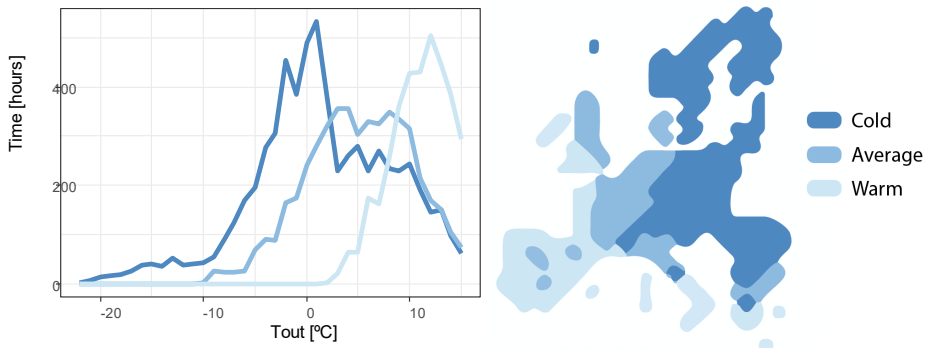


Figure 1.2: Climate profiles according to the standard (European Commission, 2018a)

Additionally, heat pump technology tends to reduce its capacity as external temperatures drop, so if sufficient capacity is needed at extreme working conditions, that would imply having an overpowered device the rest of the time, which would incur higher consumption and a loss in comfort.

Different technologies arise to adapt the capacity to the load (summarized in Figure 1.3), all of which imply reducing the compressor operation time or the amount of refrigerant displaced by it.

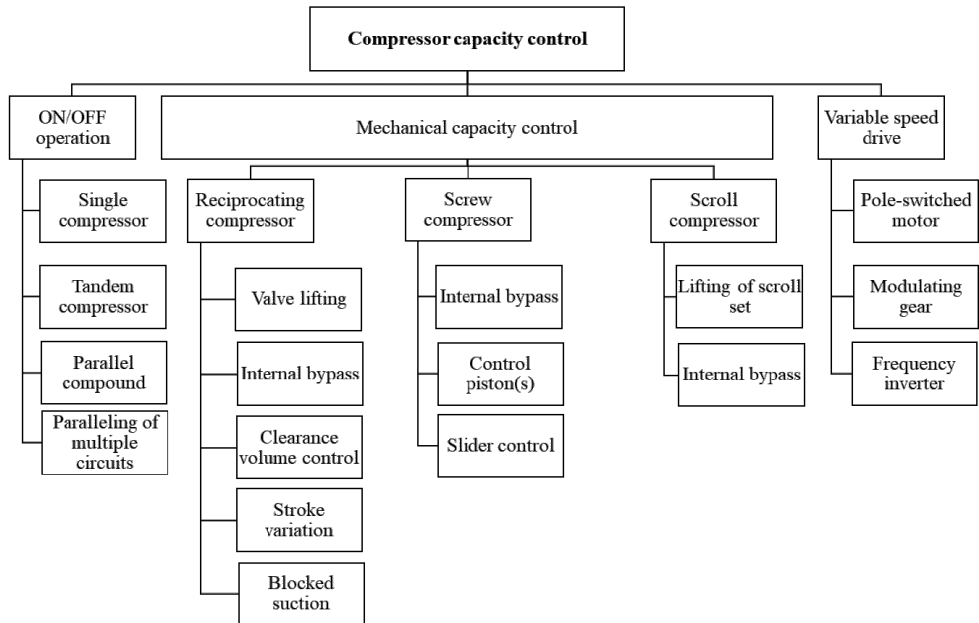


Figure 1.3: Capacity control techniques (Inspired from Bitzer, 2016)

The traditional control method is cycling the device between On and Off compressor states. This technique can reduce operating times and consequently consumption but has inherent problems related with cycling: lowering the compressor expected lifetime, heat exchanger unloading during off states, lower average compressor efficiencies, comfort loss, and more need for defrosting (Cecchinato, 2010; Garstang, 1990).

Other technologies implied reducing the effective refrigerant flow displaced by the compressor with different techniques depending on compressor technology. Most of the methods involved bypassing compressor discharge with suction or partially blocking the suction port. These technologies keep the compressor running and consequently dramatically drop the compressor's total efficiency.

Finally, with the development of power electronics and the drastic decrease in semiconductor costs, the possibility of controlling the compressor speed became viable and has been spreading since Toshiba introduced this technology to the HVAC sector in 1981 (Toshiba Air Conditioning, Pioneer of Modern Inverter Air Conditioning, n.d.). This technology has been reported to offer superior

energy efficiency when compared to On/Off systems in many applications (Bergman, 1985; Marquand et al., 1984; Miller, 1988; Tassou & Qureshi, 1998)

Figure 1.4 shows a comparative between part load technologies working at 50% of the load and concludes that the variable-speed technique is the one with a lower consumption.

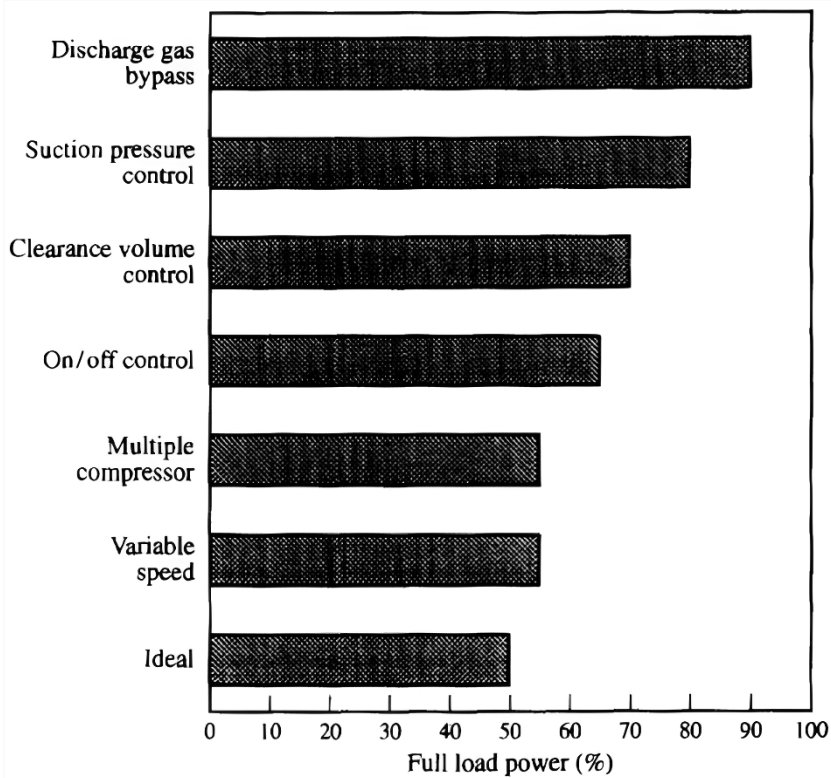


Figure 1.4: Comparison of various capacity control techniques at half load (Qureshi & Tassou, 1996)

1.1.4. Inverter technology

In order to modulate the compressor's speed, an additional device is needed which is able to adjust the frequency and voltage supplied to the compressor's electric motor.

This device is called Variable Frequency Drive (VFD) but it is also known as inverter or Variable Speed Drive (VSD), and its most common principle of work is described in Figure 1.5.

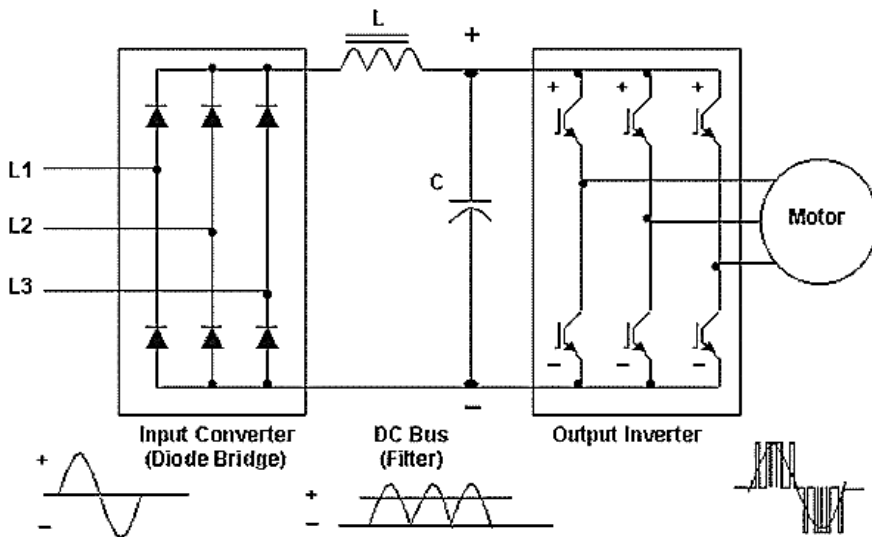


Figure 1.5: Internal schematic of a Variable Frequency Drive (VFD)

In the first stage, the input sinusoidal line is converted to DC by a diode bridge rectifier, then it is filtered by a DC bus filter and finally a set of IGBT switches commanded by a microcontroller chop the DC signal with a Pulse Width Modulation (PWM) to generate a new sinusoidal line at the desired frequency which will dictate the compressors speed.

VFDs have revolutionized the way electric motors operate by providing precise control over motor speed, soft starts/stops and having a high energy efficiency. Extensive research has been conducted on inverter performance within the electrical domain, yielding reliable prediction models by considering input variables such as output currents, DC bus voltages, technology of the switching

devices, and control algorithms. In contrast, such comprehensive information is seldom accessible in the Heating, Ventilation and Air Conditioning (HVAC) field.

In this field, Afjei and Jenni (Afjei & Jenni, 1994) divided inverter losses into two: primary losses, which included conduction, commutation and base power losses (produced in the inverter itself), and secondary losses generated in the compressor and related to the harmonics created by the inverter. Other studies as Cuevas and Lebrun (Cuevas & Lebrun, 2009) claimed that inverter losses were basically dependent on output power and was in the range of 2-5%.

1.1.5. Compressor modeling

System modeling is a fundamental process in engineering that involves creating abstract representations of real-world systems. It helps capture a system's essential characteristics, behaviors, and interactions to gain insights, make predictions, and facilitate decision-making.

When modeling a system, three approaches can be followed, each offering unique advantages and being suited to different scenarios based on the level of understanding and information available:

White Box Models (detailed): They are characterized by a transparent structure where the internal processes and components of the system are explicitly known. They offer high precision and adaptability when contour conditions vary. But, on the other side, they need a deep knowledge of the system, which may not always be feasible.

Black Box Models (empirical): They treat the system as an opaque entity focusing solely on inputs and outputs without explicit knowledge of the internal workings. Statistical or data-driven methods are used to understand the system's behavior. Typically, their formulation is very simple, making their integration in broader systems uncomplicated. They are suitable when limited information on the internal processes is available. However, they need extended empirical data and, even if they can have good accuracy, they show limited robustness to provide good results when predicting new data outside the trained range (extrapolating).

Grey Box Models (semi-empirical): They strike a balance between black and white models. They model the internal processes according to their physical

formulations and then empirical data is used to fit some coefficients which are difficult to estimate a priori. Their accuracy is very dependent on the made assumptions and on the level of detail of the internal process submodels.

System modeling in heat pumps brings about a notable reduction in the need for prototyping and streamlines the design process. By creating virtual representations of HVAC systems, engineers can simulate and test various configurations, optimizing designs before physical prototypes are constructed. This not only accelerates the design phase but also minimizes costs associated with multiple prototyping iterations.

Typically, compressor models are used when modeling the consumption and capacity of heat pumps as it is the primary energy-consuming component in the system and is responsible of moving the refrigerant and thus, providing capacity.

In the HVAC field a standardized model is typically used for fixed-speed compressors (AHRI_540, 2020; EN 12900, 2014). It is an empirical model based on condensing and evaporating temperatures and uses ten fitting coefficients for either electric consumption and mass flow rate. Its formulation is displayed in Eq.(1.1). This correlation has been extensively used but some studies declared that, for certain compressor typologies, this model could incur significant extrapolation errors and needed too many compressor tests to be fitted (Marchante-Avellaneda, Corberan, et al., 2023; Marchante-Avellaneda, Navarro-Peris, et al., 2023)

$$\dot{W}_c |\dot{m} = k_1 + k_2 T_e + k_3 T_c + k_4 T_e^2 + k_5 T_e T_c + k_6 T_c^2 + k_7 T_e^3 + k_8 T_e^2 T_c + k_9 T_e T_c^2 + k_{10} T_c^3 \quad (1.1)$$

However, there is no general characterization procedure when talking about variable-speed compressors (VSC). Typically, VSC are studied as a family of fixed-speed compressors, and the performance of the VSC is provided with an AHRI 10 coefficient correlation for each different speed. In its selector software, Bitzer uses this methodology (BITZER Software, n.d.), and it appears in some publications (Park et al., 2001). This methodology would imply interpolations between speeds and testing a great number of different compression conditions at each speed, which is cumbersome and time-consuming.

Nowadays, the state of the art of VSC modeling is to use an expanded version of the widely known 10-coefficient AHRI correlation Eq.(1.1). The new

function introduces ten additional speed-dependent coefficients, resulting in a 20-coefficient correlation.

This polynomial expression is used by manufacturers such as Emerson or Danfoss in their catalog data (Coolselector, n.d.) and has been used in the literature for modeling variable-speed heat pumps (Guo et al., 2017). It tends to adjust well train data due to the high number of fitting coefficients. However, many tests are required to fit the model correctly, and the extrapolation capabilities are limited.

Apart from the 20-coefficient correlation, other variable-speed models have been published among which it should be remarked the ones of Shao et al., 2004, Li, 2013, Santos et al., 2019, Mendoza-Miranda et al., 2016 and Winandy et al., 2002a. Other studies also proposed the use of Artificial Neural Networks to model compressor performance as Ma et al., 2020 or Kizilkan, 2011. All of them have strengths and weaknesses and more recent studies from important institutions as Oklahoma State University (Gabel & Bradshaw, 2023) and CEEE (Wan et al., 2021) make a review analysis to compare their pros and cons.

In order to carry out fair comparisons among models, extensive variable-speed empirical data obtained from high-fidelity test stands are required. However, there is limited performance data published in the literature for variable-speed compressors and most of the existing ones have limitations:

Cuevas and Lebrun (Cuevas & Lebrun, 2009) provided a dataset with 48 different conditions at five different speeds. Even if the test matrix maps present quite an orthogonal design it maps a narrow range of speeds and the tested conditions are for very high temperatures which are not common in the refrigeration field. Additionally, the experimental uncertainty was low.

Shao et al. (Shao et al., 2004) tested a rotary compressor working with R22. However, in his study, only the experimental ratio of mass flow and consumption for nominal speed seems to be provided, not the absolute results (as for nominal speed only a 6-coefficient correlation is presented). Consequently, this dataset is partially filtered by the model used and not exclusively empirical.

Winandy et al. (Winandy et al., 2002a) published an experimental data set of a mechanically-driven open-type reciprocating compressor working with R12. The piston had a significant displacement and the tested speeds were very low,

which is unusual for domestic heat pumps. The dataset consists of only 25 conditions tested at three different speeds ranging from 6 to 11 Hz. Both power and mass flow measurements were indirect, with a high stated uncertainty of 5 and 3 %, respectively.

Finally, Moradi et al. (Moradi et al., 2017) studied the performance map of a heat pump and published a performance data set with 44 test results over five different speeds. The test matrix was not centered on the compressor envelope but on the HP instead. Consequently, higher pressure ratios are tested as compressor speed increases, so studying the speed effect *ceteris paribus* is challenging. Additionally, the mass flow measurement was indirect and the power meter resolution was 100W, resulting in a high observed experimental uncertainty.

Another challenge that arises when characterizing the consumption of variable-speed compressors is to independently model the compressor and its inverter. Figure 1.6 shows the scheme compressor + inverter. In this scheme typically only \dot{E}_1 is measured and consequently what it is modelled is the overall compressor + inverter efficiency (considering both components as a black-box).

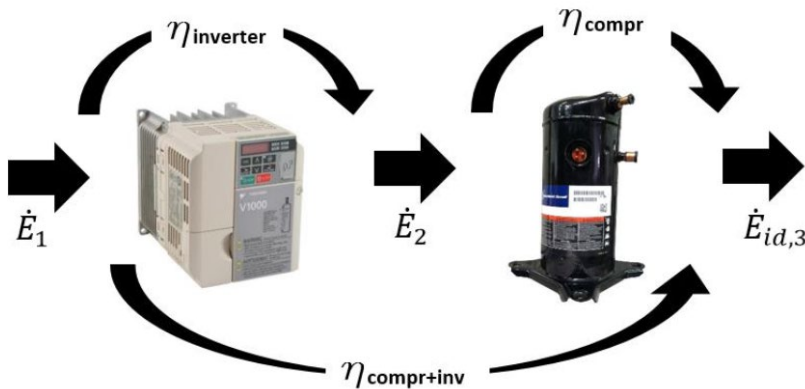


Figure 1.6: Compressor + Inverter scheme

Measuring only \dot{E}_1 is in part due to the challenge of obtaining accurate power measurements on the line connecting the inverter and the compressor (\dot{E}_2). This power line presents a high-frequency square wave with high harmonic distortion which needs specialized equipment with a very high sampling frequency and a broad sample window.

Treating the system as a black box introduces uncertainty when the inverter and the compressor are sold independently. In those cases, if another inverter is installed (different from the one used to fit the consumption model), significant discrepancies between the actual and predicted consumption can arise.

1.1.6. Oil Management

Another challenge that arises from the use of variable-speed compressors is the oil management.

A common typology in compressors is to use a drill in the shaft that acts as a centrifugal pump to move the lubricant from the oil sump to the key spots. The pumping action depends on rotational speed and thus, if the system is designed to have good lubrication at low speeds it will end up pumping an excess of lubricant when the speed increases, which eventually will be discharged by the compressor into the system.

In the system, oil is considered a contaminant as it changes the thermodynamic properties of the refrigerant, reduces the heat transfer coefficient in the heat exchangers and, in worst cases, can block the expansion device (Kruse & Schroeder, 1985). Moreover, excessive oil migrating into the system may result in insufficient oil remaining inside the compressor, compromising its lubrication and ultimately limiting its operational lifespan.

All the mentioned issues are especially important with variable-speed compressors. However, limited literature was published at the beginning of the research.

1.1.7. Heat pump design and sizing

Traditionally, heat pumps have been optimized for a rated condition, and its component selection was made to maximize the efficiency/cost ratio at that working condition.

In particular, the size of heat exchangers was typically chosen following techno-economic analysis, such as the one proposed by Bäckström in his study "Economic Optimum Problems in Connection with Refrigeration" (Bäckström, 1940). In his research, the heat exchangers were selected to achieve an optimum temperature difference between the refrigerant and the secondary fluid. This

methodology is still in use today as a rule of thumb and is reflected in "Refrigerating Engineering" by Granryd and Palm (Granryd & Palm, 2003), with a table of optimum temperature differences as a function of HX technology and operation time.

However, new rating standards (Commission Delegated Regulation (EU) No 811/2013 of 18 February 2013, 2013; European Commission, 2018a) measure the seasonal efficiency taking into account a scenario where working temperatures and loads evolve over year and thus, a nominal state does not exist anymore and techno-economic analysis as Bäckström's can't be directly applied.

More recent literature assessed the selection of heat exchangers. Mancini et al. (Mancini et al., 2018) focused on the design of plate evaporators for zeotropic mixtures. Wang and Sundén (L. Wang & Sundén, 2003), Caputo et al. (Caputo et al., 2008) and Unuvar and Kargici (Unuvar & Kargici, 2004) studied the optimal design of plate heat exchangers for general use. Jiang et al. (Jiang et al., 2022) proposed a general guideline for selecting heat pump systems based on economic analysis. Finally, Dai et al. (Dai et al., 2019) (Dai et al., 2023) analyzed the design of CO₂ heat pumps in China for space heating, including in the study calculations for varying heating loads and calculations for HX required area.

However, the mentioned studies do not take into consideration new degrees of freedom, such as the ability of the compressor to modulate its speed and/or keep designing the system for a virtual rated condition.

1.1.8. Thesis Framework

This PhD thesis has been developed in the described context in the "Instituto de Ingeniería Energética" ([IIE](#)) hosted at the Polytechnic University of Valencia (UPV).

IIE is a multidisciplinary research institute that has been conducting research since 2001 in energy-related topics and is divided into five different areas.

The investigation of this thesis was developed in the Thermal Area, which focuses on topics related to heat transfer, solar energy and heat pumps, among others.

The Thermal Area has a laboratory with more than 300 m² dedicated to test heat pumps and their components, and it is adapted to work with flammable

refrigerants as hydrocarbons. Among its equipment, it should be highlighted the presence of 4 climatic chambers, 3 independent and controllable water loops and a calorimetric compressor test bench.



Figure 1.7: Areas of the research institute

Apart from testing, this area of the institute is also focused on thermal system modeling to provide tools to make the process of heat pump design more efficient. In this line, the Institute developed [IMST-ART](#), a computer simulation tool that comprises detailed modeling of the different elements of the heat pump and manages to obtain performance predictions using as input easy-to-obtain catalog data from the different components.

This thesis emerges as a research effort to further improve IMST-ART capabilities by expanding the knowledge of variable-speed heat pumps and upgrading the existing built-in correlations to allow the simulation of these new heat pump typologies which is required for their design and for generating guidelines to select their components.

1.2. Identified gaps

From the mentioned context it can be concluded that variable-speed heat pumps are a key technology for ecological transition in Europe. However, contrary to fixed-speed heat pumps, they lack the methodologies to design and model their components correctly.

Fixed-speed compressors have been intensely studied, and a characterization standard is broadly accepted in the HVAC field. However, regarding their variable-speed counterparts, there is not a standard characterization procedure and there is limited published performance data, in part due to the number of tests required to completely map the entire working conditions (which increases the characterization costs dramatically). Additionally, the existing published data tends to study the system inverter-compressor as a black box and the power losses of the inverter are not deeply studied.

Regarding the sizing of the heat exchangers, they have typically been designed for a fixed capacity and a barely constant working temperature/pressure. However, the reality is that, for variable-speed heat pumps, either capacity and environmental conditions can fluctuate significantly over time, which may affect the design criteria.

Finally, during the development of the first experimental campaign of the thesis, high circulation rates of lubricant in the system were measured compared to the published data on fixed-speed heat pumps. This fact motivated a deeper study of oil circulation rates in variable-speed heat pumps and the evaluation of their impact on global performance as they can affect the design of the components.

1.3. Aims of the thesis

Given the context described above, the broad objective of the present thesis is to provide optimal design guidelines to design and select components for variable-speed heat pumps. For that matter, particular goals were proposed, which are focused on providing new insights into the performance of the different components and can be divided into three distinct groups:

Compressor Modeling:

- Test variable-speed compressors to provide a high-fidelity and well-structured data set in which the efficiency of the compressor and the inverter can be studied independently.
- Model the inverter losses as a function of easy-to-access variables.
- Study the evolution of compressor performance with compression conditions and compressor speed.
- Evaluate the performance of existing variable-speed compressor models.
- According to the limitations observed in the existing models, propose new compact correlations to predict the main performance indicators (mass flow, compressor consumption and discharge temperature).
- Evaluate the minimum number of characterization tests to adjust the proposed models and give insights on how to position them.

Heat exchanger design and sizing:

- Design simple correlations for predicting heat exchanger performance under varying loads and compressor speed.
- Propose a general technique to select and size heat exchangers in a heat pump working under varying loads and with a variable speed compressor.

Oil management

- Study how variable-speed compressors manage lubrication.
- Quantify the discharged oil and its dependence on compressor speed.
- Study how circulating oil in the system could affect the heat pump's performance.

1.4. Structure

This thesis is a compendium of published articles related to modeling and designing variable-speed heat pumps. **Chapter 1** introduces the context of the thesis, highlights the importance of heat pump design, and introduces the limitations of the state-of-the-art and the objectives of the investigation.

The middle chapters correspond to individual papers published. Each chapter is self-contained, presenting the study, methodology, and results separately. These chapters can be grouped into three different groups according to their objectives:

1.4.1. Compressor Modeling

The paper in **Chapter 2** presents the empirical data obtained from the experimental test campaign. In total, three inverters and two scroll compressors are tested. The evolution of performance is analyzed, and the different models proposed in the literature to model compressor consumption are evaluated. For the models that perform better, an optimal technique to design test matrices is presented that allows the models to be adjusted with the minimum data possible. Regarding the inverters, a model to predict heat losses is presented and the effect of the switching frequency is evaluated.

The paper in **Chapter 3** conducts a detailed analysis of how compressor energy consumption, mass flow, and discharge temperature evolve with compressors' working conditions and speed. Compact correlations are proposed for each performance variable, and they are generalized for varying suction conditions. The models are validated with different data sets and were proved to be robust even if tested with limited data.

1.4.2. Heat Exchanger design for variable-speed heat pumps

The paper in **Chapter 4** reviews the classical design criteria for selecting and sizing heat exchangers and proposes a new methodology to optimize the sizing of heat exchangers according to a techno-economic analysis that takes into account the climate profile and the ability of the compressor to adapt the capacity to the ever-changing load. In order to make this technique possible, simple

correlations are proposed to predict heat exchanger performance as a function of optimizing variables.

1.4.3. Effect of oil in heat pump

The paper in **Chapter 5** studies the amount of oil discharged by a variable-speed compressor and its evolution with speed. A new measuring technique is presented to analyze the oil discharged based on a discrepancy method rather than the standard weighting procedure, which is cumbersome and time-consuming. The results show that variable-speed compressors can release much more lubricant to the system compared to traditional fixed-speed compressors. Additionally, a simplified correlation is provided to predict oil discharge evolution with compressor speed.

The paper in **Chapter 6** shows the limitations of the existing oil-refrigerant miscibility correlations to provide realistic predictions when they are extrapolated at conditions close to pure refrigerant. Predicting miscibility in these conditions is key to evaluating how lubricants can affect the heat exchange in heat exchangers. This study proposes a new miscibility correlation using only a single coefficient, which can be used as a miscibility index and has the advantage of not obtaining predictions with no physical sense.

In **Chapter 7**, a theoretical evaluation of the impact of oil circulation in the system is carried out. Three different impact contributions were studied: the heat transfer reduction in the evaporator at high oil circulation rates, the effect of refrigerant being solved in oil and finally, the impact of oil in the compressor itself.

Finally, **Chapter 8** comprises the main conclusions, future work, and the scientific production obtained within the framework of the present thesis. **Chapter 9** lists the literature references used during the investigation and in the different Appendixes a summary of the empirical results is shown.

1.5. Chronology

It should be noted that the order of the chapters does not follow a chronological sequence; they are grouped according to their objectives for improved readability. To give the reader a broader perspective, the followed research path is described in the following paragraphs:

This thesis started with the characterization of the variable-speed compressor, which is the core of the heat pump, responsible for producing capacity and the primary energy consumer; consequently, it is the first element to study when designing a heat pump. However, due to the limited data published it was decided to carry out an extensive experimental campaign in which the compressor and the inverter could be studied independently.

In the early stages of the testing, some tests were conducted to measure the oil circulation, which demonstrated that variable-speed compressors could discharge more lubricant compared with its fixed-speed counterparts. This finding motivated the design of an additional test campaign, the results of which were reported in the publication of **Chapter 5**. This publication has received particular attention with around 20 citations, among which a study from the Illinois group (Haider et al., 2022) stands out, in which the reported evolution of oil circulation with speed was reproduced.

After the first publication, and in parallel to the variable-speed compressor testing, the theoretical impact of the circulating oil on the heat pump's performance was investigated, and the results were published in the publication of **Chapter 7**. To conduct this investigation, an internship in TU Dresden was planned. It consisted of 4 months of research in the Schaufler Chair of Refrigeration, Cryogenics and Compressor Technology, a research institute with a lab to investigate mixture properties. During the internship, the miscibility of lubricants and refrigerants was studied; obtaining a general solubility correlation using only a single fitting coefficient (the solubility index). The mentioned miscibility model was used for the publication in **Chapter 7** and was presented in detail in a posterior short publication (**Chapter 6**).

From this point, the research divided into two: finishing/analyzing the experimental results of the variable-speed compressor campaign and studying standards for part load performance to provide design guidelines for the selection of

component. Being the latter the main objective of the thesis. Those two research objectives finished in rapid succession with the publication of their respective papers in ***Chapter 2*** and ***Chapter 4***.

Finally, a deeper analysis of the results of the experimental campaign was carried out to provide compact correlations to model mass flow, consumption and discharge temperatures in variable-speed compressors. The results obtained from this study are displayed in ***Chapter 3*** and are currently under peer review to be published in a high-impact journal.

Chapter 2:

FIRST PUBLICATION





Applied Thermal Engineering

Volume 230, Part B, 25 July 2023, 120725



Research Paper

Testing of Variable-Speed Scroll Compressors and their inverters for the evaluation of compact energy consumption models

Rubén Ossorio  , Emilio Navarro-Peris

<https://doi.org/10.1016/j.applthermaleng.2023.120725>

Testing of Variable-Speed Scroll Compressors and their inverters for the evaluation of compact energy consumption models

Rubén Ossorio, Emilio Navarro-Peris

Instituto Universitario de Investigación en Ingeniería Energética (IUIIE)
Universitat Politècnica de València, Camino de Vera s/n, ed. 8E cubo F 5º, Valencia,
46022, Spain

2.1. Abstract

Prediction models for energy consumption in heat pumps are critical for design, selection, control and fault detection. However, nowadays, the methodology for characterizing variable-speed compressors has not been standardized, and typically the pair compressor-inverter is studied as a whole. In this study, disaggregated energy consumption results of compressor and inverter is obtained by using a double-wattmeter scheme. The compressor results are used to compare the existing performance models and to establish guidelines to define minimal test data required to characterize this type of compressor. The widely used 20-coefficient correlation overfits the compressor behavior, introducing significant deviations when extrapolations are performed. Optimal Design methodologies to create rating test matrixes gave excellent results compared with classical clustering techniques. Regarding inverter results, a compact empirical model was proposed to model inverter power losses depending on total consumption and compressor speed. The proposed model used only five fitting coefficients, and most predictions are inside a 5% error band for all tested inverters. Finally, the tested compressors and inverters suffered a significant efficiency loss at very low speeds, which could make cycling more profitable under certain circumstances.

Keywords: Variable speed compressor, inverter, efficiency, modeling, consumption

2.2. Introduction

Heat pump systems have spread into the heating and air conditioning industry as they offer an efficient, affordable, and reliable solution. The EU considers them the path to follow in heating and cooling to reach the objectives of reducing CO₂ emissions.

As thermal loads tend to be highly variable, heat pumps have to work at part load for most of their lifetime. Consequently, capacity control techniques have to be applied, among which the use of variable speed compressors (VSC) stands out (Qureshi & Tassou, 1996) (Granryd & Palm, 2003). This technology enhances energy savings compared with On/Off systems using single-speed compressors (Bagarella et al., 2016) (R.S.Adhikari et al., 2012), which have been gradually replaced by variable speed solutions since Toshiba introduced the technology into the HVAC sector in 1981 (*Toshiba Air Conditioning, Creator of Modern Inverter Air Conditioning*, n.d.).

The compressor is the heart of a heat pump and its most complex element. Consequently, a compressor simulation model that provides information about consumption is essential in designing or studying an HVAC system. In the literature, three different approaches are typically found when modeling a single-speed compressor (Wan et al., 2020):

Detailed models (Duprez et al., 2007) (Chen et al., 2002) consider internal geometries, leakages, oil properties and heat dynamics inside the compressor. They require many parameters based on information that only manufacturers have and are computationally intensive. They provide accurate results but are used mainly for compressor design.

Semi-empirical models (Cuevas et al., 2010; Jahnig et al., 2000; Winandy et al., 2002b) (Koury et al., 2001). These models are derived from the physical work equation of vapor compression and use experimental data to deduce parameters that are hard to determine as polytropic coefficients, losses to the ambient and heat transfer coefficients, among others. These are models with a low number of fitting parameters. However, they may be difficult to adjust as they involve non-linear equations, typically with exponents, and their accuracy is limited.

Map-based models (or Empirical) (AHRI_540, 2020) (Shao et al., 2004) (C. Aprea and C. Renno & Department, 2008). They don't require any physical

information about the internal processes of the compressor. They typically consist of polynomial equations whose coefficients are fitted with experimental data.

The problem with map-based models is overfitting. A model with many coefficients will constantly adjust the training dataset better; however, it may result in fitting non-useful information as experimental error. When this happens, the model will fail to perform accurately against unseen data (Hu et al., 2020). To avoid underfitting or overfitting, the model needs to have a suitable complexity in agreement with the level of information embedded in the train data. Choosing between model accuracy and model complexity is critical for map-based model development.

When modeling a fixed-speed compressor, the most extended methodology is the AHRI correlation which uses ten coefficients (Standard, 2017) (AHRI_540, 2020) (represented in Eq.(2.1)) . It is a map-based model that uses evaporating and condensing temperatures as modeling variables and can be used to predict compressor consumption and refrigerant mass flow, among others.

$$\dot{W}_{compr} = k_1 + k_2 T_e + k_3 T_c + k_4 * T_e^2 + k_5 T_e T_c + k_6 T_c^2 + k_7 T_e^3 + k_8 T_e^2 T_c + k_9 T_e T_c^2 + k_{10} T_c^3 \quad (2.1)$$

According to Aute et al. (Aute et al., 2015), manufacturers typically take more than 14 experimental points to fit the correlation and test 2-3 different units for accounting for unit-to-unit variations.

However, there is no general characterization procedure when talking about variable-speed compressors. Typically, VSC are studied as a family of fixed-speed compressors, and the performance of the VSC is provided with an AHRI 10 coefficient correlation for each different speed. In its selector software, Bitzer uses this methodology (*BITZER Software*, n.d.), and it appears in some publications (Park et al., 2001). This methodology would imply interpolations between speeds and testing 14 different compression conditions at each speed which is cumbersome and time-consuming.

Nowadays, the state of art of VSC modeling is to use an expanded version of the widely known 10-coefficient AHRI correlation (AHRI_540, 2020). The new function introduces ten additional speed-dependent coefficients resulting in a 20-coefficient correlation which will be called from now on AHRI-20 (displayed in Eq.2).

$$\begin{aligned}
\dot{W}_{compr} = & k_1 + k_2 T_e + k_3 T_c + k_4 f + k_5 T_e^2 + k_6 T_c^2 + k_7 f^2 \\
& + k_8 T_e T_c + k_9 T_e f + k_{10} T_c f + k_{11} T_e^3 + k_{12} T_c^3 \\
& + k_{13} f^3 + k_{14} T_e^2 T_c + k_{15} T_e^2 f + k_{16} T_c^2 T_e \\
& + k_{17} T_c^2 f + k_{18} f^2 T_e + k_{19} f^2 T_c + k_{20} T_e T_c f
\end{aligned} \tag{2.2}$$

This polynomial expression is used by manufacturers such as Emerson or Danfoss in their catalog data (*Coolselector*, n.d.) and has been used in the literature for modeling variable-speed heat pumps (Guo et al., 2017) (Wan et al., 2021). It tends to adjust well train data due to the high number of fitting coefficients. However, many tests are required to fit the model correctly, and the extrapolation capabilities are limited.

Apart from AHRI-20, other variable-speed models have been published (Shao et al., 2004) (Li, 2013) (Santos et al., 2019) (Mendoza-Miranda et al., 2016), which are reviewed in the following section. To compare the performance of the different correlations, real experimental data is needed. Performance data can be found in compressor datasheets; however, the provided data is typically not actual test results but predictions from a pre-adjusted model instead. Consequently, that data cannot be used to perform a fair comparison among models as it will perfectly fit the model from which it was generated.

In the literature, there are few experimental datasets of variable-speed compressor performance. Shao et al. (Shao et al., 2004) presented performance data of a rotary compressor. However, the study did not provide individual results but the fitted correlations instead and did not declare the number of training points and where they were positioned. In Darr and Crawford's study (Darr et al., 1992), individual experimental results are given for different temperatures and speeds for an automotive reciprocating compressor. However, the data was not evenly distributed, and only a local portion of the envelope was tested. Consequently, significant extrapolations are needed to model the complete envelope. Cuevas and Lebrun [8] also provided experimental data (50 different compression conditions distributed at five different speeds) for a variable-speed scroll compressor working with R134a.

In addition to introducing a new variable in the compressor modeling (the speed), using variable-speed compressors introduces another component, the inverter or Variable Frequency Drive (VFD). This element also generates losses which are challenging to characterize due to the difficulty of measuring electrical

power at the inverter outlet. As a consequence, the pair compressor-inverter is typically considered a black box, and only the global consumption is measured.

The inverter performance has been studied thoroughly in the electrical field, where good prediction models can be obtained using as input variables: output currents, DC bus voltages, technology of the switching devices, control algorithms... However, this information is rarely available in the HVAC field, and correlations based on easy-to-obtain variables such as consumption or speed would be of particular interest.

According to Afjei and Jenni (Afjei & Jenni, 1994), two separate losses are introduced when using an inverter. The firsts are primary losses which are produced in the inverter itself. They include conduction, commutation and base power losses. Secondary losses are generated in the compressor and are related to the PWM signal's harmonics created by the inverter. They typically can be neglected when the switching frequency exceeds 1kHz (Afjei & Jenni, 1994).

Cuevas and Lebrun (Cuevas & Lebrun, 2009) studied the inverter power losses through a calorimetric method. They concluded that the inverter efficiency depended mainly on the output power, not the speed. The reported losses were in the range of 2-5% and a correlation to model power losses wasn't proposed.

In this study, a complete experimental characterization of variable-speed systems is made. This study is split into two parts; the first focuses on heat pump compressors and the second on inverter performance.

The first part starts analyzing the compressor's experimental results. Then, the experimental data is used to review the performance of already published compressor models. And finally, the problem of how to select the rating points is assessed.

The second part focuses on inverter power losses. A novel mathematical model is proposed to predict the power losses of the tested inverters, and the carrier frequency influence is evaluated.

2.3. Methodology

2.3.1. Test bench description

The compressor test bench described in Figure 2.1 has been used to characterize variable-speed compressors. It has been designed to satisfy the Standard EN13771 (EN13771, 2017) for compressor rating and can evaluate the typical compression cycle conditions varying condensing and evaporating pressure, subcooling (SC), superheat (SH) and compressor speed. The test bench comprises a set of PID controllers that can keep any operating condition stable within a range of 1kPa and 0.1°C from its setting without manual adjustments.

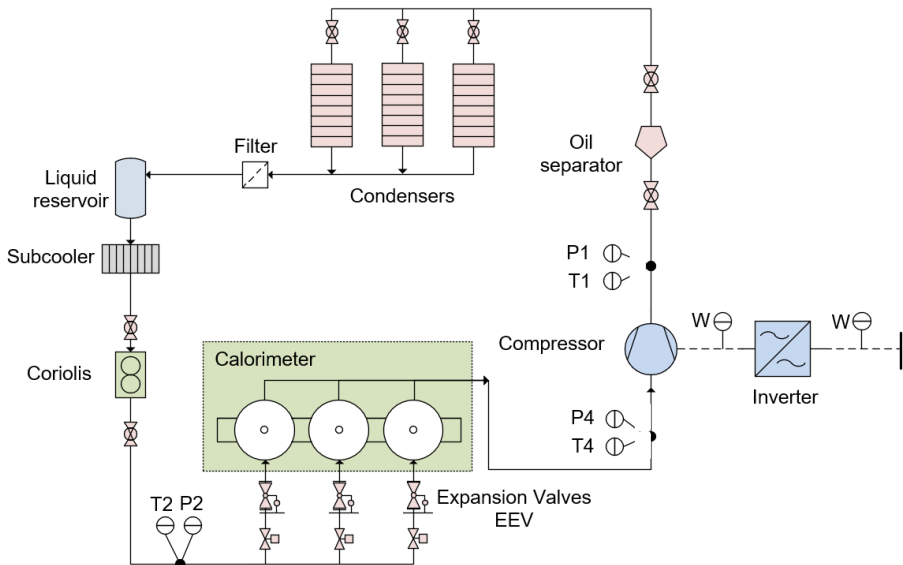


Figure 2.1: Variable-Speed Compressor Test Bench

The sensors installed are described in Table 2.1 and their uncertainty is displayed at a confidence interval of 95%. The temperature readings were taken by immersion RTDs (Class 1/10 DIN) placed in an elbow facing upstream. Methods A and E of the Standard EN13771 (EN13771, 2017) were implemented to measure mass flow: a Coriolis sensor placed in the refrigerant liquid line and a calorimetric balance in the evaporator. Regarding energy consumption, a double-wattmeter scheme was used to determine power losses in the inverter and the global consumption. A YOKOGAWA WT1030 (Hisashi et al., 1997) power meter

was implemented in the line connecting the inverter and the compressor, as it is capable of measuring electrical power in this line¹. This line cannot be measured with typical power meters as it presents a high-frequency square wave voltage in the range of the kHz result of the pulse width modulation (PWM) needed to control the compressor speed (Afjei & Jenni, 1994).

The power lines connecting the inverter and the compressor were always in the suggested range provided by the manufacturer. The inverter configuration parameters were the ones provided by the manufacturer or in its absence the ones obtained by an autotuning procedure.

Table 2.1 Sensors used and their uncertainty

Variable	Equipment	Uncertainty
T	RTD-PT100 (1/10 DIN)	±0,05°C
P	Fisher-Rosemount 3051	±0,02%
<i>m</i>	Coriolis CMF025M	±0,025gs-1
Win	Fluke 1735	±51W
Wout	Yokogawa WT1030	±13W

Sensor readings were logged with a Keysight 34970A, and the final result was the average of all the measurements taken in a stable window of at least 15 minutes (typically 30 minutes). The thermodynamic database used was REFPROP v10.0 (Huber et al., 2022), which was used to calculate evaporating and condensing temperatures as a function of the corresponding pressures.

2.3.2. Experimental data

In this test bench, two variable-speed scroll compressors from various manufacturers working with different refrigerants were tested: Compressor A and

¹ For ompressor speeds of 110 Hz the sampling speed is 28 kHz with a sampling window of 32 periods which, compared with the PWM frequency of 6kHz, satisfies the Niquist's theorem (4.6 frequency ratio). For other fundamental frequencies (compressor speeds) the frequency ratio ranges from 4.5 to 5.

Compressor B. Both presented the same typology: the compression chamber at the top position (above the electric motor and the carter). The lubrication mechanism consists of a borehole in the shaft that acts as a centrifugal pump to lubricate the main bearings and the scroll.

Compressor A has a displacement of 46cm³ and works with R290 and POE68 oil. It has been tested at distributed conditions of evaporating and condensing temperatures, trying to map the entire envelope homogeneously and orthogonally. To correctly map the complete speed range (15-120Hz), that pattern was repeated at speeds of 30, 50, 70, 90 and 110Hz, resulting in a total of 134 experimental tests. The tested conditions for each speed are represented in Figure 2.2.

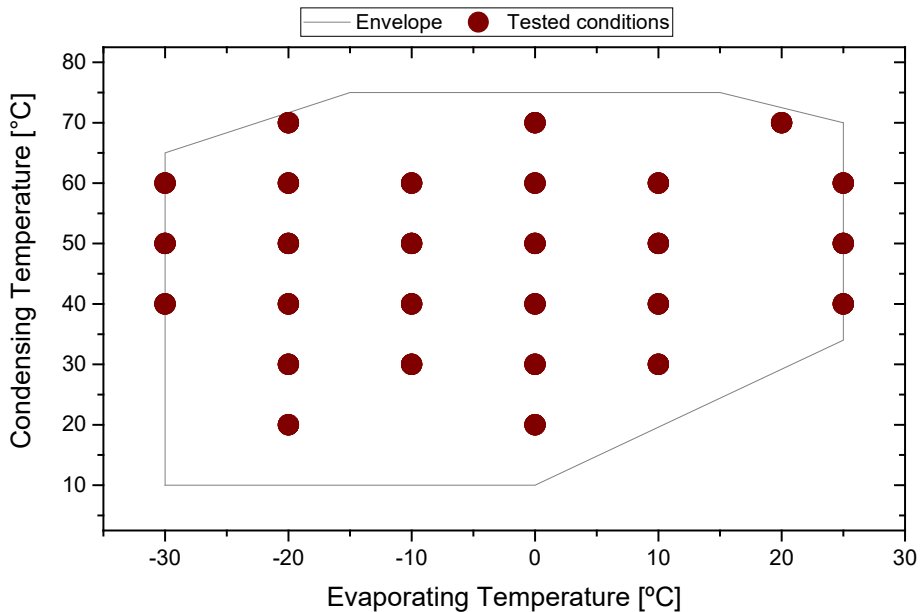


Figure 2.2: Test Matrix of Compressor A

Compressor B is a variable-speed scroll compressor with a displacement of 44.5cm³ and works with R410A and PVE32 as a lubricant. In total, 35 different compression conditions were tested, 14 at the nominal speed of 60Hz, and the rest distributed along the envelope at different frequencies.

Additionally, the experimental data obtained by Cuevas and Lebrun (Cuevas & Lebrun, 2009) was also included, so the models were evaluated against three different compressors with three different refrigerants.

In Table 2.2, a summary of the used datasets is displayed.

Table 2.2: Experimental Data set used for the evaluation of the consumption models

	<i>Compressor A</i>	<i>Compressor B</i>	<i>Compressor C</i>
<i>Source</i>	Experimental	Experimental	Cuevas & Lebrun, 2009
<i>Technology</i>	Scroll	Scroll	Scroll
<i>Displacement</i>	46cm ³	44.5 cm ³	54.25 cm ³
<i>Refrigerant</i>	R290	R410A	R134a
<i>Lubricant</i>	POE 68	PVE 32	-
<i>Speed Range</i>	15-110 Hz	15-100 Hz	35-75 Hz
<i>Nominal Speed</i>	70	60	50
<i>Tests</i>	134	35	48

Apart from the compressors, the mentioned test bench was also used to characterize three different inverters from different manufacturers. All of them used the same control strategy (Advanced Open Loop Control for Permanent Magnet Motors) to adjust the compressor speed with carrier frequencies ranging from 6.6kHz to 5kHz. As the electrical motors are synchronous, the slip ratio has not been considered, and the mechanical speed of the compressor has been supposed to be the same as the one configured in the inverter. A summary of the specifications of each tested inverter is displayed in Table 2.3.

Table 2.3: Experimental Inverter data

	<i>Inverter A</i>	<i>Inverter B</i>	<i>Inverter C</i>
<i>Tests</i>	133	17	35
<i>Carrier Frequency</i>	6 kHz	6.6 kHz	5 kHz
<i>Tested Power</i>	0.7-7 kW	0.7-5 kW	0.6-7 kW
<i>Max Power</i>	15 kW	5.5 kW	10 kW
<i>Tested Speed</i>	15-110 Hz	15-110 Hz	15-100 Hz
<i>Efficiency</i>	0.87-0.96	0.91-0.94	0.90-0.98
<i>Control mechanism</i>	Open Loop Control for Permanent Magnet Motors		

2.4. Compressor performance

2.4.1. Analysis of the experimental results

In this section, the experimental data of Compressor A will be studied in detail as it is the one with more tested conditions. The detailed experimental results of compressors A and B are included in the appendixes.

The experimental mass flow results are displayed in Figure 2.3. It should be noted that the main variables affecting the mass flow are evaporating temperature and speed.

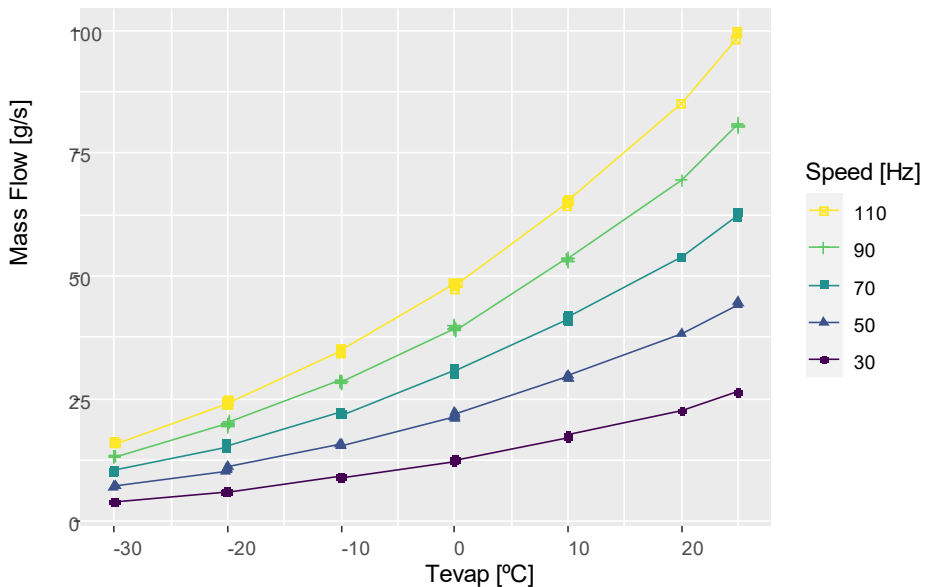


Figure 2.3: Experimental Mass Flow evolution with compression condition and speed [Compressor A]

In Figure 2.4, the experimental results of the compressor consumption (including inverter losses) are displayed at different compression conditions. The peak consumption was close to 7kW and was produced at maximum speed and PR.

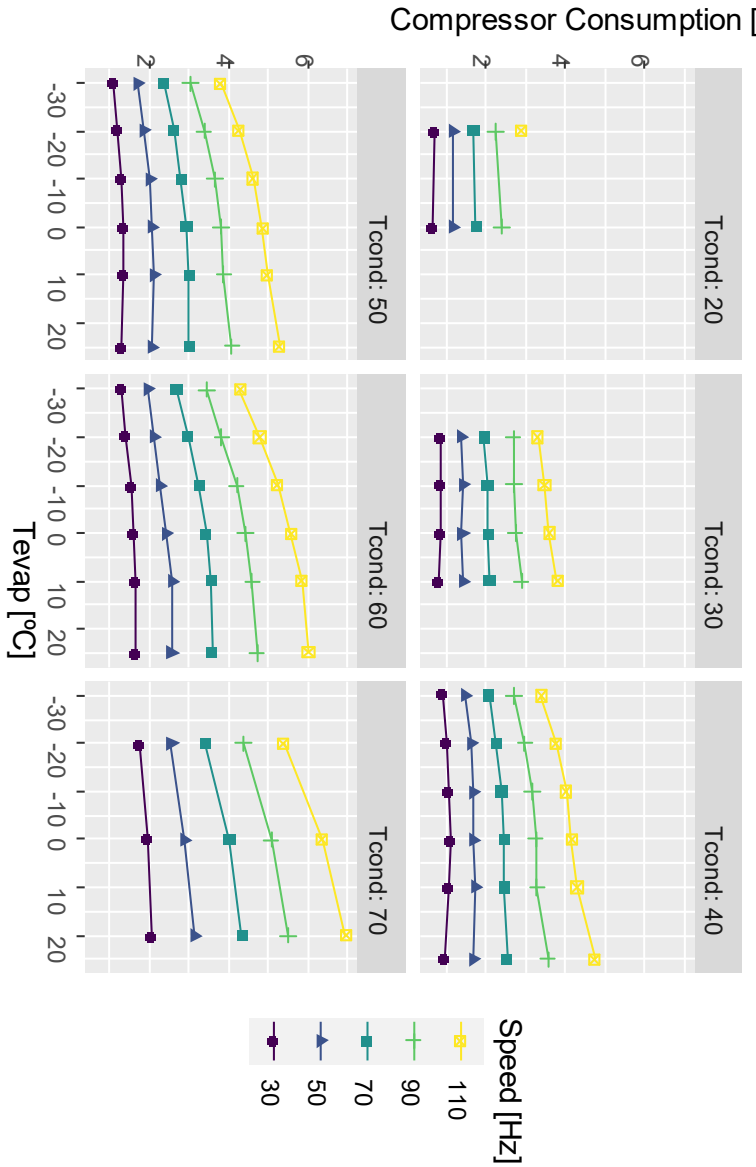


Figure 2.4: Consumption results of Compressor A and its evolution with the compression condition and speed

Compressor efficiency is defined in Eq.(2.3), and its evolution with the compression conditions can be seen in Figure 2.5.

$$\eta_{compr} = \frac{\dot{m} (h_{d,is} - h_s)}{W_{compr}} \quad (2.3)$$

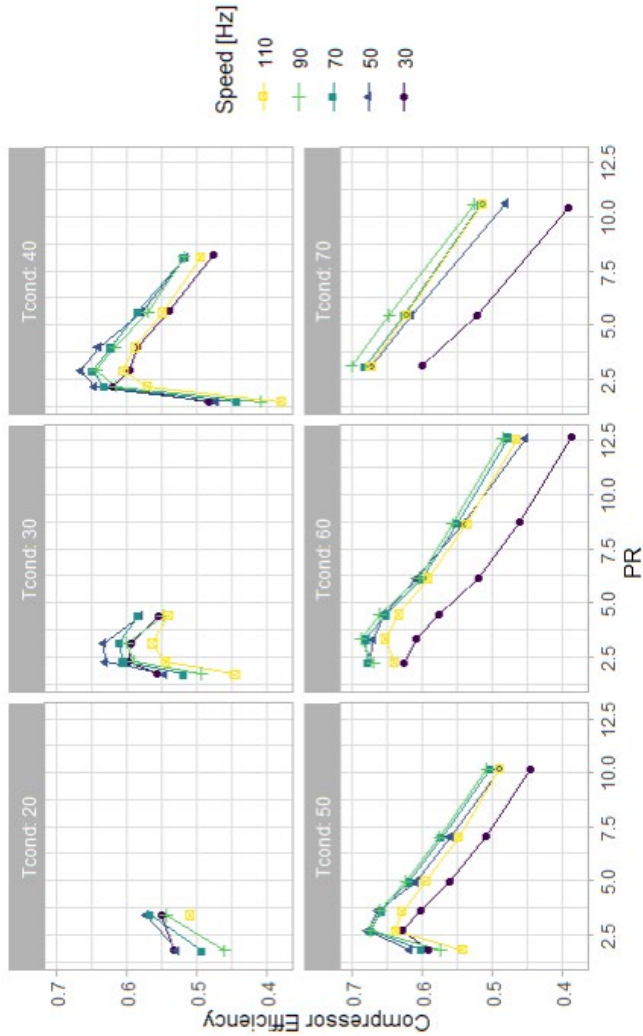


Figure 2.5: Compressor A efficiency and its evolution with the working variables

It should be pointed out that compressor efficiencies behave homogeneously, showing a maximum at PR close to 2.5 and sharply decreasing as PR decreases or increases. At central speeds (50, 70 and 90 Hz), compressor efficiency doesn't show a significant dependence on speed. However, a decrease in compressor efficiency is manifested at low frequencies and high condensing temperatures. A possible explanation for this phenomenon is a lack of lubrication in the scrolls at low speeds, which increases internal leakages and could increase frictional losses too. The internal leakages are related to the pressure difference, which explains why these become more relevant at high condensing temperatures. The hypothesis of low lubrication at low speeds was analyzed in a previous study (Ossorio & Navarro-Peris, 2021) and was also pointed out by Cuevas and Lebrun (Cuevas & Lebrun, 2009).

Compressor efficiency also decreases at high speeds and low condensing temperatures due to increased mechanical losses. These mechanical losses do not depend heavily on working temperatures; consequently, at lower condensing temperatures where the compressor has a lower consumption, they have a higher impact on efficiency.

2.4.2. Characterization models

This section compares the performance of the main proposed models in the literature for variable-speed compressors. A summary list of the tested correlations is presented in Table 2.4.

AHRI-20 and Shao are linear empirical correlations that can be easily fitted with ordinary regression tools. However, Santos, W.Li and Mendoza consider fitting exponents whose convergence is more problematic and need more complex regression tools. Santos model is coupled with the mass flow model, and thus, if the mass flow measurements have a significant experimental uncertainty, it will also propagate to the consumption estimation. In this study, to minimize this effect, the values of mass flow introduced in the consumption model will be the ones predicted by the pre-adjusted mass flow model. That way, the experimental uncertainty of mass flow is partially filtered and will lower the consumption estimation error.

All these correlations were fitted using the different compressors' complete experimental dataset, and the fitting results are displayed in Figure 2.6. For comparing the results, the Coefficient of Variation (CV) of the Root Mean Square Error (RMSE) was used (Eq.(2.4)), a dimensionless parameter that measures the relative dispersion of the error in the modelled variable. As the RMSE is divided by the tested consumption mean, the results from the different compressors can be compared even if their sizes are not the same. RMSE (in W) is also shown in the plot to compare it with the sensor accuracy (in the range of 50W).

$$CV(RMSE) = \frac{RMSE}{\bar{X}} = \frac{1}{\bar{X}} \sqrt{\frac{\sum_{n=1}^N (\hat{y}_t - y_t)^2}{N}} \quad (2.4)$$

Table 2.4: List of models fitted with the experimental data

ID	Expression	Coef	Var
AHRI-20 (Guo et al., 2017)	$\dot{W}_{compr} = k_1 + k_2 T_e + k_3 T_c + k_4 f + k_5 T_e^2 + k_6 T_c^2 + k_7 f^2 + k_8 T_e T_c + k_9 T_e f + k_{10} T_c f + k_{11} T_e^3 + k_{12} T_c^3 + k_{13} f^3 + k_{14} T_e^2 T_c + k_{15} T_e^2 f + k_{16} T_c^2 T_e + k_{17} T_c^2 f + k_{18} f^2 T_e + k_{19} f^2 T_c + k_{20} T_e T_c f$	20	3
Mendoza (Mendoza-Miranda et al., 2016)	$\eta_{compr} = \left(\frac{P_d}{P_s}\right)^{k_1} \left(\frac{f_{nom}}{f}\right)^{k_2} \left(\frac{f^3 V}{\Delta h_{iso}^{\frac{3}{2}}}\right)^{k_3} \left(\frac{\Delta h_{iso} \rho_s}{P_s}\right)^{k_4} \left(\frac{T_s}{\left(\frac{T_s + T_{d,is}}{2}\right)}\right)^{k_5}$ $W_{compr} = \frac{\dot{m} (h_{d,is} - h_s)}{\eta_{compr}}$	6	8
Santos (Santos et al., 2019)	$\dot{W}_{compr} = \dot{m} \left[k_1 T_s \left[\left(\frac{P_d}{P_s}\right)^{k_2} - 1 \right] + k_3 \right]$ $\dot{m} = \frac{P_s f}{T_s} \left\{ b_0 + b_1 \left[\left(\frac{P_d}{P_s}\right)^{b_2} - 1 \right] \right\}$	3	4
Shao (Shao et al., 2004)	$\dot{W}_{compr} = (k_1 + k_2 T_e + k_3 T_c + k_4 T_e^2 + k_5 T_c^2 + k_6 T_e T_c) \cdot [s_0 + s_1 \Delta f + s_2 \Delta f^2] \text{ (rotary)}$	9	3
W.Li (Li, 2013)	$\dot{W}_{compr} = \left\{ P_s V f_c k_1 \left[\left(\frac{P_d}{P_s}\right)^{k_2 + \frac{\kappa-1}{\kappa}} + \frac{k_3}{P_d} \right] + k_4 \right\} \cdot [s_0 + s_1 (f/f_{nom}) + s_2 (f/f_{nom})^2]$	6	4

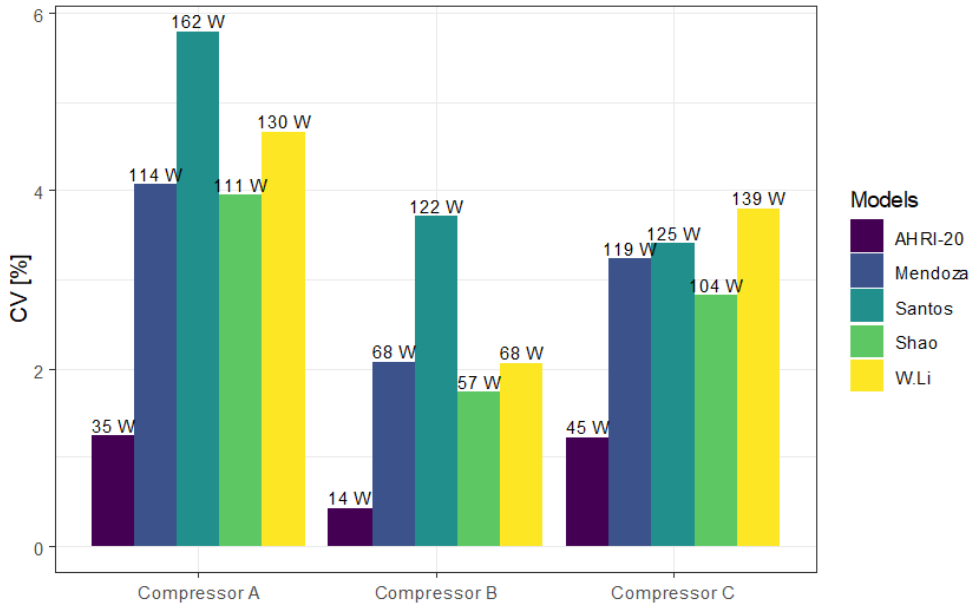


Figure 2.6: Performance of the different models fitted to various compressor datasets

The correlation with better performance is AHRI-20 with RMSE values lower than 50W in all the studied compressors. It is followed by Shao correlation, and then, the other correlations change order depending on the tested compressor. In general, the one having higher errors is Santos. However, it should be noted that it is also the correlation with fewer coefficients (only 3).

Remark that the results were obtained using all available data and models containing more coefficients will always perform better when the dataset is extensive. However, when the training data decreases, they can overfit it and fail to predict new unseen data correctly. Train-test fitting can be performed to check for overfitting, which consists of adjusting the correlations with a limited dataset (train) and then calculating the goodness of predictions for the complete dataset (test). If the correlation is overfitted, it will try to model the experimental noise in the train set, giving poor predictions with the entire data.

2.4.3. Design of Experiments

According to Aute et al. (Aute et al., 2015), manufacturers typically take 14-20 conditions when characterizing a fix-speed compressor. However, to fit the AHRI-20 correlation, at least 20 tests are needed, 21 if statistics to measure the goodness of fit are required (RMSE, MRE, CV...). Figure 2.7 shows the result of the train-test procedure repeated 100 times. In the first plot, the 21 train tests were selected randomly. In the second one, the selection was made by distributing the training samples homogeneously along the envelope with a clustering technique. It should be noted that the same 100 train sets were applied to the different correlations, so a poorly chosen trainset would affect all models. The red dots in the plot represent the fitting accuracy of each of the 100 runs and the shapes describe a violin plot representing a vertical density function of the results in which the horizontal black line describes the median.

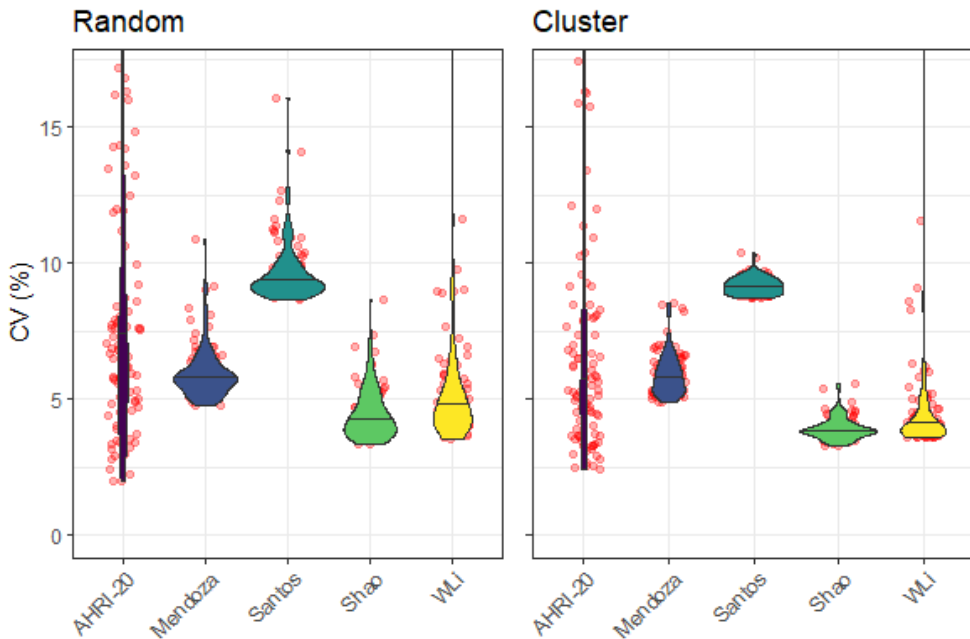


Figure 2.7: Robustness of the different models when adjusted with 21 tests selected randomly (Left) or with a clustering methodology (right)

Results show significant variability for AHRI-20, even if the samples are evenly distributed along the envelope. This indicates that this correlation tends to

overfit the train data and, a lot of experimental data is required to adjust it correctly, increasing the compressor characterization cost. Regarding the rest of the data, Shao tends to perform best most of the time with limited variability. W.Li follows Shao but presents a higher variability with a couple of points in which the solution did not converge. And finally, the one with a worse average performance is Santos which was expected with only 3 fitting coefficients.

Another conclusion from Figure 2.7 is that the results' variability also depends on the strategy followed to select the train data, as selecting distributed points improves the performance. Hence, another way of decreasing the variability would be to choose the position of the train tests wisely.

According to Aute (Aute et al., 2015) there isn't a well-established methodology among manufacturers to address the positioning of the train data. Aute [4] used a conventional approach called Latin Hypercube Sampling for fixed-speed compressors and presented a new methodology for non-rectangular domains. This new method was called Polygon Design of Experiments (PDOE) which combined the clustering technique with manually picking extreme conditions at the vertices of the envelope. Lately, Marchante (Marchante-Avellaneda, Corberan, et al., 2023) suggested the use of Optimal Design (OD) methodologies (Atkinson, 2015); these methodologies take as input the model equation, the required number of train test and a list of candidates points and return the train set that minimizes the generalized variance for the fitting coefficients. The involved calculations entangle some intensive statistical calculations, but open-source tools implement the algorithms, resulting in an easy-to-use methodology to obtain optimized train sets. In this study, the function `optFederov` of the package `AlgDesign` (Wheeler, n.d.) was used with the D-Optimal criteria (Atkinson, 2015) for linear models. It should be noted that, when either the candidate and the train set size are big, it does not exist a clear optimum and multiple train sets can be obtained from the algorithm if it is run multiple times.

In this study, the OD methodology was extrapolated to the rating point selection of variable-speed compressors. Figure 2.8 shows a train set resulting from applying OD to the model AHRI-20 with a train set size of 21. The optimization algorithm considered extreme points close to the vertexes of the envelope and some at medium speeds, which would reassemble the train points obtained if PDOE method (Aute et al., 2015) had been used.

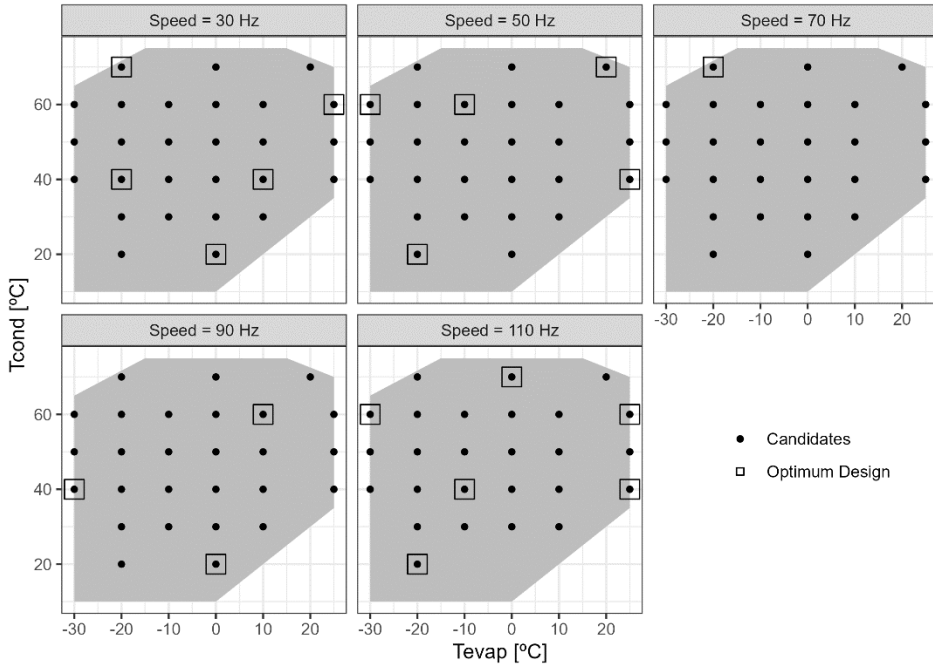


Figure 2.8: Train set selection using Optimal Design for AHRI-20 model

If this approach is followed to fit the AHRI-20 model with 21 train conditions, a RMSE of 80W is obtained when the model is used to predict the entire dataset. This value lies in the lower portion of the results obtained in Figure 2.7 using clustering.

In order to apply this methodology to Shao’s model, it was divided into two decoupled models as originally presented by his author: one for a nominal speed with 6 coefficients and the other with 3 coefficients to consider the speed effect. The OD methodology was applied for the nominal speed with a desired train size of 7, and then 2 points were added at extreme speeds to adjust the speed effect. Those 2 points at extreme speeds were added in the center of the envelope as those points tend to be easier to test and Shao states that the speed effect does not depend on the compression conditions. The complete test matrix is displayed in Figure 2.9, it can be noted how the OD algorithm also selected rating points close to the envelope vertexes and one in the center.

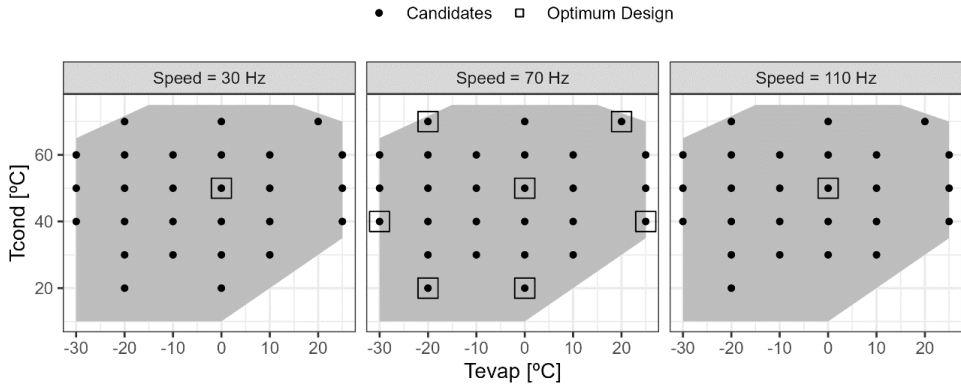


Figure 2.9: Train set selection using Optimal Design for Shao

If Shao's model is fitted with this train set and then it is used to predict the entire dataset, a RMSE of 101W is obtained, which is remarkable with only 9 train tests. Better fit even compared to using the whole dataset.

The results of this chapter highlight the importance of a good rating matrix design (number of rating points and their location) for compressor characterization. Using the Optimum Design methodology allowed to obtain high-precision fits for all the envelope using only 9 rating points. These same 9 rating points could also be used to fit mass flow correlations as its behavior is smoother and easier to model compared with power consumption (Marchante-Avellaneda, Corberan, et al., 2023).

2.5. Inverter Performance

2.5.1. Inverter Model

This section aims to study how inverter losses depend on the compression condition and speed and then an empirical correlation based on accessible variables such as global consumption and speed is provided. The obtained data for all three tested inverters can be accessed in the complementary materials, but only the inverter A dataset will be shown in this section due to space limitations.

Figure 2.10 shows the evolution of efficiency and power losses of the tested Inverter A as a function of speed and total consumption. Inverter efficiency mainly depends on power consumption; as consumption decreases, efficiency drops to values lower than 90%. In this inverter, the efficiency homogeneously increases as consumption increases; however, in other inverters (e.g. Inverter B), the efficiency finds a maximum, and then the efficiency starts decreasing as consumption keeps rising.

Furthermore, it has been found that speed also impacts efficiency, contrary to what Cuevas and Lebrun (Cuevas & Lebrun, 2009) found using the calorimetric method. This discrepancy can be explained due to the fact that Cuevas and Lebrun (Cuevas & Lebrun, 2009) tested over a limited speed range, and the efficiency variation due to speed fell in the method's uncertainty band.

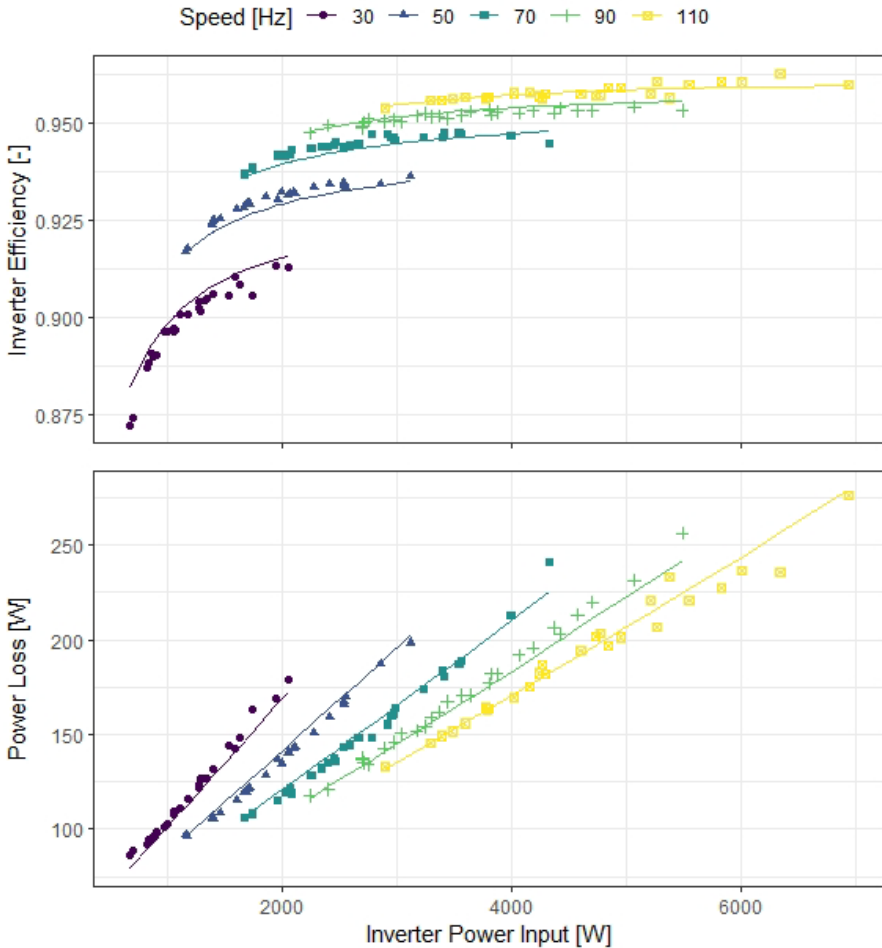


Figure 2.10: Experimental results and predicted performance of inverter A

To model the behavior of the inverter, it was preferred to model the evolution of power loss instead of efficiency, as it resulted in a more linear tendency with consumption and speed. The resulting model (Eq.(2.5)) has five fitting coefficients and can be adjusted easily with conventional regression tools.

$$\dot{W}_{loss} = c_0 + [s_0 + s_1\Delta f + s_2\Delta f^2] \dot{W}_{in} + c_2 \dot{W}_{in}^2 \quad (2.5)$$

The proposed model fits reasonably well all VSDs tested. The model performance is displayed in Figure 2.11, showing an RMSE of 5W and around 95% of

the experimental results fall in the range of 5% error. The model performance can also be checked in Figure 2.10, where the lines represent the predicted values of the proposed model applied to Inverter A.

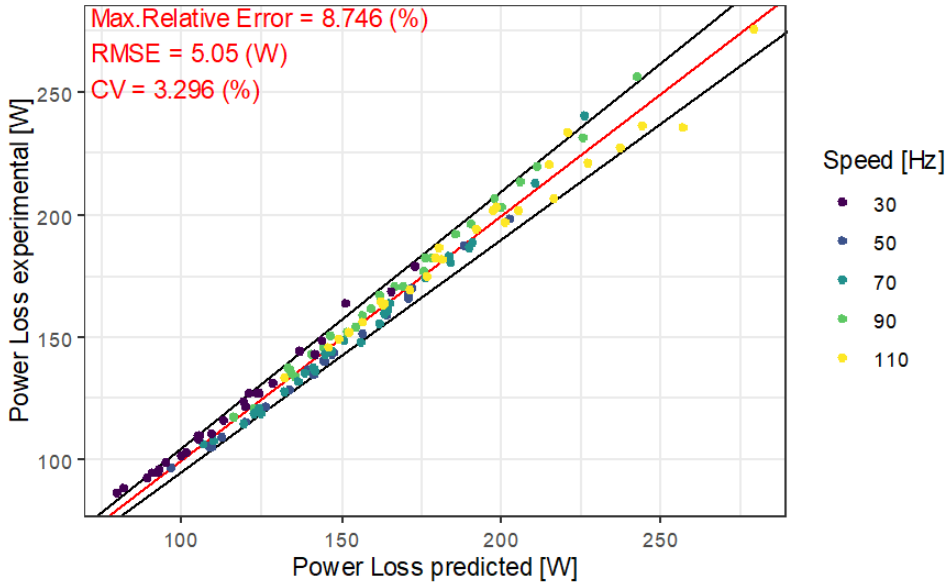


Figure 2.11: Performance of the inverter model applied to Inverter A

The fitted parameters of all three tested inverters are listed in Table 2.5, and it's worth noting that the order of magnitude of the different coefficients is similar for the various inverters. The intercept provides information about the device's no-load consumption, which can be accessed directly from the datasheets. Additionally, it has been included the significance level of the different coefficients using the following standard notation (+ $p < 0.1$, * $p < 0.05$, ** $p < 0.01$, *** $p < 0.001$). The significance of C2 can give information about the general behavior at high inverter consumption. For low significance (Inverter A), efficiency keeps increasing as consumption increases, but for high significance (Inverter B), inverter efficiency finds a maximum and decreases as consumption further increases. This behavior also is present in inverter C but only at very high speeds and consumptions.

Table 2.5: Model summary for the tested inverters

	<i>Inverter A</i>	<i>Inverter B</i>	<i>Inverter C</i>
<i>c0</i>	3.47e+01***	2.02e+01***	3.27e+01***
<i>s0</i>	5.25e-02***	5.53e-02***	1.23e-02**
<i>s1</i>	-3.01e-02***	-2.02e-02***	-1.51e-02***
<i>s2</i>	1.11e-02***	3.99e-03***	1.72E-03
<i>c2</i>	4.20e-07+	4.79e-06***	1.71e-06**
<i>Num.Obs.</i>	133	17	35
<i>RMSE</i>	5.05	1.76	5.91
<i>MRE</i>	8.75	5.26	25.55
<i>CV</i>	3.3	0.91	6.82

For Inverter C, the fitting errors are greater because the model, due to its simplicity, didn't fit a particular behavior correctly at low speeds. Nevertheless, apart from those samples, most predictions entered in the range of 5% error and RMSE was lower than 6W.

2.5.2. Effect of the carrier frequency

Carrier frequency is the rate at which the transistors are switched, which tends to be in the range of kHz. The higher the frequency the smaller number of harmonics produced at the output signal. However, it comes at the cost of increasing commutation losses.

To check the effect of the inverter switching frequency on its performance, a parametric study has been carried out with Inverter C. A total of 4 tests at different switching frequencies in the range of 2-10kHz were carried out at the same compression condition and using the same setup (conductor length and routing). The results are displayed in Figure 2.12.

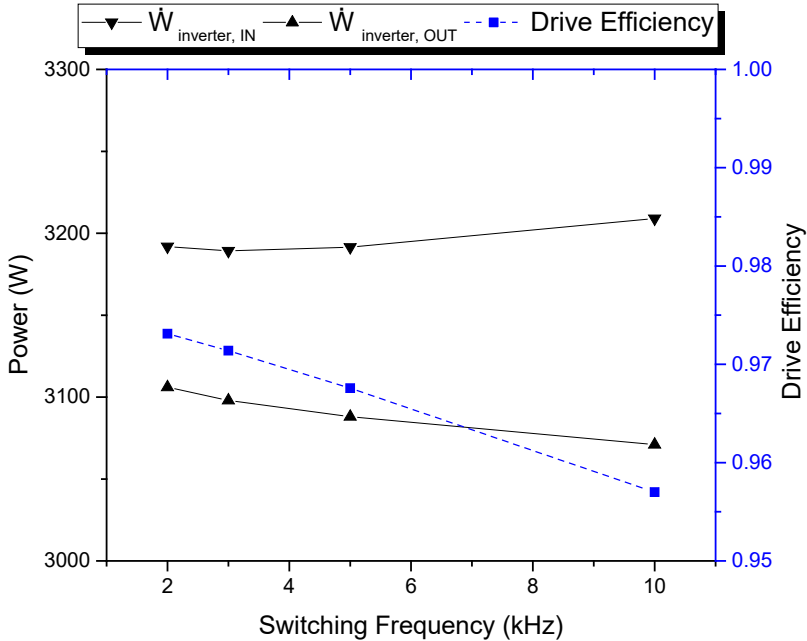


Figure 2.12: Evolution of Drive Efficiency and Inverter Power Flows with Switching Frequency

Driver efficiency clearly decreases as the switching frequency increases. In the studied range, the reduction was 1.6 percentual points, and it showed quite a linear behavior. This decrease in efficiency is attributed to higher commutations losses due to the increase in the switching frequency.

Another effect that can be observed in Figure 2.12 is a reduction of the power consumed by the compressor ($\dot{W}_{inv,out}$). The compressor works at the same load and speed in all tests; consequently, its consumption should remain constant. Hence, the decrease in consumption could be explained by a reduction of secondary losses generated in the compressor windings due to harmonics in the electrical power signal, which are reduced as the switching frequency increases.

Consequently, as the carrier frequency increases, two opposite effects appear: an increase in power losses in the inverter due to the rise of commutation losses and a reduction in the compressor's secondary losses due to fewer harmonics. The total power at the input of the inverter ($\dot{W}_{inv,in}$ in Figure 2.12) takes

into account both contributions and seems to have an optimum between 2 and 5kHz for this inverter. For higher switching frequencies, the increase of commutation losses predominates and the total consumption increases.

The effect of the switching frequency has not been considered in the inverter model as it is not a variable that tends to be modified under regular operation, and its impact on total consumption is secondary.

2.6. Conclusion

A complete energy consumption analysis has been made for variable-speed compressors studying the inverter and the compressor independently (not as an aggregated black box). Experimental results of three variable-speed scroll compressors working with three different refrigerants were used to test the performance of multiple published correlations, which raised the following conclusions:

- With a wide train set, AHRI-20 correlation gave the best accuracy with errors in the power meter's uncertainty range. However, it tended to overfit the train data when it was trained with a limited number of rating points.
- A correlation with the shape of the one proposed by Shao for rotary compressors, with less than half the coefficients compared with AHRI-20, showed a decent performance with fewer overfitting problems.
- W.Li and Mendoza closely followed Shao's performance with even fewer fitting coefficients, but, on the contrary, they involved non-linear correlations that are harder to adjust.
- Correlation selection is a trade between complexity and accuracy; thus, the optimum model could differ for each application.

Another critical issue studied was the minimum number of rating points and where to place them inside the compressor's envelope; the found conclusions are:

- The Optimal Design methodology permitted the selection of rating points to adjust the correlations with the minimum amount of experimental information.

- With only 9 rating points, predicting the global compressor behavior with decent accuracy was possible using Optimal Design and a Shao's shape correlation.

To study the power losses in the inverter three different devices were tested and the conclusions from the data analysis are:

- The double-wattmeter methodology allowed to detect that power losses depend on either consumption and speed independently.
- A linear five-coefficient correlation is proposed to predict power losses based on easy-to-measure variables, such as total consumption or compressor frequency, and with typical errors in the band of 5%.
- The switching frequency effect in the complete system is low and was not included in the inverter model as it typically is a predefined parameter that is not changed during regular operation.
- In all tested inverters, the efficiency plummeted at low speeds and total consumption reached losses in the range of 10% (far from the typical 3% constant power loss that is typically considered in the literature). Suppose the decrease of compressor efficiency at low speeds is also considered. In that case, the total penalty of running the compressor at very low frequencies could be so high that other control techniques such as cycling could be more profitable under certain circumstances.

These findings were obtained from a finite amount of 3 different datasets. Nevertheless, a previous study (Marchante-Avellaneda, Corberan, et al., 2023) stated that scroll compressors behave relatively homogeneously, so the given conclusions are expected to be confirmed with future data. Additionally, as future work, the strengths and weaknesses of the reviewed models will be analyzed to propose new improved models for consumption, mass flow and discharge temperature.

2.7. Nomenclature

Abbreviations

CV	coefficient of variance of RMSE
MRE	maximum relative error
POE	polyol ester oil
PDOE	Polygon Design of Experiments
PR	Pressure Ratio
PVE	polyvinyl ether oil
OD	optimal design
RMSE	root mean square error
SC	subcooling
SH	superheat

Sub index

amb	ambient
c	condensing
compr	compressor
d	discharge
e	evaporating
in	input
inv	inverter
is	isentropic
nom	nominal
out	output
ref	at nominal speed
s, suc	suction
v	volumetric

Symbols

f	compressor speed [Hz]
$k_{\#}, s_{\#}, c_{\#}$	fitting coefficients
\dot{m}	mass flow [g/s]
MW	molecular weight [g/mol]
P	pressure [bar]
R	8.314 [J/(K·mol)]
T	temperature [K]
V	compressor displacement [m ³]
\dot{W}	electrical power [W]

Greek letters

η	efficiency
κ	isentropic exponent [-]
ρ	density [kg/m ³]

Chapter 3:

SECOND PUBLICATION



Applied Thermal Engineering



Available online 15 February 2024, 122666

In Press, Journal Pre-proof  [What's this?](#)



Research Paper

Development of compact empirical models for variable-speed compressors for the prediction of energy consumption, mass flow and discharge temperature

Rubén Ossorio  , Javier Marchante-Avellaneda, Emilio Navarro-Peris

<https://doi.org/10.1016/j.applthermaleng.2024.122666>

Development of compact empirical models for variable-speed compressors for the prediction of energy consumption, mass flow and discharge temperature

Rubén Ossorio, Javier Marchante-Avellaneda, Emilio Navarro-Peris
Instituto Universitario de Investigación en Ingeniería Energética (IUIIE)
Universitat Politècnica de València, Camino de Vera s/n, ed. 8E cubo F 5º, Valencia, 46022, Spain

3.1. Abstract

In the context of heat pumps, developing prediction models for compressor performance holds significant importance for design, selection, control, and fault detection. Nevertheless, there is no established standard for characterizing variable-speed compressors. Various published models offer different advantages and trade-offs in terms of accuracy and simplicity; however, none of them strike the right balance between complexity and data fidelity, which is paramount, especially when working with limited or low-fidelity data.

This study analyzes how compressor performance evolves within the compressor envelope, focusing on the speed effect. From this analysis, novel compact empirical models are obtained to predict mass flow rate and energy consumption. A study of discharge temperature is also presented in this work due to its relevance in quantifying heating capacity and power losses. To model it, a correlation based on electro-mechanical efficiency is proposed, which can be generalized for different suction conditions without introducing additional coefficients. The proposed models are data-driven by high-fidelity calorimetric tests and aim to maintain simplicity, using no more than six coefficients, while delivering acceptable accuracy with average prediction errors lower than 5%. Finally, a robustness analysis is carried out, which analyzes the required training data needed to fit the model and concludes that the proposed models can compete in accuracy with models that use much more coefficients when limited training data.

Keywords: Variable speed compressor, modeling, consumption, mass flow, discharge temperature

3.2. Introduction:

System modeling, particularly in the domain of HVAC systems, has become increasingly important due to a rapidly changing regulatory environment that places greater emphasis on mitigating climate change and global warming. Compressors play a critical role in refrigeration systems, and accurately predicting their performance is essential for optimizing energy efficiency and reducing environmental impact.

Modeling approaches can be broadly categorized as either detailed models (white-box), empirical models (black-box) and semi-empirical models (grey-box). While all approaches have their merits, the choice of modeling approach depends on the available data, computational resources, desired accuracy and final application. White-box models, which are based on fundamental physical principles, provide detailed insights into the underlying physical phenomena but are more computationally intensive, are less integrable and require extensive knowledge of the system, which is typically unavailable (utilized mainly by component designers and manufacturers). Grey-box models are formulated using equations describing physical processes and use experimental data to fit parameters such as polytropic coefficients, heat transfer coefficients, death volumes, etc. Their accuracy is limited and related to the assumptions taken. They typically involve fitting exponents or solving complex equations, making them harder to fit for general users and more challenging to implement in bigger simulation systems. In contrast, black-box or empirical models only rely on data-driven relationships, and although they may lack physical interpretability, they offer simplicity and flexibility by capturing the observed behavior of the system.

Manufacturers commonly have used a black-box model for characterizing fixed-speed compressors (standard AHRI-540 (AHRI_540, 2020, p. 5)). The standard defines a 10-term and third-degree polynomial for predicting energy consumption and mass flow rate as a function of evaporating and condensing temperatures. Nevertheless, this standard is becoming outdated today because heat pump and chiller manufacturers are now moving to use variable-speed compressors, where the compressor speed plays a crucial role in its performance.

Unfortunately, currently, there is no established standard for characterizing variable-speed compressors, and a common solution adopted by manufacturers

is to use a similar approach to the one described in the AHRI-540 but introducing the speed as an extra independent variable (*Coolselector*, n.d.; *Select Online*, n.d.; Guo et al., 2017; Wan et al., 2021). This results in a total of 20 terms considering a second-order polynomial and three independent variables (T_e , T_c and f_c) [Eq.(3.1)]. This model will be called AHRI-20 from now on.

$$\begin{aligned} \dot{m}|W_c = & k_1 + k_2T_e + k_3T_c + k_4f_c + k_5T_e^2 + k_6T_c^2 + k_7f_c^2 \\ & + k_8T_eT_c + k_9T_e f_c + k_{10}T_c f_c + k_{11}T_e^3 + k_{12}T_c^3 \\ & + k_{13}f_c^3 + k_{14}T_e^2T_c + k_{15}T_e^2f_c + k_{16}T_c^2T_e \\ & + k_{17}T_c^2f_c + k_{18}f_c^2T_e + k_{19}f_c^2T_c + d_{20}T_eT_c f_c \end{aligned} \quad (3.1)$$

One crucial aspect when proposing a compressor model based on experimental information (especially for black-box models) is adapting its complexity to the information embedded in the available data. If the model becomes too complex, it will start capturing noise rather than authentic underlying patterns. This behavior is called overfitting and can lead to inaccurate predictions, particularly in cases of limited or low-fidelity data. A previous study (Ossorio & Navarro, 2023) highlighted the limitations of AHRI-20 and showed that it tends to overfit when data is scarce or lacks fidelity. To avoid such issues, it is essential to carefully select and justify the complexity of the proposed model to ensure accurate interpolation and extrapolation.

Other studies have explored using Artificial Neural Networks (ANNs) to model compressors (Ekren et al., 2010; Kizilkan, 2011; Ma et al., 2020; Yang et al., 2009). While ANNs can capture complex relationships within the data, their integration into other systems and reporting fitted parameters can be challenging. The difficulty lies in the opaque nature of ANNs, making it difficult to interpret the underlying relationships and understand the model's behavior. In contrast, compact linear models with justified complexity offer a promising alternative, providing acceptable accuracy while remaining transparent and interpretable.

In Ossorio and Navarro-Peris (Ossorio & Navarro, 2023), the performance of the most used compact models to predict energy consumption for variable speed compressors were analyzed. In the analysis, either empirical or explicit semi-empirical models were included, and they were evaluated with a train test procedure. Semi-empirical models performed generally well, showing an acceptable accuracy with a limited number of fitting equations. However, due to

their non-linear formulation, they had convergence problems during coefficient fitting. Among the studied models, Shao's model [Eq.(3.2)] offered a good trade-off between complexity and accuracy when applied to scroll compressors, even if it was originally tested only for rotary technology. However, the number of coefficients used was not analyzed. Additionally, a model for discharge temperature was not proposed, and the effect of SH on performance was not analyzed.

$$\begin{aligned} \dot{m}_{nom}|\dot{W}_{c,nom} &= k_1 + k_2T_e + k_3T_c + k_4T_e^2 + k_5T_c^2 + k_6T_eT_c \\ k_{m|p} &= \frac{\dot{m}}{\dot{m}_{nom}} \text{ or } \frac{\dot{W}_c}{\dot{W}_{c,nom}} \\ &= c_1(f_c - f_{c,nom})^2 + c_2(f_c - f_{c,nom})^2 + c_3 \end{aligned} \quad (3.2)$$

Modeling discharge temperature in compressors is also vital as it provides information about power losses, heating capacity and condenser inlet temperature. However, it remains a topic of limited study compared with the proposed mass flow and energy consumption models. The most common approaches assume constant isentropic efficiencies or introduce a term dependent on energy consumption to model energy losses (e.g., Ashrae Toolkit (Bourdouxhe et al., 1994)). Others try modeling ambient losses as a function of a virtual compressor shell temperature (Winandy et al., 2002a).

Given the introduced state of the art, this study proposes compact map-based models to predict mass flow rate, compressor energy consumption and discharge temperature with a low number of coefficients. The proposed models can also model the effect of speed on the compressor performance and show average prediction errors lower than 5%, having no more than six fitting coefficients. Moreover, the impact of suction conditions on the modeled variables is assessed, and a general correlation is proposed to model it without introducing new fitting coefficients. Finally, a robustness analysis is carried out based on a train-test methodology, which analyzes the required number of train data needed to fit the model, avoiding overfitting.

3.3. Methodology

The methodology followed to obtain compact prediction models starts with studying a high-fidelity experimental data set obtained from a variable-speed compressor, which will be used as a reference. For this step, it is essential to use real empirical data obtained from a laboratory test bench rather than catalog data, as the latter tends to be predicted from pre-fitted models instead. However, the amount and quality of published empirical results of variable-speed compressors is limited.

The data used for this study has been obtained from a compressor test bench whose complete description is available in a previous study (Ossorio & Navarro, 2023). On this test bench, a variable-speed scroll compressor working with R290 was tested over an extensive envelope of condensing and evaporating temperatures (Figure 3.1). This same pattern was repeated at different speeds ranging from 30 to 110 Hz to study the influence of speed on performance. It has to be noted that the test matrix was designed to be as orthogonal as possible to make it possible to study how each variable affects the performance independently. In total, 133 different conditions were tested, and each individual result can be accessed at (Ossorio & Navarro, 2023).

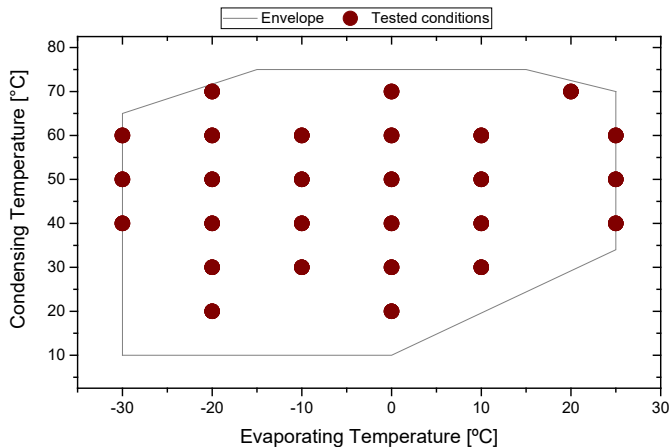


Figure 3.1: Test matrix and compressor envelope

From the study of the empirical data, the main trends are retrieved, which are then employed to design and improve predicting correlations for mass flow, consumption and discharge temperature, focusing on the dependence of these variables with speed.

Then, to ensure that the conclusions obtained for this compressor technology can be generalized for multiple compressor models and technologies, the obtained correlations will be validated against the experimental datasets summarized in Table 3.1.

Table 3.1: Summary of variable-speed compressor datasets

	SCROLL- R290	SCROLL- R410A	SCROLL- R454C	SCROLL- R134a	ROTARY- R22	PISTON- R12	PISTON- R134a
Source	Exp.	Exp.	Exp.	Cuevas[13]	Shao[14]	Winandy[12]	Moradi[15]
Technology	scroll	scroll	scroll	scroll	rotary	piston	piston
Displacement [cm ³]	46	44.5	44.5	54.25	20.7	680	74.83
Refrigerant	R290	R410A	R454C	R134a	R22	R12	R134a
Tevap Range [°C]	-30 / 25	-30 / 7	-15 / 44	14 / 68	-10 / 15	-26 / 23	-13 / 2
Tcond Range [°C]	20 / 70	25 / 49	28 / 85	39 / 101	40 / 60	8-68	19 / 65
Speed Range [Hz]	30 / 110	15 / 100	15 / 100	35 / 75	30 / 120	6-11	30 / 50
Nominal Speed [Hz]	70	60	60	50	60	6	45
Sh [K]	10	10	10	7	11	28	12
Tests	133	35	87	48	296	25	44

In Table 3.1, the first three columns represent experimental data obtained by the authors in the compressor test bench described in [6]; the rest represent datasets of variable-speed compressors published in other studies.

Cuevas and Lebrun (Cuevas & Lebrun, 2009) provided a dataset with 48 different conditions at five different speeds. Even if it does not cover the complete compressor envelope, the test matrix maps a significant portion of it and presents quite an orthogonal design. Additionally, the experimental uncertainty was low.

Shao et al. (Shao et al., 2004) tested a rotary compressor working with R22. However, in his study, only the experimental ratio of mass flow and consumption

for nominal speed seems to be provided, not the absolute results (as for nominal speed only a 6-coefficient correlation is presented). Consequently, this dataset is partially filtered by the model used and not exclusively empirical. Nevertheless, it was considered in this study, so a direct comparison can be made between their correlation and other alternatives.

Winandy et al. (Winandy et al., 2002a) published an experimental data set of a mechanically-driven open-type reciprocating compressor working with R12. The piston had a significant displacement and the tested speeds were very low, which is unusual for domestic heat pumps. The dataset consists of only 25 conditions tested at three different speeds ranging from 6 to 11 Hz. Both power and mass flow measurements were indirect, with a high stated uncertainty of 5 and 3 %, respectively.

Finally, Moradi et al. (Moradi et al., 2017) studied the performance map of a heat pump and published a performance data set with 44 test results over five different speeds. The test matrix was not centered on the compressor's envelope but on the HP instead. Consequently, higher pressure ratios are tested as compressor speed increases, so studying the speed effect *ceteris paribus* is challenging. Additionally, the mass flow measurement was indirect and the power meter resolution was 100W, resulting in a high observed experimental uncertainty.

All the mentioned variable-speed compressors were tested at constant superheat conditions and consequently, the effect of suction conditions on performance cannot be studied. That is why the effect of suction conditions will be studied in another section using the dataset AHRI21 (Som Shrestha et al., 2013) for a fixed-speed compressor and the conclusions are expected to be extrapolated for variable-speed compressors.

In the AHRI21(Som Shrestha et al., 2013) dataset, five different refrigerants were tested in the same compressor, and for each refrigerant, three complete experimental maps were obtained for different suction conditions; one for SH=11K, other at SH=22K and the last keeping the suction temperature at 18°C. A summary of the complete dataset is displayed in Table 3.2.

Table 3.2: Summary of multiple SH dataset

	SH11	SH22	T1_18
Compressor Model	ZS21KAE-PFV		
Technology	Hermetic scroll		
Displacement [m ³]	204		
Refrigerants	R404A, ARM31a, D2Y65, L40, R32_R134a		
Tevap Range [°C]	-23 / 1.6		
Tcond Range [°C]	21 / 60		
Nominal Speed [Hz]	60		
Suction Conditions	SH=11 K	SH=22 K	T1=18 °C
Tests	63	63	63

For the evaluation of the accuracy (goodness of fit) of the proposed models, RMSE and CV estimators will be used. Root Mean Squared Error (RMSE) represents the standard deviation of the prediction errors and it is reported with the same units of the modeled variable. Coefficient of Variation of RMSE (CV) constitutes a normalized RMSE and could be used as an estimator of the expected relative error. It can be used to compare models when applied to different ranges.

$$CV = \frac{RMSE}{\bar{X}} = \frac{1}{\bar{X}} \sqrt{\frac{\sum_{n=1}^N (\hat{y}_t - y_t)^2}{N}} \quad (3.3)$$

3.4. Mass flow Results

3.4.1. Experimental results

In this section the obtained mass flow results of the intensively tested scroll-290 compressor are analyzed.

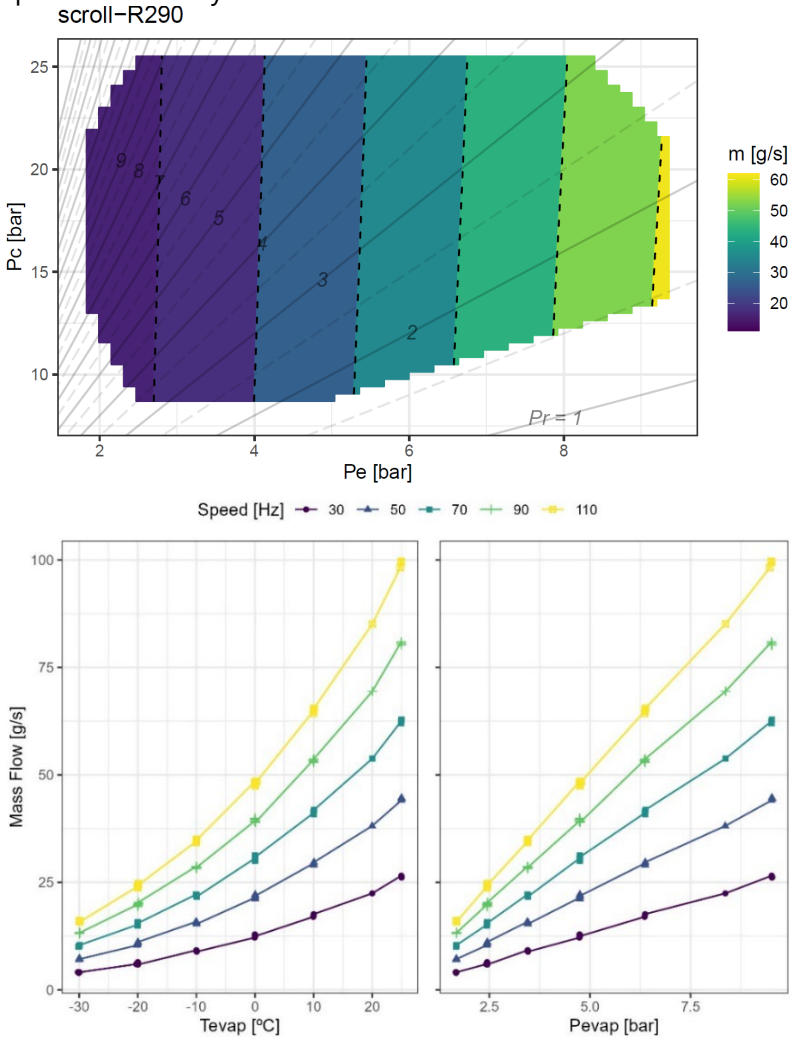


Figure 3.2: Evolution of mass flow with compression conditions at nominal speed (Up). Evolution of mass flow as a function of evaporating temperatures (Down-left) and pressures (Down-right)

The variables that affect mass flow the most are compressor speed and the evaporation condition. It should be noted that the influence of condensing temperature is very subtle and the variation of mass flow with it is barely perceptible with the scale of the graph. It is also worth mentioning that the response surface is almost linear if mass flow is plotted against the evaporating pressure.

In Figure 3.3, the experimental volumetric efficiency – defined with Eq.(3.4)– is plotted against pressure ratio (PR), and the different lines represent the different tested speeds.

$$\eta_v = \frac{\dot{m}}{\rho_1 f_c displ} \quad (3.4)$$

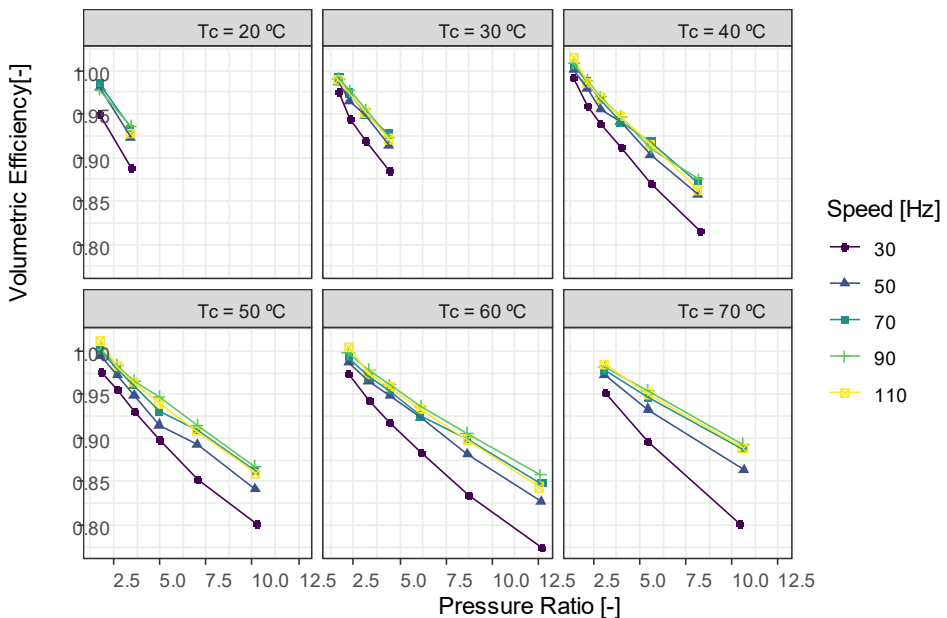


Figure 3.3: Evolution of volumetric efficiency with pressure ratio and speed

Volumetric efficiency is close to 1 at low PR and decreases quite linearly as PR increases. Volumetric efficiency does not show a strong dependency on speed at medium and high speeds. However, volumetric efficiency clearly decreases at low speeds, and this decrease is more significant as RP increases.

This reduction in volumetric efficiency can be explained by internal leakages in the compressor chamber. As compression speed decreases, the compression

is slower and refrigerant has more time to leak. Additionally, in the tested compressor, the carter is in the bottom part of the compressor, and a borehole in the shaft (acting as a centrifugal pump) is responsible for pumping the oil from the carter to the compressor chamber and the main bearings. The centrifugal action is significantly reduced at low speeds, and the pumped oil can be insufficient to create a hydrodynamic film to correctly seal the compression chamber, increasing the leakages and dropping the volumetric efficiency.

3.4.2. Model

As introduced in the first section, historically mass flow has been modelled with correlation based on working temperatures (T_e and T_c). However, as deduced from Figure 3.2, the fact of using pressures instead of temperatures as modeling variables could significantly reduce the required model complexity. The AHRI-540 standard (AHRI_540, 2020) uses 10 coefficients for fixed-speed compressors, including up to cubic terms, but if pressures are used as modeling variables, an acceptable accuracy could be obtained using fewer coefficients. In this line Marchante-Avellaneda et al. (Marchante-Avellaneda, Corberan, et al., 2023) proposed a model based on working pressures and using only four coefficients Eq.(3.5) for fixed-speed compressors.

$$\dot{m} = k_0 + k_1 P_e + k_2 P_c + k_3 P_e P_c \quad (3.5)$$

In order to model the effect of speed in mass flow, Shao et al. (Shao et al., 2004) proposed an approach using a 3-coefficient quadratic equation to model the ratio between mass flows at any speed and the nominal one (k_m) [Eq.(3.2)] and proved that these ratios were dependent only on speed not on working conditions. This methodology allows to model the compressor decoupled: with one equation representing how mass flow evolves at one speed (typically the rated one) and another to model the mass flow variation with speed.

However, the ratio k_m is heavily dependent on speed differences and it is known a priori that doubling speed will approximately double the mass flow. Consequently, modeling k_m as a function of speed differences ends up adjusting this pre-known behavior resulting in a linear term very close to unity, an intercept very close to zero and a quadratic term with low significance.

In this study, to solve that limitation, the ratios of volumetric efficiencies (k_v) will be used instead to model the speed influence on the performance. The process of deducing k_v from k_m is represented in Eq.(3.6) and concludes that the relation between one and the other is just the speed ratio between any speed and the nominal one ($f_{c,rat}$).

$$k_m = \frac{\dot{m}}{\dot{m}_{nom}} = \frac{f_c}{f_{c,nom}} \frac{\eta_v}{\eta_{v,nom}} \frac{\cancel{displ} \rho_1}{\cancel{displ} \rho_1} = f_{c,rat} k_v \quad (3.6)$$

In Figure 3.4, the k_m and k_v evolution with speed is displayed for two different compressors; Shao's compressor in the first column and the reference compressor in the second column.

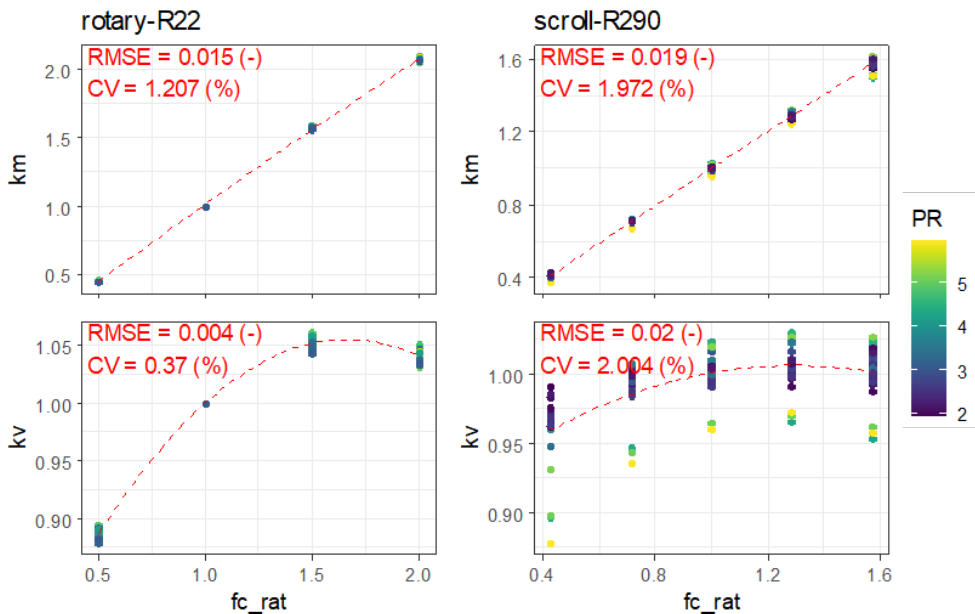


Figure 3.4: k_m and k_v evolution with speed for two different compressors

In the first row the quadratic fit of k_m is represented with a dashed red line, it should be noted that it is practically indistinguishable from a straight line of slope 1. However, if k_v are represented, the quadratic evolution becomes clear and the decrease of volumetric efficiency at low speeds becomes evident. Figure 3.4 also shows that the variation range of k_v is very narrow compared with k_m

and typically values close to one are achieved meaning that the effect of speed on η_v is reduced and consequently a simplified model as Eq.(3.7) could be used.

$$\begin{aligned} \dot{m} &= \dot{m}_{nom} k_m = \dot{m}_{nom} f_{c,rat} k_v \\ &= (k_0 + k_1 P_e + k_2 P_c + k_3 P_e P_c) f_{c,rat} \end{aligned} \quad (3.7)$$

Additionally, from Figure 3.4 it is observed that k_v reaches a maximum at a given speed and the overall behavior is parabolic. Accordingly, if extra accuracy is needed and the effect of speed in volumetric efficiency needs to be acquainted the proposed correlation in Eq.(3.8) was proposed.

$$k_v = k_m \frac{1}{f_{c,rat}} = \frac{\dot{m}}{\dot{m}_{nom}} \frac{f_{c,nom}}{f_c} \sim k_4 \left(f_{c,rat} - \frac{k_5}{f_{c,nom}} \right)^2 + k_6 \quad (3.8)$$

By definition, k_v must be 1 at nominal speed and thus, that constraint can be used to define k_6 as a function of the other two fitting coefficients k_4 and k_5 (Eq.(3.9)), resulting in a correction expression with only two coefficients instead of three as the one proposed by Shao et al.

$$k_6 = 1 - k_4 \left(1 - \frac{k_5}{f_{c,nom}} \right)^2 \quad (3.9)$$

Furthermore, due to the formulation of the correlation, both fitting coefficients represent important information: k_5 represents the speed at which the volumetric efficiency reaches its maximum and k_4 represents the curvature of the parabola, in other words the influence of speed on η_v .

Finally, if equations Eq.(3.7) and Eq.(3.8) are combined, a general expression is obtained to predict mass flow at any given condition of working pressures and speed [Eq.(3.10)].

$$\begin{aligned} \dot{m} &= \dot{m}_{nom} f_{c,rat} k_v = (k_0 + k_1 P_e + k_2 P_c + k_3 P_e P_c) \cdot \\ &\cdot f_{c,rat} \left[k_4 \left(f_{c,rat} - \frac{k_5}{f_{c,nom}} \right)^2 + k_6 \right] \end{aligned} \quad (3.10)$$

It is important to note that the general equation has only 6 coefficients as k_6 is calculated with Eq.(3.9).

Figure 3.5 represents the correlation graph of the presented model applied to "scroll-R290" compressor. The resulting modeling error is low, with a RMSE of 0.219 g/s and a CV lower than 1%.

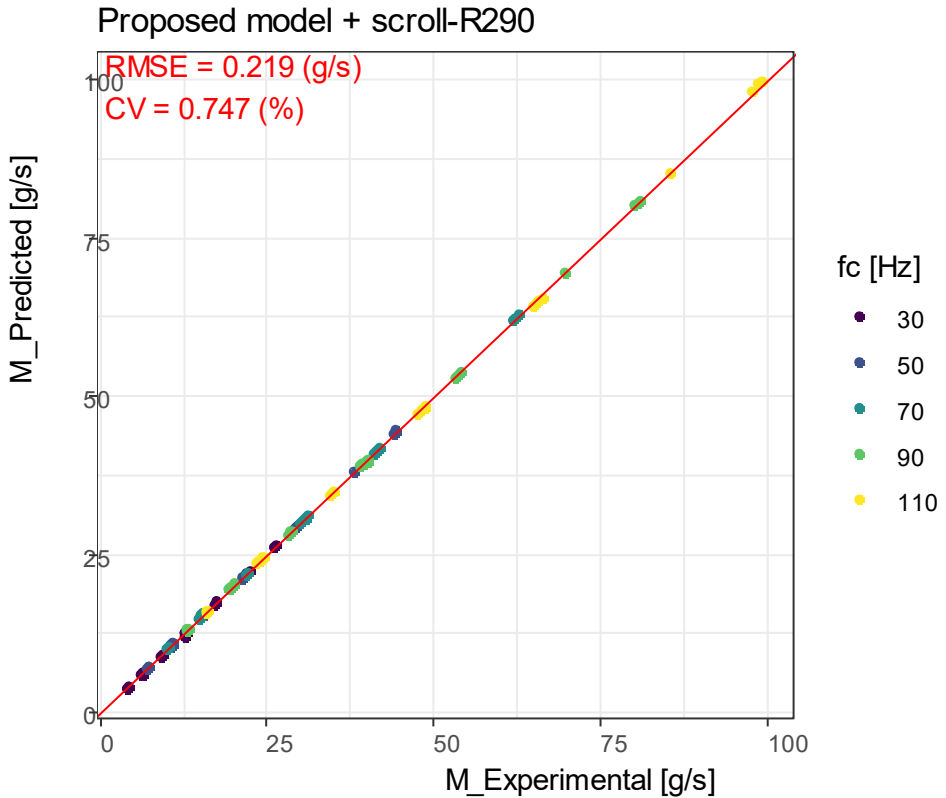


Figure 3.5: Correlation plot of mass flow model applied to reference compressor

To validate the obtained result, the model was also tested against the other experimental datasets described in Table 3.1 and the obtained RMSE and CV are displayed in Figure 3.6.

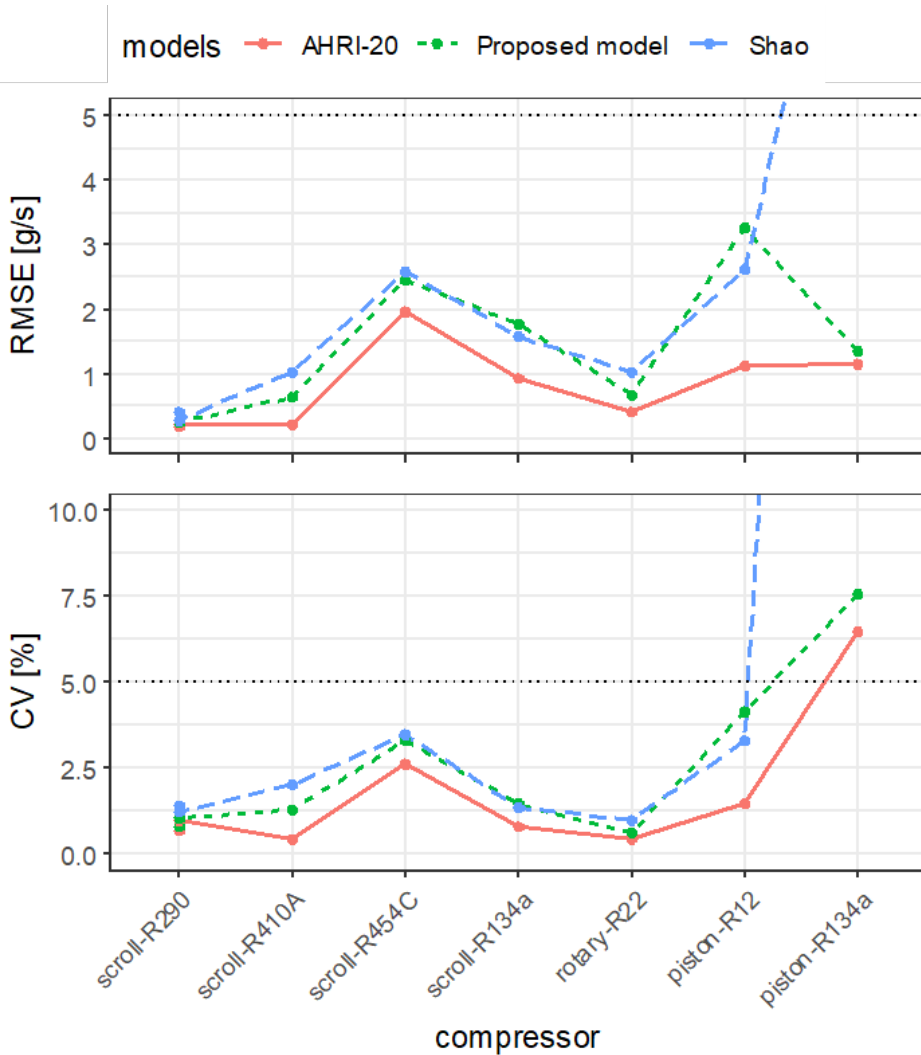


Figure 3.6: Goodness of fit of mass flow models applied to different data sets

In Figure 3.6 the baseline is reported by the AHRI-20 model which, when fitted with all the experimental data set, provides the highest accuracy as it has many fitting coefficients (20 coefficients in total). It should be remembered though, that the number of coefficients in AHRI-20 model was not justified and having a high number of coefficients will always adjust better the train data but

risks overfitting; incurring in higher prediction errors with unseen data as seen in Section 3.8.

Additionally, to AHRI-20 results, the modeling errors of Shao correlation and the new proposed model are also displayed. It is remarkable how, with less than half the number of fitting coefficients, both obtain similar fitting results compared to AHRI-20 in most compressors. This is other indicator that using 20 coefficients is overmuch.

Comparing Shao and the proposed correlation, the proposed correlation performs better consistently, even with less fitting coefficients (six versus nine). The only data set that Shao had better accuracy is piston-R12 in which the difference in accuracy falls in the experimental uncertainty band.

In the piston-R12 compressor, the difference between the modeling accuracy of AHRI 20 and the compact models increases which can be explained by the high experimental error and the low number of tests. AHRI-20 has 20 fitting coefficients and the dataset only 25; consequently, the chances are high that AHRI-20 is overfitting the given dataset.

Finally, in piston-R134a the obtained CV surpass the 5% threshold even for AHRI-20 model which clearly indicates a high experimental error. However, what is remarkable is the impossibility of Shao's model to adjust the data. This fact can be explained as the tested temperature range was not the same for all tested speed and thus important extrapolations are involved.

Proven the accuracy of the proposed model, the obtained fitted coefficients for the different compressors are listed in Table 3.3 (using g/s, bar and Hz) together with its fitting accuracy expressed as RMSE, MRE and CV. Note that the coefficient k_5 represents the speed at which the volumetric efficiency becomes maximum and, in the studied compressors, it tends to be in the high-speed domain of each compressor.

Table 3.3: Model coefficients and goodness of fit of the mass flow model applied to the different compressors

Mass flow - Proposed model							
	scroll-R290	scroll-R410A	scroll-R454C	scroll-R134a	rotary-R22	piston-R12	piston-R134a
k0	-0.810***	-2.910	-5.716**	3.873	-7.894***	-12.569*	1.130
k1	6.815***	10.290***	12.281***	12.441***	20.278***	26.817***	8.789**
k2	-0.019*	-0.215**	-0.121	-0.681***	-0.298***	-0.241	0.466
k3	-0.008***	-0.008	-0.059***	0.021+	-0.128***	-0.269+	-0.300
k4	-0.026***	-0.073***	-0.088**	-0.198***	-0.125***	0.143	-0.050
k5	104.386***	92.450***	72.354***	55.535***	99.723***	7.850***	79.378
Num.Obs.	133	35	87	48	296	25	44
RMSE	0.22	0.64	2.46	1.76	0.66	3.25	1.34
CV	0.75	1.23	3.28	1.47	0.60	4.12	7.54

3.5. Energy Consumption results

3.5.1. Experimental results

This section analyses the energy consumption results of the intensively tested scroll-290 compressor.
scroll-R290

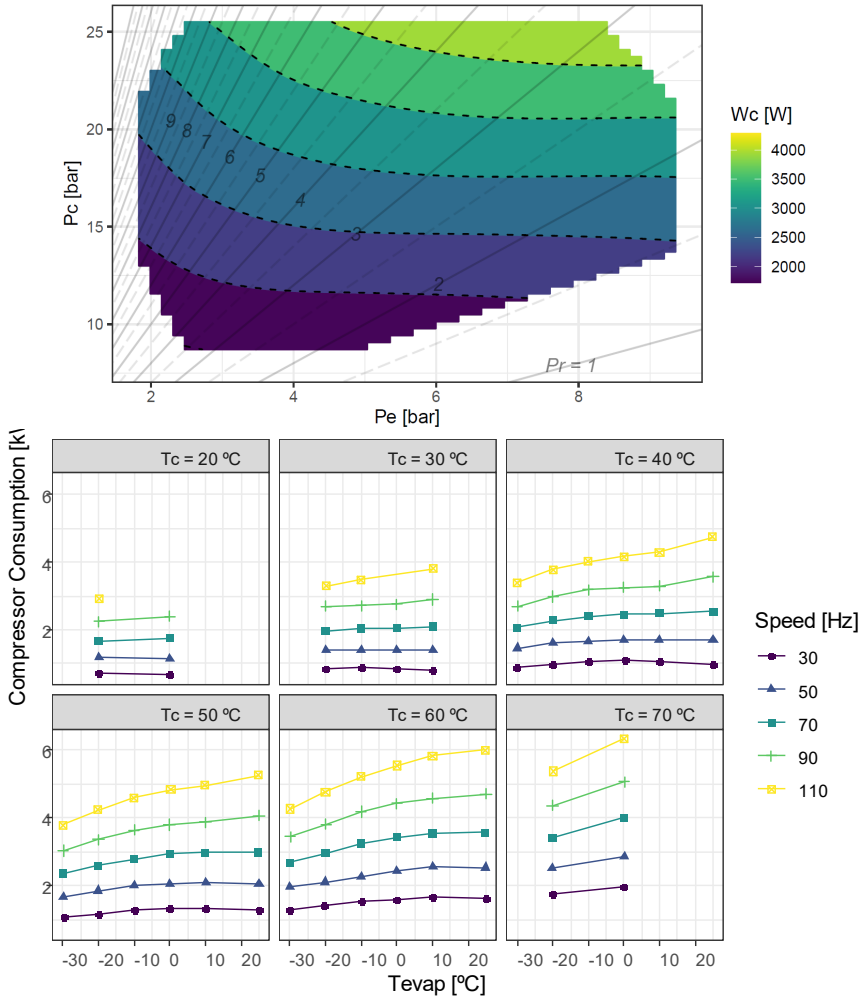


Figure 3.7: Evolution of energy consumption with compression conditions at nominal speed (Up). Evolution of energy consumption as a function of evaporating temperatures and speed (Down)

In Figure 3.7 the evolution of energy consumption with working temperatures and speed is displayed.

The main variable affecting consumption is the compressor speed, which affects the energy consumption proportionally. For a given speed, the variable affecting the most the energy consumption for the analyzed compressor is the condensing temperature. Regarding the evaporating temperature, when it increases two counteracting phenomena occur: firstly, the suction pressure and density increase, increasing the mass flow and thus increasing the expected energy consumption; secondly, the pressure ratio reduces thus decreasing the expected consumption. These counteracting phenomena make the energy consumption practically independent of suction temperatures for pressure ratios higher than three for the selected compressor working at nominal speed. This analysis was conducted with a scroll compressor and it could be different for piston as stated in (Marchante-Avellaneda, Navarro-Peris, et al., 2023).

Figure 3.8 shows the evolution of compressor efficiency (defined with Eq.(3.11) with pressure ratio and speed – at different condensing temperatures –

$$\eta_c = \frac{\dot{m}(h_{2,is} - h_1)}{\dot{W}_c} \quad (3.11)$$

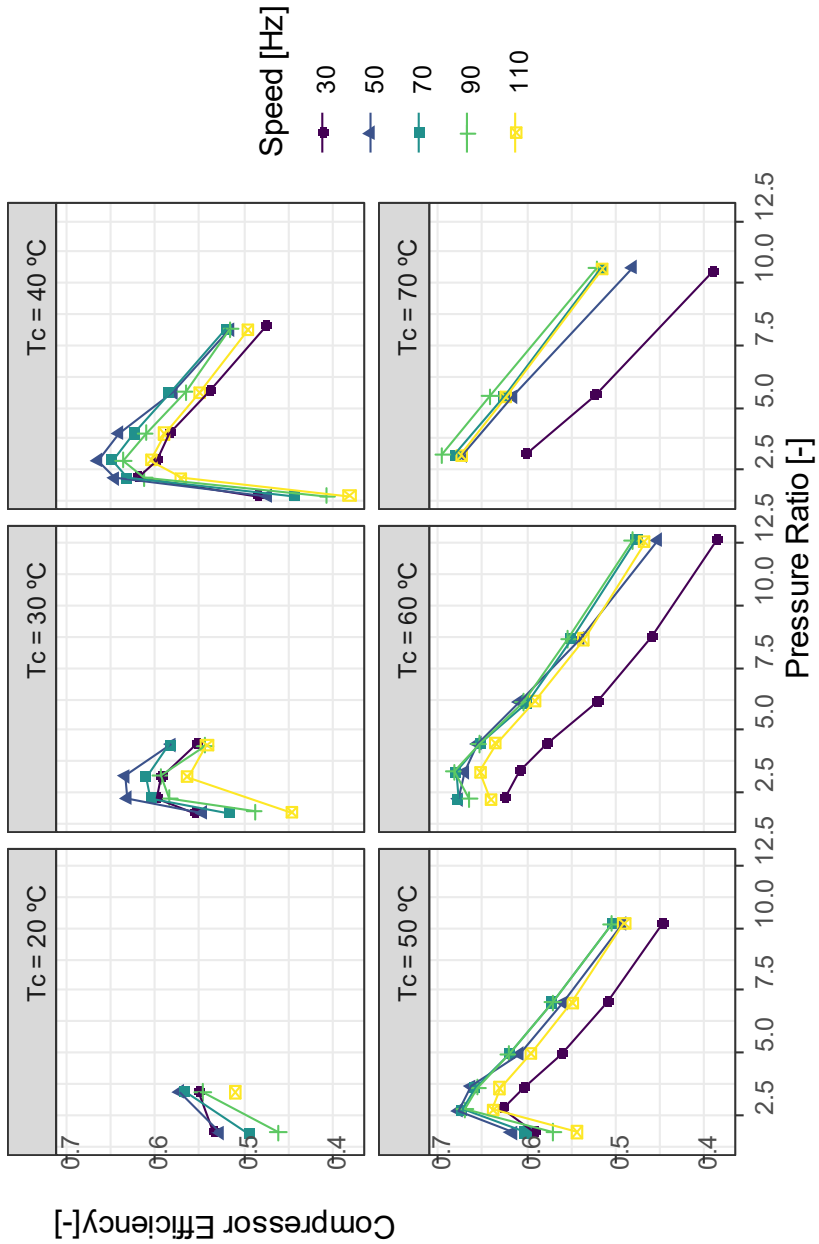


Figure 3.8: Evolution of compressor efficiency

It should be pointed out that compressor efficiencies at central speeds (50, 70 and 90 Hz) behave homogeneously, having a maximum close to $PR = 2.5$, which correlates with the built-in volume ratio with which the compressor was designed.

At low speeds and high condensing temperatures, a decrease in compressor efficiency is manifested. Cuevas and Lebrun (Cuevas & Lebrun, 2009) suggested a possible explanation of this effect: a lack of lubrication at low compressor speeds, which increased internal leakages and possibly also frictional losses. The internal leakages are related to the pressure difference, which explains why these become more relevant at high condensing temperatures.

Additionally, the compressor efficiency decreased also slightly at high speeds due to increased mechanical losses. These mechanical losses do not depend heavily on the working temperatures; thus, at lower condensing temperatures where the compressor has a lower consumption, they have a major impact on efficiency.

Another variable that can be analyzed is the specific consumption, defined as the ratio between energy consumption and mass flow [Eq.(3.12)]. Its evolution with compression conditions is displayed in Figure 3.9.

$$\dot{W}_{esp} = \dot{W}_c / \dot{m} \quad (3.12)$$

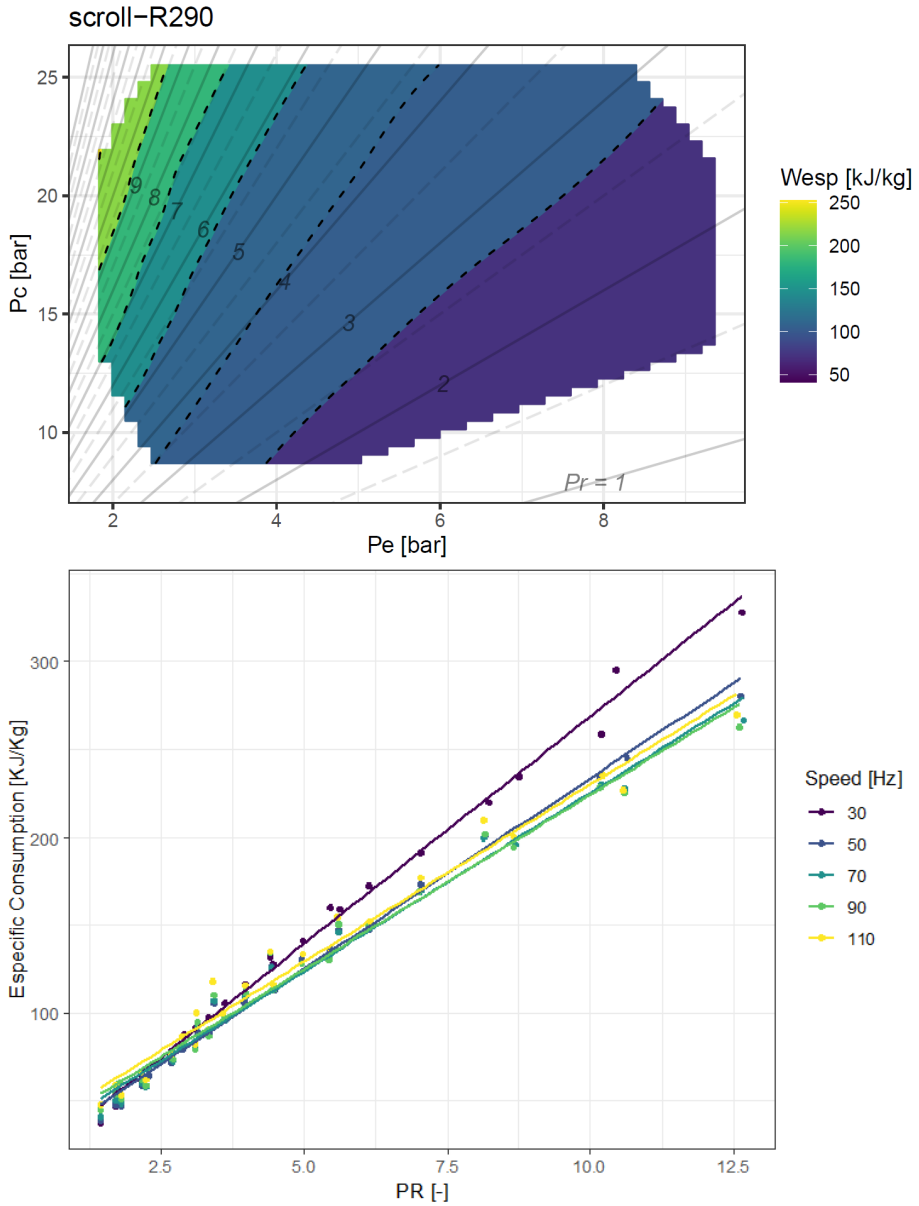


Figure 3.9: Specific consumption evolution with operating pressures (UP). Evolution of specific consumption with pressure ratio and speed (DOWN)

The evolution of the specific energy consumption seems to have a correlation with the pressure ratio as the isolines tend to be quite parallel to the pressure ratio lines. However, the isolines tend to converge at a virtual point lower than the convergence point of pressure ratio lines (Marchante-Avellaneda, Navarro-Peris, et al., 2023).

On the other hand, specific consumption seems to be independent with speed except for the lowest speed in which an increase of specific consumption is evident and it becomes more significant at higher pressure ratios. The increase in specific consumption at low speeds is explained by a decrease of volumetric and compressor efficiency due to lubrication problems and could be used to limit the compressor envelope.

3.5.2. Model

As observed in the obtained results, the specific consumption is the simplest variable to model due to its smooth and linear behavior. The modeling of power consumption through a correlation based on specific consumption was already proposed for fixed-speed compressors by Marchante-Avellaneda et al. (Marchante-Avellaneda, Navarro-Peris, et al., 2023), whose general expression is displayed in Eq.(3.13). In his study, Marchante-Avellaneda et al. (Marchante-Avellaneda, Navarro-Peris, et al., 2023) also concluded that this correlation could apply to both reciprocating and scroll compressors as they behave homogeneously in the domain of specific consumption.

$$\dot{W}_{esp} = \dot{W}_c / \dot{m}_{pred} = k_0 + k_1 PR' + k_2 PR'^2 + \dots + k_n PR'^n \quad (3.13)$$

$$\text{with } PR' = \frac{P_c - z_c}{P_e - z_e}$$

Being $k_{\#}$, z_c and z_e the fitting parameters and the determination of the order (n) of the correlation is done iteratively. The required order of Eq. (3.13) for the studied dataset was one, as adding a quadratic term did not significantly improve the model accuracy. Regarding z_c and z_e they represent a translation of the cartesian origin to the convergence point of the iso-specific-consumption lines in Figure 3.9-UP as stated in (Marchante-Avellaneda, Navarro-Peris, et al., 2023).

It should be noted that the specific energy consumption correlation is coupled with the mass flow model. Consequently, the uncertainty of mass flow

measurements will affect the accuracy of the energy consumption model. That is why using predicted values obtained from a pre-fitted mass flow model is generally preferred over empirical results, as using a correlation partially filters the noise level introduced by experimental uncertainty.

This correlation also has the advantage of partially accounting for the speed effect (as it normalizes the consumption with the mass flow) and thus, it can be used to extrapolate energy consumption to different speeds, especially if the compressor efficiency is not greatly affected, which typically happens at speeds close to rated speed.

If higher precision is required in the analysis of the speed effect, an approach similar to the one followed by Shao et al. (Shao et al., 2004) can be followed. Shao et al. (Shao et al., 2004) defined a power ratio with respect to rated speed (k_p) and modelled it with a 3 coefficients quadratic equation [Eq.(3.1)]. However, as happened with mass flow, it ends up modeling a pre-known behavior as consumption is expected to approximately double when speed is doubled.

To correct that, the ratio k_c will be studied instead of k_p . k_c is defined in Eq. (3.14) as the ratio of specific consumptions. It should be noted, that this ratio also represents the inverse of the ratio of compressor efficiency and can be deduced from k_p and k_m ratios [Eq.(3.15)].

$$k_c = \frac{\dot{W}_{esp}}{\dot{W}_{esp,nom}} = \frac{\frac{\dot{W}_c}{\dot{m}_{pred}}}{\frac{\dot{W}_{c,nom}}{\dot{m}_{pred,nom}}} = \frac{\frac{\dot{m}_{pred,nom} \Delta h_{is}}{\dot{W}_{c,nom}}}{\frac{\dot{m}^{\#} \Delta h_{is}}{\dot{W}_c}} = \frac{\eta_{c,nom}}{\eta_c} \quad (3.14)$$

$$k_c = \frac{\frac{\dot{W}_c}{\dot{m}_{pred}}}{\frac{\dot{W}_{c,nom}}{\dot{m}_{pred,nom}}} = \frac{k_p}{k_m} \quad (3.15)$$

Figure 3.10 shows a comparison between the evolution of k_p and the inverse of k_c with speed for two different compressors (Shao's compressor in the first column and the reference compressor in the second column). The inverse of k_c was plotted (instead of k_c) as it represents the compressor efficiency ratio, and its maximum represents the most efficient condition.

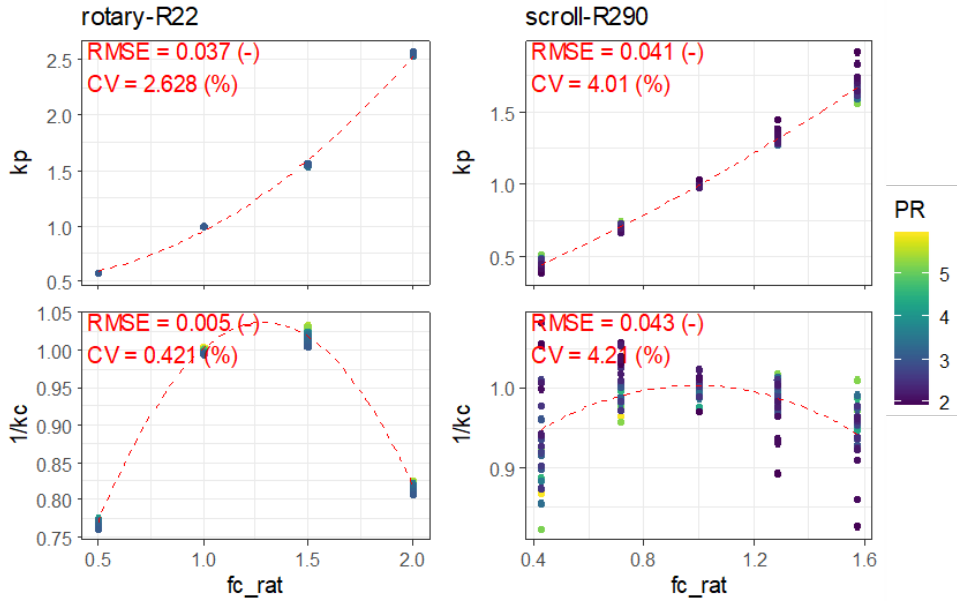


Figure 3.10: k_p and k_c evolution with speed for two different compressors

The evolution of k_p with speed ratio is plotted in the first row. The evolution presents a slight curvature but it is not far from a straight line with 45° slope which implies that k_p has a strong dependence with speed ratio. This linear dependence is normalized in the case of k_c which allows to retrieve more significant results from its study. In particular, it permits to analyze how speed affects compressor efficiency. In both compressors the optimum compressor efficiency is obtained at speeds close to the nominal and in the rotary-R22 data set the effect of speed in compressor efficiency is much more significant reaching a decrease in efficiency close to 25% at low and high speeds.

To model the evolution of k_c with compressor speed, the same parabola equation used to model k_v in Eq.(3.8) is proposed.

$$k_c = \frac{\dot{W}_{esp}}{\dot{W}_{esp,nom}} = \frac{\eta_{c,nom}}{\eta_c} \sim k_4 \left(f_{c,rat} - \frac{k_5}{f_{c,nom}} \right)^2 + k_6 \quad (3.16)$$

$$\text{with } k_6 = 1 - k_4 \left(1 - \frac{k_5}{f_{c,nom}} \right)^2$$

With this formulation k_5 represents the speed at which compressor efficiency reaches its maximum and k_4 represents the influence of speed on k_c .

If both Eq.(3.13) and Eq.(3.16) are combined, a general expression for the energy consumption of variable-speed compressors can be written as Eq.(3.17).

$$\dot{W}_c / \dot{m}_{pred} = \left(k_0 + k_1 \frac{P_c - k_2}{P_e - k_3} \right) \left[k_4 \left(f_{c, rat} - \frac{k_5}{f_{c, nom}} \right)^2 + k_6 \right] \quad (3.17)$$

Resulting in a correlation with six coefficients which, compared with Shao et.al (Shao et al., 2004) model with nine, implies a reduction of three coefficients. The result of training the proposed correlation in with the complete data set of the reference compressor is displayed in Figure 3.11.

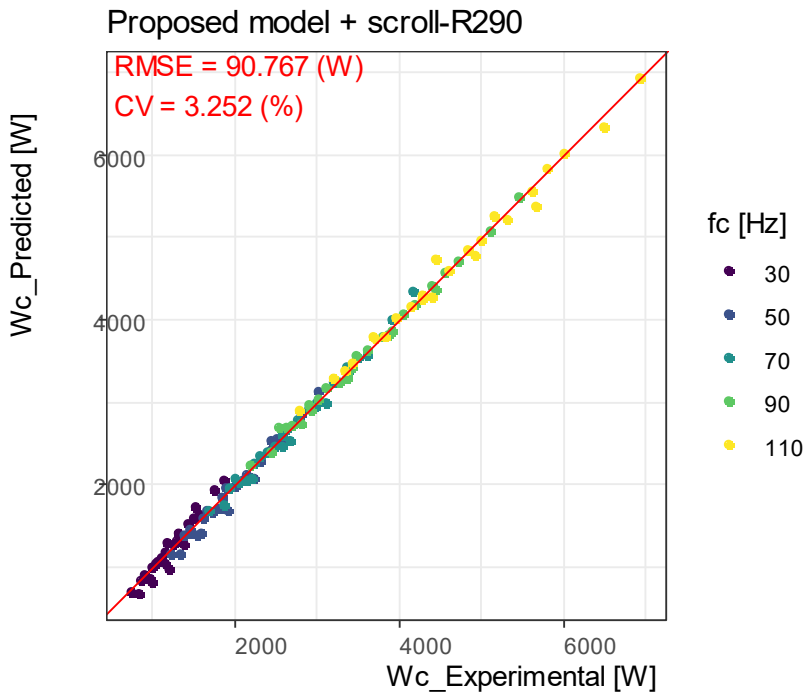


Figure 3.11: Correlation plot of energy consumption model applied to reference compressor

The obtained RMSE is lower than 100W and the CV is close to 3% for the reference compressor. In order to validate that result, the energy consumption model in Eq.(3.17) was fitted for all the presented data sets in Table 3.4 and the

model accuracy is plotted in Figure 3.12 among the fitting results obtained by Shao et al. (Shao et al., 2004) model and using as baseline the goodness of fit of AHRI-20 model.

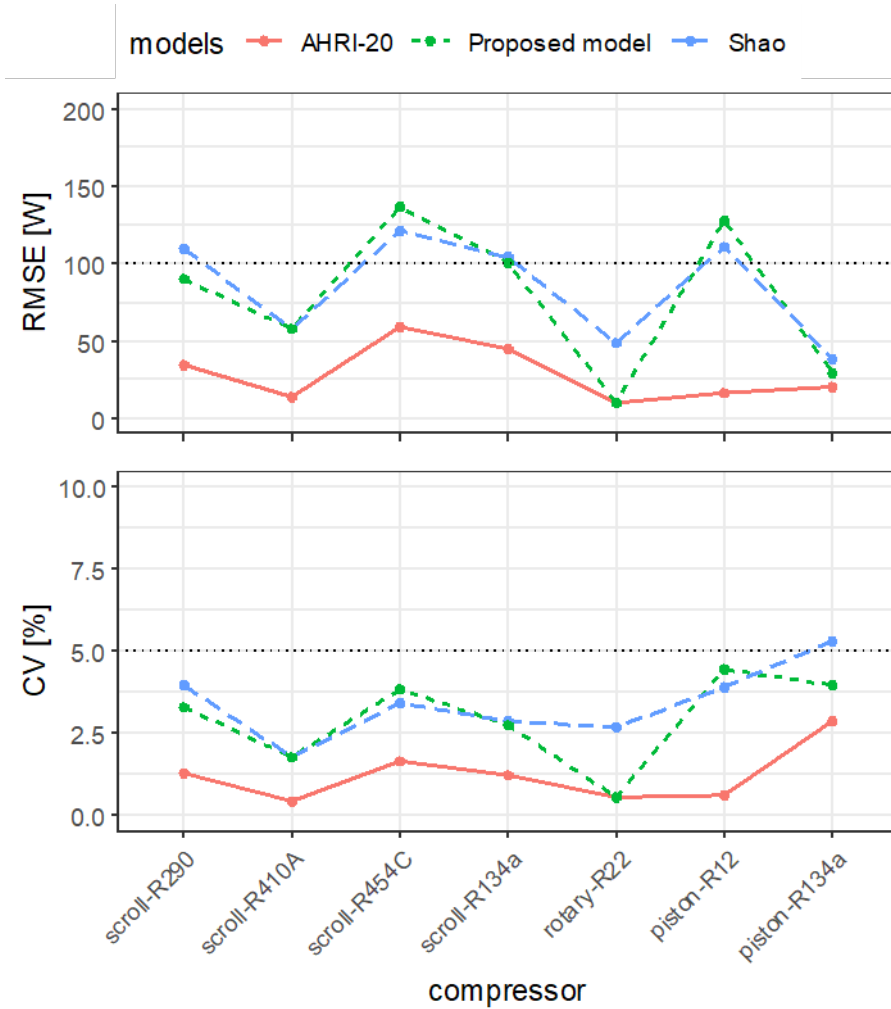


Figure 3.12: Goodness of fit of energy consumption models applied to different data sets

Both compact models have similar modeling errors and tend to achieve less than 5% CV values. Despite having more coefficients (9 vs 6), only two data sets were adjusted better by Shao et.al (Shao et al., 2004) model and with very subtle

differences. Additionally, it should be noted the case of the rotary-R22 compressor, which was reported in Shao et.al (Shao et al., 2004), and how the proposed model managed to perfectly fit the dependence of compressor efficiency with the speed, performing significantly better than Shao et.al (Shao et al., 2004) model itself and obtaining very similar results compared with AHRI-20 model (but using less than one-third of coefficients). However, even if the proposed model fitted very accurately, it should be remembered that the rotary-R12 data set was partially reconstructed using pre-fitted models and more experimental data from rotary compressors would be needed to generalize the results to all rotary compressors.

AHRI-20 model managed to fit all datasets with reduced prediction errors, but it should be noted that the coefficient fit was made using the complete data set and, when this happens, models having a great number of coefficients tend to perform better but risk overfitting when adjusted with limited train data. The overfitting in AHRI-20 model was evaluated in Section 3.8.

In Table 3.4 the fitted coefficients of the proposed model are displayed for the different compressor data sets (using kJ/kg, bar and Hz as units). k_1 tends to be the most significant parameter as it models the variation of specific consumption with the corrected pressure ratio. It should also be noted that k_1 and k_2 represent z_c and z_e respectively which represent how the point of convergence of specific consumption isolines are displaced from the origin in Figure 3.9-UP. The displacement tends to be more relevant in the condensing pressure axes and negative (which was expected to account for no-load losses). Finally, k_5 represents the speed at which the compressor runs more efficiently; the obtained optimum speeds tend to be slightly lower than the ones obtained for volumetric efficiency which indicates that the compressor efficiency drop at very high speeds is lower than the drop seen in volumetric efficiency.

Table 3.4: Model coefficients and goodness of fit of the energy consumption model applied to the different compressor data sets

Energy consumption - Proposed model							
	scroll-R290	scroll-R410A	scroll-R454C	scroll-R134a	rotary-R22	piston-R12	piston-R134a
k0	-0.251	-2.783+	-11.618***	-5.468***	-0.662***	0.665	1.436
k1	21.030***	14.283***	18.378***	12.970***	4.315***	9.862***	11.941*
k2	-6.696***	-2.328*	-1.921*	-0.029	-1.487***	-2.578*	-2.076
k3	-0.511***	0.214	-0.539**	0.629**	-0.092**	-0.398	-1.000
k4	0.185***	0.139***	0.144***	0.545***	0.533***	-0.165	0.183
k5	72.916***	65.960***	64.293***	58.650***	77.625***	11.013***	34.480+
Num.Obs.	133	35	87	48	296	25	44
RMSE	90.77	57.73	137.15	99.88	9.89	127.34	30.77
CV	3.25	1.75	3.84	2.72	0.54	4.46	4.23

3.6. Discharge temperatures

3.6.1. Experimental results

The variable-speed scroll compressor working with R290 was tested with a suction temperature 10 K higher than the evaporating temperature and at a controlled ambient temperature of 35°C.

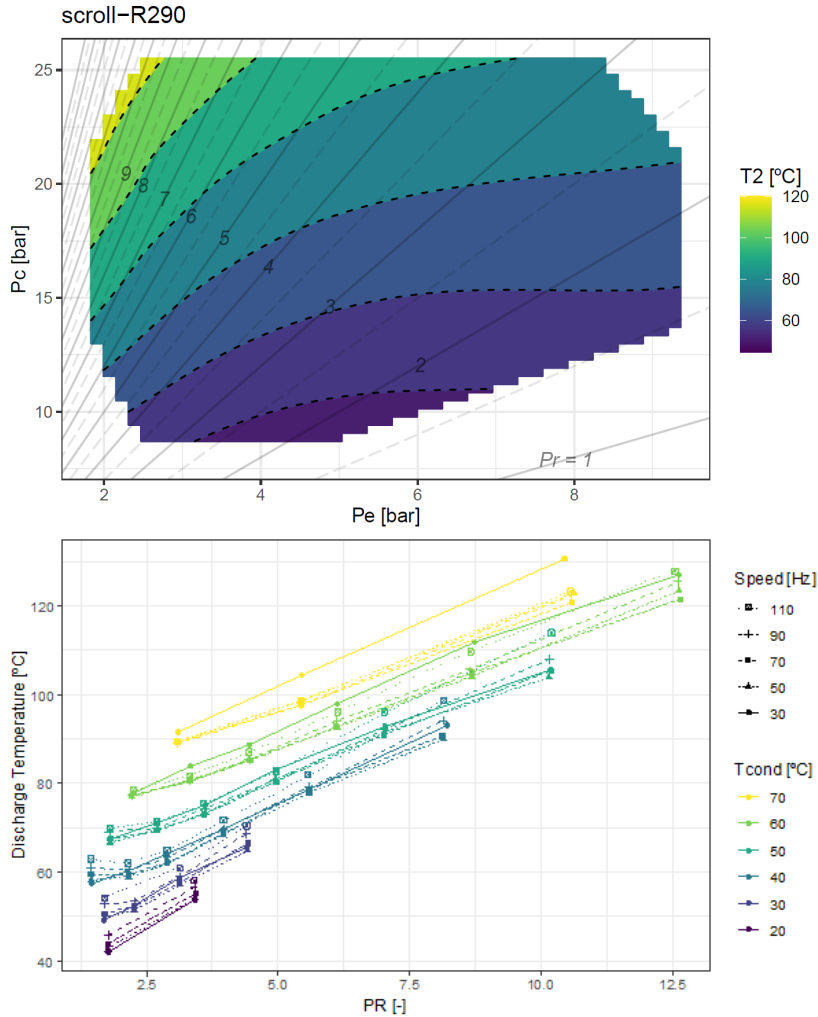


Figure 3.13: Discharge temperature as a function of working pressures for nominal speed (UP). Discharge temperatures as a function of pressure ratio, compressor speed and condensing temperature (DOWN)

In Figure 3.13, the experimental discharge temperatures are plotted. The left graph displays the evolution of discharge temperatures around the envelope at rated speed. And in the graph at the right, all the tested results are displayed as a function of pressure ratio, compressor speed and condensing temperatures.

Figure 3.13 – UP shows that the highest obtained discharge temperatures are produced in the high-pressure ratio region; in fact, the working envelope is typically limited in the high-pressure region by the allowable discharge temperature, as most frequently used lubricating oils degrade at temperatures around 120-130 °C.

Figure 3.13– DOWN, discharge temperature shows a high dependence on pressure ratio and condensing temperature. However, the effect of compressor speed in discharge temperatures is small and typical variations lower than 5K are obtained from minimum to maximum speed.

Typically, modeling discharge temperatures directly is not recommended as the obtained predictions are only valid for the defined SH. That is why, modeling other variables less dependent on the suction conditions is typically preferred. Figure 3.14 plots the compressor isentropic efficiencies defined in Eq.(3.18).

$$\eta_{is} = \frac{h_{2,is} - h_1}{h_2 - h_1} \quad (3.18)$$

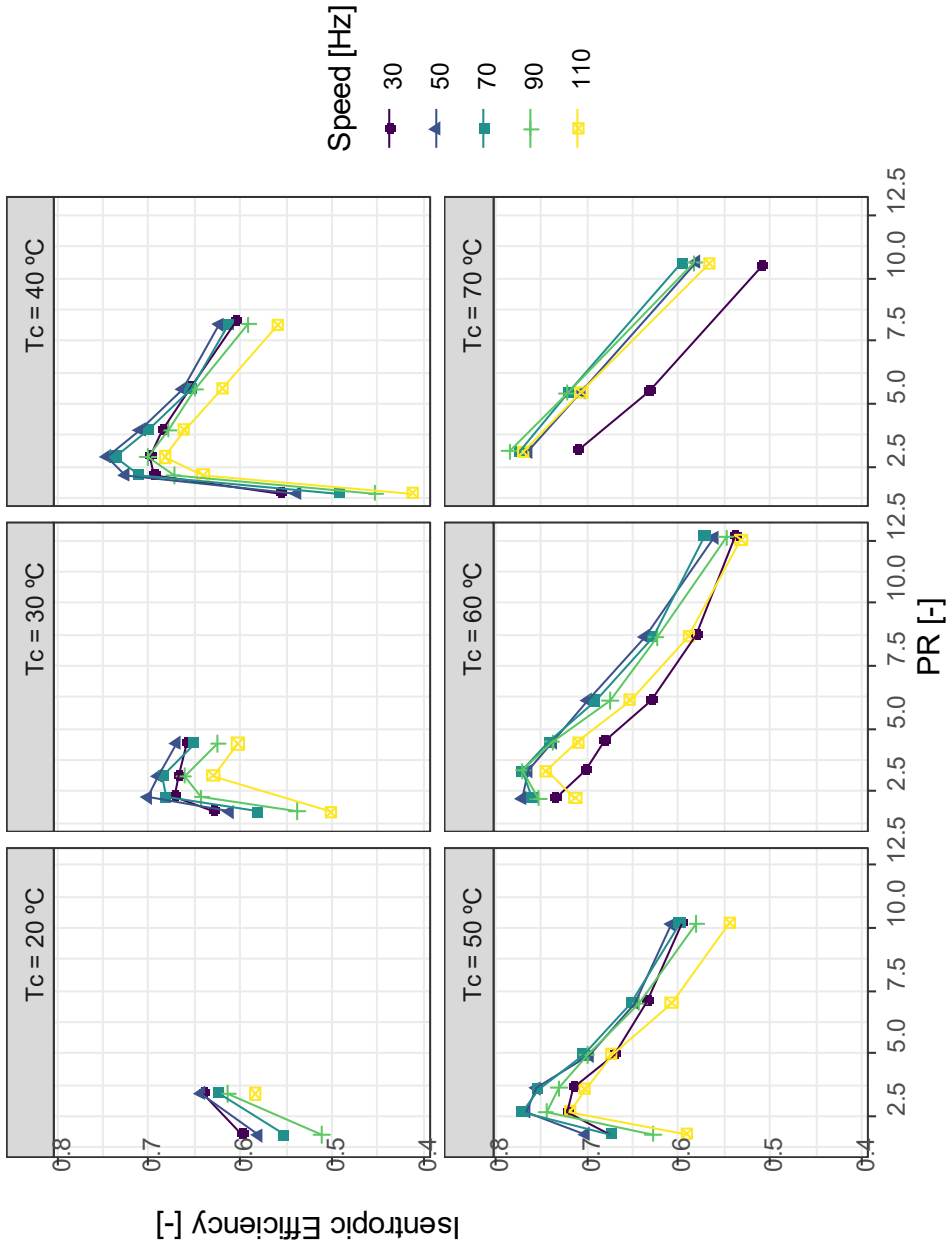


Figure 3.14: Isentropic efficiency as a function of RP, compressor speed and condensing temperatures

It can be noted that the evolution of isentropic efficiency is very similar to the observed evolution of the compressor efficiency, with a maximum at the built-in pressure ratio. This variable is still significantly dependent on compression conditions and complex models would be needed to model their behavior accurately.

Another dimensionless variable that could be studied is the electro-mechanical efficiency. It is defined as the ratio between the energy transferred to the refrigerant and the energy consumption [Eq.(3.19)] and its evolution with the compression conditions is displayed in Figure 3.15.

$$\eta_{em} = \frac{\eta_c}{\eta_{is}} = \frac{\dot{m}(h_2 - h_1)}{\dot{W}_c} \quad (3.19)$$

Electro-mechanical efficiency shows low dependence with compression conditions for medium and high speeds with stable values between 0.85 - 0.9. However, as speed decreases, a strong dependence with pressure ratio appears and the efficiency drops as pressure ratio increases.

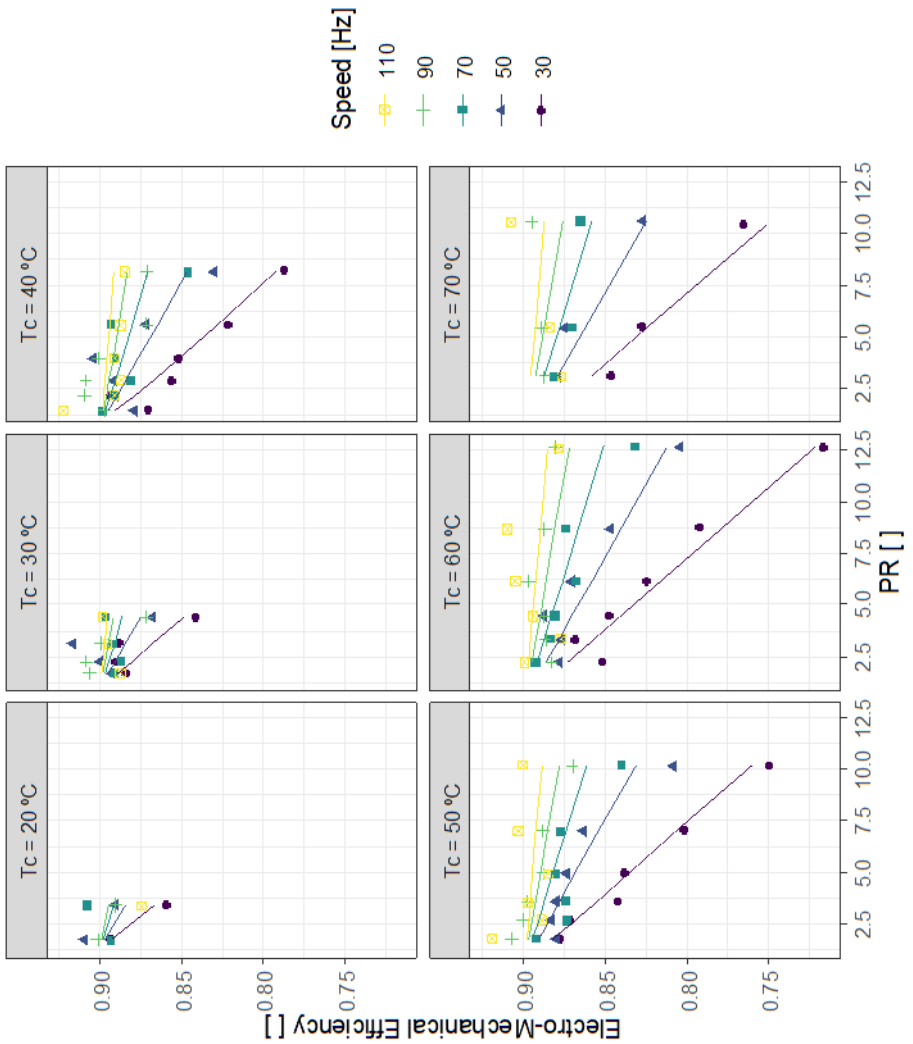


Figure 3.15: Evolution of Electro-Mechanical efficiency with pressure ratio, condensing temperature and speed. Lines represent proposed model predictions.

3.6.2. Model

As already mentioned, predicting discharge temperature with a model based only on condensing and evaporating temperatures is not a good idea, as the model would give accurate results only for the suction conditions at which the model was fitted. Consequently, a model like the presented AHRI-20 won't be viable.

In the literature, the most extended approach is to assume a constant isentropic efficiency or to model power losses as two terms: a term depending on total compression work and a constant term. This last methodology is the one proposed by ASHRAE in Toolkit (Bourdouxhe et al., 1994), and its formulation is displayed in Eq.(3.20) where the two fitting parameters are: the constant power losses (W_{loss0}) and the fraction of usefull energy that is lost as heat (α).

$$\dot{W}_c = \dot{m}(h_2 - h_1)(1 + \alpha) + W_{loss0} \quad (3.20)$$

Eq.(3.20) can also be rewritten as a function of the previously introduced electro-mechanical efficiency, resulting in Eq.(3.21).

$$\eta_{em} = \frac{\dot{m}(h_2 - h_1)}{\dot{W}_c} = \frac{1}{1 + \alpha} \left(1 - \frac{W_{loss0}}{\dot{W}_c} \right) = k_0 - \frac{k_1}{\dot{W}_c} \quad (3.21)$$

However, this expression does not consider pressure ratio or compressor speed, which were proven to affect electro-mechanical losses in variable speed compressors (Figure 3.15). Consequently, if extra accuracy is needed, additional terms can be added, resulting in the model of Eq.(3.22). The predicted electro-mechanical efficiencies with this latter model are displayed in Figure 3.15 as solid lines.

$$\eta_{em} = 1 - k_0 - k_1 PR - k_2 \frac{PR}{f_{c,rat}} - k_3 \frac{1}{\dot{W}_c} \quad (3.22)$$

Eq.(3.22) was the result of the analysis of the specific power losses and their dependence with the studied variables. For more information, please refer to Appendix 1: Electro-mechanical losses.

Once electro-mechanical losses are modelled, the predicted discharge enthalpy can be calculated using Eq.(3.19). And finally, knowing discharge enthalpy

and pressure, the predicted discharge temperature can be computed using any thermodynamic database (Huber et al., 2022).

If the proposed model in Eq.(3.22) is fitted with the reference compressor, the correlation graph in Figure 3.16 is obtained with a RMSE lower than 1 K for discharge temperatures.

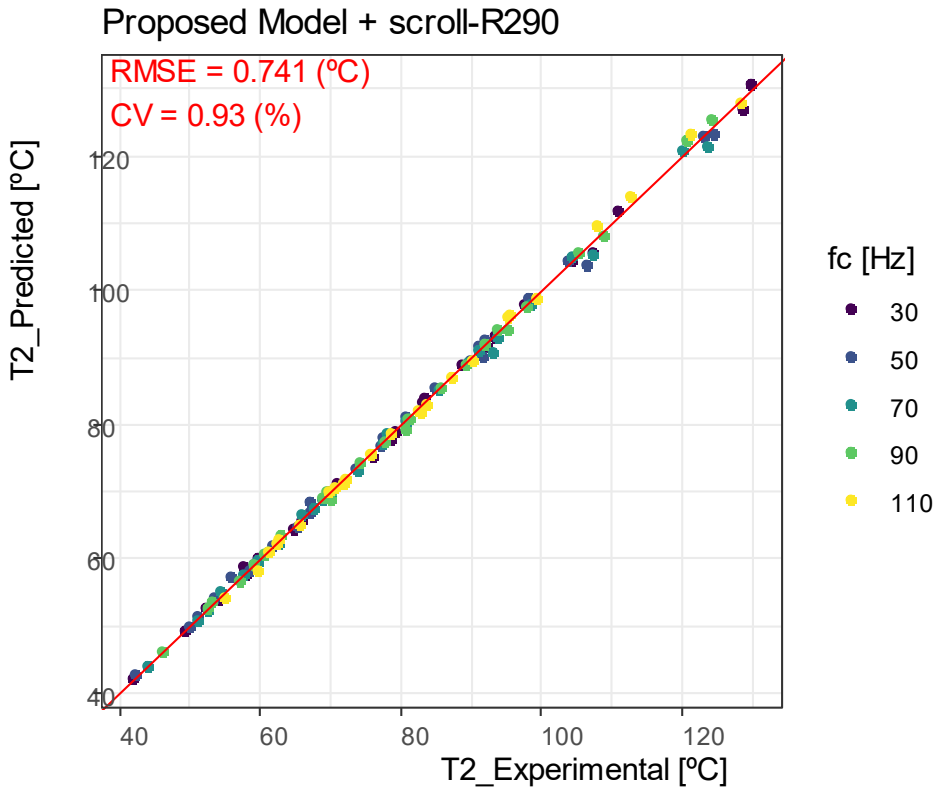


Figure 3.16: Correlation plot of discharge temperature model applied to reference compressor

To validate the presented model, it was fitted to the other compressors in the dataset and the obtained results are displayed in Figure 3.17, together with the fitting performance of the reference Toolkit model (Bourdouxhe et al., 1994).

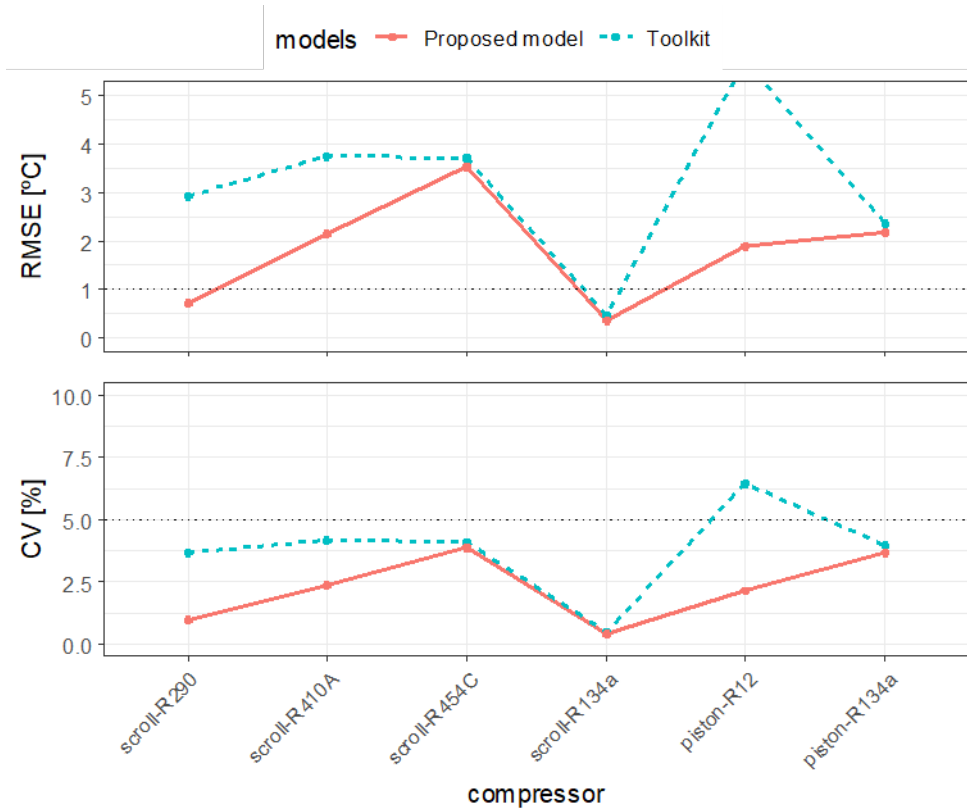


Figure 3.17: Goodness of fit of discharge temperature models applied to different data sets

From the results in Figure 3.17 the studied compressors can be separated into two different groups: one that shows a significant modeling improvement when PR and f_c are considered and other that does not. The grouping does not correlate with the compression technology and could be related to dispersion in the empirical results, tested range or another non-studied factor.

In Table 3.5, all the proposed model's fitted coefficients [Eq.(3.22)] are displayed for the different compressor data sets. k_0 represents the base percentage of the compressor consumption that is lost as ambient temperature and for the reference compressor is close to 10%.

Table 3.5: Model coefficients and goodness of fit of the proposed discharge temperature model applied to the different compressor data sets

Electro-Mechanical Efficiency - Proposed model						
	scroll-R290	scroll-R410A	scroll-R454C	scroll-R134a	piston-R12	piston-R134a
k0	1.03e-01***	1.30e-02	2.75e-01***	8.45e-02***	1.29e-01***	3.10e-01+
k1	-3.90e-03***	6.34e-04	-1.86e-02+	-2.69e-02***	-3.24e-03	-5.76e-02
k2	8.00e-03***	1.31e-02***	6.97e-03	1.89e-02***	3.40e-02**	4.36e-02+
k3	-1.48e+01**	-3.63e+01	-1.59e+02**	9.27e+00	-1.40e+01	-1.39e+02*
Num.Obs.	133	35	87	48	25	43
RMSE	0.01	0.03	0.09	0.01	0.03	0.06
CV	1.31	3.10	10.47	1.48	3.95	6.82

*It should be noted that RMSE and CV indicate the modelling error of electro-mechanical efficiency, RMSE and CV referred to discharge temperatures are displayed in previous Figure.

3.7. Effect of suction conditions

This section describes how to modify the presented models to account for a change in the vapor superheat temperature.

Regarding mass flow and compressor consumption, extensive research is available in the literature. For mass flow, Dabiri and Rice (Dabiri & Rice, 1981) correlation is proposed to correct the effect of suction conditions. Its formulation is displayed in Eq.(3.23).

$$\dot{m} = \dot{m}^{\#} \left(1 + F \left(\frac{\rho_1}{\rho_1^{\#}} - 1 \right) \right) \quad (3.23)$$

Regarding $\dot{m}^{\#}$ it represents the mass flow at a rated suction conditions whose correlation is given in Eq.(3.10). The F parameter introduced in the expression can be assumed to be 0.75, value that has been generally used in the literature. However, if extra accuracy is needed and datasets at different superheats are available the parameter F can be fitted using experimental data.

The literature also mentions that compressor consumption tends to be relatively unaffected by suction conditions, and the impact of superheat on consumption is usually disregarded. Consequently, Eq.(3.24) can be applied directly with $\dot{W}_{esp}^{\#}$ being the specific consumption obtained at rated suction conditions in Eq.(3.17) and $\dot{m}^{\#}$ the mass flow at the same suction conditions at which the coefficients in Eq.(3.17) were adjusted.

$$\dot{W}_c = \dot{W}_c^{\#} = \dot{W}_{esp}^{\#} \dot{m}^{\#} \quad (3.24)$$

As mentioned in the previous section, suction conditions greatly affect discharge temperatures, so its modeling was based on electro-mechanical efficiencies rather than on working temperatures. Considering $\eta_{em}^{\#}$ as the electro-mechanical efficiency at a reference suction condition, the ratio expressed in Eq.(3.25) can be written as:

$$\frac{\eta_{em}}{\eta_{em}^{\#}} = cc = \frac{\dot{m}}{\dot{m}^{\#}} \frac{\dot{W}_c^{\#}}{\dot{W}_c} \frac{\Delta h}{\Delta h^{\#}} \quad (3.25)$$

Then, if it is supposed that consumption and enthalpy difference are not affected by the suction conditions, the proposed ratio can be simplified as a ratio

of mass flows, which in turn can be approximated by Dabiri and Rice correlation (Dabiri & Rice, 1981), resulting in the general expression for different suction conditions displayed in Eq.(3.28).

$$\eta_{em} = \eta_{em}^{\#} \frac{\dot{m}}{\dot{m}^{\#}} = \left(k_0 + k_1 PR + k_2 \frac{PR}{f_{c, rat}} + k_3 \frac{1}{\dot{W}_c} \right) \left(1 + F \left(\frac{\rho_1}{\rho_1^*} - 1 \right) \right) \quad (3.26)$$

The F parameter introduced in the expression can be assumed to be 0.75, value that has been generally used in the literature. However, if extra accuracy is needed and datasets at different superheats are available the parameter F can be fitted using experimental data.

This general correlation was tested with the dataset summarized in Table 3.2, consisting of a fixed-speed scroll compressor working with different refrigerants. Each refrigerant was tested at three suction conditions (SH = 11 K, SH = 22 K and T1 = 18 °C). First, the electro-mechanical model was fitted with the dataset at SH = 11 K and then it was used to predict discharge temperatures for the other suction conditions without using any correction - Figure 3.18 (Left) - and using the Dabiri and Rice correction with $F = 0.75$ - Figure 3.18 (Right) - .

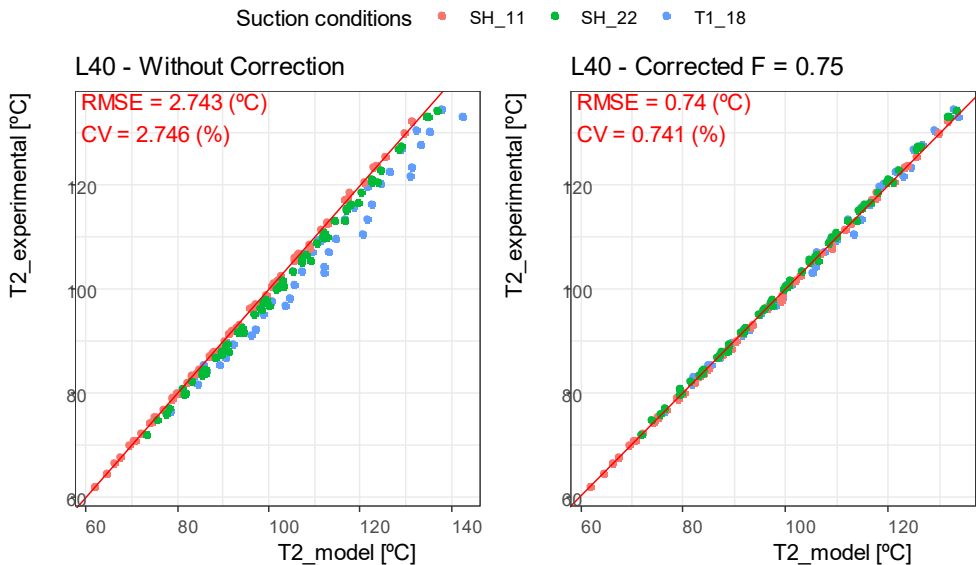


Figure 3.18: Discharge temperature correlation graphs. Without correction (LEFT). Using the correction term with $F = 0.75$

The results in Figure 3.18 show that the correction effectively reduces the prediction errors when the model is extrapolated to different suction conditions. For the particular case shown in Figure 3.18 Dabiri and Rice correction reduced the prediction RMSE from 2.7 °C to values lower than 1 °C without introducing any further fitting parameters. To confirm that this result can be generalized, the same methodology was applied to the rest of the tested refrigerants and the results are summarized in Table 3.6.

Table 3.6: Improvement of prediction errors when Dabiri correction is implemented

REFR	NO CORRECTED		CORRECTED ($F=0.75$)	
	RMSE [K]	CV [%]	RMSE [K]	CV [%]
R404A	1.66	2.03	0.92	1.12
ARM31A	2.46	2.58	0.70	0.73
D2Y65	2.21	2.32	0.80	0.84
L40	2.74	2.75	0.74	0.74
R32_R134A	2.74	2.61	0.91	0.87

With all the tested refrigerants, the correction significantly decreased the prediction errors of the discharge temperature without introducing new fitting parameters.

3.8. Robustness Analysis

As introduced in the first section, when fitting empirical models, a recurrent problem is overfitting, which occurs when the complexity of the model is higher than the information imbibed in the data. When overfitting occurs, the model seems to fit well the train set but will fail to predict new data. To test the model against overfitting a train-test methodology is needed in which the data set is split into two groups; one will be used to fit the model coefficients and then the complete dataset is used to check the accuracy of new predictions.

This train-test procedure was applied to both AHRI-20 model and the new proposed models and two questions are answered for each model: which is the minimum number of tests required to fit a model avoiding overfitting and which is the influence of the position of this train tests.

To apply the train-test methodology to the models, 50 different training sets were generated, each with a specific number of samples. These train sets were then used to estimate the model coefficients and then the complete dataset is used to evaluate the prediction errors (CV [%]). In total 50 different prediction errors are computed for each case which are represented aggregated using box-whiskers diagrams.

For selecting the position of the train tests different methodologies arise. The simplest one is choosing train tests randomly, however this methodology does not map the complete working range homogeneously. Clustering techniques solve this problem but these tend to exclude train tests located in the borders of the working range which will force the models make extrapolations.

To ensure comprehensive coverage of the complete working range, including its limits, maxDissim methodology will be followed. It involves adding train tests that maximize the dissimilarity between new and existing ones. Additionally, with this technique 50 different train sets can be obtained by randomly selecting a first seed of three tests. It is important to note that the train sets selected were the same for the evaluation of both models, so a poorly trainset choice will affect the performance of both tested models. The other sampling techniques, such as fully random or clustering were tested but tended to penalize AHRI-20 model more aggressively as they introduced more important extrapolations.

When less than 20 observations were selected, the AHRI-20 model was truncated, discarding high-order terms to check whether a simplified AHRI-like model could compete in accuracy with the proposed model.

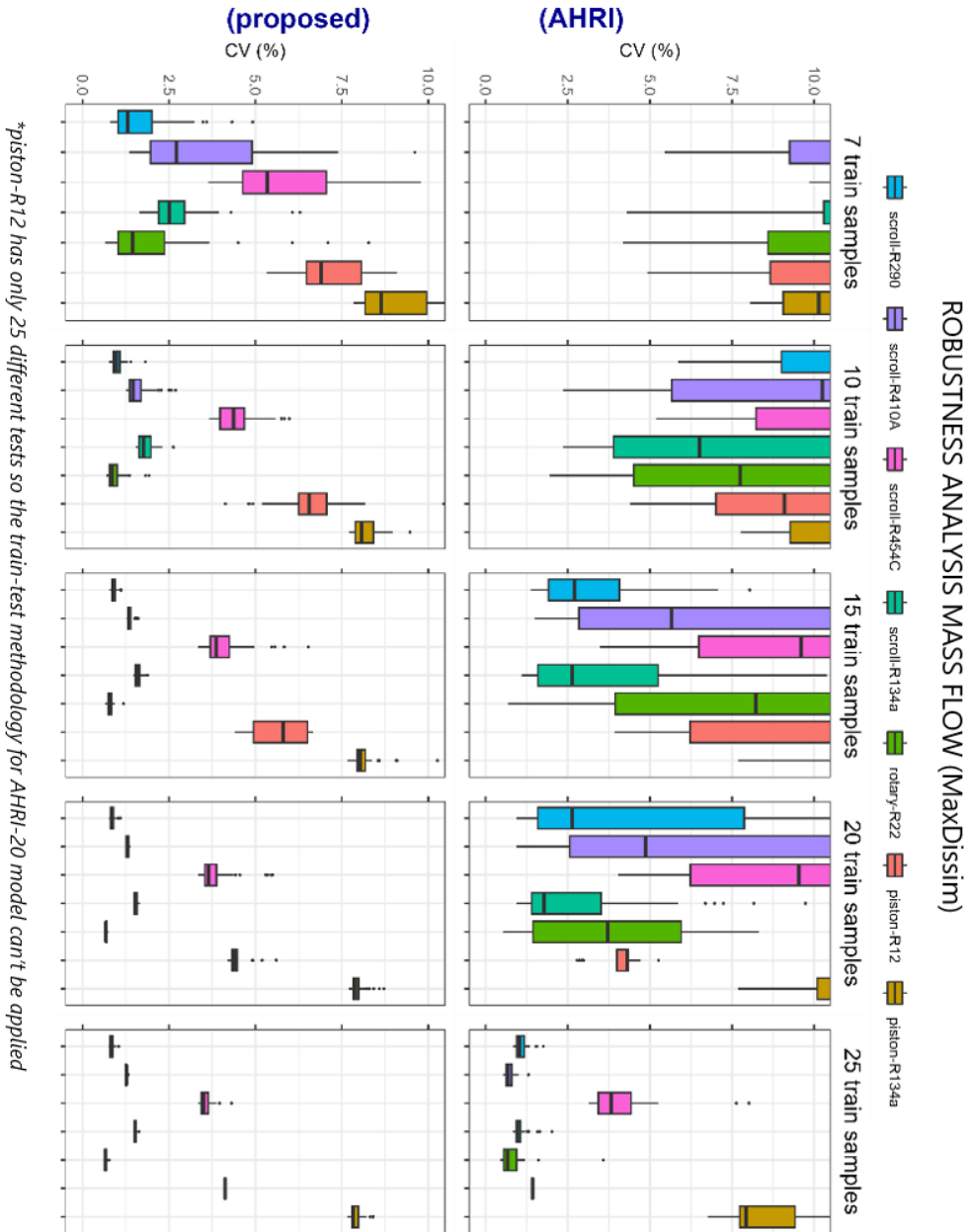


Figure 3.19: Train-Test methodology to evaluate the robustness of the studied mass flow models

Figure 3.19 shows that on average, the proposed mass flow model's accuracy when fitted with 7 samples is better than AHRI-20 fitted with 20 samples as it tends to overfit less. Additionally, Figure 3.19 shows that increasing the fitting sample above 10 observations does not further improve the accuracy of the proposed model for the studied dataset. In turn, the AHRI-20 model needs to reach 25 samples to avoid overfitting and reach accuracy values similar to those obtained by the proposed model. Finally, from Figure 3.19, it can also be concluded that the proposed model has better accuracy than a scaled-down AHRI-20.

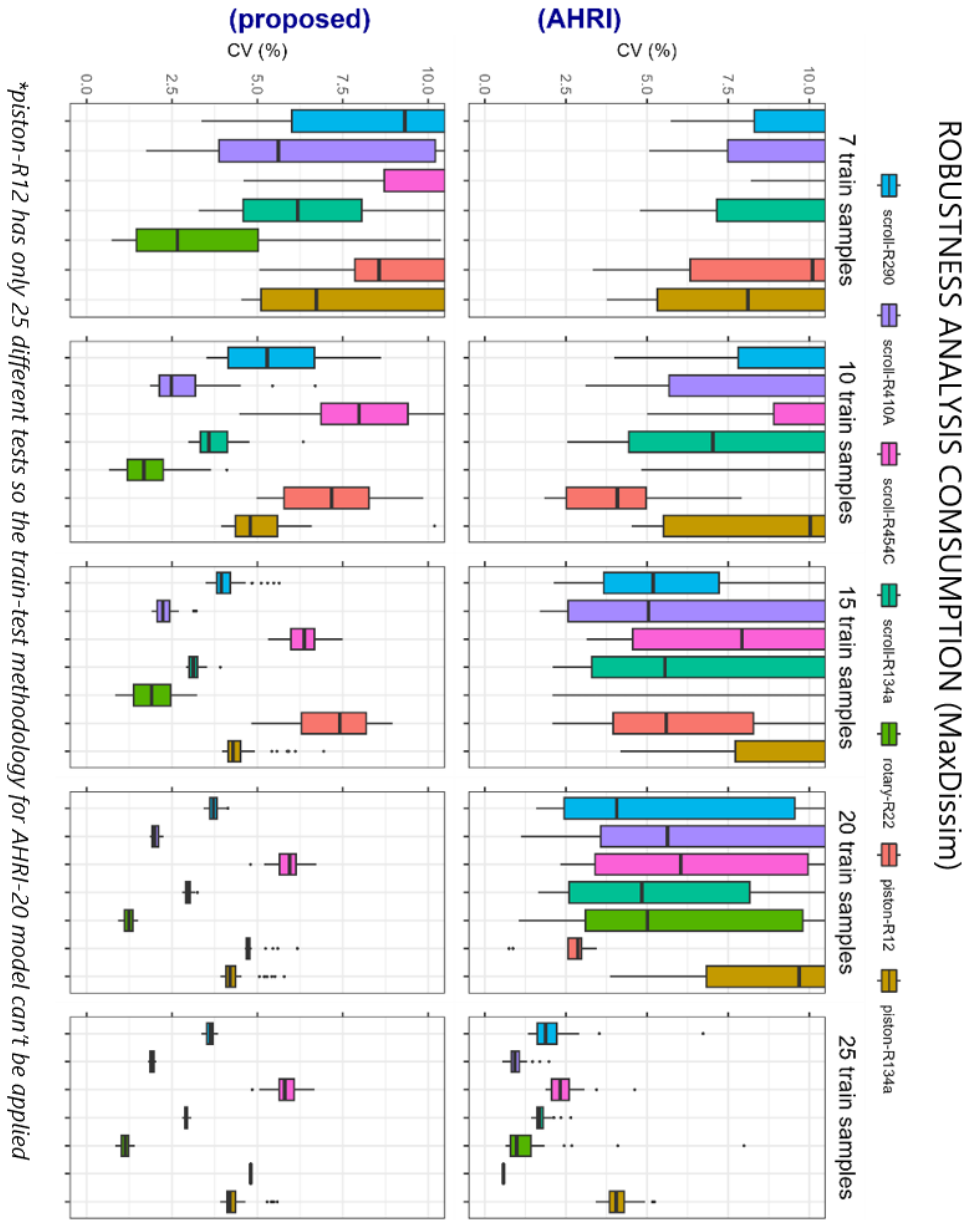


Figure 3.20: Train-Test methodology to evaluate the robustness of the studied consumption models

Figure 3.20 shows that the proposed consumption model also reaches a good accuracy with 10-15 distributed samples, but on the contrary AHRI-20 needs 25. The proposed model trained with only 10 samples performs comparable to AHRI-20 fitted with 20, and the proposed model works better than a truncated AHRI-20 model for low train sample conditions. Finally, AHRI-20 starts giving more accurate predictions for train sets with more than 25 tests for some compressors, so the latter would be preferred if a high amount of train data is available for the studied case. However, in the rotary-R22 and piston-R134a datasets, even with a high number of train samples, AHRI-20 does not manage to outperform the proposed model. It should be remarked though, that the train samples were chosen trying to map the complete compressor envelope so extrapolations were limited, in the case of using other sampling techniques, AHRI-20 model could incur in higher prediction errors especially due to the third-degree coefficients.

3.9. Conclusions

Analyzing the performance of variable-speed compressors presents a significant challenge due to the extensive data requirements, which may explain the limited availability of published data on the subject. This study conducted an exhaustive analysis of a high-fidelity calorimetric dataset of a variable-speed compressor. The observed tendencies were crucial to designing data-driven empirical correlations using no more than six coefficients to predict mass flow, consumption and discharge temperatures. The obtained models were validated with other published datasets and the following conclusions arise:

- Mass flow

- o A correlation with four coefficients is proposed
- o Correlating mass flow as a function of saturating pressures, rather than temperatures, is preferred due to the resulting linear relationship
- o Compressor speed affects volumetric efficiency, which is modeled with a quadratic expression, adding two more fitting coefficients.

- Consumption

- o A correlation with four coefficients is proposed.
- o Correlating specific consumption, rather than base consumption, is favored as it partially filters the speed effect by dividing it by mass flow.
- o If higher precisions is needed a quadratic expression is proposed to consider speed effect on compressor efficiency.

- Discharge temperature,

- o the chosen modelled variable was the electro-mechanical efficiency, which was correlated using four coefficients dependent on pressure ratios and compressor speed.
- All the proposed models were generalized for changing suction conditions without adding additional coefficients to be fitted.
- Finally, a robustness analysis concluded that the proposed models are preferable to models with many coefficients, especially when the amount and quality of

the empirical data is scarce and extrapolations are needed. A set of 15 tests is enough to adjust the coefficients of the proposed model. However, a model with 20 coefficients would require a minimum of 25.

In conclusion, the insights gained from this study and the robust models developed offer a practical approach to enhance the accuracy and efficiency of variable-speed compressor performance predictions. These findings contribute to the advancement of compressor technology, providing essential tools for design, selection, control, and fault detection in HVAC systems.

3.10. Appendix 1: Electro-mechanical losses

This appendix studies in depth the influence of working variables on electro-mechanical efficiency and serves as a justification for the electro-mechanical efficiency correlation proposed in Eq.(3.19).

The study starts with a reformulation ASHRAE expression of electro-mechanical efficiency in which $\dot{W}_{loss,0}$ is the base power loss and α is defined as the specific power losses (the fraction of total consumption that is lost as ambient heat (Eq.(3.27)):

$$\eta_{em} = 1 - \alpha - \frac{\dot{W}_{loss,0}}{\dot{W}_c} \tag{3.27}$$

$$\text{with } \alpha = \frac{\dot{W}_{loss}}{\dot{W}_c} = \frac{\dot{W}_c - m(h_2 - h_1)}{\dot{W}_c}$$

In Figure 3.21 the evolution of specific power losses (α) with the working conditions is plotted:

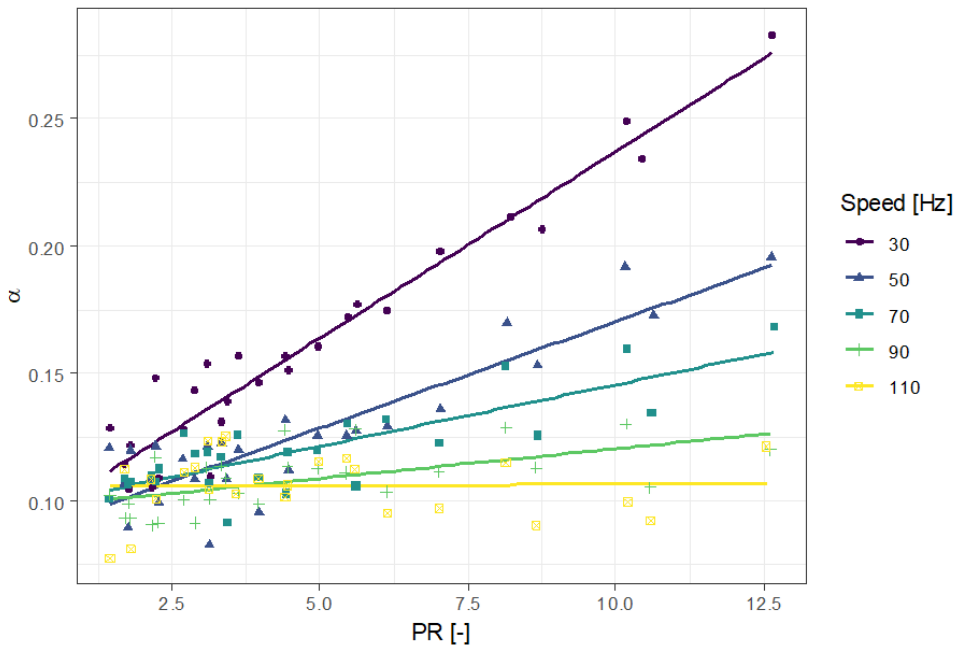


Figure 3.21: Evolution of specific losses as a function of pressure ratio and speed

Figure 3.21 shows a clear dependence of α with PR which can be modelled with a linear equation as Eq.(3.28).

$$\alpha = \alpha_0 - k_1 PR \quad (3.28)$$

According to the given formulation k_1 represents the effect of PR in specific losses and the experimental values of k_1 are plotted in Figure 3.22.

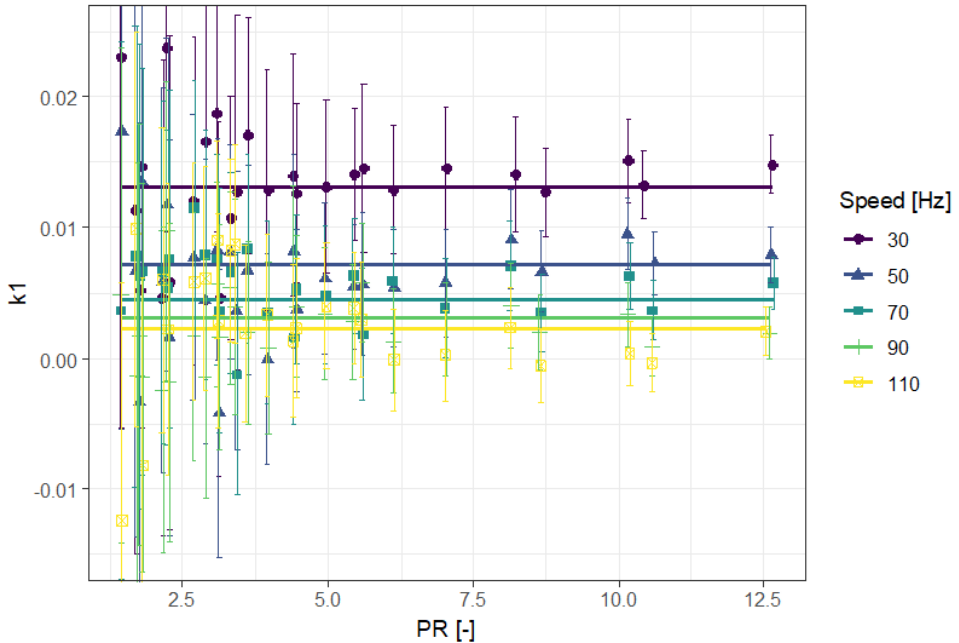
**Figure 3.22: Evolution of k_1 as a function of pressure ratio and speed**

Figure 3.22 shows high data dispersion at low PR which can be explained by empirical error, specially by the power meter uncertainty (check the uncertainty bars). On the other hand, at medium and high PR the empirical uncertainty decreases allowing the study of the effect of speed in k_1 : at low speeds the effect of PR in specific losses is high and tends asymptotically to zero as speed reduces. This effect can be modelled with the correlation in Eq.(3.29) whose predictions are displayed in Figure 3.22 with solid lines.

$$k_1 = k_{10} + k_{11} \frac{1}{f_{c,rat}} \quad (3.29)$$

Once the effect of the different variables in compressor losses has been analyzed, Eq.(3.27), Eq.(3.28) and Eq.(3.29) can be fusion into a final correlation for η_{em} [Eq. (3.30)] from where Eq.(3.22) is deduced.

$$\eta_{em} = \left(1 - k_0 - \left(k_1 + k_2 \frac{1}{f_{c, rat}} \right) RP \right) - \frac{W_{loss,0}}{\dot{W}_c} \quad (3.30)$$

3.11. Nomenclature

Abbreviations

CV	coefficient of variance of RMSE
displ	compressor displacement
PR	Pressure Ratio
RMSE	root mean square error

Symbols

f_c	compressor speed [Hz]
$k_{\#, S\#, C\#}$	fitting coefficients
k_c	compressor efficiency ratio
k_m	mass flow ratio
k_p	consumption ratio
k_v	volumetric efficiency ratio
\dot{m}	mass flow [g/s]
P	pressure [bar]
SH	Super Heat [K]
T	temperature [K]
\dot{W}_c	compressor consumption [W]
\bar{X}	Magnitude average

Sub index

0	at no load
1	suction
2	discharge
c	condensing
e	evaporating
esp	specific (divided by \dot{m})
is	isentropic
nom	at reference speed
rat	ratio with nominal conditions

Super index

#	at reference SH
'	redefined

Greek letters

α	loss fraction of effective work
η_c	compressor efficiency
η_{em}	electromechanical efficiency
η_{is}	isentropic efficiency
η_v	volumetric efficiency
ρ	density [kg/m ³]

Chapter 4:

THIRD PUBLICATION





Thermal Science and Engineering Progress

Volume 46, 1 December 2023, 102229



A novel methodology to assist manufacturers in the heat exchanger sizing for variable-speed heat pumps based on part load conditions and economic assessment

Rubén Ossorio  , Emilio Navarro-Peris, Javier Marchante-Avellaneda

<https://doi.org/10.1016/j.tsep.2023.102229>

Heat Exchanger sizing for Variable-Speed Heat Pumps based on part load conditions and economic assessment

Rubén Ossorio, Emilio Navarro-Peris, Javier Marchante-Avellaneda
Instituto Universitario de Investigación en Ingeniería Energética (IUIIE)
Universitat Politècnica de València, Camino de Vera s/n, ed. 8E cubo F 5º, Valencia,
46022, Spain

4.1. Abstract

Matts Bäckström assessed the selection criteria of heat exchangers for single-speed heat pumps in 1940, and his methodology and conclusions have been kept practically unchanged for almost a century. However, heat pump systems have evolved, especially with the introduction of variable-speed heat pumps. These new systems introduced a new degree of freedom to the heat pump design - the compressor speed - which is not considered by traditional design criteria.

This study proposes novel design criteria to optimize the heat exchanger size when the heat pump unit can work under part-load conditions. The proposed method models how heat exchangers and variable-speed compressors perform under different loads and sizes. It considers part-load requirements based on climatic data (which are typically available in the standards) and considers economic factors such as initial investment and operation costs (which are dependent on the components' size). Given the mentioned information, a multivariable optimization algorithm is implemented to find the optimum heat exchanger size that minimizes the total cost. To validate the proposed approach's effectiveness, it was exemplified by determining the optimum size of a coil and a plate heat exchanger for a domestic variable-speed heat pump. The results demonstrate that using traditional criteria could lead to over-dimensioning heat exchangers in variable-speed heat pumps, which could incur a cost increase of 5% for the studied case.

Keywords: Variable-speed heat pump, selection criteria, heat exchanger, part load, optimization, design

4.2. Introduction

Heat pumps (HP) have become an increasingly popular choice in the heating and air conditioning sector due to their efficiency, reliability and affordability. That is why the European Union has recognized them as a key technology to reduce CO₂ emissions and achieve the objectives proposed in the European Green Deal to become climate-neutral by 2050 (European Commission, 2021).

Heat Pumps, especially those with an external unit, work under varying climatic conditions, which strongly affects their performance. Consequently, an annual performance evaluation is needed to fairly compare HP among them and to their counterparts (gas and electric boilers). In Europe, the standards (European Commission No 811/2013, 2013; European Commission, 2018a) establish a letter code (from A+++ to G) for each device to rank the different solutions based on its yearly efficiency, which is calculated according to three different weather profiles: Cold, Intermediate and Warm, based on Helsinki (Finland), Strasbourg (France) and Athens (Greece) reference temperatures respectively. Figure 4.1 shows the required heating hours for the three different climate profiles and which profile applies to each region.

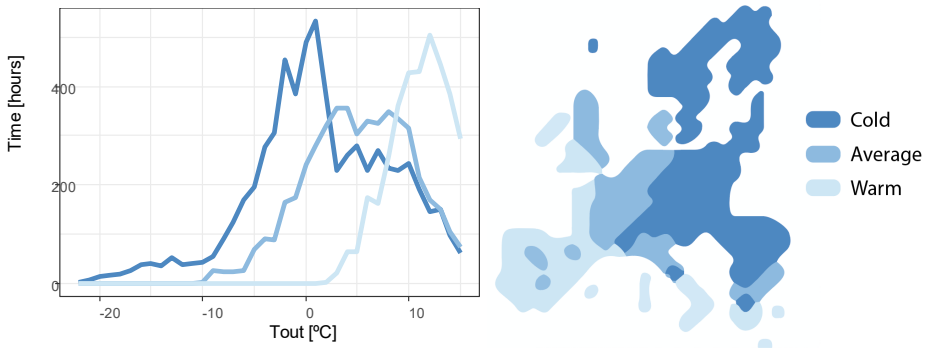


Figure 4.1: Climate profiles according to the standard (European Commission, 2018a)

The standard also provides information about the relation between the required heating capacity at each external temperature and the rated conditions of the heat pump. Eq.(4.1) represents this relation consisting of a straight line starting from the rated heating capacity at the nominal temperature and reaching null heating requirements at external temperatures of 16 °C.

$$\dot{Q}_{req} = \frac{t_{ext} - 16}{t_{nom} - 16} \dot{Q}_{nom} \quad (4.1)$$

As shown in Figure 4.1, thermal loads significantly fluctuate throughout the year, and thus, capacity control in HP is necessary. Historically, ON/OFF cycling was the preferred control strategy; however, since the introduction of variable-speed compressors (VSC), the modulation of the compressor speed to modify the HP capacity has become more attractive as it can result in significant energy savings and better comfort (Qureshi & Tassou, 1996) (R.S.Adhikari et al., 2012).

However, with variable-speed heat pumps (VSHP), a new degree of freedom in the analysis of these devices arises – the speed – which directly affects the methodologies to model, select and design its components.

In recent years, numerous papers have been published studying VSHPs, which are collected in the review articles of Aynur (Aynur, 2010), Lin Lee et al. (Lin et al., 2015) and Zhang et al. (Zhang et al., 2019). Additionally, other studies focused on modeling VSCs proposing correlations to predict compressor mass flow and energy consumption (Shao et al. (Shao et al., 2004), Mendoza-Miranda et al. (Mendoza-Miranda et al., 2016), Ossorio and Navarro-Peris (Ossorio & Navarro, 2023)). And others focused on inverter power losses (Cuevas and Lebrun (Cuevas & Lebrun, 2009) and Ossorio and Navarro-Peris (Ossorio & Navarro, 2023)).

Regarding sizing criteria, Bagarella et al. (Bagarella et al., 2016) studied the influence of cycling losses in the sizing strategy of on-off and variable-speed compressors. However, there is a lack of studies evaluating the sizing criteria of heat exchangers for variable-speed heat pumps, as this topic is only treated for fixed-speed heat pumps.

For the selection of HX in fixed-speed heat pumps, the work of Matts Bäckström has to be highlighted, which already in 1940 assessed the selection criteria of heat exchangers in his study "Economic Optimum Problems in Connection with Refrigeration" (Bäckström, 1940). In his research, Bäckström selected the temperature difference between the HX and the source or sink as an optimization parameter and proposed a techno-economic methodology considering investment capital and operational cost. This methodology is still in use today and is reflected in "Refrigerating Engineering" by Granryd and Palm (Granryd & Palm,

2003), in which a table with optimum temperature differences is displayed for either evaporators and condensers as a function of its technology and operation time.

More recent literature also assessed the selection of heat exchangers. Mancini et al. (Mancini et al., 2018) focused on the design of plate evaporators for zeotropic mixtures. Wang and Sundén (L. Wang & Sundén, 2003), Caputo et al. (Caputo et al., 2008) and Unuvar and Kargici (Unuvar & Kargici, 2004) studied the optimal design of plate heat exchangers for general use. Jiang et al. (Jiang et al., 2022) proposed a general guideline for selecting heat pump systems based on economic analysis. Finally, Dai et al. (Dai et al., 2019) (Dai et al., 2023) analyzed the design of CO₂ heat pumps in China for space heating, including in the study calculations for heating loads and calculations for HX required area.

However, the mentioned methodologies do not consider new degrees of freedom, such as compressor speed and/or designing the system for a fixed and stationary condition (not including the variation of the external temperatures and loads). Moreover, it should be pointed out that, if a heat exchanger is designed for its maximum capacity, it would be over-dimensioned when the VSHP works at part load (most of its lifetime).

To assess these issues, this study proposes a new methodology for sizing heat exchangers for a VSHP. It combines an improved techno-economic analysis including the speed modulation and incorporates climatic weather profiles available in the standards to account for the variation of external conditions. The methodology is meant to be simple and comprehensible so it can be easily implemented in the first steps of the heat pump design process. To exemplify the proposed method, it has been applied to the sizing of the heat exchangers of an air-to-water HP for domestic space heating and its results have been compared with the ones obtained by Bäckström classical criteria. Furthermore, for modeling the HP performance, simplified correlations for predicting temperature differences between the HX and the secondary fluids have been proposed for either the coil and the plate HX. Regarding the compressor modeling, a simple correlation is proposed, which takes into account its working limits.

4.3. Methodology

4.3.1. Bäckström

As mentioned in the introduction, in 1940 Matts Bäckström published a study which settled the bases of HX selection. The chosen selection variable was the optimum temperature difference between the sink or the source and the evaporating or condensing temperature, respectively. This optimum temperature difference is a parameter that directly depends on the heat exchanger's size and global transfer coefficient.

To choose the optimum temperature difference in the HXs, Bäckström minimized the cost function displayed in Eq.(4.2).

$$C = aI + \kappa_e \tau \dot{E} + \text{constants} \quad (4.2)$$

In which the first term represents the yearly capital costs (I representing the total capital investment and a the annuity factor) and the second represents the annual operational cost (κ_e representing the energy cost, τ the working hours and \dot{E} the power consumption of the unit). To define the variables as a function of HX temperatures, the investment was expressed with the marginal investment cost κ_{HX} , representing how capital costs increase with the HX size (Eq.(4.3)).

$$I = \kappa_{HX} UA = \kappa_{HX} \frac{\dot{Q}_{HX}}{\Delta T_{HX}} \quad (4.3)$$

And for energy consumption, the expression in Eq.(4.4) was used, assuming a constant Carnot efficiency.

$$\dot{E} = \frac{\dot{Q}_{cond}}{COP} = \frac{\dot{Q}_{cond}}{\eta_{Ct} \frac{T_{cond}}{T_{cond} - T_{evap}}} = \dot{Q}_{cond} \frac{T_{cond} - T_{evap}}{\eta_{Ct} T_{cond}} \quad (4.4)$$

Eq.(4.5) can be obtained by substituting both Eq.(4.3) and Eq.(4.4) in Eq.(4.2). And finally, Eq.(4.5) can be solved for an optimum temperature difference (ΔT) in either the condenser or in the evaporator.

$$C = a \left[\frac{\kappa_{evap} \dot{Q}_{evap}}{\Delta T_{evap}} + \frac{\kappa_{cond} \dot{Q}_{cond}}{\Delta T_{cond}} \right] + \kappa_{el} \tau \dot{Q}_{cond} \frac{(t_{sink} + \Delta T_{cond}) - (t_{source} - \Delta T_{evap})}{\eta_{Ct} (t_{sink} + \Delta T_{cond})} \quad (4.5)$$

Eq.(4.5) depends on the following:

- Economically linked variables which are the result of an economic assessment as: a (the annuity factor), κ_{evap} , and κ_{cond} (the marginal cost of the HX per "size") and κ_e (the cost of the energy needed to operate the HP).
- Characteristic parameters of the HP as \dot{Q}_{evap} , \dot{Q}_{cond} and η_{Ct} (which is considered by Bäckström constant in the range of interest).
- External working parameters, as t_{sink} , t_{source} (working temperatures) and τ (total operation hours), which depend on the application and on the working condition.
- HX temperature differences ΔT_{cond} and ΔT_{evap} , which mainly depend on the size and typology of the heat exchangers. They are the optimization variables that are chosen to minimize the total cost (C).

Once this function is built, Bäckström performs the partial derivatives of the cost function with ΔT_{cond} and ΔT_{evap} respectively and equals the new expressions to zero to look for minimum cost. This methodology results in two formulas that can be used to calculate the optimum ΔT directly and in a semi-independent manner (it is not entirely independent as for the optimization of one HX information of the optimum ΔT of the other HX is needed, which is approximated or guessed).

The main limitation of this methodology is that the optimization is made for a single condition and, as it is known, air-water HP working conditions significantly vary over time, especially in the external air unit as external temperature changes. One simplistic approach could be to design the HP at the rated or at the most repeated condition, which has been a common methodology.

However, a better solution would be to combine Bäckström methodology with the information provided in the HP rating standard. The standard offers information regarding working hours and required heating capacity at each external condition Eq.(4.1). For example, the conditions in Figure 4.2 would apply for

a HP working in an intermediate climate with a rated heating capacity of 6.5 kW at -10 °C.

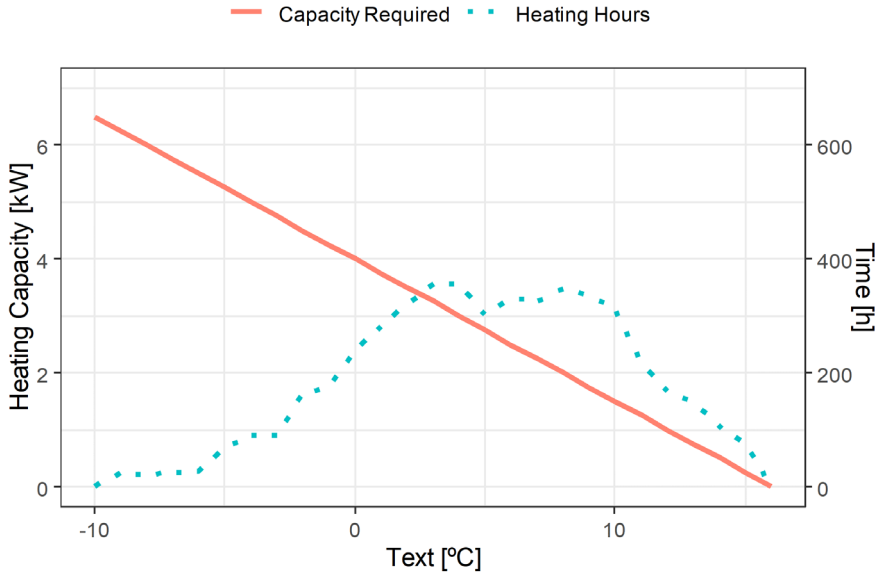


Figure 4.2: Operating hours and heat capacity required as a function of external temperature for a HP with a rated capacity of 6.5kW working in an intermediate climate

Consequently, the required heating capacity and expected heating hours in a year can be obtained for a given HP and for each external temperature. And with the given information, the cost equation can be rewritten as shown in Eq.(4.6):

$$\begin{aligned}
 C &= a \left[\frac{\kappa_{evap} \dot{Q}_{evap,nom}}{\Delta T_{evap,nom}} + \frac{\kappa_{cond} \dot{Q}_{cond,nom}}{\Delta T_{cond,nom}} \right] \\
 &+ \sum_{bin} \kappa_e \tau_{bin} \dot{Q}_{cond,bin} \frac{(t_{sink,bin} + \Delta T_{cond,bin}) - (t_{source,bin} - \Delta T_{evap,bin})}{\eta_{Ct} (t_{sink,bin} + \Delta T_{cond,bin} + 273.15)} \quad (4.6)
 \end{aligned}$$

In this way, the operational costs are divided into bins (one for each external temperature), and for each bin, the standard gives information of τ , \dot{Q}_{cond} and t_{source} . Regarding t_{sink} , the standard defines four different conditions (35, 45, 55

and 65 °C) depending on the application. The only still missing parameter is $\dot{Q}_{evap,nom}$ that can be approximated with Eq.(4.7):

$$\dot{Q}_{evap,nom} = \dot{Q}_{cond,nom} - \dot{W}_{compr} = \dot{Q}_{cond,nom} \left(1 - \frac{1}{\eta_{ct} COP_{ct}}\right) \quad (4.7)$$

Consequently, if the economic parameters are also known, the only non-defined information is how ΔT evolves in the HX for different external conditions (ΔT_{bins}). Nevertheless, a heat exchanger model can be used to predict ΔT_{bins} based on a ΔT_{nom} and on the working condition of each bin. With that, the only non-defined parameters would be the optimum temperature differences in both HXs ($\Delta T_{evap,nom}$, $\Delta T_{cond,nom}$), which are the optimization variables of the proposed methodology as they dictate the size of the heat exchanger.

4.3.2. Evaporator model

The objective of this section is to provide a correlation that predicts the temperature difference between the refrigerant and the external environment (ΔT) in a coil HX as a function of:

- Heating capacity: which can be easily retrieved from the standard for each external condition
- Sizing parameter: for example, coil width, a design parameter that increases total exchange area without significantly affecting the heat exchange mechanism and flow patterns.

IMST-ART, a detailed heat pump model, was used to study the effect of these variables in ΔT . IMST-ART (IMST,2023), is an advanced heat pump simulation software that combines accurate and fast correlations to model HP systems using as input only geometric and easy-to-obtain data from catalogs. This tool allows a detailed description of HXs (row number, tubes per row, tube spacing, number of parallel circuits and their distribution, fin pitch, material properties...). IMST-ART implements heat transfer coefficient and pressure drop correlations discretized for virtual discrete volumes in the heat exchanger and solves a complete simulation of the whole system in less than 20 seconds. Additionally, it has been proven to be robust and has been validated against extensive experimental data at steady-state conditions (Corberan et al., 2008; Corberán et al., 2011; Piscopiello et al., 2016; Pitarch et al., 2017) with prediction errors between 5%

and 10% of Maximum Relative Error. It should be remarked that for this study the frost formation won't be considered to keep it simpler and more readable.

Figure 4.3 displays the IMST-ART results obtained for ΔT at different heating capacities and different coil sizes. The modified sizing parameter was the coil width, and the various heating capacities were introduced in the detailed model by varying the external temperatures and compressor speeds. Regarding the other HX parameters defined in the simulations, the studied evaporator had 3 rows, 8 parallel circuits, 32 tubes per row, a longitudinal tube spacing of 19 mm, a transversal tube spacing of 25 mm and a fin pitch of 2 mm. The air velocity was considered to be 1.5 m/s and the airflow is variable with the coil width; as the coil gets wider, more fans will be installed.

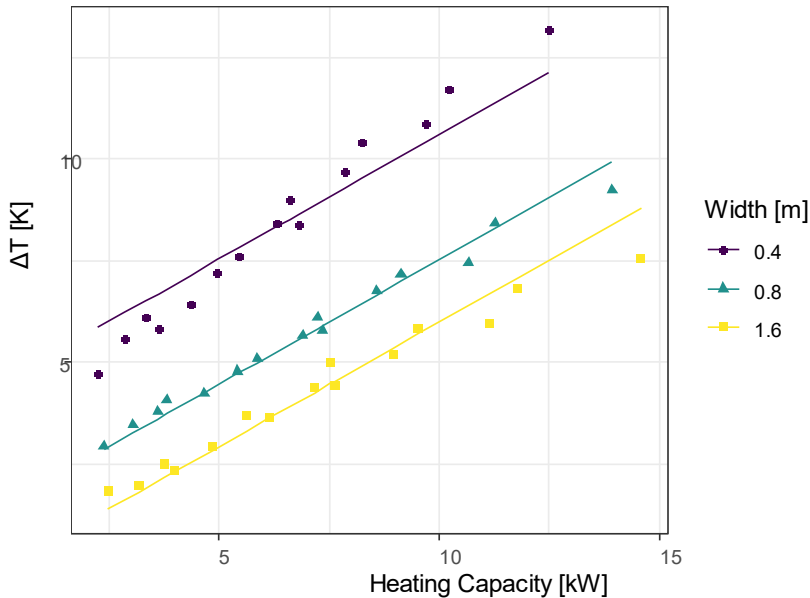


Figure 4.3: Dependence of ΔT in the evaporator as a function of heating capacity and coil width and prediction of the used model

The results show a linear correlation between Heating Capacity and ΔT in the evaporator. Regarding the effect of the coil size, as width diminishes, the total exchange area decreases and ΔT increases accordingly, just as expected. What is remarkable is that the dependence between heat capacity and ΔT (slope) does

not seem to be significantly affected by the width change. With those results, the following simplified evaporator model is proposed:

$$\Delta T_{evap} = \left(k_{00} + \frac{k_{01}}{Width} \right) + k_1 \dot{Q}_{cond} \quad (4.8)$$

The term between brackets is a constant that only depends on the size and consequently, for a given HX, it disappears if the expression is given in differences with respect to a nominal condition ($\Delta T_{e,nom}$ and $\dot{Q}_{cond,nom}$). The result of expressing the model with respect to nominal conditions is shown in Eq.(4.9).

$$\Delta T_{evap,bin} = \Delta T_{evap,nom} + k_1 (\dot{Q}_{cond,bin} - \dot{Q}_{cond,nom}) \quad (4.9)$$

Eq.(4.9) only uses one coefficient and can be substituted in the general cost expression [Eq.(4.6)], so all the terms inside the summation are referenced to the optimization parameter that is $\Delta T_{evap,nom}$. Additionally, once the optimum ΔT_{nom} has been obtained, Eq.(4.10) can be used to predict an optimum coil width.

$$Width_{opt} = \frac{k_{01}}{\Delta T_{evap,nom_{opt}} - k_1 \dot{Q}_{cond,nom} - k_{00}} \quad (4.10)$$

4.3.3. Condenser Model

With the condenser, a similar methodology was used to obtain a simplified correlation to estimate ΔT as a function of heating capacity and a sizing parameter.

First, the detailed heat pump model IMST-ART was used to study the dependence of operating variables on ΔT . IMST-ART allows the simulation of different lengths, widths, number of plates and can also define the plate's pitch, thickness and used material. Additionally, a parametric study of the inlet water temperature and its mass flow can also be carried out. In case IMST-ART is not available, other alternatives, such as SSP calculator from SWEP (SWEP, 2023) could be used to obtain the fitting coefficients.

Figure 4.4 shows the obtained ΔT simulated with IMST-ART in the condenser at different heating capacities, number of plates and water temperature steps. The modelled condenser had a length and width between ports of 0.478 m and 0.073 m respectively and the plates had a pitch of 2.35 mm and thickness of 0.4 mm. Regarding the waterside, the outlet water temperature was 35 °C and the

water mass flow was the one required to reach the desired temperature step in the waterside (ΔT_{water}).

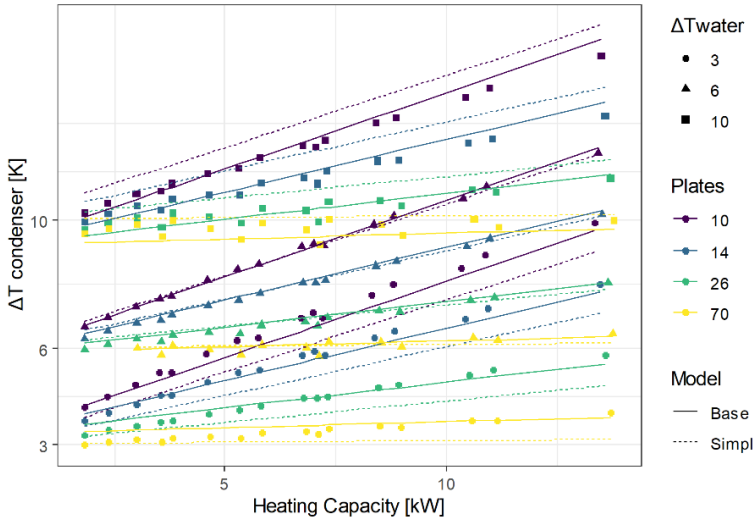


Figure 4.4:: Dependence of ΔT as a function of heating capacity and number of plates and prediction of the used models

The results also show a linear dependence of ΔT_{cond} with heating capacity. Modifying the number of plates mainly affects the slope of the dependence with heating capacity, not the intercept (contrary to the coil heat exchanger). In fact, it can be checked that a common intercept exists, which has been proven to depend mainly on the water temperature difference. With the information provided by the simulations, the simplified model in Eq.(4.11) was proposed:

$$\Delta T_{cond} = k_0 + \left(k_{10} + \frac{k_{11}}{Plates} \right) \dot{Q}_{cond} \quad (4.11)$$

$$k_0 = \begin{cases} \Delta T_{water} \\ k_{00} + k_{01} \Delta T_{water} \end{cases}$$

The definition of the intercept k_0 has two different approaches:

The simplified one considers it to be equal to ΔT_{water} , it is the simpler one and fits well the general trend but incurs more significant errors at high and low ΔT_{water} . Its predicted values are displayed in Figure 4.4 with dotted lines.

On the other side, if more precision is required, k_0 can be defined as a linear function of ΔT_{water} giving excellent results. Its performance can be checked out in Figure 4.4 with solid lines.

Regarding ΔT_{water} and the service temperature, the standard defines them as a function of:

- **Application:** the reference service temperature is 35, 45, 55 or 65 °C for low, intermediate, medium and high-temperature applications, respectively.
- **Water pump:** if it can vary its speed, then $\Delta T_{water} = 5 K$ is assumed for all conditions. Else, the water flow is established to provide $\Delta T_{water} = 5 K$ for the standard rating condition given in EN 14511-2 and then that water flow is kept constant for the rest of the conditions.

Given the model in Eq.(4.11), its slope (k_1) can be calculated with Eq.(4.12) given a nominal condition ($\Delta T_{nom}, \dot{Q}_{cond,nom}$).

$$k_1 = \left(k_{10} + \frac{k_{11}}{Plates} \right) = \frac{\Delta T_{cond,nom} - k_0}{\dot{Q}_{cond,nom}} \quad (4.12)$$

And if Eq.(4.11) and Eq.(4.12) are combined and rearranged Eq.(4.13) is obtained:

$$\Delta T_{cond,bin} = \Delta T_{cond,nom} \frac{\dot{Q}_{cond,bin}}{\dot{Q}_{cond,nom}} + k_0 \left(1 - \frac{\dot{Q}_{cond,bin}}{\dot{Q}_{cond,nom}} \right) \quad (4.13)$$

With this equation, each ΔT_{bin} is calculated based on ΔT_{nom} . Consequently, this equation can be substituted into the modified Bäckström expression in Eq.(4.6) so the only unknown temperature difference on the condenser side is $\Delta T_{cond,nom}$.

Once the optimum $\Delta T_{cond,nom}$ has been obtained, Eq.(4.12) can be used to calculate the optimum number of plates in the condenser (taking into account that it should be a pair number). It should be noted that if the simplified model is considered ($k_0 = \Delta T_{water}$), Eq.(4.13) won't contain any fitting coefficient and thus, no condenser model would be needed to calculate the optimum $\Delta T_{cond,nom}$.

4.3.4. Compressor model

The compressor is the device in charge of modulating the heating capacity to adapt it to the load. The modulation is carried out by varying the compressor speed in a range that can differ from model to model but typically ranges from less than 30 Hz to values slightly higher than 120 Hz. A typical modulating scheme is displayed in Figure 4.5.

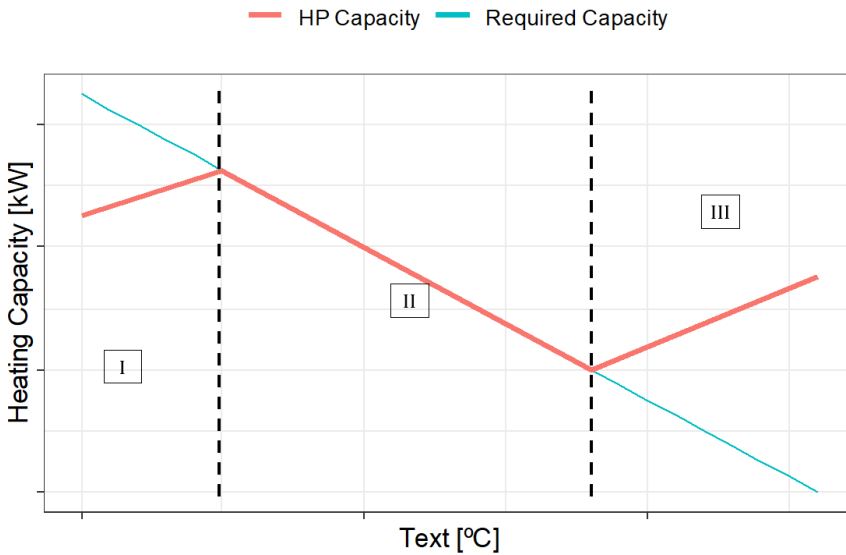


Figure 4.5: Heat pump operational zones

Figure 4.5 shows three different operating zones. In the middle part, the VSHP manages to modulate its capacity to exactly fit the thermal load. At low external temperatures, the compressor speed reaches its maximum, the heat pump is unable to provide enough heating capacity and a backup heating system is required (typically a boiler or an electric heater). On the other hand, when the outdoor temperature is warmer, the compressor reaches its lowest speed, starts providing more heat than required and starts to cycle between ON/OFF states.

To correctly model the three differentiated areas, a compressor model is required to correlate the compressor speed with the provided heating capacity. In

order to provide a simplified expression, the heating capacity was modeled only as a function of evaporating temperature and speed, as shown in Eq.(4.14).

$$\dot{Q}_{cond} = c_0 + c_1 f_c + c_2 t_{evap} f_c + c_3 t_{evap}^2 f_c \quad (4.14)$$

It can be justified to model the capacity only with evaporating temperature as it determines the refrigerant mass flow which directly affects the provided capacity. Condensing temperature also affects heating capacity, but the effect is weaker, and in the described application, the condensing temperature remains relatively constant as the service water temperature does not vary significantly over the year.

The model performance can be visualized in Figure 4.6, in which the dots represent the results obtained from IMST-ART and the lines represent the model predictions. The maximum relative error is close to 5% and the RMSE is lower than 100 W.

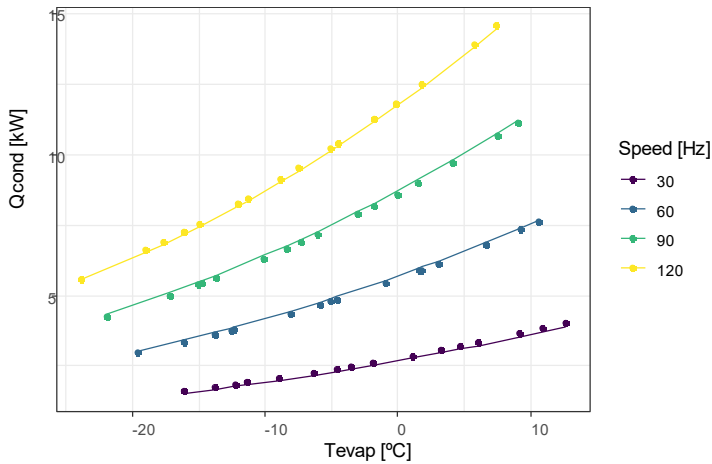


Figure 4.6: Compressor model performance

Consequently, knowing the heating requirements and the evaporating temperature ($T_{evap} = T_{ext} - \Delta T_{evap}$), it is possible to calculate the compressor's working speed with Eq.(4.14). However, ΔT_{evap} is not known *a priori* as it is a result of applying the evaporator model, which in turn needs to know the operation zone of the HP. Therefore, an iterative calculation is needed, which will be detailed in the following section.

Additionally, when using Eq.(4.14), the required working speeds can result in values higher than the compressor's maximum speed. In that case, the compressor model uses as input $f_{c,max}$ to calculate the maximum heating capacity that the compressor is able to produce at that condition. This procedure will also be used when the required speed is less than $f_{c,min}$ to calculate the actual capacity produced.

For zone I, the backup system will start working to reach the desired capacity and thus, another power-consuming element will appear in the system which, in the case of an electrical heater, can be modeled by adding the term appearing in Eq.(4.15) to the general cost equation in Eq.(4.6).

$$\sum_{bin} \kappa_e \tau_{bin} \dot{Q}_{aux,bin} \quad (4.15)$$

Being $\dot{Q}_{aux,bin}$ the extra capacity needed to reach the required one ($\dot{Q}_{req,bin}$). It can be calculated with Eq.(4.16).

$$\dot{Q}_{aux,bin} \begin{cases} \dot{Q}_{req,bin} - \dot{Q}_{cond,bin} & \text{if } \dot{Q}_{req,bin} > \dot{Q}_{cond,bin} \\ 0 & \text{if } \dot{Q}_{req,bin} < \dot{Q}_{cond,bin} \end{cases} \quad (4.16)$$

For zone III, the compressor will oscillate between on and off states, so the total operating time in the third zone should be reduced using the following formula Eq.(4.17).

$$\tau_{bin} \dot{Q}_{cond,bin} = \tau_{req} \dot{Q}_{req,bin} \quad (4.17)$$

4.3.5. Optimum temperature difference

Once a simplified model is proposed for each key element of the system, all the information can be put together to find the optimum economic HX size.

As mentioned in the previous section, an iterative calculation is needed to determine the different compressor zones. A diagram showing the general calculation flow is displayed in Figure 4.7 for better understanding.

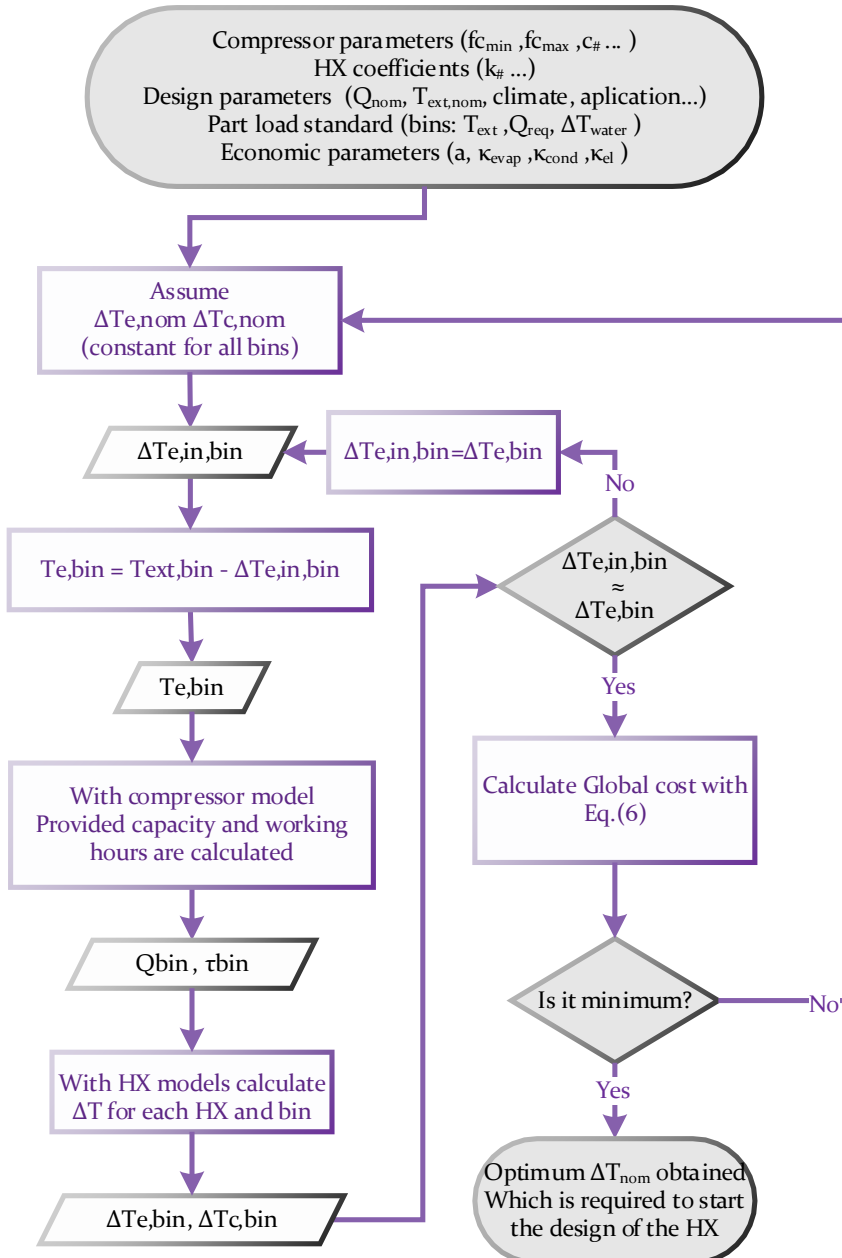


Figure 4.7: Calculation flow for sizing HXs

First a HX size is assumed for the evaporator and condenser which translates in assuming a ΔT_{nom} , which is the temperature difference between the refrigerant and the secondary fluid at nominal conditions ($T_{ext,nom}, \dot{Q}_{nom}$). Initially, ΔT_{nom} is considered to be constant under all external conditions. Then, the evaporating temperature is calculated and the compressor zones are established. The new Q_{bins} are calculated for zone I and III with $f_{c,max}$ and $f_{c,min}$ respectively, and total operating time is corrected with Eq.(4.17) in zone III. Once Q_{bins} are calculated, both HX models are used to calculate their respective ΔT which won't be constant for all conditions anymore. With this new ΔT_{evap} the compressor model and HX correlations are used again in an iterative way until the solution converges (the convergence is often achieved in a couple of iterations). Once the performance of the HP is modelled, the cost formula in Eq.(4.6) can be used to estimate the total cost. The described procedure is repeated changing ΔT_{nom} in evaporator and condenser until the minimum cost is reached. Once $\Delta T_{nom,opt}$ has been found for both HX, Eq.(4.10) and Eq.(4.12) can then be used to obtain the optimum width of the coil and the optimum number of plates in the condenser.

This procedure can be performed independently for the evaporator and condenser, assuming approximate data for the other heat exchanger. However, if higher accuracy is needed, multivariable optimization algorithms can be used so both optimizations are carried out simultaneously.

4.4. Results

4.4.1. Optimization of HX size

The described methodology has been exemplified with the HX optimization of an air-to-water HP for a low-temperature application with a required nominal capacity of 6.5 kW at external conditions of $-10\text{ }^{\circ}\text{C}$ and working in an intermediate climate profile. A preliminary analysis has decided to use the typology of HXs described in the methodology section, whose model parameters are displayed in Table 4.1:

Table 4.1: Model coefficients of the HXs and Compressor

	Model coefficients					
	k0		k1		RMSE	CV
	k00	k01	k10	k11		
Coil Evaporator	0.7814	0.77332	0.73083		0.328	4.61
Plate Condenser	0.8963	0.81633	-0.03324	5.3225	0.258	3.852
	c0	c1	c2	c3	RMSE	CV
Compressor	0.1795	3.12E-03	3.21E-05	-0.3137	0.129	1.904

The supplied hot water is provided at $35\text{ }^{\circ}\text{C}$ and is circulated with a variable speed pump that ensures a water temperature difference of 5 K. The compressor starts cycling at speeds lower than 30 Hz and it is able to provide the desired rating capacity at its maximum speed of 120 Hz, so there is no need for auxiliary systems. The different working zones of the compressor in the exemplified application are displayed in Figure 4.8. The cycling starts at external temperatures close to $5\text{ }^{\circ}\text{C}$, and from there, the operating hours are reduced by applying Eq.(4.17).

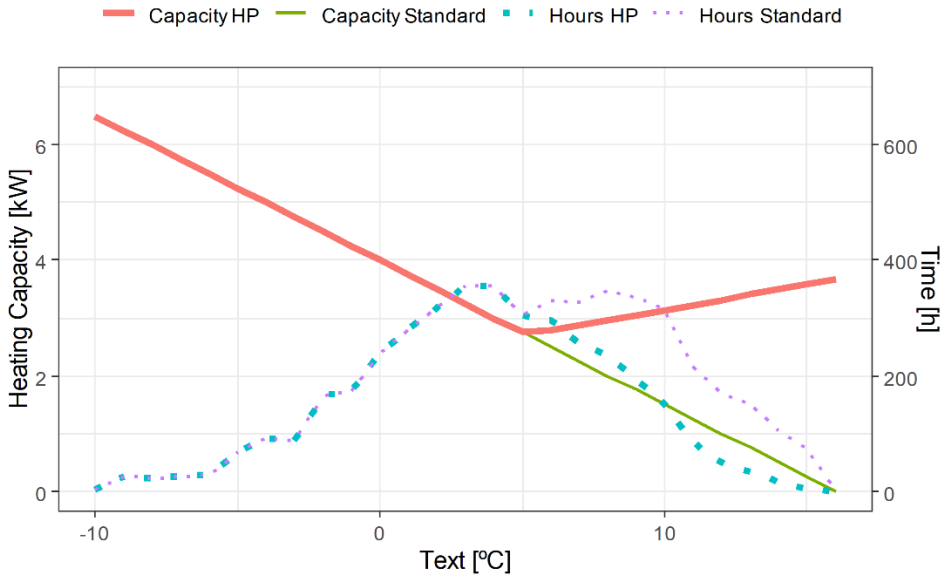


Figure 4.8: Compressor zones in the optimum condition and working hours for each bin

The rest of the input parameters were considered to be the same used in “Refrigeration Engineering” (Granryd & Palm, 2003) when exemplifying Bäckström methodology so a direct comparison could be performed. Regarding economic parameters: $a = 0.25$, $k_e = 0.5 \frac{SEK}{KWh}$, $k_{evap} = 2000 \frac{SEK}{KW \cdot K}$ and $k_{cond} = 1430 \frac{SEK}{KW \cdot K}$. And last but not least, Carnot efficiency was considered constant and equal to 0.45 (as also stated in (Granryd & Palm, 2003)).

Given the input information, the iterative procedure described in Figure 4.7 was coded in R-language (R Core Team, 2022), and a genetic algorithm (Scrucca, 2013) was implemented for the multivariable optimization so both temperature differences in the evaporator and condenser are optimized simultaneously for more accurate results.

In Figure 4.9, the evolution of the costs with the ΔT in the HX is displayed for the optimum solution. The total cost is the result of adding the capital and operational costs and it is represented with a solid line.

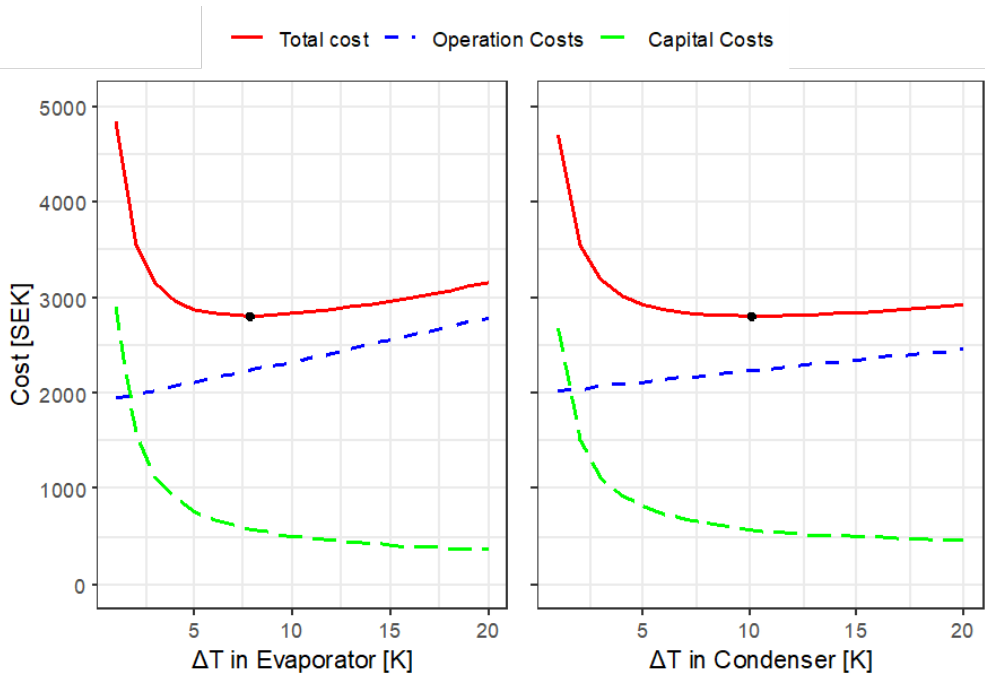


Figure 4.9: Optimization of temperature differences in heat exchangers using (4.6)

An increase in ΔT implies using a smaller HX, which reduces the capital costs. On the contrary, a high ΔT increases the difference between evaporating and condensing conditions reducing COP and increasing the operational cost. If both effects are added the total costs are obtained, whose minimum is found with the optimization algorithm and is marked with a dot in Figure 4.9. For the studied case, the optimum temperature difference in the coil evaporator is 7.78 K and 10.1 K in the plates condenser resulting in a total cost of 2803 SEK.

With these results, Eq.(4.10) and Eq.(4.12) can be used to select the HX dimensions, which results in a coil width close to 0.5 m (0.448 m) for the evaporator and a condenser with six plates. The resulting number of plates is relatively small so other plate HX with a lower length between ports could be selected.

Note that the difference in the slope of the operational cost is steeper in the case of the evaporator, even if the energy cost is the same for both cases. That results in a flatter total cost for high ΔT in the condenser, which in turn makes the optimum cost less sensitive to variations of the selected ΔT in the optimum

range. The explanation for this different behavior is that, as ΔT_{evap} changes, the compressor working zones change accordingly, varying the working hours and affecting the operational costs. On the other hand, the operational costs are more stable with the variation of ΔT_{cond} as it does not affect the compressor working zones.

A rigorous direct comparison with the pure method presented by Bäckström can't be made as the variation of the external conditions can't be considered. However, if Eq.(4.5) is applied and it is assumed that the HP is operated consistently at the nominal conditions ($t_{source} = -10\text{ }^{\circ}\text{C}$ and $t_{sink} = 35\text{ }^{\circ}\text{C}$) the solution in Figure 4.10 is obtained.

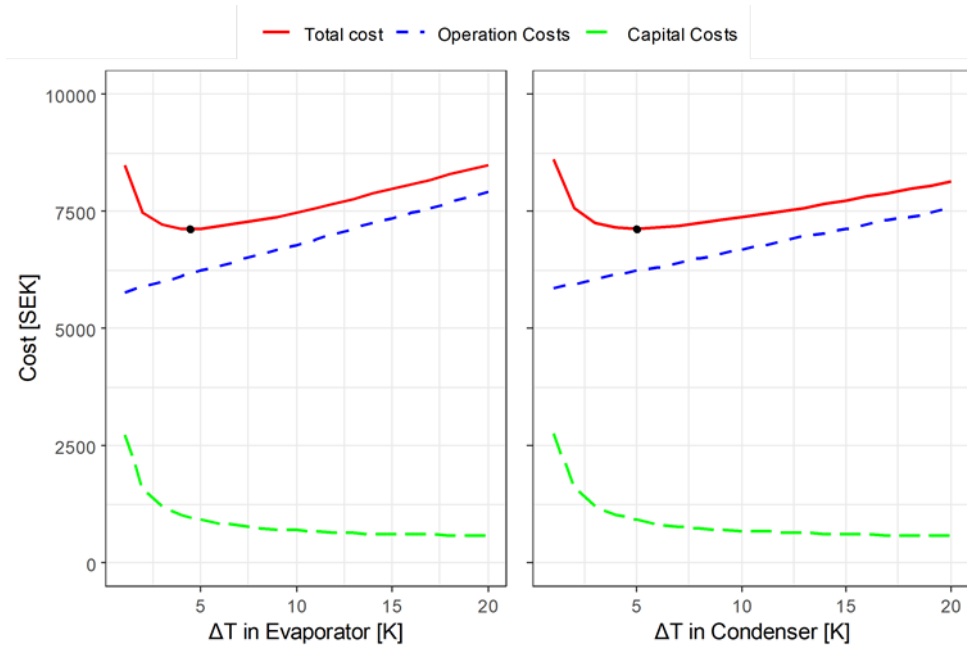


Figure 4.10: Optimization of temperature differences in heat exchangers with Bäckström method

The optimum ΔT in the evaporator and condenser would be $4.46\text{ }^{\circ}\text{C}$ and $4.98\text{ }^{\circ}\text{C}$ respectively and the annual minimum cost ascends to 7130 SEK, double as much as the part-load solution. This is unrealistic due to the fact that the HP is always working at its maximum consumption zone, which also affects the

sensibility of the solution, which is steeper for both cases compared to the part-load solution.

To conclude this section, it will be assessed the potential cost savings associated with the proposed methodology when compared to conventional approaches. In order to do that, the optimal solution obtained with Bäckström criteria has been integrated to the cost function of the proposed new method (which is capable of accurately calculate the total cost considering all part load available information).

As a result, if the new part-load cost equation is evaluated with a ΔT close to 5K in either the condenser and evaporator (representing the Bäckström-designed configuration), the obtained total expense incurred amounts to 2943 SEK. This represents a 5% cost increase compared with the optimized solution. It is essential to highlight that this incremental cost is specific to the particular application under analysis and it is expected to vary across different applications, potentially reaching substantially higher values.

4.4.2. Influence of the economic parameters on the optimization

The optimization solution depends on the chosen economic parameters that must be obtained from an economic analysis. In the following, the influence of these parameters on the optimal solution will be studied.

The described optimization methods were applied varying each economic parameter *ceteris paribus* and the results are displayed in a grid of plots in Figure 4.11. In each row a different cost equation was used: in the first row, Bäckström original formula was used without considering part-load [Eq.(4.5)], while in the second, part-load was considered using Eq.(4.6). Regarding the columns, each represents the parametric study of a different economic variable: k_e , k_{evap} and k_{cond} respectively. In each plot, the different cost curves obtained in the parametric study are represented with solid lines and the optimums are marked with a dot.

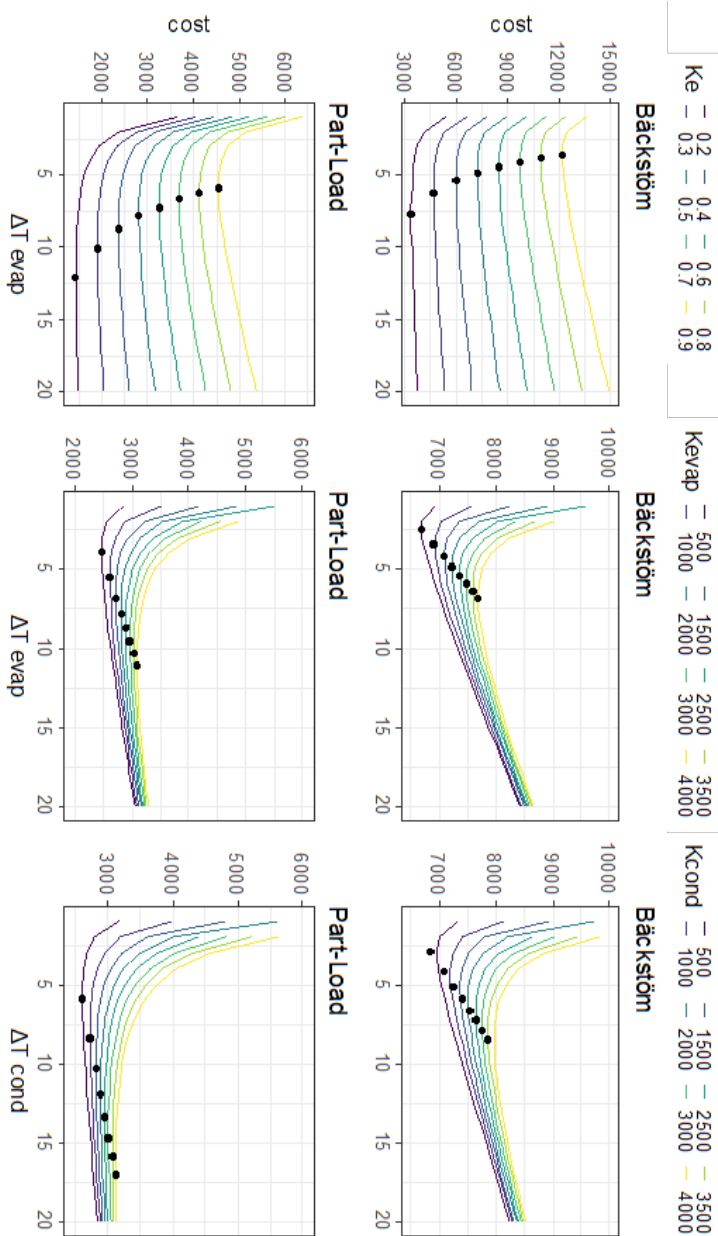


Figure 4.11: Study of the influence of the different economic parameters in the optimization of HXs

The most evident result is that the optimum ΔT displaces to the right (to smaller HXs) as the cost of the HXs (k_{evap} and k_{cond}) increases and the contrary occurs with the cost of energy; as the cost of energy grows, bigger HXs are preferred as they are more energy efficient.

For the same parameter values, optimum ΔT are always smaller when part-load is not considered and the gap is enhanced as HXs cost increase or when energy costs decrease. The highest difference in ΔT_{opt} is found when k_{cond} is modified, the explanation of this comes to the fact that the cost curves of the condenser are flatter. On the other hand, the variable that has a higher impact on the total cost is the cost of energy.

It should be pointed out that the energy cost also affects the HX cost. However, in the parametric study this was not analyzed and k_e was modified maintaining constant the HX cost.

4.5. Discussion and limitations of results

The HX design methodology proposed in the study followed a detailed and rigorous modeling of the system and it was exemplified with a particular case scenario. To further enhance the precision when applying the methodology the following modifications could be applied: utilize local standards and climatic registries to calculate the operating hours at each external temperature according to the final location (e.g. ANSI/ASHRAE 116-2010 for EEUU), incorporate updated economic data for components using the particular manufacturer information and, last but not least, consider the dependence of Carnot's Efficiency with compressor speed rather than treating it as a constant (Shao et al., 2004).

Additionally, compressor cycling (Figure 4.5: Zone III) introduces a COP reduction which has not been taken into account in the present study for better readability. To include it, the standard (European Commission, 2018a) proposes the correction factor described in Eq.(4.18), which can be multiplied to each bin of Eq.(4.6) (being $Cd=0.9$ the default value for air-to-water HPs for water heating).

$$\frac{COP_{bin,corrected}}{COP_{bin}} = \frac{CR}{Cd \cdot CR + (1 - Cd)} \quad (4.18)$$
$$with CR = \frac{Q_{req,bin}}{Q_{cond,bin}}$$

It is also important to highlight that simplified correlations were proposed for coil and plate heat exchangers Eq.(4.8). These models could be applied to other typologies or capacity ranges, but prior validation is required.

Finally, the method was presented for heating heat pumps. However, the methodology is meant to be general and applicable to most heat pumps applying little modifications. For cooling heat pumps the same methodology could be followed redefining the operational costs term Eq.(4.4)(4.4): the desired heating capacity is substituted with cooling capacity and the heating COP is substituted by refrigerating COP which results in Eq.(4.19).

$$\dot{E} = \frac{\dot{Q}_{evap}}{COP_{refr}} = \frac{\dot{Q}_{evap}}{\eta_{ct,refr} \frac{T_{evap}}{T_{cond} - T_{evap}}} = \dot{Q}_{evap} \frac{T_{cond} - T_{evap}}{\eta_{ct,refr} T_{evap}} \quad (4.19)$$

With the mentioned changes the general cost equation would result in Eq.(4.20).

$$\begin{aligned} &\text{Cost} \\ &= a \left[\frac{\kappa_{evap} \dot{Q}_{evap,nom}}{\Delta T_{evap,nom}} + \frac{\kappa_{cond} \dot{Q}_{cond,nom}}{\Delta T_{cond,nom}} \right] \\ &+ \sum_{bin} \kappa_e \tau_{bin} \dot{Q}_{evap,bin} \frac{(t_{sink,bin} + \Delta T_{cond,bin}) - (t_{source,bin} - \Delta T_{evap,bin})}{\eta_{ct,refr} (t_{source,bin} + \Delta T_{evap,bin} + 273.15)} \end{aligned} \quad (4.20)$$

Moreover, the Standard EN 14825 (European Commission, 2018a, p. 14825) also includes a climate profile for space cooling with the reference amount of hours expected at each external temperature and part load capacity at each condition [Figure 4.12] which is necessary to define the different bins in Eq.(4.20)(4.20).

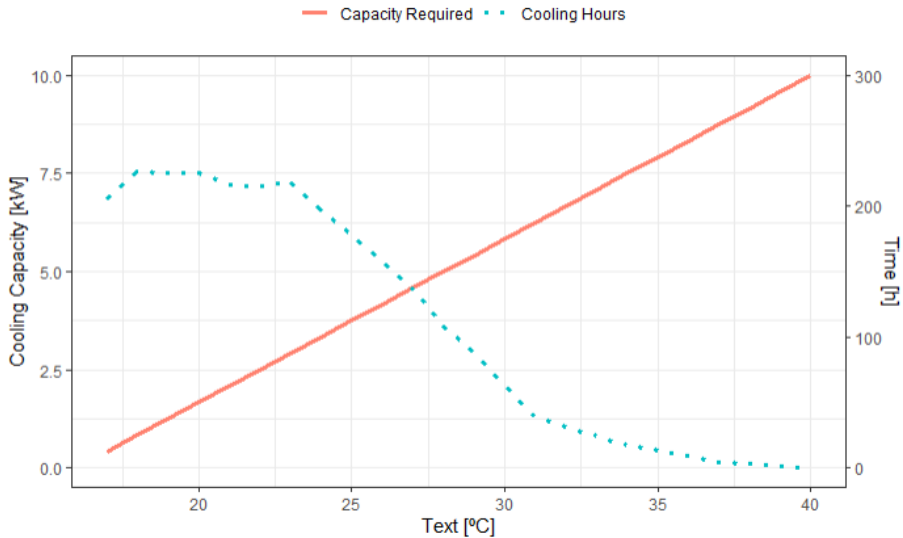


Figure 4.12: Operating hours and cooling capacity required as a function of external temperature for a HP with a rated capacity of 10 kW

4.6. Conclusion

A new systematic methodology for selecting heat exchangers in variable-speed heat pumps working at part load has been proposed. Some of the more relevant aspects of the procedure are:

- The evolution of the external working temperatures over time is considered as it affects the working time, the required capacity and the heat pump's performance.
- The chosen heat exchangers' design parameters were the coil's width and the number of plates. Simple heat exchanger models are proposed that predict the temperature difference as a function of the operating conditions and the design parameters.
- The methodology takes into account the compressor working range and establishes three differentiated working zones. A simplified compressor model is presented for the calculation of the provided capacity at the different zones.
- The obtained optimal solutions suggest using smaller heat exchangers compared to when classical rules are followed. Additionally, the cost function seems flatter, so a slight deviation from the optimum will have a smaller effect on total cost.
- For the studied case, savings close to 5% are obtained when using the proposed methodology compared with the classical one. However, the savings could vary for other applications reaching higher values.

Overall, this study provides a general approach to assist system designers in heat exchanger selection based on a cost-based analysis, which could lead to a better design of future heat pumps, increasing total efficiency and making these systems more attractive compared with classical boilers or electrical heaters.

4.7. Nomenclature

Abbreviations

COP	Coefficient of Performance
CV	Coefficient of Variance of the RMSE ($\frac{RMSE}{\bar{x}}$)
HP	Heat Pump
HX	Heat Exchanger
RMSE	Root Mean Square Error
VSC	Variable Speed Compressor
VSHp	Variable Speed Heat Pump

Symbols

A	heat exchange area [m ²]
a	annuity factor [year ⁻¹]
C	cost [SEK]
$c_{\#}$	model coefficient for VSC
\dot{E}	Heat Pump Power Consumption [kW]
f_c	compressor speed [Hz]
I	Investment [SEK]
$k_{\#}$	model coefficients for HX
\dot{Q}	heating capacity [kW]
t	temperature [°C]
T	temperature [K]
ΔT_{evap}	$ T_{ext} - T_{evap} $ [K]
ΔT_{cond}	$ T_{cond} - T_{water,service} $ [K]

U	heat transfer coefficient [W/(m ² °C)]
-----	---

Greek letters

κ	marginal cost [SEK/(kW/K)]
η_{ct}	Carnot's efficiency [-]
τ	working hours

Sub index

aux	auxiliary heating system
bin	related to each external temperature
$compr$	related to the compressor
$cond$	related to condenser
e	related to energy
$evap$	related to the evaporator
ext	of air at outdoor conditions
HX	heat exchanger
max	maximum
min	minimum
nom	nominal, at rated conditions
opt	optimum
req	required, obtained from the standard

Chapter 5:

FORTH PUBLICATION



International Journal of Refrigeration

Volume 123, March 2021, Pages 63-71



Study of oil circulation rate in variable speed scroll compressor working with propane
Étude du débit de circulation de l'huile dans un compresseur à spirales à vitesse variable fonctionnant au propane

Rubén Ossorio, Emilio Navarro-Peris  

<https://doi.org/10.1016/j.ijrefrig.2020.12.002>

Study of Oil Circulation Rate in Variable-Speed Scroll Compressors Working with Propane

Rubén Ossorio, Emilio Navarro-Peris

Instituto Universitario de Investigación en Ingeniería Energética (IUIIE)
Universitat Politècnica de València, Camino de Vera s/n, ed. 8E cubo F 5º, Valencia,
46022, Spain
Phone: 34-96-3877000 Ext. 88280, Fax: 34-96-3879126

5.1. Abstract

The use of hydrocarbons as refrigerants is being more common in the recent years, nevertheless the solubility of propane in POE oils is significantly higher than in HFCs. This fact has made that POE oils used with hydrocarbons usually have a higher viscosity than the commonly used with HFCs. This approach solves the lubrication problem in the compressor but the way in which oil could affect the system performance is not so widely studied. In this work, an experimental analysis about the oil circulation rate of a variable speed compressor working with propane has been done. The study has analyzed the oil circulation at different compressor speeds and evaporating temperatures. The obtained results have shown that the oil circulation rate increases with the compressor speed having values higher than 5% at the higher speeds. This fact can penalize the COP of the system in more than 15% in these working conditions.

Keywords: Variable Speed Compressor, OCR, Oil separator, Compressor efficiency,

5.2. Introduction

Variable speed compressors have spread all over the refrigeration and heat pump systems thanks to its capability to adapt the cooling capacity to the demand, improving also the comfort conditions (Qureshi & Tassou, 1996). This technology introduces several advantages compared with On/Off cycling. However, one of the problems that this technology has to face is a correct lubrication in all speed range.

Lubrication using oil is necessary in the vast majority of compressors for the correct lubrication of the moving parts, to ensure a seal in the compression chamber and to lower the compressor temperature. In order to ensure a sufficient quantity of oil in the key spots different technologies arises, in scroll compressors, a drill into the shaft acts as a pump to arise the oil that lays in the bottom part to the main bearing and to the compression chamber which is typically in the upper part (Branch & Lepak, 2019). This pumping action depends mainly on the rotational speed of the shaft. Consequently, when designing variable speed compressors, having enough pumping action at low speeds implies having too much pumping action at high speeds which also implies an excess of oil discharged out of the compressor. Ribeiro and Barbosa (Ribeiro & Barbosa, 2016) suggested a model of a centrifugal oil pump based on the study of (Kim & Lancey, 2003) to estimate the oil mass flow discharged by the compressor. However, the model used hard to find geometric data and a correction factor using six correlation coefficients.

Oil, although being necessary in the compressor, it is considered as a contaminant in the rest of the system. Oil changes thermodynamic properties of the refrigerant, reduces the heat transfer coefficient in the heat exchangers and, in worst cases, can block the expansion device (Kruse & Schroeder, 1985). In addition, an excess of oil migrating to the system could led to not having enough oil inside the compressor for a correct lubrication, limiting its effective life. Consequently, it is important to estimate the quantity of oil circulating in the system and, to do so, Oil Circulation Rate (OCR) is the main parameter used in the literature, which is expressed as:

$$OCR = \frac{\dot{m}_{oil}}{\dot{m}_{oil} + \dot{m}_{refr}} \quad (5.1)$$

Where \dot{m}_{oil} is the oil mass flow circulating in the system and \dot{m}_{refr} is the refrigerant mass flow. Accordingly to Lottin study (Lottin et al., 2003b), values of OCR up to 0.5% have negligible effect in the system. However, above this percentage, the performance of the unit decreases significantly. In particular, with OCR of 5%, the COP can be reduced up to 15%.

Lotting et al. studied the effect of oil circulation in the system (Lottin et al., 2003a) and concluded that the most influenced element was the evaporator as the overall heat transfer coefficient (HTC) decrease with high concentrations of oil which typically occur when vapor quality exceeds 70%. To quantify this effect, it was followed a thermodynamic approach considering the refrigerant and oil as a zeotropic mixture and applying three different HTC correlations: Yam et al. (Yam et al., 1997), Gungor and Winterton (Gungor & Winterton, 1986) and finally Bivens and Yokozeki (Bivens & Yokozeki, 1994) .

To limit the OCR, oil separators are used. These devices are placed at the discharge line of the compressor and separate the oil droplets from the refrigerant using centrifugal forces and return the separated oil to the compressor. In this way, oil circulation on the heat exchangers and expansion devices are significantly decreased as the typical efficiency of these devices is higher than 90%. In small systems though, the oil separator is discarded as it is not economically advantageous. Note that, in these cases, a noticeable decrease of the performance can occur compared with expected values announced by the manufacturer as the latter are reported using oil separator and testing OCR is never displayed.

The procedure to determine the oil circulation rate (OCR) is described in ASHRAE 41.4 standard (ASHRAE, 2015) and it is based on taking samples from the liquid line of the refrigeration circuit. Summarizing, the steps of the procedure are the following: take a refrigerant sample and weight it, then the refrigerant in the sample is slowly evacuated letting it evaporate through a capillary tube, create vacuum in the sample cylinder, weight it again, clean the interior with acetone, let it evaporate... The described methodology results in accurate results when all the steps are rigorously followed but it is a time-consuming procedure with tedious steps which limits the number of tests that can viably be done. Additionally, it is needed a scale with great

accuracy and resolution and, what it is more important, the sampling is invasive as it affects the overall quantity of oil and refrigerant in the studied system (Wujek et al., 2007).

With such a cumbersome procedure, generating a wide map of OCR values depending on the working conditions for a variable speed compressor can be very problematic as the required number of tests are significantly increased as a consequence of including the speed in the study.

To solve the problems of the previously explained procedure other methods have appeared which calculates the OCR non-invasively and in an online configuration (meaning continuously and not having to extract samples). These methods are based in thermal conductivity (Wujek et al., 2007), dielectric constant (Hwang et al., 2008), high speed cameras (Xu & Hrnjak, 2017), UV absorption (Kutsuna et al., 1991), speed of sound (Lebreton et al., 2001) and refraction (Fukuta et al., 2006) among others. However, these techniques require high end and experimental equipment with specific calibrations for each test bench, refrigerant and lubricant.

Regarding existing OCR experimental data in the literature, most of them only provides OCR data for the validation for OCR estimations methods. Therefore, these existing tests do not provide information about how OCR varies with the working condition. Other studies focus on fixed speed compressors and only measure a limited amount points as (Navarro et al., 2005) which tested 5 propane single speed compressors at 3 different conditions each. As other example, Wujek (Wujek et al., 2014) focuses on the effect of the chosen oil in OCR, testing 6 different oils in 4 different conditions (all at the same speed).

Regarding the studies of OCR in variable speed compressors also some studies can be found in the literature. In (Sarntichartsak et al., 2006) two variable speed commercial unit (rotary compressor) in the working range of 30-50Hz using R22/MO and R407C/POE/MO are tested, the behavior with the speed of the compressor and the charge and type of the oil are analyzed. However, the compressor speed range is limited, and the tests are not carried out in a calorimeter so the evaporating and condensing temperature are not controlled. Yoon (Yoon et al., 2011) study a variable speed high shell pressure scroll in a speed range of 30-120Hz working with R410A/PVE. A refractive

index sensor was used to measure the OCR and a wide test matrix was proposed in which the influence of speed, superheat and suction pressure on OCR could be retrieved with high accuracy.

As reviewed experimental results of OCR in variable speed scroll compressors are limited and are carried out using HFCs. However, most of them have a high global warming potential and are phased out being substituted by new alternatives more environmentally friendly among which hydrocarbons as propane (R290) stands out. However, propane presents a higher solubility in POE oils than HFCs (Gas-Servei, n.d.) what makes that compressor providers recommend using high viscosity lubricants as POE ISO 68 which in turn makes it difficult to extrapolate the results obtained with HFCs to propane systems.

This study analyses the OCR of a variable speed scroll compressor of 46 cm³ and a capacity between 3.4-15.7 kW working with R290/POE as a function of the compressor speed. The compressor has been tested in more than 70 different points including evaporation temperatures from -30 °C to 25°C and compressor speeds from 30 Hz to 120 Hz. In order to be able to perform all these OCR measurements in a limited amount of time a methodology based on mass flow discrepancies has been implemented. The developed methodology has demonstrated enough accuracy to provide acceptable qualitative results. It should be pointed out that the methodology does not require any experimental set up modification and can be implemented just using the sensors included in the Standard EN13771 (EN13771, 2017) for compressor rating. With the obtained experimental results, in the second part of the study, the global oil trend in the tested variable speed compressor and how it affects the compressor performance is analyzed.

5.3. Methodology

5.3.1. Test bench

The used test bench is the calorimetric test bench represented in Figure 5.1. It has been designed to satisfy the Standard EN13771 (EN13771, 2017) for compressor rating. It is able to control Condensing and Evaporating temperatures, Subcooling (SC) and Superheat (SH). Additionally, the test bench comprises a set of PID controllers that can keep any operating condition stable within a range of 1kPa and 0.1°C from its setting without manual adjustments.

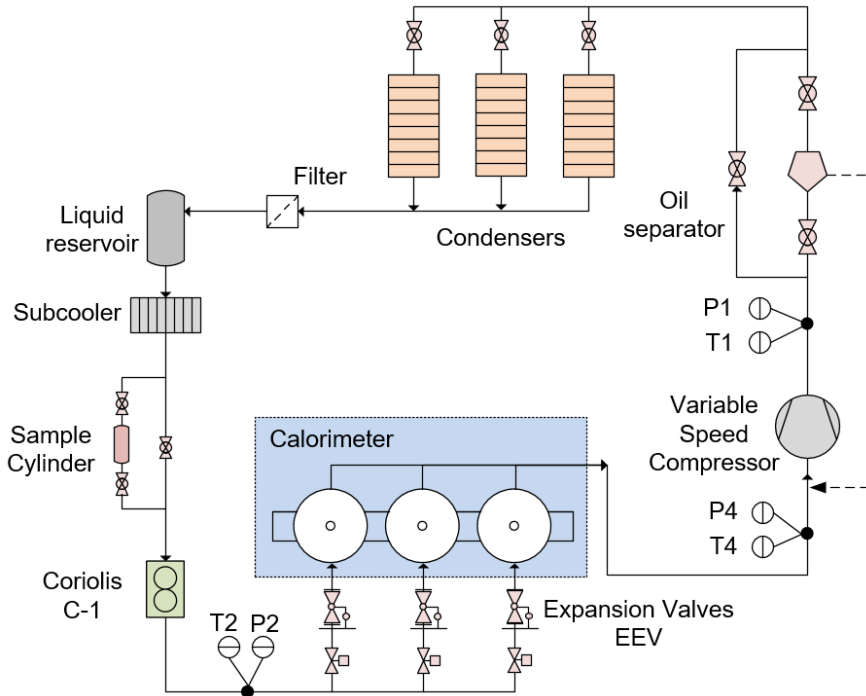


Figure 5.1: Calorimetric Test Bench

For this study the most important elements of the calorimetric test bench are: the evaporator, the oil separator and the Coriolis mass flow sensor. The evaporator consists of 3 isolated vessels in which the refrigerant exchange heat with an electric resistance. If the vessels are at constant temperature, the electrical power is measured and the heat loss to the ambient is modelled; then, the effective mass flow of refrigerant in the system can be calculated with Eq.(5.2). This method is also called calorimetric method:

$$P_{electr} - P_{loss} = \dot{m}_{refr}(h_{out} - h_{in}) \quad (5.2)$$

Regarding the oil separator, it has been used a Castel 5520/C oil separator at the discharge of the compressor which returns the discharged oil to the suction line of the compressor. Its efficiency has been experimentally tested in the test bench at different compressor speeds and it always showed efficiencies higher than 95%. This device can be bypassed so that the same condition can be tested with and without oil separator. And finally, the Coriolis mass flow sensor selected was a Micromotion sensor CMF025M which is placed in the liquid line between the subcooler and the expansion valves.

In addition to the mass flow meter, Pt100 and absolute pressure transducers have been installed all around the test bench to have an accurate estimation of the compression condition. The basic declared uncertainties of the used sensors are displayed in Table 5.1. Regarding derivate thermodynamic properties as enthalpies, they have been calculated using the REFPROP database (Lemmon & McLinden, 2002).

Table 5.1: Uncertainty of Sensors

Uncertainty of the used sensors		
<u>Variable</u>	<u>Equipment</u>	<u>Uncertainty</u>
T	RTD-PT	±0,05°C
P	Fisher-Rosemount 3051	±0,02%
\dot{m}	Coriolis CMF025M	±0,025gs ⁻¹
P _{electr}	Sineax CAM	±20W

5.3.2. Description of the methodology to estimate the oil mass flow rate (Discrepancy Method)

According to Standard EN13771 (EN13771, 2017), as the mass flow is the main variable for characterizing a compressor, two different mass flow estimations have been simultaneously carried out to lower the uncertainty and to have a validation of the results. As it has been stated previously, the used methods in this study were: 1) a coriolis mass flow meter in the liquid line 2) an estimation of mass flow using an energy balance in the evaporator (calorimetric method).

However, when testing a compressor without oil separator, a homogeneous discrepancy between the results of both methods appears (specially at high speeds) in which the Coriolis mass flow meter always shows a higher value of the mass flow rate.

It has been assumed that this discrepancy is caused by oil circulation in the system which is registered by the Coriolis sensor but not in the heat balance performed in the evaporator. In that way, the measurement of the Coriolis provided the sum of the refrigerant mass flow \dot{m}_{refr} and the mass flow of the oil \dot{m}_{oil} . On the other hand, as the evaporating \dot{m}_{refr} is the only mass flow that has cooling capacity, the result of the energy balance in the evaporator only considered \dot{m}_{refr} .

Under these assumptions the oil mass flow in the system could be easily achievable subtracting both estimations as in Eq.(5.3)

$$\dot{m}_{coriolis} - \dot{m}_{calorimeter} = (\dot{m}_{oil} + \dot{m}_{refr}) - \dot{m}_{refr} = \dot{m}_{oil} \quad (5.3)$$

Note that this assumption is an approximation as part of the refrigerant will remain dissolved in the oil and will not evaporate in the evaporator (Youbi-idrissi et al., 2003; Youbi-Idrissi & Bonjour, 2008). This is why the mass flow of refrigerant dissolved into the oil should be added to the result of Eq.(5.3). With this approach, the result of subtracting the estimation of both methods would be the ineffective mass flow: \dot{m}_{ineff} .

The OCR is a parameter typically used to estimate the impact of the oil circulation on the system performance. However, different systems with the same OCR can behave differently depending on the solubility of the refrigerant on the oil which depends also on temperature and pressure. Consequently, to add the effect of oil solubility to the OCR concept a redefinition can be carried out in which the ineffective mass flow is used instead of the oil mass flow as shown in Eq.(5.4):

$$OCR_e = \frac{\dot{m}_{ineff}}{\dot{m}_{total}} \quad (5.4)$$

5.3.3. Experimental campaign

The used compressor is a scroll variable speed compressor with a speed range from 15 to 120 Hz, with a swept volume of 46cm³ and working with propane. Regarding the lubricant oil, the compressor uses ISO 68 Polyol ester Oil (POE) which is accumulated in a carter located in the bottom part of the compressor at suction condition.

In order to validate the proposed discrepancy method a first experimental campaign was designed to compare the results with the weighting procedure described in the ASHRAE 41.4 standard (ASHRAE, 2015). A Mettler Toledo scale was used with a resolution of 0.01g and a Swagelok stainless steel sample cylinder which was placed in the liquid line as displayed in Figure 5.1.

This first experimental campaign consisted on 6 different tests in which the compressor was set to work in the same compression condition (T_{evap}=0°C | T_{cond}=50°C) but varying the working speed.

Once the methodology was validated, to study the compressor OCR as a function of the working conditions, the experimental campaign shown in Figure 5.2 was carried out. It includes the variation of 3 parameters: speed, evaporation temperature and the existence of oil separator. The frequencies of 30, 45, 60, 85, 110 and 120 Hz have been tested at evaporation temperatures from -30 to 25°C. Assuming that condensing temperature has a second order effect in OCR and in order to reduce the number of tests it has been decided to maintain the condensing temperature constant in this study.

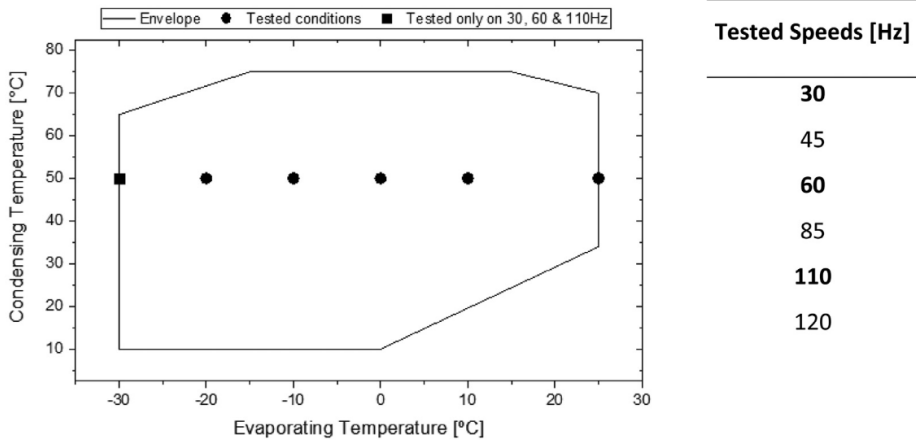


Figure 5.2: Envelope of the compressor and tested conditions

In total there are a set of 6 different conditions of evaporating temperature for each of the 6 chosen speeds and each condition is tested with and without oil separator. In total 66 different tests were carried out.

The methodology for each test was:

1. Setting the compression condition and speed.
2. Letting it stabilize and then log for 15 minutes with oil separator.
3. Bypassing the oil separator.
4. Letting the system stabilize and then log for 15 minutes without oil separator.

It should be noted that the stabilization includes also the stabilization of the level of oil inside the compressor which was monitored using a sight tube. The results of each test are the average of the measured variables along the logging time.

5.4. Experimental results

5.4.1. Validation of the methodology

Figure 5.3 represents the OCR values obtained with both methodologies as a function of compressor speed. The errors are calculated with a 95% of confidence and considering the sensors and dataloggers uncertainty besides repeatability and random errors.

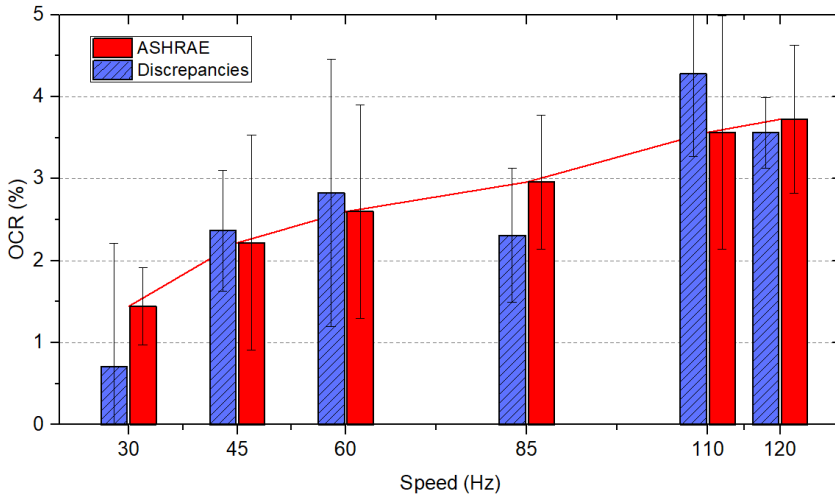


Figure 5.3: Comparison between OCR against speed for both methodologies ASRHARE and Discrepancies

The results show that despite the higher dispersion of the discrepancy method, both methodologies follow the same trend and there is an overlap in the error bars between both methodologies showing that they are compatible in the tested range.

5.4.2. Oil circulation results

Based on the previous results, the experimental campaign described in Figure 5.2 was carried out and the obtained results are described in this section.

Figure 5.4 shows the evolution of oil mass flow (5.4a and 5.4b) and OCR (5.4c and 5.4d) as a function of the total mass flow (measured with a Coriolis

sensor) with and without oil separator. The oil mass flow has been calculated with Eq.(5.3) and the OCR with Eq.(5.1). The lines spotted in the figures represent the trends shown by tests carried out with the same compressor speed.

Remark that, if the rest of the compression conditions remain constant, an increase of the evaporating temperature implies an increase of the total mass flow (as the suction specific volume increases with the evaporating temperature). Consequently, moving to the right in the X axis implies an increase of mass flow but also an increase of evaporating temperature for each speed.

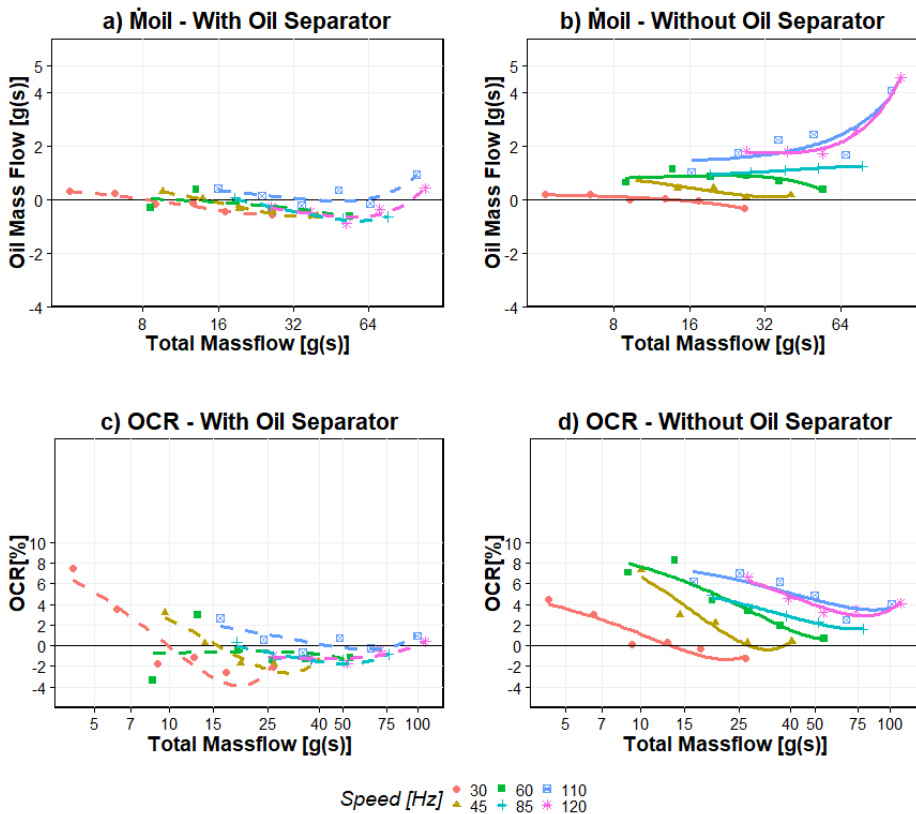


Figure 5.4: Evolution of moil and OCR against total mass flow with and without oil separator a) Results of moil with oil separator b) Results of moil without oil separator c) Results of OCR with oil separator d) Results of OCR without oil separator

Regarding the oil separator, it keeps a low circulating mass flow of oil close to zero at all the speeds. Remark that at very low mass flows the error in the OCR calculation increases significantly, this fact must be taken into account interpreting the high OCR obtained at low mass flows. The negative values of oil mass flow must be viewed also in the frame of the uncertainty of the sensors and the followed methodology. Nevertheless, this fact does not avoid to extract qualitative conclusions from the data analyzed.

With the information shown in Figure 5.4b, it can be concluded that at low speeds the oil mass flow is reduced and tends to zero, even without using oil separator. At 60Hz, the amount of oil mass flow begins to increase significantly, obtaining oil flows around 1g/s. And lastly, at high speeds (110Hz), the oil mass flow increases reaching values close to 4 g/s. This trend is in the same direction of the increase of the total mass flow with the compressor speed.

Analyzing the OCR can supply some more information as it allows to normalize the oil mass flow values relatively to the total mass flow. Figure 5.4d shows an increase of OCR with the speed. Regarding the evaporating temperature, OCR values decrease as evaporating temperature increases. This behavior is produced because the oil circulation depends mainly on the rotational speed of the shaft which is responsible of pumping up the oil from the carter to the main bearings and the compression chamber. Consequently, the effect of an increase in the evaporating temperature, keeping the speed constant, will increase the refrigerant mass flow but the oil mass flow won't be influenced so much by the evaporating temperature.

In Figure 5.5, OCR has been plotted against the speed and each data series represent a different Evaporating temperature. In this plot the effect of evaporating temperature and speed on OCR can be visualized without taking into account the total mass flow, a variable that depends on the chosen compressor.

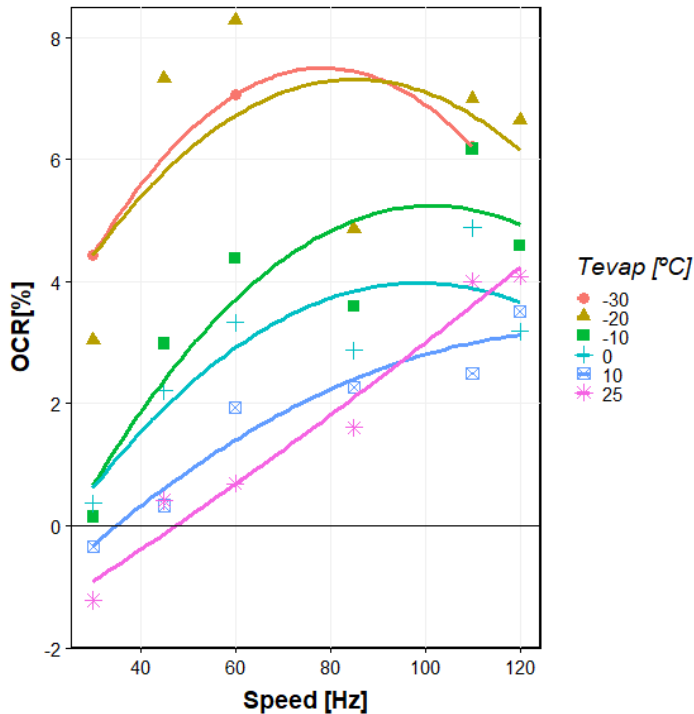


Figure 5.5: Effect of the Evaporating Temperature and Speed in OCR

In general, there is an increase of OCR with the rotational speed of the compressor. This tendency is particularly clear at high evaporating temperatures in which the increase is homogeneous. On the other side, at low evaporating temperatures the tendencies split in two parts: the first, characterized by a rapid increase of OCR with speed and a second in which the trend tends to change and the OCR starts to reduce. This local maximum could be explained by a saturation in the oil pump mechanism which in turn seems to get reached at lower speeds as the evaporating temperature decreases. Remark that the saturation affects the oil mass flow (not the OCR) and, as the refrigerant mass flow keeps rising with speed, the OCR starts decreasing. The authors also want to point out that a sharp decrease of OCR has been detected at 85Hz at different evaporating temperatures. The authors do not have strong evidences that could explain this behavior, but some hypotheses could be a resonant effect at that speed, which is very close from the nominal speed (90Hz), or a set of outliers.

5.4.3. Oil mass flow correlation

From the experimental data and in order to be able to extrapolate the obtained results to other working conditions an empirical correlation of the oil circulation has been obtained.

Ribeiro and Barbosa (Ribeiro & Barbosa, 2016) suggested a semi-empirical model based on a centrifugal pump and a correction factor composed by 6 fitting coefficients depending on speed and pressure ratio. However, it needed geometric information of the interior of the compressor which is not declared by the manufacturer. This fact and the great number of coefficients makes the model difficult to be applied in our study.

The model used in this study only depends on the rotational speed of the compressor and follows the equation:

$$\frac{\dot{m}_{oil}}{\dot{m}_{oil_max}} = \left(\frac{N}{N_{max}} \right)^2 \quad (5.5)$$

In which \dot{m}_{oil_max} is the fitting coefficient and equals 2,517 when \dot{m}_{oil} is expressed in g/s and N is the rotational speed, being N_{max} the maximum speed declared by the manufacturer. Note the similarity of the proposed correlation with the affinity laws of pumps and fans.

In Figure 5.6, the result of applying the single-coefficient correlation is displayed. For each speed. The dots are the model predictions, the black and solid line represents the evolution of the correlation and the boxplot represents the experimental data for each speed.

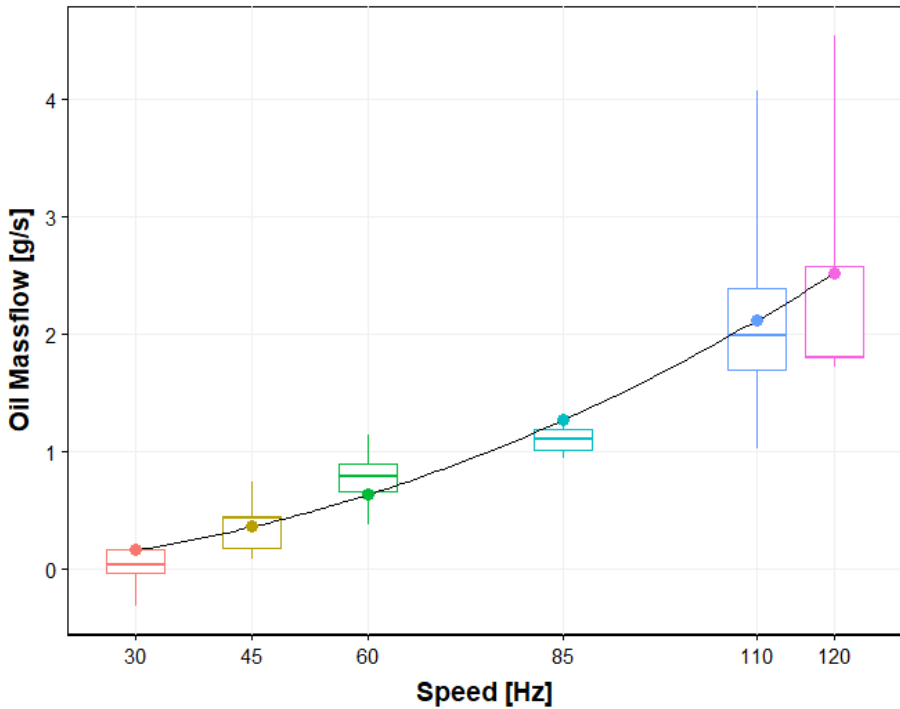


Figure 5.6: Evaluation of the model estimation of oil mass flow as a function of speed compared with the experimentally estimated values of oil mass flow.

In the graph it can be seen how the model fits properly the evolution of the oil mass flow. The result of the correlation provides a R-square value of 0.85 which is assumed to be acceptable considering the dispersion of the experimental data. Ribeiro and Barbosa (Ribeiro and Barbosa, 2016) considered also the pressure ratio in their model but in this study adding coefficients depending on the pressure ratio didn't improve the accuracy of the model. Consequently, only the coefficient depending on the quadratic term of the speed was considered which, in turn, allows to fit the model performing only one test. The authors consider that, even if only one compressor has been tested, this correlation would apply for other vertical scroll compressors as long as they implement the same oil pump mechanism.

5.5. Discussion

Once the results of the experimental campaign have been presented, in this section the effects of the oil in the compressor performance are analyzed. The analysis will be focused mainly on compressor and volumetric efficiencies when the compressor works a 110 Hz. That condition has been selected because it is the condition in which the compressor is pumping a higher amount of oil and therefore where its effects become more significant.

When considering the compressor efficiency, also known as isentropic efficiency, AHRI Standard 571 and ASHRAE Standard 23.1 define it as:

$$\eta_c = \frac{\dot{m}(h_{2s} - h_1)}{P_{electr}} \quad (5.6)$$

In this equation \dot{m} represents the refrigerant mass flow, however, it is common to consider the total mass flow (oil + refrigerant) for the value of mass flow.

Even if the increase of enthalpy on the oil is not useful for the cycle, the compressor is using some energy to increase its pressure and temperature. Consequently, the compressor consumption can be extended with 2 new terms to consider the effects on the oil [Eq.(5.7)]. This equation could help to compare data of the same compressor with different lubricants (Wujek et al., 2014).

$$\eta_c = \frac{\dot{m}_{ref}(h_{2s} - h_1) + \dot{m}_{oil}c_p(T_{2is} - T_1) + \dot{m}_{oil}v_{oil}(P_2 - P_1)}{P_{electr}} \quad (5.7)$$

In conclusion, three different ways of calculating the compressor efficiency can be derived:

- 1) Assuming the total mass flow (refrigerant+oil) measured with a Coriolis sensor.
- 2) Assuming only the refrigerant mass flow calculated with the calorimetric method and Eq.(5.2) .
- 3) Considering both the refrigerant and the lubricant terms according Eq.(5.7).

P_{electr} and the enthalpy difference are the same independently of the presence of the oil separator in the system, therefore the differences observed in the different ways of calculating the compressor efficiency will be related to the refrigerant mass flow and the oil term.

In Figure 5.7, the results of the different possible definitions of compressor efficiency are displayed for different evaporating temperatures and for 110Hz, which is considered high speed with a significant OCR of 5% average.

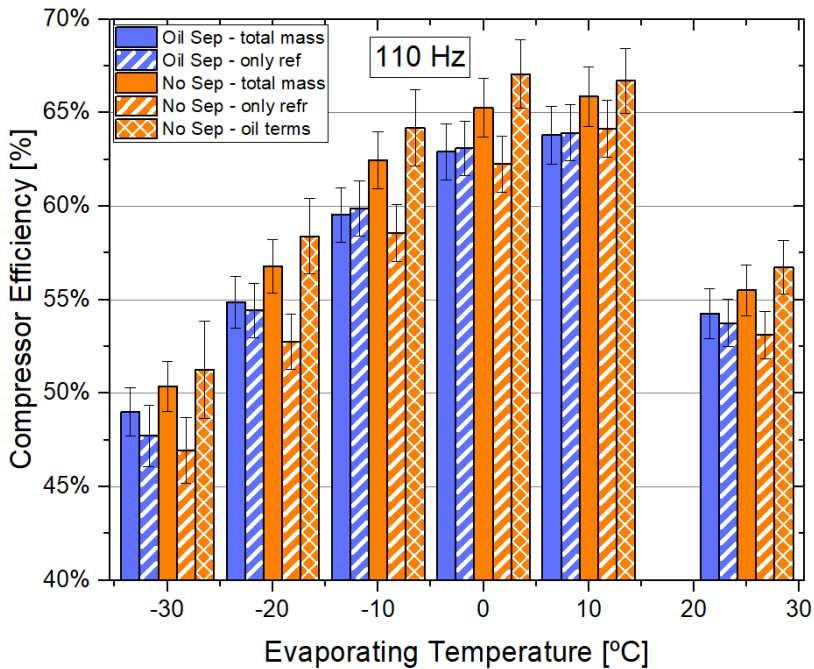


Figure 5.7: Compressor Efficiency calculated for different Evaporating Temperatures at 110Hz with different approaches

The solid bars represent the compressor efficiency assuming the mass flow measured with the Coriolis sensor, the stripped ones considering the mass flow obtained with the calorimeter and the rhomboid bar considering also the oil to calculate the efficiency [Eq.(5.7)]. Remark that the first two columns (blue) correspond to the test in which the oil separator was connected and they give very similar results. The point at -30°C of evaporating temperature shows a higher divergence but, in that point, the experimental installation presents higher errors.

The results show a homogeneous increase of the compressor efficiency when the compressor is tested without oil separator and the Coriolis mass flow is considered (between solid bars), showing that the oil contribution to the total mass flow is significant. When the mass flow measured with the calorimeter is considered (stripped bars), a decrease of efficiency appears in most cases when no oil separator is used showing that part of the refrigerant remains solved in the oil. Regarding the oil terms of Eq.(5.7), the weight of the third term (the compression of oil) is negligible but the second one (the increase in temperature of oil) has an important contribution to the global efficiency, increasing the compressor efficiency up to 5%. This apparent increase in efficiency is actually a loss as it is power delivered to the oil instead of to the refrigerant. In case the amount of oil pumped by the compressor could be reduced this loss of efficiency would be reduced too.

Regarding volumetric efficiency, it is defined as the ratio between refrigerant mass flow pumped by the compressor and its swept volume:

$$\eta_v = \frac{\dot{m}v_{suc}}{V f c} \quad (5.8)$$

In this case, the same distinction about the consideration of the mass flow rate in the compressor efficiency can be done.

The compressor also displaces oil and this fact can be taken into account with a new term displayed in Eq.(5.9).

$$\eta_v = \frac{\dot{m}v_{suc} + \dot{m}v_{oil}}{V f c} \quad (5.9)$$

Figure 5.8 represents the different results of volumetric efficiency for different evaporating temperatures and for 110Hz. The format used is the same as in Figure 5.7, the first 2 columns for each evaporation temperature represent tests with oil separator and the other 3 without it. In addition, the solid, stripped and rhomboid bars correspond to the different definitions of volumetric efficiency respectively: 1) considering the mass flow measured with the Coriolis sensor 2) with the calorimetric method 3) including also the oil term [Eq.(5.9)].

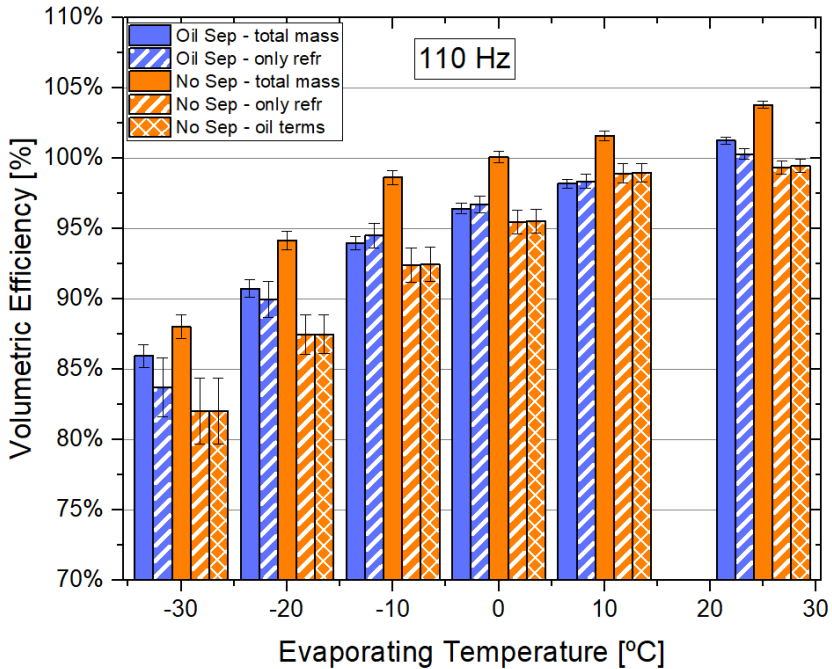


Figure 5.8: Compressor Efficiency calculated with different approaches for different Evaporating Temperatures at 110 Hz.

When using oil separator (the first two bars), the graph shows that the chosen mass flow estimation does not have a great effect on the result as the oil mass flow is maintained negligible. In contrast, when considering the results without oil separator, a great discrepancy up to 8% appears between the mass flow estimation methods (between the 3rd and 4th bar) which, in some cases, results in a volumetric efficiency higher than one when the Coriolis estimation is used. This variation is due to consider the oil mass flow as vapor refrigerant which have very different specific volume. Regarding the oil term in Eq.(5.9), it does not contribute significantly to the volumetric efficiency (no sensible difference between 4th and 5th bar), this can be explained by the fact that the specific volume of the liquid oil is significantly smaller than the one of the vapor refrigerant. Additionally, another interesting result is that the volumetric efficiency considering the calorimetric mass flow tends to decrease when the oil separator is present (difference between stripped bars). Assuming that the compressor operates in a similar way in both

situations, these values indicate that when the oil separator is not present some refrigerant can be maintained dissolved in the oil in the evaporator, not contributing to the refrigerant effect and therefore reducing the performance of the system, hence the introduction of an oil separator in these heat pumps, although increasing the total charge of the system could increase significantly the cooling capacity and the COP. This point also reveals that characterizing a compressor in a test bench with an oil separator could introduce a significant deviation in the estimation of the effective mass flow rate when this compressor is working in a real system not equipped with that device.

The results shown correspond to 110Hz which is considered “high speed” for this compressor but the obtained conclusions are similar for the rest of compressor speeds where noticeable values of OCR have been measured.

5.6. Conclusions

In this paper an analysis of the OCR in a scroll variable-speed compressor at different operating conditions and working with propane has been carried out. In order to do that it has been used a methodology based on the discrepancy between two mass flow estimation methods (calorimetric and Coriolis sensor). The developed methodology has demonstrated to supply enough accuracy to detect different oil behavior in the system with the advantage of supplying an online and non-invasive compared to the ASHRAE standard.

Based on this technique the following conclusions related to oil behavior in the compressor have been obtained:

- Measurements based on Coriolis and on calorimeter can diverge significantly if an oil separator is not present.
- OCR increases as evaporating temperature decreases.
- OCR increases with compressor speed. This is a consequence of the way in which compressor lubrication is performed in scroll compressors, and the OCR values can be significantly high at high speeds.

- A correlation of the oil mass flow with the square of the compressor speed has been found. The correlation allows a first estimation of oil mass flow requiring just one coefficient for vertical scroll compressors.
- At high OCRs, evaluating the compressor and volumetric efficiency with the Coriolis mass flow estimation can give values up to 5% higher than when the calorimeter procedure is used. This deviation can be very relevant when cooling capacity is estimated with a Coriolis mass flow meter.
- The existence of oil being heated in the compression process can decrease the real compressor efficiency up to 5%.
- The evaluation of volumetric efficiency has demonstrated, for the tested compressor, that a system without oil separator could have a reduction in the cooling capacity up to 2% at high speeds associated to the reduction of effective refrigerant mass flow caused by oil. This reduction can be explained by refrigerant which is compressed by the compressor but remains solved in the oil not supplying refrigerant effect.
- The OCR values obtained at high speeds and low evaporating temperatures are significantly high, up to 8%. And according to some estimations from literature (Lottin et al., 2003a), those OCR values could led to COP reductions up to 20%.

Finally, from all the results presented, it can be concluded that the deviations observed in the refrigerant mass flow rate depending on the employed measurement method could have an important influence in the estimation of the cooling capacity of variable speed scroll compressor working with propane. Hence, significant deviations between catalog capacity values and the real capacity values supplied by a compressor working in real systems could be expected. To avoid this, more information about how the catalog mass flow has been obtained and about the OCR evolution with the speed would reduce this uncertainty in the design of systems with these compressors.

5.7. Nomenclature

Nomenclature:


C	regression coefficient
Cp	heat capacity
displ	compressor's displacement
h	enthalpy
\dot{m}	mass flow
MO	Mineral Oil
μ_c	compressor efficiency
μ_v	volumetric efficiency
N	rotational speed
OCR	Oil Circulation Rate
P	pressure
P_{electr}	electrical power
P_{loss}	power lost to ambient
POE	polyol ester
UV	Ultra Violet
ϑ	specific volume

Subscripts:

1	at compressor inlet
2s	at compressor outlet considering isentropic compression
e	effective
ineff	not producing refrigerating effect
in / out	at evaporator inlet / outlet conditions
max	maximum
oil	lubricant oil
refr	refrigerant
total	sum of refrigerant and oil

Chapter 6:

FIFTH PUBLICATION



**13th National and 4th International
Conference in Engineering Thermodynamics**

Castellón de la Plana
29/11–01/12/2023

13ENIT | **UNIVERSITAT
JAUME I** | **FUNDACIÓ
DE L'ENGINYERIA
I LA CIÈNCIA**

Communication number: 804

A Novel and Compact Correlation for the Prediction of Oil-Refrigerant Miscibility

6.1. Introduction

The primary function of oil lubricants in heat pumps is to reduce wear and improve the seal between the discharge and suction sides. Additionally, it acts as a coolant homogenizing the temperatures inside the compressor.

When designing a heat pump, the oil selection is based on its viscosity; high-viscosity lubricants seal better but, on the other side, increase frictional losses (ASHRAE, 2010) and therefore, a compromised solution is needed. Another lubricant parameter that must be considered is its miscibility with the used refrigerant; a high miscibility is required to avoid oil retention in the evaporator and ensure oil return to the compressor. However, having refrigerant dissolved in the oil reduces its viscosity and reduces the effective refrigerant charge in the system, which is especially critical when there are charge limitations.

Oil, albeit being necessary in the compressor, is not desired in the rest of the system as it reduces heat transfer in heat exchangers and can block the expansion devices (Kruse & Schroeder, 1985). Additionally, if both solubility and oil quantity in the evaporator are high, the refrigerant will be kept solved in the lubricant and won't evaporate (not providing cooling capacity)(Ossorio et al., 2023).

In order to characterize viscosity and solubility, multiple correlations have been published. Regarding viscosity, oils are standardized according to an ISO viscosity grade as specified by ASTM Standard D2422 and its temperature dependence is declared in ASTM Standard D341. However, there is no a standardized solubility correlation, and the most relevant equations to model it are summarized in Table 6.1.

P represents the pressure of the mixture and P_{sat} the saturation pressure of pure refrigerant (both in bar). Mixture temperature (T) and refrigerant critical temperature (T_{crit}) are given in K. The mass concentration of refrigerant in the mixture is represented as x_{ref} and finally $k_{\#}$ are the model coefficients.

The mentioned equations are typically fitted for compressor conditions which involve high oil concentrations and they show high extrapolation errors. Therefore, they cannot be applied if the refrigerant concentration (x_{ref}) is higher than 30-40%. However, values of x_{ref} closer to 1 are found if oil-refrigerant interactions are studied in the evaporator.

Additionally, Göpfert et al. isn't a linear equation which can make the coefficient fitting challenging. Seeton does not converge at P_{sat} when $x_{ref} = 1$ and at 0 bar when $x_{ref} = 0$, and all of them can incur predicting values higher than P_{sat} at $x_{ref} < 1$.

Finally, all of them show a high number of coefficients which could involve overfitting when adjusted in all the concentration range and do not allow a direct comparison between oils comparing their fitting parameters as they do not have any physical meaning.

In this study, the miscibility of a POE ISO68 oil and propane is experimentally obtained as a function of x_{ref} and temperature, and then, the obtained data is used to test the equations in Table 6.1. Additionally, a new correlation is proposed, designed to be as simple as possible, to avoid non-physical predictions and to allow the comparison between mixtures by only comparing the fitting parameters.

Table 6.1: Equations for the characterization of Oil-Refrigerant Miscibility

Id	Model	Expression	Coefs	Var	Linear
Seeton	Seeton and Hrnjak [4]	$\log_{10}(P) = k_1 + \frac{k_2}{T} + \frac{k_3}{T^2} + \log_{10}(x_{ref}) \left(k_4 + \frac{k_5}{T} + \frac{k_6}{T^2} \right) + \log_{10}^2(x_{ref}) \left(k_7 + \frac{k_8}{T} + \frac{k_9}{T^2} \right)$	9	3	Yes
Cavestri	Cavestri [5]	$P = P_{sat}x_{ref} + P_{sat}(1 - x_{ref}) \left(k_1 + k_2 \frac{T}{T_{crit}} + k_3 \left(\frac{T}{T_{crit}} \right)^2 + k_4 x_{ref} + k_5 x_{ref} \frac{T}{T_{crit}} + k_6 x_{ref} \left(\frac{T}{T_{crit}} \right)^2 \right)$	6	5	Yes
Göpfert	Göpfert et al [6]	$P = P_{sat}x_{ref} \left[k_1(1 - x_{ref})^{k_2} + k_3 \frac{T}{T_{crit}} + k_4(1 - x_{ref}) \frac{T}{T_{crit}} + k_5(1 - x_{ref})^2 + k_6 x_{ref} \left(\frac{T}{T_{crit}} \right)^2 + k_7(1 - x_{ref})^2 \left(\frac{T}{T_{crit}} \right)^2 \right]$	7	5	No

6.2. Experimental data

The test bench displayed in Figure 6.1 was used to test the oil-refrigerant miscibility. It consists of isochoric sample tubes made from borosilicate glass in which temperature, pressure and the volume of the phases are monitored. Those are placed inside a climatic chamber whose temperature can be controlled in the range of $-40\text{ }^{\circ}\text{C}$ to $80\text{ }^{\circ}\text{C}$.



Figure 6.1: Miscibility test bench

Each sample tube is charged with a specific oil-refrigerant concentration, and then they are vibrated at a certain chamber temperature until the internal pressure stabilizes. Then the liquid height is measured and, with that, the liquid and vapor volume can be calculated, which is needed to obtain the corrected oil-refrigerant concentration of the liquid fraction (x_{ref}).

Regarding the instrumentation, Keller M5HB transmitters with an accuracy of 0.06 bar were used for measuring pressure and immersion PT100 for measuring temperature. A National Instrument interface was used for data logging and monitoring.

It should be noted that the main uncertainty source is the repeatability of the tests due to the temperature control algorithm and how long it takes to reach miscibility equilibrium.

6.3. Results

The described test bench was used to characterize the miscibility of propane and a POE oil. The experimental results from the tests are displayed in Figure 6.2 as solid dots.

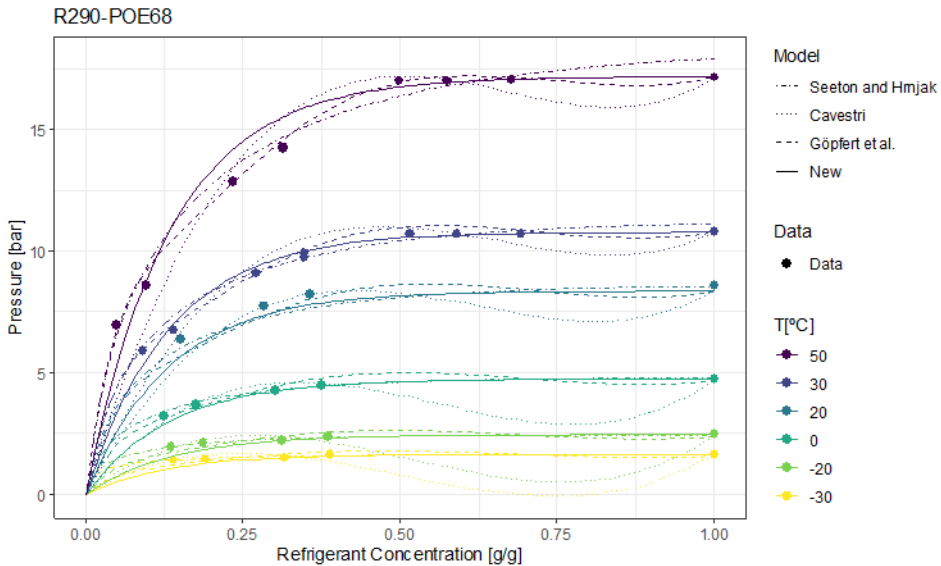


Figure 6.2: Test results and model predictions

Figure 6.2 represents how the mixture pressure varies with either the refrigerant concentration and temperature. The general trend is clear, pressure tends to zero as concentration approaches pure oil and, as concentration approaches pure refrigerant, pressure tends to its saturating pressure. The evolution of pressure between pure oil and pure refrigerant is determined by its solubility; if both are not very miscible, pressure will reach values close to saturation at lower refrigerant concentrations.

The presented data was used to fit the models in Table 5.1. Their predictions are also displayed in Figure 6.2. and their fitted parameters are displayed in Table 6.2.

- Seeton and Hrnjak model provides a smooth evolution of pressure with refrigerant concentration and that evolution is homogenous (there is not a decrease of pressure as x_{ref} increases). On the other hand, it has numerous fitting coefficients and does not converge to the saturating pressure when $x_{ref} = 1$ (this discrepancy is especially important at higher temperatures).
- Cavestri model forces P_{sat} when $x_{ref} = 1$ and 0 bar when $x_{ref} = 0$. However, it fails to describe the general behavior of pressure with concentration as the predicted behavior contains oscillations which are especially important at low temperatures (even negative pressures are predicted).
- Göpfert et al. model performs best compared with the previous ones. It fits closely the tests data and, even if P_{sat} is not forced when $x_{ref} = 1$, the deviation is rather small (always lower than 0.1bar). Nevertheless, it is not a linear correlation that makes it difficult to fit and keeps having oscillations which do not have physical sense.

As shown, the most used solubility models fail to correctly predict the general behavior of the mixture. That is why, another model was designed with the focus on eliminating oscillations and forcing P_{sat} when $x_{ref} = 1$. It was also desired to obtain an easy correlation with the fewer number of fitting coefficients. With that in mind, the correlation in Eq.(10) was designed, whose predictions are represented with a solid line in Figure 6.2.

$$P = P_{sat} \left(1 - e^{\frac{-x_{ref}}{k}} + e^{\frac{-1}{k}} \right) \quad (10)$$

Being P_{sat} the saturation pressure of the pure refrigerant at a certain temperature. It can be calculated using a refrigerant database as Refprop (Lemmon & McLinden, 2002) or by using the Antoine equation as a function of temperature.

Table 6.2 Fitting coefficients of the different models

	SEETON AND HRNJAK	CAVESTRI	GÖPFERT ET AL.	NEW
K1	4.900	68.15	8.462	0.1333
K2	1305	-144.7	15.00	
K3	4.101e+04	81.568	2.363	
K4	8.799	-225.7	-0.516	
K5	-4.913	512.9	6.333	
K6	6.789e+05	-296.5	-1.392	
K7	9.469		-4.796	
K8	-5597			
K9	8.013e+05			
RMSE [BAR]	0.303	0.723	0.184	0.464

The proposed model has only 1 coefficient which additionally is dimensionless and thus can be treated as a Miscibility Index (higher values of k would imply higher miscibilities). This allows to compare the miscibility of different mixtures by only checking the fitting parameters, which was impossible with the other correlations.

The term $e^{\frac{-1}{k}}$ was added to force P_{sat} when $x_{ref} = 1$. However, its presence is not crucial, especially for solubility indexes lower than 0.21 as the introduced error would be lower than 0.01 bar. In the case of not introducing this additional term, the correlation could be linearized by applying logarithms and solved with ease with the simplest regression algorithms. Additionally, in the extreme case, the value of k could be found by solving the equation with only one test result.

This model corrects the previously mentioned issues and fits well most of the experimental data. Additionally, it was proved to be robust when applied to different oil-refrigerant mixtures with completely different miscibility indexes as shown in Figure 6.3.

The Root Mean Squared Error (RMSE) was also displayed in Table 6.2 to evaluate the goodness of fit. The lowest error is obtained by Göpfert et al. model and the new model has a RMSE lower than 0.5 bar.

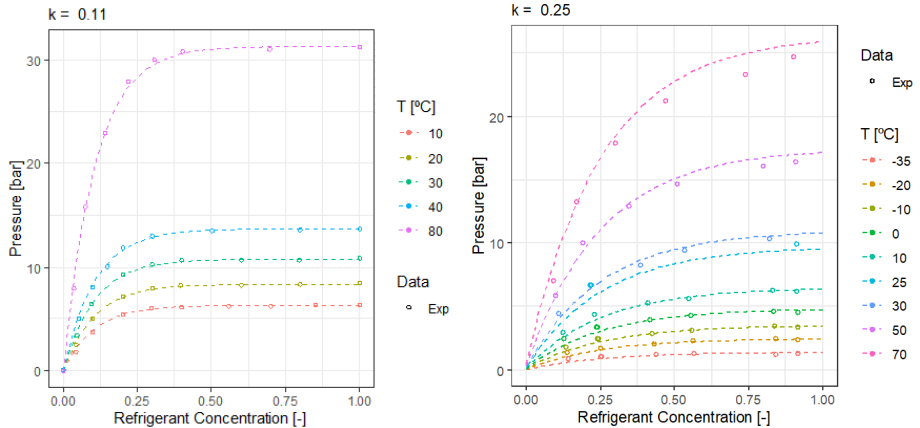


Figure 6.3: New model predictions of low miscibility mixtures ($k=0.11$) [Left] and high miscibility mixtures ($k=0.25$) [Right]

6.4. Conclusions

In this study, the limitations of the most used models to predict solubility are highlighted, and a new model is proposed whose main characteristics are:

- Compactness.
- Miscibility Index: It uses only one dimensionless fitting coefficient which can be used to compare mixtures.
- It can be simplified and linearized with ease.
- It can be fitted with scarce experimental data. In worst-case scenario only with one test.
- Robustness: can be applied to very different mixtures without overfitting

In conclusion, this new equation could have a higher performance compared with classical correlations when realistic predictions are needed over the complete concentration range and could allow the standardization of the miscibility thanks to the use of a Miscibility Index (similar to the Viscosity Index).

Chapter 7:

SIXTH PUBLICATION





International Journal of Refrigeration

Volume 145, January 2023, Pages 436-445



Impact of lubricant in the performance of
variable speed heat pumps working with
R290

Impact du lubrifiant sur les performances
des pompes à chaleur à vitesse variable
fonctionnant au R290

Rubén Ossorio^a, Emilio Navarro-Peris^a ,  Riley B. Barta^b

<https://doi.org/10.1016/j.ijrefrig.2022.10.003>

Impact of Lubricant in the Performance of Variable Speed Heat Pumps

Rubén Ossorio¹, Emilio Navarro-Peris¹, RileyB.Barta²

¹ Instituto Universitario de Investigación en Ingeniería Energética (IUIIE)
Universitat Politècnica de València, Camino de Vera s/n, ed. 8E cubo F 5º, Valencia, 46022,
Spain

² Bitzer Chair for Refrigeration, Cryogenics and Compressor Technology, Technische Universität Dresden, 01062 Dresden, Germany

7.1. Abstract

Modulating the speed of the compressors and adapting its capacity to the required load has led to a decrease in the annual energy consumption in many applications. However, in the compressor, having adequate lubrication at low speeds usually implies discharging too much lubricant at higher speeds. Although necessary for compressor operation, lubricating oil acts as a contaminant in the rest of the system. Consequently, manufacturers have to consider the oil circulation rate (OCR), as it limits the speed range of the compressor. In a previous study, a compressor was tested over its speed range (30 to 110Hz), working with R290 and POE68 as a lubricant. Experimental data confirm the increase of OCR with speed and suggests that working with R290-POE68 could imply higher OCR values compared to other refrigerant-oil mixtures. In this study, the impact of the OCR in the performance of a R290 heat pump was theoretically assessed. Three contributions were studied: The heat transfer coefficient (HTC) reduction in the evaporator, the effect of refrigerant being solved in oil and finally, the impact of oil in the compressor. It was found that OCR values of 5% could decrease the coefficient of performance (COP) by more than 20%.

Keywords: OCR, Heat Transfer Coefficient, Solubility, Oil effect

7.2. Introduction

Lubrication is necessary for most compressors for the lubrication of their moving parts. It also ensures a seal in the compression chamber and acts as a coolant, transferring heat from the bearings to the crankcase sump (ASHRAE, 2010). Different technologies arise to provide a sufficient amount of oil in the key spots. In scroll compressors, it is common to use a drill into the shaft that acts as a pump to lift the oil from the oil sump to the main bearing and the compression chamber, which is typically located in the upper part (Branch & Lepak, 2019). This pumping action depends mainly on the rotational speed of the shaft. Consequently, when designing variable speed compressors, having enough pumping action at low speeds implies having too much-pumping action at high speeds, having an excess of oil discharged out of the compressor. Ribeiro and Barbosa (Ribeiro & Barbosa, 2016) suggested a model of a centrifugal oil pump based on the study of (Kim & Lancey, 2003) to estimate the oil mass flow discharged by the compressor. However, the model used hard-to-find geometric data and a correction factor using six correlation coefficients.

Although necessary in the compressor, oil is considered as contaminant in the rest of the system; oil changes the thermodynamic properties of the refrigerant, reduces the heat transfer coefficient in the heat exchangers, and, in worst cases, can block the expansion device (Kruse & Schroeder, 1985). Consequently, it is essential to estimate the quantity of oil circulating in the system, and to do so, Oil Circulation Rate (OCR) is the main parameter used in the literature, which is expressed as:

$$OCR = \frac{\dot{m}_{oil}}{\dot{m}_{oil} + \dot{m}_{ref}} \quad (7.1)$$

Where \dot{m}_{oil} is the oil mass flow circulating in the system and \dot{m}_{ref} is the refrigerant mass flow.

In a previous study (Ossorio & Navarro-Peris, 2021), a variable speed scroll compressor working with R290 and POE68 was tested and the evolution of OCR and \dot{m}_{oil} was studied as a function of variables such as T_{cond} , T_{evap} and compressor speed. The results at high speeds shown OCR values higher than 5%, reaching peak values close to 7-8%. In that study it was also

found a strong direct dependence of \dot{m}_{oil} with speed. This dependence was in accordance with the model of (Ribeiro & Barbosa, 2016), which considered the spinning shaft of the compressor as a centrifugal pump.

Lottin studied the effect of oil circulation in the heat pump (Lottin et al., 2003a), he followed a thermodynamic approach to quantify the effect of HTC considering the refrigerant and oil as a zeotropic mixture and applying three different HTC correlations: Yam and Lin (Yam et al., 1997), Gungor and Winterton (Gungor & Winterton, 1986) and finally Bivens and Yokozeki (Bivens & Yokozeki, 1994). In his book *Engineering Data Book III* (John R Thome, 2010), Thome also reviewed in-depth the effect of oil in the evaporator HTC. Thome states that, at high vapor qualities, the HTC is sharply reduced due to the significant increase in local liquid viscosity due to high local concentrations of oil. Furthermore, he proposes a procedure to determine the actual HTC considering the oil. First, he uses the flow boiling model of Kattan et al. (Kattan et al., 1998) which is based on flow pattern maps and has been widely recommended in the literature. And then a correction factor is introduced which is dependent on the viscosity of the oil.

Another effect that has to be taken into account when analyzing the effect of oil in the system is the refrigerant solubility in oil. Refrigerant solved in the oil does not evaporate, and thus, it does not provide cooling capacity. The effect of solubility in the evaporator was studied by (Youbi-Idrissi et al., 2003; Youbi-Idrissi et al., 2004; Youbi-Idrissi & Bonjour, 2008). Youbi-Idrissi proposes a methodology to create pressure-enthalpy-quality diagrams for the combined mixture refrigerant-lubricant. This methodology considers that, as the evaporation of the refrigerant takes place, the fraction of oil in the liquid phase increases and, when it is significant, the mixture temperature starts increasing compared to the expected saturation temperature. This apparent superheat can affect the control on thermostatic expansion valves and the enthalpy calculations based on temperature and pressure at the output of the evaporator. Different authors have used this methodology to different mixtures (Sun et al., 2021; Zhelezny et al., 2009).

Apart from the effect on the evaporator, Lottin (Lottin et al., 2003a) also took into account an increase in compressor consumption due to oil. If both contributions are taken into account, the unit's performance can decrease significantly. In particular, with OCR values of 5%, the coefficient of

performance (COP) can be reduced by more than 15%. These results though, were obtained for hydrofluorocarbons (HFC)s, which have liquid densities higher than hydrocarbons such as R290. As OCR is given as a mass fraction, it is possible that, for the same oil flow, R290 systems will present higher values of OCR compared to the HFCs, and consequently, Lottin's results can't be applied to hydrocarbons directly.

In this contribution, the effect of oil in variable speed heat pumps working with R290 and POE68 will be studied. The expected impact on the performance of the obtained OCR measurements in (Ossorio & Navarro-Peris, 2021) will be analyzed. Three significant contributions will be explored independently: HTC reduction, refrigerant solved in oil and oil being heated in the compressor. For the HTC, the flow boiling model of Kattan et al. (Kattan et al., 1998) based on flow pattern maps will be used. The effect of the oil in the model will be taken into account with the proposed correlation in Engineering Data Book III (Thome, 2010). Regarding the solubility of R290 in POE68, it has been characterized empirically and the methodology proposed by Youbi-Idrissi was followed to calculate the effect in the cooling capacity of the evaporator. And finally, the effect of heating the oil in the compressor will be analyzed and compared with the values obtained by Lottin et al. (Lottin et al., 2003a). The increase of pressure drop at the end of the evaporator and in the liquid line due to the presence of oil has not been considered in this study.

7.3. Methodology

As explained in the introduction, the HTC reduction, the solubility effect, and the effect of the oil in the compression will be studied independently. Their contribution to lower the performance will be added afterward.

7.3.1. Impact of lubricant on HTC

A theoretical analysis has been carried out to estimate the impact of OCR in the global system. The reduction of the evaporating temperature due to a decrease of the HTC in the evaporator is assessed. It should be noted that the goal of this study is not to give an exact value but an approximate order

of magnitude of the effect that could have the oil. Consequently, simplifications and assumptions will be made. For example, the correlations used are proposed for high OCRs and do not model the improvement of HTC at very low OCRs due to wettability and foaming.

In this study, the procedure, correlations and correction factors proposed by Thome (Thome, 2010) will be followed to calculate the drop of the overall HTC due to the presence of oil. Once the difference in HTC has been estimated, the decrease of the evaporating temperature is calculated with the LMTD method using the following system of equations:

$$\left\{ \begin{array}{l} Q_{evap} = U \cdot A \cdot LMTD \\ Q_{evap} = \dot{m}_{ref} \cdot (h_{evap,out} - h_{evap,in}) \\ Q_{evap} = \dot{m}_{air} \cdot c_{p,air} \cdot (T_{air,in} - T_{air,out}) \end{array} \right. \quad (7.2)$$

To exemplify this methodology, it will be applied to a virtual heat pump which presents a cooling capacity close to 10kW at air temperatures of 0°C. The evaporator of the heat pump has been considered to be designed with an inner tube diameter of 8.6mm and 2.5m² of total exchange area in the refrigerant part. The number of circuits are designed to ensure a vapor speed of 8.6 m s⁻¹ and the HTC of the refrigerant and air sides have been considered equivalent by design ($U = 0,5$ HTC). Typically, the air part has a much lower HTC but it has been assumed that it was compensated by increasing the exchange area in the air part introducing fins. Regarding the secondary fluid, a fan circulates 7000 m³ h⁻¹ of air at different $T_{air,in}$. For the tested range of temperatures, a constant c_p of 1.012 kJ kg⁻¹ for the air has been considered. Additionally, no superheat (SH) has been considered at the evaporator's output and the inlet quality has been calculated as a function of T_{evap} considering no subcooling (SC) in the condenser and an isenthalpic expansion. All the thermodynamic properties have been calculated using Refprop10 (Lemmon & McLinden, 2002).

Refrigerant mass flow is calculated with Eq.(7.3) assuming a displacement of $0.00506 \text{ m}^3 \text{ s}^{-1}$ (46 cm^3 at 110 Hz), a volumetric efficiency following Eq.(7.4) and the inlet density is expressed as a function of T_{evap} assuming $SH=0K$.

$$\dot{m}_{ref} = displ \cdot \eta_v \cdot \rho_{suc}(T_{evap}) \quad (7.3)$$

$$\eta_v = 9.648e^{-1} + 2.522e^{-3} \cdot T_{evap} - 2.923e^{-5} \cdot T_{evap}^2 \quad (7.4)$$

The main unknowns of the presented system are T_{evap} , Q_{evap} , and $T_{air,out}$. Consequently, the only parameter that remains undetermined is the heat transfer coefficient of the refrigerant. It will be calculated using the Kattan, Thome and Favrat correlation (Kattan et al., 1998) based on flow pattern maps. This correlation requires as inputs the refrigerant properties at the evaporation temperature and parameters of the heat exchanger as; inner tube diameter, heat flux [W m^{-2}], and mass velocity [$\text{kg m}^{-2} \text{ s}^{-1}$]. With this information, the correlation provides a HTC for each local vapor quality. The resulting overall HTC will be assumed to be equivalent to the average HTC calculated along the complete evaporator. Note that the model inputs for the determination of HTC depend on the evaporating temperature, which, in turn, is an unknown of the system. Consequently, an iterative procedure is needed, which is described in Figure 7.1.

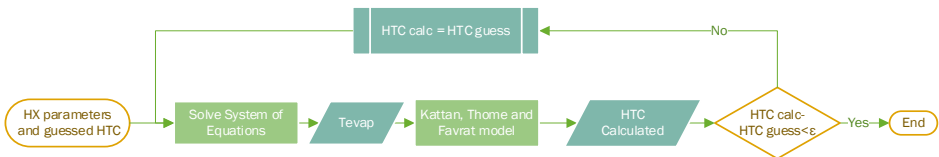


Figure 7.1: Diagram of the iterative procedure to obtain the Heat Transfer Coefficient and T_{evap}

For calculating the new evaporating temperature affected by the oil, the system is solved again but changing HTC. As mentioned, HTC is greatly affected by the presence of oil, especially at the end of the evaporator, where the local concentration of lubricant is higher. Thome in (Thome, 2010) proposes the following correction factor to quantify the reduction of HTC:

$$HTC_{ratio} = \frac{HTC_{ref+oil}}{HTC_{ref}} = \left[\frac{\mu_{ref}}{\mu_{oil}} \right]^{0.26 \cdot x_{oil}} \quad (7.5)$$

Being μ_{ref} and μ_{oil} the dynamic viscosity of the refrigerant and the oil respectively at the evaporating temperature. And being x_{oil} the local oil mass concentration in the liquid phase calculated with Eq.(7.6), being x_e the local vapor quality:

$$x_{oil} = 1 - x_{ref} = \frac{OCR}{1 - x_e} \quad (7.6)$$

Regarding the dynamic viscosity of the lubricant in Eq.(7.5), it was estimated using the correlation of Guzman-Andrade:

$$\mu_{oil} = A \cdot e^{B/T} \cdot \rho_{oil} \quad (7.7)$$

Where T is the evaporating temperature in K, ρ_{oil} the lubricant density (987 kg m⁻³) and A=4.54e-4 and B=3730 are the fitting coefficients calculated using the viscosity catalog data at 40°C and 100°C.

Once the iteration process has been solved, and the reduction in T_{evap} due to the decrease in HTC has been calculated, the potential COP reduction is calculated using the compressor model proposed by Shao (Shao et al., 2004) using experimental data to adjust the coefficients in Table 7.1:

$$W_c | \dot{m}_t = a_0 + a_1 T_{cond}^2 + a_2 T_{cond} + a_3 T_{cond} T_{evap} + a_4 T_{evap}^2 + a_5 T_{evap} \quad (7.8)$$

	a₀	a₁	a₂	a₃	a₄	a₅	R²
W_c	2.32E+03	3.23E-01	3.44E+01	6.91E-01	-3.70E-01	-1.07E+01	0.9984
\dot{m}	4.93E+01	-9.51E-05	-1.92E-02	-4.85E-05	1.75E-02	1.57E+00	0.9994

Table 7.1: Fitting parameters and R² of the compressor models

Being COP defined as:

$$COP = \frac{\dot{Q}_{evap}}{\dot{W}_c} = \frac{\dot{m} \Delta h_{evap}}{\dot{W}_c} \quad (7.9)$$

Where \dot{W}_c and \dot{m} are obtained with the compressor model defined in Eq.(7.8) and Δh_{evap} is obtained at a certain T_{cond} and T_{evap} , assuming SC=SH=0 K.

7.3.2. Impact of lubricant solubility on the evaporator

The first step to analyze the impact of the solubility is to characterize the solubility of refrigerant in oil. To do so, an experimental campaign was designed which provided the results of Figure 7.2 (with x_{ref} being the mass fraction of refrigerant in the liquid mixture):

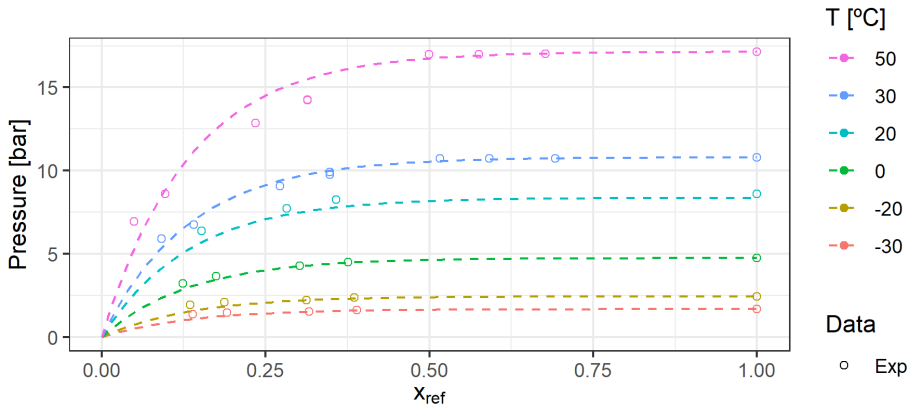


Figure 7.2: Liquid-Vapor-Equilibrium diagram of R290 and POE68

The experimental data were fitted using a new correlation based on the Weibull distribution, which appears to fit well even when reduced experimental data is available and there is no accurate value of molar weight to obtain the molar concentration. The equation used is the following:

$$P = P_{sat}(1 - e^{-k \cdot x_{ref}} + e^{-k}) \quad (7.10)$$

Being P_{sat} the saturation pressure of pure refrigerant at a specific T , x_{ref} the mass fraction of refrigerant in the liquid and k the only fitting coefficient that, for the studied mixture, equals 7.5. To be noted is that, by definition, mixture pressure tends to P_{sat} with pure refrigerant and to zero when pure oil. Note also that the relation between x_{ref} and the vapor quality is given by Eq.(7.6).

The solubility formula presented explains how pressure is affected by the lubricant. Regarding the effect of oil on enthalpy, the method proposed by (M. Youbi-Idrissi et al., 2004) has been applied. This method is based on a three terms equation as a function of vapor quality; the first term quantifies

the enthalpy of the not evaporated refrigerant, the second the enthalpy of the oil and the third the enthalpy of the vaporized refrigerant:

$$h_t = (1 - x_e - OCR) \cdot h_{l,ref} + OCR \cdot h_{oil} + x_e \cdot h_{v,ref} \quad (7.11)$$

$h_{l,r}$ and $h_{v,r}$ are the specific enthalpy of pure refrigerant at the condition of liquid and vapor phase, respectively. Besides, x_e is the vapor quality, which is calculated as:

$$x_e = \frac{m_v}{m_{l,ref} + m_{oil} + m_v} \quad (7.12)$$

In Eq.(7.11) h_{oil} represents the specific enthalpy of the oil, which is calculated as:

$$h_{oil} = h_o + \int_{T_o}^T C_{p,oil} dT \quad (7.13)$$

h_o and T_o are the reference enthalpy and temperature which have values of 200 kJ kg⁻¹ and 273.15K respectively. $C_{p,oil}$ is the specific heat capacity of the oil which is given as a function of temperature and density by the equation of Liley and Gambill cited in (Mermond et al., 1999):

$$C_{p,oil} = \frac{0.75529 + 0.0034 T}{\sqrt{\rho_{oil}/998.5}} \quad (7.14)$$

Where ρ_{oil} is the density of oil at 15.6°C, which has the value of 984.97 kg m⁻³ for the chosen POE.

Once pressure and enthalpy have been calculated as a function of the vapor quality x_e , it is possible to:

- Generate a P-h-X plot of the mixture.
- Calculate the non-expanded quantity of refrigerant (*NEQ*) at a certain vapor quality:

$$NEQ = \frac{m_{l,ref}}{m_{l,ref} + m_v} = 1 - \left(\frac{x_e}{1 - OCR} \right)_{evap,outlet} \quad (7.15)$$

- Calculate the apparent superheat SH^* , with $T_{sat,pure}$ calculated at the evaporating pressure considering pure refrigerant.

$$SH^* = T_{evap,out} - T_{sat,pure} \quad (7.16)$$

- Calculate the enthalpy ratio R_h , which represents the enthalpy difference reduction in the evaporator at a specific outlet temperature when oil is circulating in the system.

$$R_h = \frac{\Delta h_{ref,oil}}{\Delta h_{r,pure}} \quad (7.17)$$

with $\Delta h_{ref,oil} = h_{evap,out}(T_{out}, P_{out}, OCR) - h_{evap,in}(T_{in}, P_{in}, OCR)$

7.3.3. Impact of lubricant in compressor

During the compression process, the oil in the compression chamber also gets compressed and heated, and additionally, in this process, part of the refrigerant that was solved vaporizes. Those processes require energy, which has to be supplied by the compressor. Consequently, if the oil is considered, the formula of the ideal compression work should be expanded with new terms:

$$W_c = \dot{m}_{ref} (h_{2s} - h_1) + \dot{m}_{oil} c_p (T_{2s} - T_1) + \dot{m}_{oil} \vartheta_{oil} (P_2 - P_1) + \dot{m}_{exp} \Delta h_{vap} \quad (7.18)$$

The first term represents the isentropic compression work of the refrigerant. The second and the third stand for the work needed to compress and heat the oil to the discharge conditions. Remark that as ϑ_{oil} is very low, that term can be easily neglected. And finally, the last term is related with the vaporization of the refrigerant solved into the oil due to an increase of temperature during the compression.

7.4. Results

7.4.1. Impact of lubricant on HTC

An example of the effect of oil in HTC and its evolution with the vapor quality is displayed in Figure 7.3. It is the result of applying the (Kattan et al., 1998) flow map model and the (Thome, 2007) correction for oil presence. The input parameters are: a T_{evap} of $-10\text{ }^{\circ}\text{C}$, an OCR of 5%, a tube inner diameter of 8.6 mm, a heat flux of $4000\frac{\text{W}}{\text{m}^2}$ and $72\frac{\text{kg}}{\text{m}^2\text{s}}$ mass velocity.

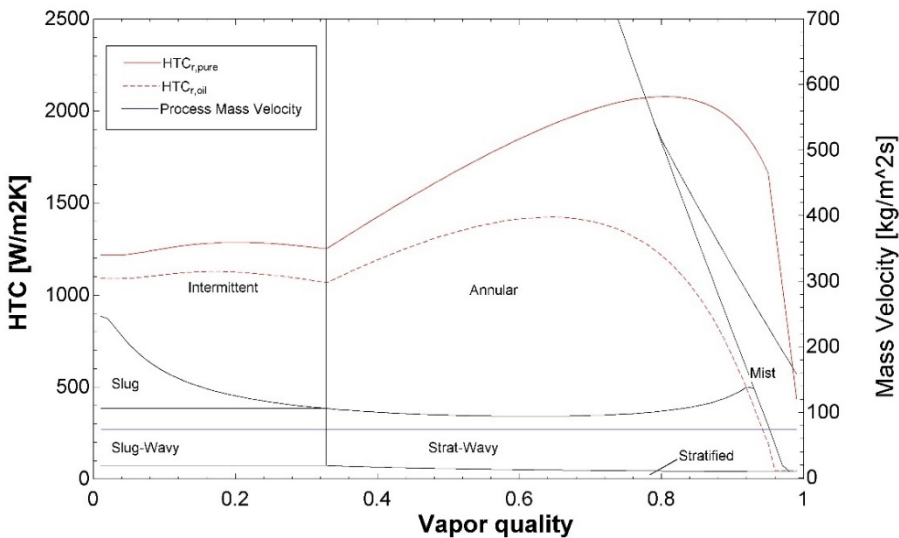


Figure 7.3: Evolution of heat transfer as a function of vapor quality

In Figure 7.3, the black lines represent the limits between flow regimens, which are defined as a function of vapor quality and mass velocity. The horizontal blue line represents the mass velocity of the refrigerant during the process of evaporation. It determines the flow pattern that will appear in the different parts of the evaporator. And finally, the red lines represent the evolution of the HTC during the evaporation, being the dashed line the reduced HTC due to the oil presence. If it is assumed that the evolution of vapor quality is homogeneous along the evaporator length and that the input vapor quality is 0.35, the average HTC considering pure refrigerant and considering

the influence of the lubricant would be 1.73 and $1.10 \text{ W}/(\text{m}^2\text{K})$ respectively (a HTCratio of 0.63) for the example case.

The impact of oil in T_{evap} can be estimated solving the equation system (7.2) with the iterative procedure described in Figure 7.1. If we repeat this methodology for different $T_{air,in}$ and OCR values, the results displayed in Figure 7.4 are obtained. In the bottom subplot, a slice of the upper figure is presented, fixing a $T_{air,in} = 0^\circ\text{C}$.

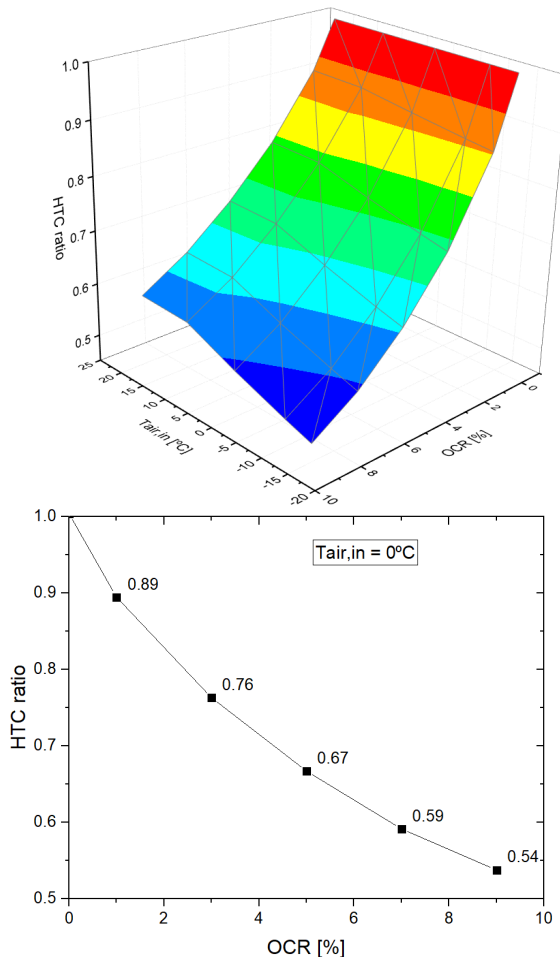


Figure 7.4: HTC ratio evolution with: OCR and $T_{air,in}$ (up), HTC ratio evolution with OCR, assuming $T_{air,in} = 0^\circ\text{C}$ (down)

Figure 7.4 (up) shows that the HTC ratio depends much more on the OCR than on $T_{air,in}$. And Figure 7.4 (down) shows that HTC ratio decreases with OCR. At OCR levels of 5% the HTC ratio is 0.67.

The effect of oil in T_{evap} is studied in Figure 7.5.

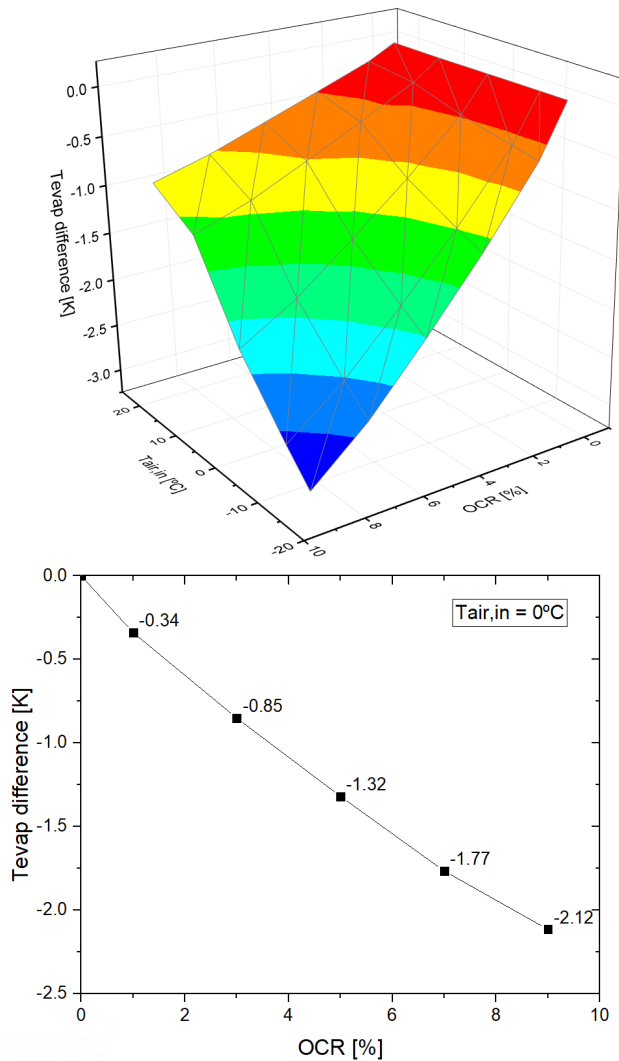


Figure 7.5: Evolution of the drop in T_{evap} with OCR and $T_{air,in}$ (up). Dependence of the drop in T_{evap} and the decrease of COP with of OCR $T_{air,in} = 0^\circ\text{C}$ (down)

As expected, when OCR increases, HTC decreases and T_{evap} decreases too. For OCR values of 5% the expected reduction in T_{evap} is 1.3K at $T_{air,in}$ of 0°C. This decrease is more significant at higher OCR and lower $T_{air,in}$. With Eq.(7.8) and Eq.(7.9) it is possible to convert this decrease in T_{evap} into a decrease of COP. This conversion is displayed in Figure 7.6.

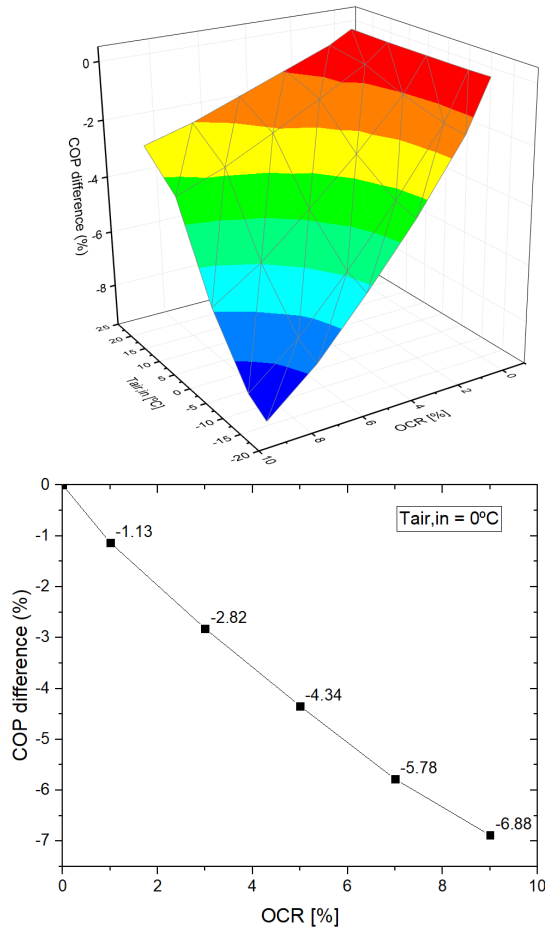


Figure 7.6: Evolution of COP with OCR and $T_{air,in}$ (up). Dependence of COP reduction with OCR assuming $T_{air,in} = 0^\circ\text{C}$ (down)

For OCR values of 5% the expected reduction in COP is 4.3% at $T_{air,in}$ of 0°C. This decrease is more significant at higher OCR and lower $T_{air,in}$ reaching a peak value of 9.3%.

7.4.2. Impact of solubility on performance

Knowing how to calculate the effect of oil in pressure (7.10) and specific enthalpy (7.11) it is possible to create a P-h-X diagram of the refrigerant-oil mixture. The particular case of R290 and a 5% of POE68 is displayed in Figure 7.7.

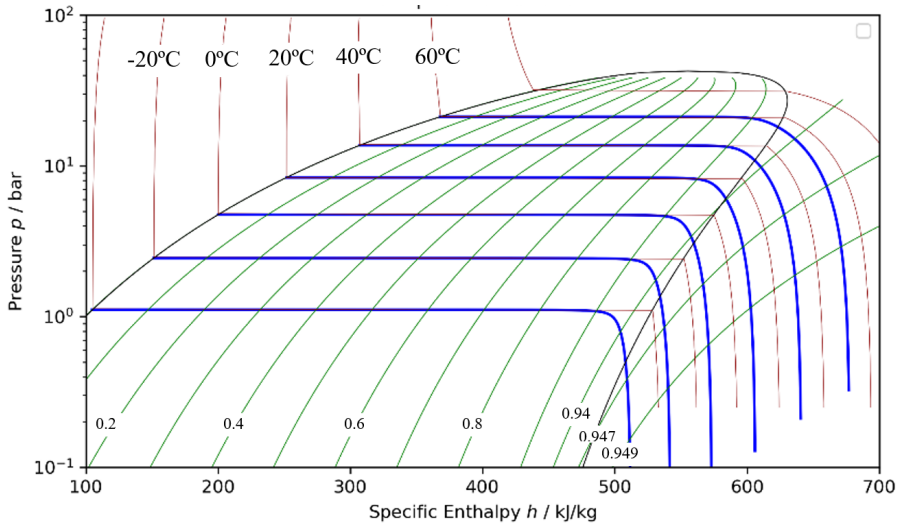


Figure 7.7: P-h-X diagram of R290 and POE68 (OCR=5%)

In the new diagram, the iso-quality lines extend out of the two-phase region of the pure refrigerant and, as the oil is considered to remain in the liquid state in the studied range, no qualities higher than 1-OCR are obtained. To be noted is also that there are two differentiated regions during the evaporation; one in which the mixture behaves as pure refrigerant (quasi isothermal evaporation), and one in which the sensible heat starts being significant and an apparent SH appears. This apparent superheat means a temperature rise even if there is still refrigerant in liquid state and occurs when the local liquid concentration of oil is high, at the end of the evaporator, with high vapor qualities. The relation between these variables (vapor quality, liquid concentration of oil and apparent SH) can be studied in Figure 7.8.

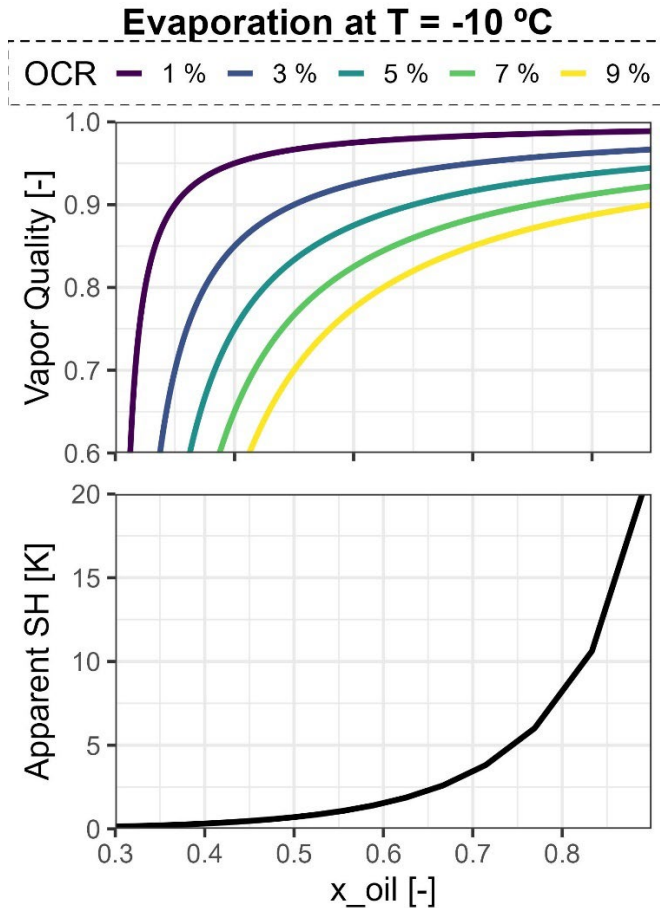


Figure 7.8: Relation between vapor quality, oil concentration in the liquid and apparent SH

This apparent SH will affect the control algorithm of thermostatic expansion valves and also, it will affect the energy balances in the evaporator. For example, looking at Figure 7.7, if we have $T_{evap} = -10^{\circ}\text{C}$ and $\text{SH}=1$ at the outlet of the evaporator, an enthalpy of 580 kJ kg^{-1} is expected (according to the pure refrigerant diagram). However, if an OCR of 5% is taken into account, the outlet enthalpy would be closer to 540 kJ kg^{-1} for 21°C at the output of the evaporator. If the enthalpy at the inlet of the evaporator is 336 kJ kg^{-1} for both cases (assuming $T_{cond}=50^{\circ}\text{C}$ and $\text{SC}=0$), the enthalpy difference ratio R_h would be 0.84 (applying Eq(7.17)). The effect of the apparent SH and OCR on the R_h is shown in Figure 7.9 (up).

Another way of studying the effect of having oil in the evaporator is considering that part of the refrigerant is solved in the oil and never evaporates, which lowers the cooling capacity in the evaporator. The more the apparent SH at the output of the evaporator the lower the not evaporated quantity (NEQ), this relation is shown in Figure 7.9 (down).

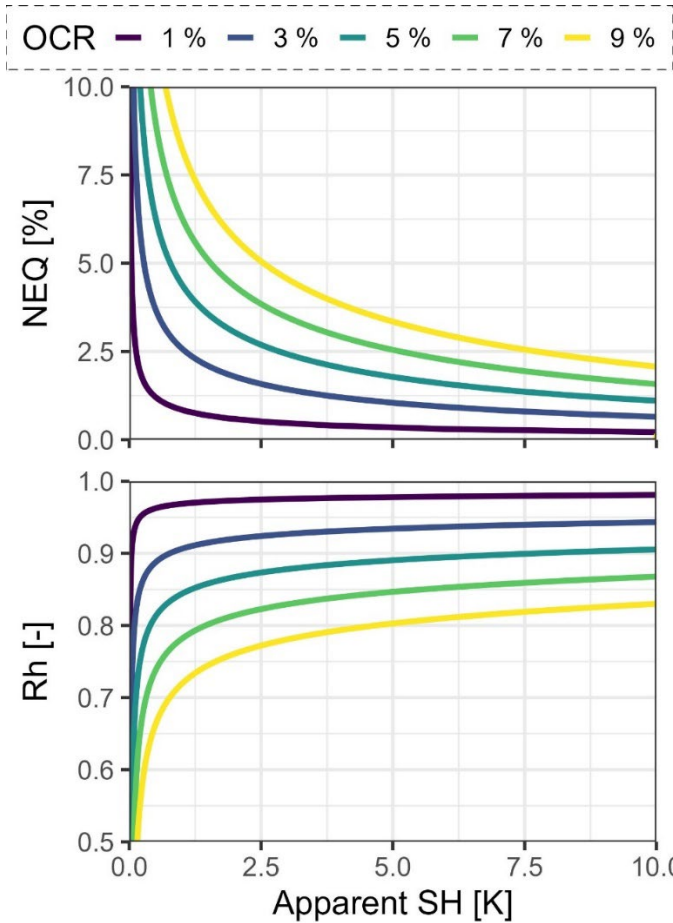


Figure 7.9: Evolution of Rh (up) and NEQ (down) with apparent SH for different OCR values

This evolution is greatly affected by the solubility of the refrigerant in oil. In this case, even with a low miscible oil, we obtain $Rh=0.943$ and $NEQ=1.11\%$ for $SH=10K$ and OCR of 5%. It should be noted that Rh and NEQ are manifestations of the same phenomena so, to study the effect of solubility on the

cooling capacity, we will focus on the effect of NEQ with the following equation:

$$\frac{Q_{evap,oil}}{Q_{evap,pure}} = \frac{\dot{m}_{ref,exp}}{\dot{m}_{ref}} \frac{\Delta h_{ref,pure}}{\Delta h_{ref,pure}} = 1 - NEQ \quad (7.19)$$

If we substitute in the formula the values obtained for SH=10K and OCR=5%, a capacity ratio of 98.89% is achieved. Which is translated to a reduction in COP of 1.11%. In Figure 7.10, the results for different OCR values are displayed, keeping the rest of the variables constant:

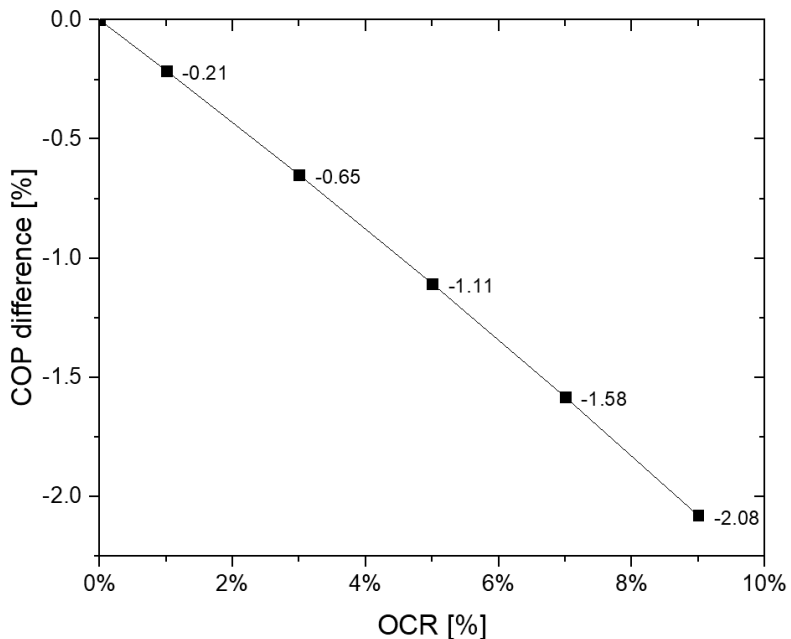


Figure 7.10: COP reduction due to refrigerant solved in oil as a function of OCR and the methodology used.

The graph shows an almost linear dependence between OCR and the COP reduction reaching a value of 2% for OCR values of 9%.

7.4.3. Impact of oil in compressor consumption

To exemplify the methodology, the impact of oil will be analyzed for a representative compression condition of a tested variable speed compressor (46 cm³) working with R290 and with 1200ml of POE68 on it (Ossorio &

Navarro-Peris, 2021). The compression condition was: $N=110\text{Hz}$, $T_{evap} = -10^\circ\text{C}$, $T_{cond} = 50^\circ\text{C}$ and $SH=10$ K. For that particular condition, an OCR of 5% was obtained experimentally.

For this analysis, it has been assumed $c_{p,oil}=1738\frac{\text{J}}{\text{kg K}}$, $\rho_{oil}=979\frac{\text{kg}}{\text{m}^3}$, $\Delta h_{vap}=580.3\frac{\text{kJ}}{\text{kg}}$. Regarding \dot{m}_{exp} , to calculate the maximum effect of this term, it is considered that, at the discharge of the compressor, due to the increment of temperature, the solved refrigerant in the oil is close to zero and $\dot{m}_{exp} = \dot{m}_{ref} \cdot NEQ$ (with $NEQ = 1.11\%$ from last section).

$$W_c = \dot{m}_{ref} (h_{2s} - h_1) + \dot{m}_{oil} c_{p,oil} (T_{2is} - T_1) + \dot{m}_{oil} \vartheta_{oil} (P_2 - P_1) + \dot{m}_{exp} \Delta h_{vap} \quad (7.20)$$

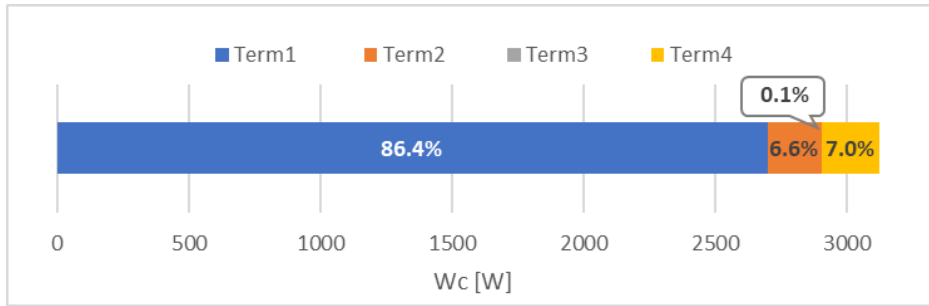


Figure 7.11: Contribution to the total compressor consumption of the different terms of Eq.(7.20)

The results are displayed in Figure 7.11 and shows that, from the total consumption, the 86.4% is used to compress the refrigerant and, from the other 13.6% of the compressor power consumption, 6.6 % is used to heat the oil and 7% to vaporize the solved refrigerant. The work used to compress the oil can be neglected as ϑ_{oil} is very low. Note that the compressor model presented is based in the theoretical calculations carried out by Lottin and it is highly dependent on the made assumptions and has not been validated by experimental data. Additionally, this impact cannot be avoided by introducing an oil separator and consequently it is not easy to study.

Regarding the impact on the performance for the studied case with $OCR=5\%$, oil increases the compression work by 15.8%, which translates to a decrease of COP of 13.6%. In Figure 7.12, the results for different OCR values are displayed, keeping the rest of the variables constant:

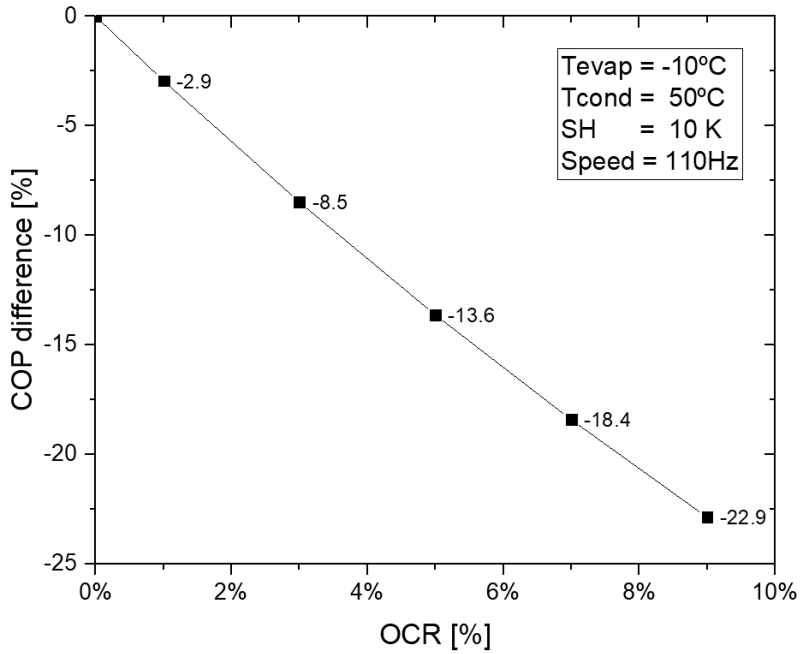


Figure 7.12: Evolution of the COP reduction due to the heating of oil during compression for different OCR values.

The results show that the COP reduction can achieve values higher than 20% for OCR values of 9%.

7.5. Conclusions

In this study, the theoretical effect of oil presence on the performance of a heat pump is analyzed. Three effects were studied, the decrease of heat transfer in the evaporator, refrigerant being solved in oil and the effect of oil being heated during compression. The results are studied as a function of the amount of oil circulation rate in the system which, in scroll compressors working with R290, is higher than refrigeration systems working with HFCs. This could be explained as propane has lower density and the oil circulation ratio is mass based. In particular, with oil circulation rate of 5%, value that, according previous works, has been found in scroll compressors working at high speeds with R290, the following results arises:

- The lowering of HTC translates into a COP decrease of 4.3% for a representative working condition. This impact could increase for higher OCR and lower evaporating temperatures.
- The impact of solubility in the evaporator in the evaluated conditions is in the range of 1%. In other situations, this impact can be more significant, especially when lower SH is selected and when the solubility of refrigerant and oil is higher.
- A decrease in COP higher than 5% is expected if we add up the impact of oil in the evaporator due to HTC and solubility.
- The highest losses due to the oil presence are found in the compressor, where a COP reduction close to 15% can be found. These losses appear as energy is wasted heating the lubricant during the compression.

If all contributions are supposed to be independent (to have an estimation of the maximum theoretical impact), a decrease of COP of around 20% could be reached for OCR values easily found at high compressor speeds. With this significant decrease in performance, a redesign of the pumping system of these compressors may be considered to reduce the oil circulation at high speeds and the use of oil separators is highly recommended to reduce the amount of oil reaching the heat exchangers. Additionally, the reduction of discharged oil could help reducing the refrigerant charge of the system, especially important with flammable refrigerant that have charge restrictions as R290.

7.6. Nomenclature

Abbreviations

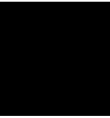
A	area (m^2)
h	enthalpy (kJ kg^{-1})
displ	compressor displacement ($\text{m}^3 \text{s}^{-1}$)
HTC	Heat Transfer Coefficient ($\text{W m}^{-1} \text{K}^{-1}$)
LMTD	Log Mean Temp. Diff. (K)
\dot{m}	mass flow (g s^{-1})
NEQ	Not Expanded Quantity (%)
OCR	Oil Circulation Ratio (-)
R_h	enthalpy ratio (-)
SC	sub cooling (K)
SH	super heat (K)
U	global HTC ($\text{W m}^{-2} \text{K}^{-1}$)
x_e	vapor quality (-)
x	mass concentration (-)
η	efficiency (-)
ρ	density (kg m^{-3})
μ	viscosity (cPs)

Subscript

1	suction
2	discharge
air	air
cond	condensing
evap	evaporator/evaporating
exp	expanded
in	inlet
l	liquid
o	reference
out	outlet
pure	pure
s	isentropic
sat	saturating
ref	refrigerant
v	vapor
vap	vaporization

Chapter 8:

THESIS CONCLUSIONS



8.1. Conclusions

In the pursuit of the outlined objectives aimed at advancing the understanding and design of components for variable-speed heat pumps, this thesis has traversed a multifaceted journey. This research embarked on a mission to fill critical gaps and provide valuable insights within the field, encompassing the study of compressor modeling, heat exchanger design, and oil management. In the following, the obtained conclusions on each topic will be listed.

8.1.1. Variable-speed compressor modeling

The presented compressor test bench allowed studying the compressor and the inverter separately, which permitted the study of inverter losses. In this test bench, three different compressors and three different inverters were tested.

The empirical results showed that the efficiency of all inverters drastically decreased at low speeds and loads, reaching losses in the range of 10% (significantly higher than the typically assumed 3%). Thanks to the resolution of the double-wattmeter measurement, it was possible to detect that power losses depended on consumption and speed independently. From the study of the results an empirical linear model was proposed using only five coefficients. The effect of inverter switching frequency – even if studied – was not included in the model as its effect was secondary, and it is typically a parameter that is not modified under normal operation.

The performance of variable-speed compressors was evaluated, analyzing its evolution with working conditions and speed. The empirical results were used to design new compact correlations that could predict compressed refrigerant mass flow rate, compressor consumption and discharge refrigerant temperature. The mentioned performance variables were modeled with empirical models using only four coefficients and an additional two terms correction factor was suggested to increase the prediction accuracy at extreme speeds for mass flow and consumption models. The proposed expressions are easily generalizable to varying suction conditions without adding new adjusting coefficients and shown robustness when adjusted with scarce training data.

Some methodologies were evaluated for the generation of test matrixes to characterize compressors. Random and clustering techniques were of limited

utility with a low number of training tests. On the contrary, Optimal Design Algorithms and maxDissim selection criteria proved to select test locations more efficiently. If the latter was selected, the proposed models could be adjusted with fewer than 15 experimental tests.

The obtained results in this section provide a simple but robust model of the general performance of the pump in terms of consumption and capacity. This is essential to develop system simulations which are necessary for the design, rating and component selection.

8.1.2. Heat Exchanger design for variable-speed heat pumps

A general and systematic optimization methodology has been proposed for the selection of the geometry of heat exchangers in variable-speed heat pumps. The selected design geometry for coil heat exchangers was the length of the tubes (the coil's width) and for plate heat exchangers, the number of plates. The motivation behind selecting these variables is that the coil's width is the geometry that affects less the heat transfer mechanisms and the flow patterns; and the number of plates is the main configuration parameter for these kinds of devices.

To know how the geometry, the required capacity, and the working conditions affect the heat exchanger, simple correlations were proposed, which were validated using a detailed commercial model.

The sizing criteria perform a cost-based analysis that consider the capital investment and the operational cost. The methodology considers the evolution of the external working temperatures, which affects the working time, the required capacity and the heat pump's performance. Additionally, the ability of the compressor to change speed and its working limits were also taken into account.

The optimal solutions obtained with the described methodology propose the utilization of smaller heat exchangers compared with classical design algorithms for fixed-speed heat pumps. The obtained methodology can reduce total costs, and it can be generalized to different heat pump typologies with little changes.

8.1.3. Oil impact

A new methodology based on discrepancies was implemented to evaluate the oil circulation ratio produced by a compressor, which was validated against the standard procedure described in ASHRAE 41.4 (ASHRAE, 2015). This

methodology permitted the evaluation of the circulating oil in a compressor test bench in a non-invasive manner and without using specialized devices.

The tested variable-speed compressors discharged significantly higher oil ratios when running at high speeds compared to their fixed-speed counterparts'. The oil circulation ratios increased at low evaporating temperatures and high speeds and could reach values close to 6-8%. Additionally, the obtained results were validated by another independent laboratory in Illinois (Haider et al., 2022) and mentioned in SAE and ASHRAE publications (Shah et al., n.d.; X. Wang et al., 2023)

Given the high oil circulations observed in the system, an evaluation of how they could impact the heat pump performance was conducted. Three different penalty contributions were identified and theoretically analyzed: the heat transfer reduction in the evaporator at high oil circulation rates, the effect of solved refrigerant in oil that does not evaporate and finally the impact of oil on the compressor consumption. Combining all three contributions resulted in a theoretical COP reduction that could reach 20% in some case scenarios or 15% if oil separators are installed at compressor discharge.

The obtained results highlight the importance of a correct oil management in the heat pump design, especially when variable speed compressors are used.

8.2. Future Work

This research assessed some challenges that have to be overcome when designing variable-speed heat pumps. The conclusions from the thesis result in a deeper knowledge of these systems and can be used as a seed for new studies to further analyze the broad field of heat pump design. In the following, some possible future research related to the presented thesis are suggested:

Regarding oil analysis, the study could be continued by extending the oil circulation characterization to other compressor technologies, such as rotary or reciprocating, and using different oil-refrigerant mixtures and oil pumping mechanisms that are less dependent on shaft speed. It could also be continued by experimentally validating the modelled effect of oil circulation in COP reduction and once it is validated include it in the heat pump consumption model which may influence the system design and the decision of introducing or not an oil separator.

In the described selection methodology, the compressor size was given as an input parameter, which has been typically the case. However, when variable-speed compressors are considered, a new degree of freedom appears in the design, and the compressor selection is not direct anymore. The proposed method to minimize heat pump costs and select heat exchangers could be extended to help sizing compressors too.

Designers do not always want to optimize the system for total life costs and may wish to optimize just efficiency instead (putting into the market a A+++ efficiency device). In that case the methodology to calculate the heat exchanger optimum size could be implemented the other way around to guess which would be the approximated heat exchanger size that would be needed to obtain the yearly consumption that would reach the target efficiency class.

Additionally, the method to design variable-speed heat pumps and calculate their seasonal consumption accounting for variation in external conditions and loads could be used to make comparisons among different technologies for a given application. For example, it would be of particular interest to compare which system could have a lower total life cost for a given application: a direct expansion variable flow system with a variable-speed heat pump or a hydronic system with a fixed-speed heat pump.

8.3. Science Production

8.3.1. Journal Contribution

Ossorio, R., & Navarro-Peris, E. (2021). Study of oil circulation rate in variable speed scroll compressor working with propane. *International Journal of Refrigeration*, 123, 63–71. <https://doi.org/10.1016/j.ijrefrig.2020.12.002>

Ossorio, R., NAVARRO-PERIS, E., & BARTA, R. B. (2022). Impact of Lubricant in the Performance of Variable Speed Heat Pumps Working with R290. *International Journal of Refrigeration*, 145(October 2022), 436–445. <https://doi.org/10.1016/j.ijrefrig.2022.10.003>

Ossorio, R., & Navarro, E. (2023). Testing of Variable-Speed Scroll Compressors and their inverters for the evaluation of compact energy consumption models. *Applied Thermal Engineering*, 230, 120725. <https://doi.org/10.1016/j.applthermaleng.2023.120725>

Ossorio, R., Navarro-Peris, E., & Marchante-Avellaneda, J. (2023). A novel methodology to assist manufacturers in the heat exchanger sizing for variable-speed heat pumps based on part load conditions and economic assessment. *Thermal Science and Engineering Progress*, 46, 102229. <https://doi.org/10.1016/j.tsep.2023.102229>

Ossorio, R., Marchante-Avellaneda, J., & Navarro-Peris, E. (2023). Development of Compact Empirical Models for Variable-Speed Compressors for the Prediction of Energy Consumption, Mass Flow and Discharge Temperature (SSRN Scholarly Paper 4642994). <https://doi.org/10.1016/j.applthermaleng.2024.122666>

8.3.2. International Congress Contributions

Ossorio, R, Emilio Navarro, José Gonzalvez, Paloma Albadalejo, y Alejandro López. «Efficiency Characterization of a Variable Speed Compressor». En CNIT, 265-75, 2018.

Ossorio, R, E Navarro, A López, y J A M Román. «Performance Analysis of a Variable Speed Drive». En CYTEF, 2020.

Ossorio, R, E Navarro, A López, y J Gonzalvez. «A NON-INVASIVE METHODOLOGY FOR ESTIMATING THE OIL MASS FLOW RATE IN REFRIGERATION CYCLES». En CYTEF, 2020.

Ossorio, R, Emilio Navarro-Peris, y Alejandro López Navarro. «Virtual Sensor of Insufficient Lubrication in Variable Speed Compressors». CYTEF, 2022. <https://doi.org/10.31428/10317/11527>.

Ossorio, R, Emilio Navarro Peris, Riley Barta, y Alejandro Lopez. «Impact of Lubricant in the Evaporator as a Function of Oil Circulation Rate in Variable Speed Heat Pumps Working with R290». Purdue, 2022.

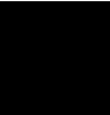
Marchante-Avellaneda, Javier, Ossorio, R, y Emilio NAVARRO-PERIS. «Characterization of Discharge Conditions in Refrigeration Compressors by Using Empirical Polynomial Models.» CNIT. Castellón, 2023.

Ossorio, R, y Emilio Navarro-Peris. «A Novel and Compact Correlation for the Prediction of Oil-Refrigerant Miscibility». CNIT. Castellón, 2023.

Chapter 9:

References

Standing on the shoulders of giants
- Isaac Newton -



- Afjei, T., & Jenni, F. (1994). The Impact of Inverter Losses on Heat Pump Performance. *International Compressor Engineering Conference*, Paper 1064.
- AHRI_540. (2020). *AHRI Standard 540: Performance rating of positive displacement refrigerant compressors*.
- ASHRAE. (2010). *ASHRAE Handbook* (Vol. 30329, Issue 404).
- ASHRAE. (2015). Standard Method for Measuring the Proportion of Lubricant in Liquid Refrigerant. *ASHRAE Journal*, 2015.
- Atkinson, A. C. (2015). Optimal Design. *Wiley StatsRef: Statistics Reference Online*, 1–17. <https://doi.org/10.1002/9781118445112.stat04090.pub2>
- Aute, V., Martin, C., & Radermacher, R. (2015). AHRI Project 8013: A Study of Methods to Represent Compressor Performance Data over an Operating Envelope Based on a Finite Set of Test Data. *Air-Conditioning, Heating, and Refrigeration Institute*.
- Aynur, T. N. (2010). Variable refrigerant flow systems: A review. *Energy and Buildings*, 42(7), 1106–1112. <https://doi.org/10.1016/j.enbuild.2010.01.024>
- Bäckström, M. (1940). Economic Optimum Problems in Connection with Refrigeration. *THE ROYAL SWEDISH INSTITUTE FOR ENGINEERING RESEARCH*, 155.
- Bagarella, G., Lazzarin, R., & Noro, M. (2016). Sizing strategy of on-off and modulating heat pump systems based on annual energy analysis. *International Journal of Refrigeration*, 65, 183–193. <https://doi.org/10.1016/j.ijrefrig.2016.02.015>
- Bergman, A. (1985). Impact of on/off control of heat pumps laboratory testing. *Bygghälsöversynsmyndigheten R111*, 67.
- Bitzer. (2016). *Kompetenz in Leistungsregelung Competence in Capacity Control*. https://www.bitzer.de/shared_media/documentation/a-600-6.pdf
- BITZER Software*. (n.d.). Retrieved May 6, 2022, from <https://www.bitzer.de/web-software/Calculate.aspx?cid=1651820569375&mod=ESC>
- Bivens, D. B., & Yokozeki, A. (1994). Heat transfer coefficients and transport properties for alternative refrigerants. *Proceedings of the International Refrigeration and Air Conditioning Conference*, 299–304.

-
- Bourdouxhe, J. P. H., Grodent, M., Silva, K. L., Lebrun, J. J., & Saavedra, C. (1994). *A toolkit for primary HVAC system energy calculation. Part 2: Reciprocating chiller models* (CONF-9406105-). Article CONF-9406105-. <https://www.osti.gov/biblio/33295>
- Branch, S. M., & Lepak, D. (2019). OIL CIRCULATION IN A SCROLL COMPRESSOR. In *Patent*.
- C. Aprea and C. Renno, Y. & Department. (2008). Experimental model of a variable capacity compressor C. *INTERNATIONAL JOURNAL OF ENERGY RESEARCH*. <https://doi.org/10.1002/er.1468>
- Caputo, A. C., Pelagagge, P. M., & Salini, P. (2008). Heat exchanger design based on economic optimisation. *Applied Thermal Engineering*, *28*(10), 1151–1159. <https://doi.org/10.1016/j.applthermaleng.2007.08.010>
- Cecchinato, L. (2010). Part load efficiency of packaged air-cooled water chillers with inverter driven scroll compressors. *Energy Conversion and Management*, *51*(7), 1500–1509. <https://doi.org/10.1016/j.enconman.2010.02.008>
- Chen, Y., Halm, N. P., Braun, J. E., & Groll, E. A. (2002). Mathematical modeling of scroll compressors. *International Journal of Refrigeration*, *25*(6), 751–764.
- Commission Delegated Regulation (EU) No 811/2013 of 18 February 2013, 239 OJ L (2013). http://data.europa.eu/eli/reg_del/2013/811/oj/eng
- Coolselector. (n.d.). Retrieved May 17, 2022, from <https://coolselectoronline.danfoss.com/>
- Corberán, J. M., Martínez-Galván, I., Martínez-Ballester, S., González-Maciá, J., & Royo-Pastor, R. (2011). Influence of the source and sink temperatures on the optimal refrigerant charge of a water-to-water heat pump. *International Journal of Refrigeration*, *34*(4), 881–892. <https://doi.org/10.1016/j.ijrefrig.2011.01.009>
- Corberan, J. M., Radulescu, C., & González-Maciá, José. (2008). Performance Characterisation of a Reversible Water To Water Heat Pump. *9th International IEA Heat Pump Conference, May*, 20–22.
- Cuevas, C., & Lebrun, J. (2009). Testing and modelling of a variable speed scroll compressor. *Applied Thermal Engineering*, *29*(2–3), 469–478. <https://doi.org/10.1016/j.applthermaleng.2008.03.016>

- Cuevas, C., Lebrun, J., Lemort, V., & Winandy, E. (2010). Characterization of a scroll compressor under extended operating conditions. *Applied Thermal Engineering*, 30(6–7), 605–615. <https://doi.org/10.1016/J.AP-PLTHERMALENG.2009.11.005>
- Dabiri, A. E., & Rice, C. K. (1981). *Compressor-simulation model with corrections for the level of suction gas superheat*. February 2017.
- Dai, B., Qi, H., Liu, S., Zhong, Z., Li, H., Song, M., Ma, M., & Sun, Z. (2019). Environmental and economical analyses of transcritical CO₂ heat pump combined with direct dedicated mechanical subcooling (DMS) for space heating in China. *Energy Conversion and Management*, 198, 111317. <https://doi.org/10.1016/j.enconman.2019.01.119>
- Dai, B., Wang, Q., Liu, S., Wang, D., Yu, L., Li, X., & Wang, Y. (2023). Novel configuration of dual-temperature condensation and dual-temperature evaporation high-temperature heat pump system: Carbon footprint, energy consumption, and financial assessment. *Energy Conversion and Management*, 292, 117360. <https://doi.org/10.1016/j.enconman.2023.117360>
- Darr, J. H., Crawford, R. R., & Conditioning, A. (1992). *Modeling of an Automotive Air Conditioning Compressor Based on Experimental Data Acustar Division of Chrysler Bergstrom Manufacturing Co. Ford Motor Company General Electric Company Harrison Division of GM ICI Americas, Inc. Modine Manufacturing Co. P. 61801*(February).
- Duprez, M. E., Dumont, E., & Frère, M. (2007). Modelling of reciprocating and scroll compressors. *International Journal of Refrigeration*, 30(5), 873–886. <https://doi.org/10.1016/j.ijrefrig.2006.11.014>
- EHPA. (2023, March 14). MEPs' vote signals end of fossil fuel boiler era. *European Heat Pump Association*. <https://www.ehpa.org/news-and-resources/press-releases/meps-vote-signals-end-of-fossil-fuel-boiler-era/>
- Ekren, O., Sahin, S., & Isler, Y. (2010). Comparison of different controllers for variable speed compressor and electronic expansion valve. *International Journal of Refrigeration*, 33(6), 1161–1168. <https://doi.org/10.1016/j.ijrefrig.2010.05.005>
- EN 12900. (2014). *EN 12900: Compressors for refrigerants*.

EN13771. (2017). *EN 13771 Compressors and condensing units for refrigeration—Performance testing and test methods*.

Energy 2020 A strategy for competitive, sustainable and secure energy, (2010). <https://eur-lex.europa.eu/legal-content/EN/TXT/?qid=1409650806265&uri=CELEX:52010DC0639>

Energy Roadmap 2050, (2011). https://eur-lex.europa.eu/legal-content/EN/ALL;/ELX_SESSIONID=pXNYJKSFbLwdq5JBWQ9CvY-WyJxD9RF4mnS3ctywT2xXmFYhInIW1!-868768807?uri=CELEX:52011DC0885

Europe's 2030 energy strategy, (2014). https://www.consilium.europa.eu/uedocs/cms_data/docs/pressdata/en/ec/145397.pdf

European Commission. (2018a). *EN 14825—Air conditioners, liquid chilling packages and heat pumps, with electrically driven compressors for space heating and cooling—Testing and rating at part load conditions and calculation of seasonal performance. 0*.

European Commission. (2021). *European Green Deal*.

Progress on competitiveness of clean energy technologies, (2022). <https://eur-lex.europa.eu/legal-content/EN/TXT/?uri=CELEX%3A52022DC0643&qid=1669913060946>

European Commission. (2018b). *A Clean Planet for all A European strategic long-term vision for a prosperous, modern, competitive and climate neutral economy*. <https://eur-lex.europa.eu/legal-content/EN/TXT/PDF/?uri=CELEX:52018DC0773>

Eurostat. (2023). *Heating and cooling from renewables gradually increasing*. <https://ec.europa.eu/eurostat/web/products-eurostat-news/w/DDN-20230203-1>

Fukuta, M., Yanagisawa, T., Shimasaki, M., & Ogi, Y. (2006). Real-time measurement of mixing ratio of refrigerant/refrigeration oil mixture. *International Journal of Refrigeration*, 29(7), 1058–1065. <https://doi.org/10.1016/j.ijrefrig.2006.03.010>

Gabel, K. S., & Bradshaw, C. R. (2023). Evaluation and quantification of compressor model predictive capabilities under modulation and extrapolation

- scenarios. *International Journal of Refrigeration*, 149(December 2022), 1–10. <https://doi.org/10.1016/j.ijrefrig.2022.11.032>
- Garstang, S. W. (1990). Variable frequency speed control of refrigeration compressors, pt. 2. *HandV Engineer*, 63(703), 12–14.
- Gas-Servei. (n.d.). *R-290 (Propane) Data-Sheet*.
- Granryd, E., & Palm, B. (2003). *Refrigerating engineering*. Royal Institute of Technology, KTH.
- Gungor, K. E., & Winterton, R. H. S. (1986). A general correlation for flow boiling in tubes and annuli. *International Journal of Heat and Mass Transfer*, 29(3), 351–358. [https://doi.org/10.1016/0017-9310\(86\)90205-X](https://doi.org/10.1016/0017-9310(86)90205-X)
- Guo, Y., Li, G., Chen, H., Hu, Y., Shen, L., Li, H., Hu, M., & Li, J. (2017). Développement d'un capteur de puissance de compresseur virtuel à vitesse variable pour un système de conditionnement d'air à débit de frigorigène variable. *International Journal of Refrigeration*, 74, 71–83. <https://doi.org/10.1016/j.ijrefrig.2016.09.025>
- Haider, S. A., Wang, X., & Elbel, S. (2022). *Oil Circulation Rate Measurements with Flow-through and Evacuated Type Sampling Cylinders*.
- Hisashi, I., Hirotaka, T., Katsuya, T., & Kazuo, H. (1997). *Models WT1010/WT1030/WT1030M Digital power meters* (p. 12). Yokogawa Technical Report.
- Hu, M., Xiao, F., & Cheung, H. (2020). Identification of simplified energy performance models of variable-speed air conditioners using likelihood ratio test method. *Science and Technology for the Built Environment*, 26(1), 75–88. <https://doi.org/10.1080/23744731.2019.1665446>
- Huber, M. L., Lemmon, E. W., Bell, I. H., & McLinden, M. O. (2022). The NIST REFPROP Database for Highly Accurate Properties of Industrially Important Fluids. *Industrial and Engineering Chemistry Research*. <https://doi.org/10.1021/ACS.IECR.2C01427>
- Hwang, Y., Radermacher, R., & Hirata, T. (2008). Oil mass fraction measurement of CO₂/PAG mixture. *International Journal of Refrigeration*, 31(2), 256–261. <https://doi.org/10.1016/j.ijrefrig.2007.05.011>

-
- Instituto Ingeniería Energética (IIE). (n.d.). *IMST-ART (4.10)* [Computer software]. Retrieved January 3, 2024, from <http://www.imst-art.com/>
- International Energy Agency. (2022). *The Future of Heat Pumps*. <https://doi.org/10.1787/2bd71107-en>
- Jahnig, D. I., Reindl, D. T., & Klein, S. A. (2000). Semi-empirical method for representing domestic refrigerator/freezer compressor calorimeter test data. *ASHRAE Transactions*, 106(February 2017).
- Jiang, J., Hu, B., Ge, T., & Wang, R. Z. (2022). Comprehensive selection and assessment methodology of compression heat pump system. *Energy*, 241, 122831. <https://doi.org/10.1016/j.energy.2021.122831>
- Kattan, N., Thome, J. R., & Favrat, D. (1998). Flow boiling in horizontal tubes: Part 1-development of a diabatic two-phase flow pattern map. *Journal of Heat Transfer*, 120(1), 140–147. <https://doi.org/10.1115/1.2830037>
- Kim, H. J., & Lancey, T. W. (2003). Numerical study on the lubrication oil distribution in a refrigeration rotary compressor. *International Journal of Refrigeration*, 26(7), 800–808. [https://doi.org/10.1016/S0140-7007\(03\)00050-1](https://doi.org/10.1016/S0140-7007(03)00050-1)
- Kizilkan, Ö. (2011). Thermodynamic analysis of variable speed refrigeration system using artificial neural networks. *Expert Systems with Applications*, 38(9), 11686–11692. <https://doi.org/10.1016/j.eswa.2011.03.052>
- Koury, R. N. N., MacHado, L., & Ismail, K. A. R. (2001). Numerical simulation of a variable speed refrigeration system. *International Journal of Refrigeration*, 24(2), 192–200. [https://doi.org/10.1016/S0140-7007\(00\)00014-1](https://doi.org/10.1016/S0140-7007(00)00014-1)
- Kruse, H. H., & Schroeder, M. (1985). Fundamentals of lubrication in refrigerating systems and heat pumps. *International Journal of Refrigeration*, 8(6), 347–355. [https://doi.org/10.1016/0140-7007\(85\)90030-1](https://doi.org/10.1016/0140-7007(85)90030-1)
- Kutsuna, K., Inoue, Y., Mizutani, T., Sudo, E., & Araga, T. (1991). Real time oil concentration measurement in automotive air conditioning by ultraviolet light absorption. *SAE Technical Papers*. <https://doi.org/10.4271/910222>
- Lebreton, J.-M., Vuillame, L., Morvan, E., & Lottin, O. (2001). Oil Concentration Measurement In Saturated Liquid Refrigerant Flowing Inside A Refrigeration Machine *. In *Int.J. Applied Thermodynamics* (Vol. 4, Issue 1).

- Lemmon, E. W., & McLinden, O. M. (2002). NIST Reference Fluid Thermodynamic and Transport Properties—REFPROP. In *U.S. Department of Commerce*. U.S. Department of Commerce. <http://www.boulder.nist.gov/div838/theory/refprop/MINIREF/MINIREF.HTM>
- Li, W. (2013). Simplified steady-state modeling for variable speed compressor. *Applied Thermal Engineering*, 50(1), 318–326. <https://doi.org/10.1016/j.applthermaleng.2012.08.041>
- Lin, X., Lee, H., Hwang, Y., & Radermacher, R. (2015). A review of recent development in variable refrigerant flow systems. *Science and Technology for the Built Environment*, 21(7), 917–933. <https://doi.org/10.1080/23744731.2015.1071987>
- Lottin, O., Guillemet, P., & Lebreton, J. M. (2003a). Effects of synthetic oil in a compression refrigeration system using R410A. Part I: Modelling of the whole system and analysis of its response to an increase in the amount of circulating oil. *International Journal of Refrigeration*, 26(7), 772–782. [https://doi.org/10.1016/S0140-7007\(03\)00064-1](https://doi.org/10.1016/S0140-7007(03)00064-1)
- Lottin, O., Guillemet, P., & Lebreton, J. M. (2003b). Effects of synthetic oil in a compression refrigeration system using R410A. Part II: Quality of heat transfer and pressure losses within the heat exchangers. *International Journal of Refrigeration*, 26(7), 783–794. [https://doi.org/10.1016/S0140-7007\(03\)00065-3](https://doi.org/10.1016/S0140-7007(03)00065-3)
- Ma, J., Ding, X., Horton, W. T., & Ziviani, D. (2020). Development of an automated compressor performance mapping using artificial neural network and multiple compressor technologies. *International Journal of Refrigeration*, 120, 66–80. <https://doi.org/10.1016/j.ijrefrig.2020.08.001>
- Mancini, R., Zühlsdorf, B., Kjær Jensen, J., Brix Markussen, W., & Elmegaard, B. (2018). Deriving guidelines for the design of plate evaporators in heat pumps using zeotropic mixtures. *Energy*, 156, 492–508. <https://doi.org/10.1016/j.energy.2018.05.026>
- Marchante-Avellaneda, J., Corberan, J. M., Navarro-Peris, E., & Shrestha, S. S. (2023). A critical analysis of the AHRI polynomials for scroll compressor characterization. *Applied Thermal Engineering*, 219(PA), 119432. <https://doi.org/10.1016/j.applthermaleng.2022.119432>

-
- Marchante-Avellaneda, J., Navarro-Peris, E., Corberan, J. M., & Shrestha, S. S. (2023). Analysis of map-based models for reciprocating compressors and optimum selection of rating points. *International Journal of Refrigeration*, S0140700723001524. <https://doi.org/10.1016/j.ijrefrig.2023.06.002>
- Marquand, C. J., Tassou, S. A., Wang, Y. T., & Wilson, D. R. (1984). An economic comparison of a fixed speed, a two speed, and a variable speed vapour compression heat pump. *Applied Energy*, 16(1), 59–66. [https://doi.org/10.1016/0306-2619\(84\)90027-8](https://doi.org/10.1016/0306-2619(84)90027-8)
- McLinden, M. O., Brown, J. S., Brignoli, R., Kazakov, A. F., & Domanski, P. A. (2017). Limited options for low-global-warming-potential refrigerants. *Nature Communications*, 8(1), 14476. <https://doi.org/10.1038/ncomms14476>
- Mendoza-Miranda, J. M., Mota-Babiloni, A., Ramírez-Minguela, J. J., Muñoz-Carpio, V. D., Carrera-Rodríguez, M., Navarro-Esbrí, J., & Salazar-Hernández, C. (2016). Comparative evaluation of R1234yf, R1234ze(E) and R450A as alternatives to R134a in a variable speed reciprocating compressor. *Energy*, 114, 753–766. <https://doi.org/10.1016/j.energy.2016.08.050>
- Mermond, Y., Feidt, M., & Marvillet, C. (1999). Thermodynamic and physical properties of mixtures of refrigerants and oils; Propriétés thermodynamiques et physiques des mélanges de fluides frigorigènes et d'huiles. *International Journal of Refrigeration*, 22(7), 569–579. [https://doi.org/10.1016/S0140-7007\(99\)00015-8](https://doi.org/10.1016/S0140-7007(99)00015-8)
- Miller, W. A. (1988). *Laboratory examination and seasonal analyses of the dynamic losses for a continuously variable speed heat pump*. <https://www.osti.gov/biblio/7174165>
- Molina, M. J., & Rowland, F. S. (1974). Stratospheric sink for chlorofluoromethanes: Chlorine atom-catalysed destruction of ozone. *Nature*, 249(5460), Article 5460. <https://doi.org/10.1038/249810a0>
- Moradi, M. H., Sohani, A., Zabihigivi, M., & Wirbser, H. (2017). A comprehensive approach to find the performance map of a heat pump using experiment and soft computing methods. *Energy Conversion and Management*, 153, 224–242. <https://doi.org/10.1016/j.enconman.2017.09.070>
- Navarro, E., Urchueguía, J. F., González, J., & Corberán, J. M. (2005). Test results of performance and oil circulation rate of commercial reciprocating

- compressors of different capacities working with propane (R290) as refrigerant. *International Journal of Refrigeration*, 28(6), 881–888. <https://doi.org/10.1016/j.ijrefrig.2005.01.010>
- Ossorio, R., & Navarro, E. (2023). Testing of Variable-Speed Scroll Compressors and their inverters for the evaluation of compact energy consumption models. *Applied Thermal Engineering*, 230, 120725. <https://doi.org/10.1016/j.applthermaleng.2023.120725>
- Ossorio, R., & Navarro-Peris, E. (2021). Study of oil circulation rate in variable speed scroll compressor working with propane. *International Journal of Refrigeration*, 123, 63–71. <https://doi.org/10.1016/j.ijrefrig.2020.12.002>
- Ossorio, R., Navarro-Peris, E., & Barta, R. B. (2023). Impact of lubricant in the performance of variable speed heat pumps working with R290. *International Journal of Refrigeration*, 145, 436–445. <https://doi.org/10.1016/j.ijrefrig.2022.10.003>
- Park, Y. C., Kim, Y. C., & Min, M. K. (2001). Performance analysis on a multi-type inverter air conditioner. *Energy Conversion and Management*, 42(13), 1607–1621. [https://doi.org/10.1016/S0196-8904\(00\)00147-3](https://doi.org/10.1016/S0196-8904(00)00147-3)
- Piscopiello, S., Mazzotti, W., Nota, C., Sawalha, S., & Palm, B. (2016). Performance evaluation of a large capacity water-water heat pump using propane as refrigerant. *Refrigeration Science and Technology*, 3(2008), 803–810. <https://doi.org/10.18462/iir.gl.2016.1129>
- Pitarch, M., Navarro-Peris, E., González-Maciá, J., & Corberán, J. M. (2017). Evaluation of different heat pump systems for sanitary hot water production using natural refrigerants. *Applied Energy*, 190, 911–919. <https://doi.org/10.1016/j.apenergy.2016.12.166>
- Qureshi, T. Q., & Tassou, S. A. (1996). Variable-speed capacity control in refrigeration systems. *Applied Thermal Engineering*, 16(2), 103–113.
- R Core Team. (2022). *R: A Language and Environment for Statistical Computing*. R Foundation for Statistical Computing. <https://www.r-project.org/>
- Ribeiro, G. B., & Barbosa, J. R. (2016). Analysis of a variable speed air conditioner considering the R-290/POE ISO 22 mixture effect. *Applied Thermal*

-
- Engineering*, 108, 650–659. <https://doi.org/10.1016/j.applthermaleng.2016.07.155>
- R.S.Adhikari, N, A., M, M., & D, M. (2012). Energy Savings through Variable Speed Compressor Heat Pump Systems. *Energy Procedia*, 14, 1337–1342. <https://doi.org/10.1016/j.egypro.2011.12.1098>
- Santos, G. Z., Ronzoni, A. F., & Hermes, C. J. L. (2019). Performance characterization of small variable-capacity reciprocating compressors using a minimal dataset. *International Journal of Refrigeration*, 107, 191–201. <https://doi.org/10.1016/j.ijrefrig.2019.07.014>
- Sarntichartsak, P., Monyakul, V., Thepa, S., & Nathakaranakule, A. (2006). Simulation and experimental evaluation of the effects of oil circulation in an inverter air conditioning system using R-22 and R-407C. *Applied Thermal Engineering*, 26(14–15), 1481–1491. <https://doi.org/10.1016/j.applthermaleng.2006.01.002>
- Scrucca, L. (2013). GA: A package for genetic algorithms in R. *Journal of Statistical Software*, 53(4), 1–37. <https://doi.org/10.18637/jss.v053.i04>
- Select Online. (n.d.). Retrieved September 9, 2022, from <https://selectonline.emersonclimate.eu/SelectOnline/main>
- Shah, V. M., Kurtulus, O., Horton, W. T., Groll, E. A., & Braun, J. E. (n.d.). *In-Situ Oil Circulation Ratio (OCR) Measurement using Separation Method in a Transport Refrigeration System with R404A and POE32*.
- Shao, S., Shi, W., Li, X., & Chen, H. (2004). Performance representation of variable-speed compressor for inverter air conditioners based on experimental data. *International Journal of Refrigeration*, 27(8), 805–815. <https://doi.org/10.1016/j.ijrefrig.2004.02.008>
- Som Shrestha, Vishaldeep Sharma, & Omar Abdelaziz. (2013). *TEST REPORT #21 Compressor Calorimeter Test of R-404A Alternatives ARM-31a, D2Y-65, L-40, and R-32/R-134a (50/50)* (TEST REPORT #21; p. 42). Oak Ridge National Laboratory. <https://info.ornl.gov/sites/publications/files/Pub42278.pdf>
- Standard, A. (2017). *Performance Rating of Modulating Positive Displacement Refrigerant Compressors*.

- Sun, Y., Wei, Q., Wang, J., Wang, X., & He, M. (2021). Impact of oil presence on the evaporator enthalpy working with R1234ze(E) and R1234yf. *International Journal of Refrigeration*, 129, 153–162. <https://doi.org/10.1016/j.ijrefrig.2021.05.004>
- SWEP. (2023). *SSP G8—Advanced brazed plate heat exchanger (BPHE) calculations* [Computer software].
- Tassou, S. A., & Qureshi, T. Q. (1998). Comparative performance evaluation of positive displacement compressors in variable-speed refrigeration applications. *International Journal of Refrigeration*, 21(1), 29–41. [https://doi.org/10.1016/S0140-7007\(97\)00082-0](https://doi.org/10.1016/S0140-7007(97)00082-0)
- Thome, J. R. (2007). Chapter 10 Boiling Heat Transfer Inside Plain Tubes. In *Wolverine tube, Inc. Engineering Thermal Innovation*.
- Thome, J. R. (2010). Engineering Data Book III. In *Wolverine tube, Inc. Toshiba Air Conditioning, Creator of modern Inverter Air Conditioning*. (n.d.). Retrieved March 8, 2023, from <https://toshiba-aircon.com.au/toshiba-air-conditioning-creator-of-modern-air-conditioning/>
- Unuvar, A., & Kargici, S. (2004). An approach for the optimum design of heat exchangers. *International Journal of Energy Research*, 28(15), 1379–1392. <https://doi.org/10.1002/er.1080>
- Wan, H., Cao, T., Hwang, Y., Chang, S.-D., & Yoon, Y.-J. (2021). Machine-learning-based compressor models: A case study for variable refrigerant flow systems. *International Journal of Refrigeration*, 123, 23–33. <https://doi.org/10.1016/j.ijrefrig.2020.12.003>
- Wan, H., Cao, T., Hwang, Y., & Oh, S. (2020). A review of recent advancements of variable refrigerant flow air-conditioning systems. *Applied Thermal Engineering*, 169(October 2019), 114893. <https://doi.org/10.1016/j.applthermaleng.2019.114893>
- Wang, L., & Sundén, B. (2003). Optimal design of plate heat exchangers with and without pressure drop specifications. *Applied Thermal Engineering*, 23(3), 295–311. [https://doi.org/10.1016/S1359-4311\(02\)00195-3](https://doi.org/10.1016/S1359-4311(02)00195-3)

-
- Wang, X., Haider, S. A., & Elbel, S. (2023). *Transient Oil Migration and Flow Behavior during Automotive Compressor Startup* (SAE Technical Paper 2023-01-0142). SAE International. <https://doi.org/10.4271/2023-01-0142>
- Wheeler, B. (n.d.). *CRAN - Package AlgDesign* [Computer software]. <https://cran.r-project.org/web/packages/AlgDesign/index.html>
- Winandy, E., Saavedra O, C., & Lebrun, J. (2002a). Simplified modelling of an open-type reciprocating compressor. *International Journal of Thermal Sciences*, 41(2), 183–192. [https://doi.org/10.1016/S1290-0729\(01\)01296-0](https://doi.org/10.1016/S1290-0729(01)01296-0)
- Winandy, E., Saavedra O, C. S., & Lebrun, J. (2002b). Experimental analysis and simplified modelling of a hermetic scroll refrigeration compressor. *Applied Thermal Engineering*, 22(2), 107–120. [https://doi.org/10.1016/S1359-4311\(01\)00083-7](https://doi.org/10.1016/S1359-4311(01)00083-7)
- Wujek, S. S., Bowers, C. D., & Okarma, P. (2014). Effect of Lubricant-Refrigerant Mixture Properties on Compressor Efficiencies. *International Compressor Engineering Conference, 2003*, 1–9.
- Wujek, S. S., Hrnjak, P. S., & Seeton, C. J. (2007). Online measurement techniques for determining oil circulation rate. *2007 Proceedings of the 5th Joint ASME/JSME Fluids Engineering Summer Conference, FEDSM 2007, 2 FORA(PART A)*, 181–186. <https://doi.org/10.1115/FEDSM2007-37640>
- Xu, J., & Hrnjak, P. (2017). Quantification of flow and retention of oil in compressor discharge pipe. *International Journal of Refrigeration*, 80, 252–263. <https://doi.org/10.1016/j.ijrefrig.2017.05.004>
- Yam, Y. Y., Lin, T. F., & Yang, B. C. (1997). Evaporation heat transfer and pressure drop of refrigerant R134a in a plate heat exchanger. *Proceedings of the ASME Turbo Expo, 121*(February). <https://doi.org/10.1115/97-AA-048>
- Yang, L., Zhao, L. X., Zhang, C. L., & Gu, B. (2009). Loss-efficiency model of single and variable-speed compressors using neural networks. *International Journal of Refrigeration*, 32(6), 1423–1432. <https://doi.org/10.1016/j.ijrefrig.2009.03.006>
- Yoon, P., Kang, D., Kim, C., Ahn, S., Chung, B., Kim, B., Lee, J., & Hwang, Y. (2011). An experimental study on oil discharge ratio at inverter-driven high shell

- pressure scroll compressor using R410A/PVE. *International Journal of Refrigeration*, 34(1), 105–112. <https://doi.org/10.1016/j.ijrefrig.2010.08.019>
- Youbi-Idrissi, M., & Bonjour, J. (2008). The effect of oil in refrigeration: Current research issues and critical review of thermodynamic aspects. *International Journal of Refrigeration*, 31(2), 165–179. <https://doi.org/10.1016/j.ijrefrig.2007.09.006>
- Youbi-Idrissi, M., Bonjour, J., Marvillet, C., & Meunier, F. (2003). Impact of refrigerant – oil solubility on an evaporator performances working with R-407C. *Refrigeration*. *Refrigeration*, 26, 284–292. [https://doi.org/10.1016/S0140-7007\(02\)00129-9](https://doi.org/10.1016/S0140-7007(02)00129-9)
- Youbi-Idrissi, M., Bonjour, J., Terrier, M. F., Marvillet, C., & Meunier, F. (2004). Oil presence in an evaporator: Experimental validation of a refrigerant/oil mixture enthalpy calculation model. *International Journal of Refrigeration*, 27(3), 215–224. <https://doi.org/10.1016/j.ijrefrig.2003.11.001>
- Zhang, G., Xiao, H., Zhang, P., Wang, B., Li, X., Shi, W., & Cao, Y. (2019). Review on recent developments of variable refrigerant flow systems since 2015. *Energy and Buildings*, 198, 444–466. <https://doi.org/10.1016/j.enbuild.2019.06.032>
- Zhelezny, V. P., Nichenko, S. V., Semenyuk, Y. V., Kosoy, B. V., & Kumar, R. (2009). Influence of compressor oil admixtures on theoretical efficiency of a compressor system. *International Journal of Refrigeration*, 32(7), 1526–1535. <https://doi.org/10.1016/j.ijrefrig.2009.03.001>

Appendix 1:

Compressor Data

“scroll-R290”

Tech.	Displ.	Refr.	Oil	Speed Range	Nominal Speed	Tests
Scroll	46cm ³	R290	POE 68	15-110 Hz	70	134

Tevap [°C]	Tcond [°C]	Speed [rps]	Tsuc [°C]	Tdisch [°C]	M_refr [g/s]	Wc [W]	Wc + Winv [W]	Vol. Eff. [-]	Isentr. Eff. [-]	Compr. Eff. [-]
-30.22	39.98	30	-19.70	93.27	4.10	804	903	0.815	0.600	0.478
-29.94	49.98	30	-20.02	105.77	4.09	948	1057	0.800	0.596	0.445
-30.07	59.98	30	-20.35	127.05	3.93	1164	1291	0.775	0.540	0.386
-20.01	20.03	30	-10.06	54.04	6.43	616	704	0.888	0.640	0.550
-19.97	29.94	30	-9.96	65.82	6.40	750	844	0.883	0.658	0.554
-20.07	39.98	30	-9.99	78.86	6.28	893	996	0.869	0.654	0.539
-20.11	49.99	30	-10.19	92.94	6.15	1058	1174	0.854	0.634	0.509
-20.27	59.99	30	-9.92	111.78	5.98	1272	1403	0.833	0.578	0.461
-19.96	69.38	30	-12.48	130.62	5.88	1572	1736	0.801	0.526	0.390
-10.02	29.96	30	0.06	58.77	9.21	776	872	0.920	0.666	0.593
-9.95	39.99	30	-0.05	69.88	9.16	955	1064	0.911	0.688	0.585
-10.01	49.98	30	0.12	83.31	8.99	1147	1271	0.897	0.669	0.562
-9.94	60.01	30	-0.30	97.96	8.88	1380	1530	0.883	0.635	0.519
-0.03	20.07	30	9.98	42.24	12.90	588	674	0.951	0.597	0.534
0.02	29.98	30	9.94	52.74	12.84	772	867	0.945	0.675	0.598
0.03	40.01	30	10.03	64.31	12.76	1007	1118	0.939	0.698	0.597

Tevap [°C]	Tcond [°C]	Speed [rps]	Tsuc [°C]	Tdisch [°C]	M_refr [g/s]	Wc [W]	Wc + Winv [W]	Vol. Eff. [-]	Iseentr. Eff. [-]	Compr. Eff. [-]
-0.03	49.98	30	9.89	75.25	12.63	1204	1331	0.932	0.717	0.603
0.05	60.00	30	9.93	88.91	12.49	1453	1595	0.918	0.683	0.576
-0.06	70.00	30	9.97	104.35	12.15	1778	1947	0.897	0.631	0.523
10.01	29.96	30	19.98	49.24	17.61	727	820	0.976	0.630	0.556
9.99	39.97	30	20.08	60.26	17.28	945	1053	0.959	0.691	0.619
9.99	49.98	30	19.96	71.18	17.25	1213	1340	0.957	0.722	0.628
9.95	59.99	30	20.00	83.85	16.99	1528	1650	0.944	0.701	0.609
20.00	69.99	30	29.93	91.70	22.45	1876	2055	0.952	0.711	0.600
24.97	39.99	30	34.94	57.55	26.56	877	978	0.991	0.558	0.484
25.02	49.98	30	35.03	67.60	26.20	1150	1272	0.977	0.674	0.592
25.00	59.99	30	35.00	77.88	26.12	1478	1627	0.974	0.735	0.626
-30.00	39.97	50	-19.98	90.16	7.27	1357	1466	0.858	0.622	0.516
-29.87	49.98	50	-19.99	103.86	7.18	1566	1685	0.842	0.609	0.490
-30.03	60.00	50	-19.86	123.37	7.00	1828	1965	0.826	0.560	0.451
-19.96	20.12	50	-9.76	54.16	11.13	1076	1173	0.921	0.640	0.572

Tevap [°C]	Tcond [°C]	Speed [rps]	Tsuc [°C]	Tdisch [°C]	M_refr [g/s]	Wc [W]	Wc + Winv [W]	Vol. Eff. [-]	Iseentr. Eff. [-]	Compr. Eff. [-]
-20.03	29.97	50	-10.15	64.88	11.02	1282	1388	0.914	0.671	0.581
-20.01	39.98	50	-10.03	77.94	10.90	1491	1607	0.903	0.664	0.578
-20.09	49.99	50	-9.94	91.71	10.72	1731	1859	0.892	0.646	0.560
-20.06	59.99	50	-10.04	104.29	10.61	1973	2116	0.883	0.637	0.540
-20.14	69.99	50	-10.06	122.96	10.36	2372	2539	0.863	0.580	0.481
-10.09	29.99	50	-0.07	57.38	15.81	1300	1405	0.949	0.690	0.633
-9.96	39.97	50	0.12	68.57	15.75	1553	1672	0.941	0.708	0.641
-9.94	49.98	50	-0.04	81.07	15.33	1861	1996	0.915	0.698	0.608
-10.01	59.99	50	0.16	92.58	15.41	2127	2278	0.923	0.698	0.609
0.03	19.98	50	10.08	42.80	22.20	1069	1166	0.980	0.579	0.528
0.04	29.98	50	10.02	51.59	21.85	1292	1397	0.964	0.702	0.631
0.02	39.96	50	9.93	61.93	21.65	1582	1703	0.957	0.748	0.665
-0.06	49.97	50	10.13	73.51	21.40	1912	2053	0.948	0.750	0.663
-0.02	59.96	50	9.98	85.51	21.45	2260	2419	0.949	0.738	0.655
0.04	69.99	50	9.99	98.72	21.14	2677	2864	0.933	0.706	0.616
10.05	29.96	50	19.96	49.76	29.69	1301	1406	0.986	0.614	0.546

Tevap [°C]	Tcond [°C]	Speed [rps]	Tsuc [°C]	Tdisch [°C]	M_refr [g/s]	Wc [W]	Wc + Winv [W]	Vol. Eff. [-]	Iseentr. Eff. [-]	Compr. Eff. [-]
9.92	39.96	50	19.96	59.11	29.38	1599	1720	0.980	0.724	0.645
10.04	49.98	50	20.19	69.57	29.22	1961	2104	0.972	0.763	0.677
10.01	59.99	50	20.01	80.98	28.99	2388	2558	0.965	0.764	0.670
19.98	69.99	50	30.03	89.67	38.13	2923	3122	0.972	0.764	0.671
24.99	40.05	50	35.09	58.30	44.69	1574	1694	1.001	0.534	0.472
25.05	49.98	50	35.01	66.85	44.49	1929	2069	0.994	0.703	0.617
24.97	59.99	50	35.03	76.95	44.08	2376	2542	0.988	0.768	0.676
-29.93	39.97	70	-20.20	90.90	10.40	1957	2079	0.872	0.616	0.518
-29.97	49.99	70	-19.97	105.40	10.25	2223	2355	0.862	0.599	0.503
-30.11	60.00	70	-19.97	121.59	10.02	2525	2673	0.848	0.571	0.477
-20.01	20.07	70	-10.11	55.30	15.76	1572	1678	0.934	0.625	0.566
-20.03	30.03	70	-10.03	66.61	15.64	1849	1963	0.927	0.651	0.584
-20.00	39.97	70	-9.99	78.81	15.50	2133	2261	0.917	0.654	0.584
-20.07	49.98	70	-10.03	91.13	15.32	2452	2596	0.910	0.651	0.572
-20.08	59.99	70	-10.22	105.05	15.14	2801	2960	0.899	0.630	0.550

Tevap [°C]	Tcond [°C]	Speed [rps]	Tsuc [°C]	Tdisch [°C]	M_refr [g/s]	Wc [W]	Wc + Winv [W]	Vol. Eff. [-]	Iseentr. Eff. [-]	Compr. Eff. [-]
-20.05	70.00	70	-9.92	120.81	14.96	3227	3410	0.886	0.595	0.515
-10.06	29.98	70	-0.01	57.74	22.17	1922	2041	0.950	0.684	0.611
-9.96	39.97	70	-0.08	68.91	22.04	2269	2404	0.940	0.702	0.623
-9.96	49.98	70	-0.05	80.55	21.80	2643	2791	0.930	0.705	0.619
-9.94	59.99	70	-0.03	92.96	21.69	3072	3246	0.925	0.692	0.599
0.01	19.92	70	9.95	43.85	31.23	1644	1751	0.985	0.554	0.493
0.07	29.98	70	9.97	52.30	30.91	1942	2062	0.974	0.684	0.605
-0.01	39.90	70	9.86	62.22	30.61	2324	2462	0.966	0.739	0.649
0.04	49.98	70	9.88	73.16	30.47	2775	2930	0.961	0.757	0.658
0.04	59.99	70	10.02	85.33	30.27	3243	3423	0.954	0.741	0.652
0.01	69.99	70	9.96	97.77	29.99	3789	4002	0.946	0.721	0.625
10.09	29.98	70	19.93	50.78	41.90	1970	2089	0.993	0.585	0.518
10.00	39.99	70	20.02	59.58	41.50	2340	2476	0.987	0.710	0.633
9.97	49.98	70	20.14	69.45	41.11	2824	2985	0.979	0.766	0.673
10.03	59.99	70	20.04	80.69	40.86	3362	3549	0.970	0.770	0.679
20.02	69.98	70	29.98	89.27	53.80	4097	4337	0.978	0.775	0.681

Tevap [°C]	Tcond [°C]	Speed [rps]	Tsuc [°C]	Tdisch [°C]	M_refr [g/s]	Wc [W]	Wc + Winv [W]	Vol. Eff. [-]	Iseentr. Eff. [-]	Compr. Eff. [-]
24.99	40.06	70	35.04	59.68	62.87	2402	2545	1.006	0.491	0.442
24.92	49.97	70	34.91	67.64	62.43	2831	2995	1.000	0.674	0.600
24.95	59.99	70	35.01	77.25	61.99	3383	3571	0.993	0.758	0.677
-29.98	39.97	90	-19.91	94.30	13.36	2565	2701	0.875	0.590	0.519
-29.91	49.98	90	-19.89	108.10	13.27	2887	3037	0.867	0.580	0.508
-29.99	60.00	90	-20.12	125.49	13.10	3273	3441	0.857	0.548	0.485
-19.89	20.03	90	-9.32	56.66	20.35	2125	2243	0.933	0.606	0.544
-19.90	29.99	90	-9.94	68.75	20.10	2556	2694	0.925	0.624	0.549
-20.00	39.98	90	-9.94	79.34	19.75	2832	2978	0.910	0.648	0.570
-20.03	49.99	90	-10.01	92.05	19.85	3205	3367	0.915	0.642	0.575
-19.97	59.99	90	-10.01	105.64	19.70	3637	3819	0.906	0.624	0.557
-20.01	69.99	90	-10.11	122.37	19.40	4161	4367	0.893	0.583	0.526
-10.05	30.07	90	-0.15	59.10	28.69	2580	2715	0.956	0.663	0.600
-10.05	39.97	90	-0.68	69.92	28.53	3022	3174	0.949	0.688	0.617
-9.94	49.98	90	0.16	80.99	28.52	3470	3641	0.943	0.699	0.623

Tevap [°C]	Tcond [°C]	Speed [rps]	Tsuc [°C]	Tdisch [°C]	M_refr [g/s]	Wc [W]	Wc + Winv [W]	Vol. Eff. [-]	Iseentr. Eff. [-]	Compr. Eff. [-]
-9.98	59.99	90	-0.05	94.33	28.19	3992	4188	0.936	0.676	0.605
-0.03	19.97	90	9.88	46.02	39.82	2281	2403	0.979	0.513	0.461
0.02	29.87	90	9.56	53.61	39.90	2615	2750	0.982	0.652	0.591
0.00	40.02	90	9.28	63.48	39.62	3094	3248	0.973	0.715	0.644
-0.06	49.96	90	9.81	74.40	39.26	3628	3805	0.965	0.733	0.660
0.04	59.96	90	9.92	85.38	39.22	4218	4421	0.963	0.740	0.660
0.07	69.97	90	10.13	97.71	38.96	4838	5069	0.956	0.721	0.647
10.03	30.33	90	19.59	52.80	53.71	2750	2892	0.993	0.548	0.493
9.93	39.96	90	19.68	60.70	53.43	3139	3298	0.988	0.679	0.616
9.96	49.98	90	19.82	70.14	53.18	3692	3874	0.983	0.748	0.675
10.01	59.97	90	20.08	80.74	52.91	4367	4580	0.977	0.769	0.687
20.02	69.98	90	30.09	89.01	69.45	5235	5491	0.982	0.782	0.701
24.95	40.00	90	35.03	61.14	80.93	3398	3569	1.008	0.451	0.408
24.99	49.95	90	35.00	68.98	80.56	3873	4065	1.002	0.628	0.574
24.98	59.99	90	35.04	77.43	80.20	4488	4708	0.998	0.751	0.670
-29.94	39.98	110	-20.04	98.72	16.13	3239	3388	0.862	0.560	0.494

Tevap [°C]	Tcond [°C]	Speed [rps]	Tsuc [°C]	Tdisch [°C]	M_refr [g/s]	Wc [W]	Wc + Winv [W]	Vol. Eff. [-]	Iseentr. Eff. [-]	Compr. Eff. [-]
-29.98	49.98	110	-19.99	113.98	16.04	3622	3785	0.859	0.544	0.490
-29.88	59.98	110	-20.09	128.04	15.82	4085	4271	0.843	0.533	0.466
-19.91	19.92	110	-10.11	58.24	24.73	2768	2901	0.927	0.586	0.509
-19.99	29.95	110	-10.15	70.64	24.48	3155	3300	0.921	0.605	0.542
-19.90	39.96	110	-10.04	81.95	24.39	3608	3772	0.915	0.621	0.549
-20.07	49.98	110	-9.92	96.06	24.02	4062	4244	0.907	0.606	0.549
-20.01	59.99	110	-10.31	109.74	23.85	4572	4775	0.899	0.592	0.537
-19.98	70.03	110	-11.22	123.39	23.73	5144	5378	0.888	0.576	0.515
-9.98	29.94	110	-0.04	61.04	35.04	3332	3484	0.953	0.630	0.564
-9.98	39.95	110	0.12	71.77	34.84	3854	4023	0.947	0.660	0.589
-10.04	49.98	110	-0.08	82.92	34.51	4410	4604	0.940	0.674	0.595
-10.04	59.99	110	-0.07	96.27	34.27	4996	5217	0.933	0.654	0.591
-0.05	30.04	110	9.95	55.97	48.43	3443	3599	0.975	0.610	0.546
0.00	39.92	110	9.97	64.97	48.22	3989	4164	0.969	0.683	0.605
0.30	49.97	110	10.00	75.62	48.49	4644	4840	0.964	0.707	0.629

Tevap [°C]	Tcond [°C]	Speed [rps]	Tsuc [°C]	Tdisch [°C]	M_refr [g/s]	Wc [W]	Wc + Winv [W]	Vol. Eff. [-]	Isentr. Eff. [-]	Compr. Eff. [-]
0.06	59.98	110	10.00	87.08	47.79	5331	5552	0.958	0.711	0.634
0.04	69.99	110	10.01	98.69	47.38	6108	6344	0.951	0.706	0.623
10.09	30.01	110	20.06	54.38	65.53	3638	3802	0.988	0.503	0.446
10.01	39.92	110	19.97	62.13	65.19	4115	4297	0.986	0.642	0.571
9.97	49.97	110	20.06	71.38	64.85	4757	4959	0.982	0.717	0.638
9.98	59.98	110	19.95	81.79	64.31	5600	5828	0.974	0.745	0.653
20.02	69.99	110	29.98	89.43	85.14	6663	6939	0.985	0.770	0.674
24.94	40.14	110	34.82	62.99	99.71	4535	4737	1.015	0.415	0.379
24.97	49.96	110	34.75	70.04	99.49	5063	5269	1.012	0.596	0.542
24.78	59.98	110	34.79	78.62	98.18	5774	6010	1.004	0.713	0.640

Appendix 2:

Compressor Data

“scroll-R410A”

Tech.	Displ.	Refr.	Oil	Speed Range	Nominal Speed	Tests
Scroll	44.5 cm ³	R410A	PVE 32	15-110 Hz	60	35

Tevap [°C]	Tcond [°C]	Speed [rps]	Tsuc [°C]	Tdisch [°C]	M_refr [g/s]	Wc [W]	Wc + Winv [W]	Vol. Eff. [-]	Is- entr. Eff. [-]	Compr. Eff. [-]
-30.00	30.01	100	-19.87	122.34	35.31	4245	4323	0.796	0.521	0.482
-25.03	25.15	100	-14.80	95.85	45.53	4030	4106	0.848	0.571	0.538
-19.98	40.01	100	-10.12	112.96	55.12	5394	5494	0.851	0.582	0.546
-9.98	45.05	100	-0.07	100.61	83.49	6300	6426	0.908	0.649	0.606
-9.97	48.03	100	-0.28	105.86	82.00	6607	6736	0.891	0.642	0.594
-0.01	48.54	100	9.76	90.40	120.30	6926	7060	0.944	0.727	0.657
-25.03	25.04	90	-15.27	94.24	41.28	3536	3611	0.852	0.577	0.552
-19.94	40.03	80	-9.92	110.51	44.25	4135	4229	0.853	0.600	0.570
-9.99	45.03	80	-0.09	99.00	66.57	4796	4906	0.906	0.666	0.633
5.06	45.02	80	14.90	78.89	115.18	5029	5149	0.965	0.773	0.696
5.95	48.02	80	14.10	81.54	119.37	5322	5446	0.962	0.759	0.701
-29.96	33.12	60	-20.17	128.17	19.07	2538	2611	0.714	0.520	0.450
-24.97	39.95	60	-14.86	127.54	24.21	2966	3050	0.750	0.543	0.482
-20.01	40.03	60	-9.91	111.21	32.13	3025	3110	0.828	0.597	0.564
-20.01	30.01	60	-9.94	89.10	34.28	2498	2568	0.883	0.635	0.620

Tevap [°C]	Tcond [°C]	Speed [rps]	Tsuc [°C]	Tdisch [°C]	M_refr [g/s]	Wc [W]	Wc + Winv [W]	Vol. Eff. [-]	Is- entr. Eff. [-]	Compr. Eff. [-]
-19.96	40.00	60	-9.26	110.87	32.74	3027	3113	0.845	0.604	0.575
-15.01	25.05	60	-5.17	71.36	41.95	2324	2384	0.904	0.665	0.642
-9.96	45.03	60	-0.15	97.82	49.21	3473	3572	0.891	0.678	0.642
-9.95	30.05	60	0.16	73.01	51.34	2602	2674	0.931	0.687	0.674
-9.94	40.03	60	-0.15	89.46	50.50	3144	3232	0.914	0.681	0.669
0.02	40.04	60	9.89	77.50	72.33	3262	3365	0.946	0.723	0.697
-0.02	32.03	60	9.87	65.55	73.02	2715	2801	0.956	0.706	0.690
4.99	40.03	60	14.90	72.73	85.67	3256	3360	0.959	0.740	0.704
5.03	45.02	60	14.99	80.20	85.17	3646	3747	0.953	0.747	0.708
4.99	48.04	60	14.91	85.09	84.93	3841	3952	0.951	0.740	0.716
-10.04	45.03	50	-0.12	99.61	40.68	2897	2989	0.887	0.660	0.636
4.07	32.03	50	14.01	61.44	69.49	2142	2224	0.961	0.724	0.705
-19.96	40.03	30	-8.01	119.44	12.69	1534	1602	0.660	0.557	0.437
-15.03	25.02	30	-4.94	71.43	19.62	1108	1155	0.847	0.666	0.622
-9.95	30.04	30	0.20	72.17	24.13	1255	1307	0.876	0.700	0.648

Tevap [°C]	Tcond [°C]	Speed [rps]	Tsuc [°C]	Tdisch [°C]	M_refr [g/s]	Wc [W]	Wc + Winv [W]	Vol. Eff. [-]	Is- entr. Eff. [-]	Compr. Eff. [-]
-10.06	45.03	30	-0.09	102.95	22.65	1756	1834	0.824	0.627	0.577
7.05	25.01	30	17.24	48.60	45.41	904	948	0.956	0.696	0.696
-15.00	25.02	15	-4.85	80.25	8.99	644	705	0.776	0.569	0.466
-10.07	30.04	15	-0.07	80.51	11.63	713	776	0.847	0.591	0.527
7.00	25.01	15	16.97	51.78	21.63	512	569	0.911	0.588	0.553

Appendix 3:

Compressor Data

“scroll-R454C”

Tech.	Displ.	Refr.	Oil	Speed Range	Nominal Speed	Tests
Scroll	44.5 cm ³	R454C	PVE 32	15-110 Hz	60	87

Tevap [°C]	Tcond [°C]	Speed [rps]	Tsuc [°C]	Tdisch [°C]	M_refr [g/s]	Wc + Winv [W]	Vol. Eff. [-]	Isentr. Eff. [-]	Compr. Eff. [-]
10.69	67.34	15	21.89	116.54	12.88	1292.47	0.71	0.47	0.35
29.23	43.64	20	39.35	60.15	36.28	651.50	0.87	0.62	0.49
-14.63	52.79	30	-4.60	122.27	9.92	1380.66	0.63	0.45	0.35
-9.22	44.91	30	0.88	86.12	14.41	1156.84	0.76	0.59	0.48
12.51	64.08	30	22.95	96.25	30.41	1842.34	0.79	0.62	0.52
23.37	66.16	30	33.72	92.25	42.51	1926.90	0.80	0.65	0.55
38.97	72.95	30	48.85	97.38	64.69	2326.46	0.79	0.58	0.50
-14.61	52.78	40	-4.72	119.67	13.69	1753.06	0.65	0.46	0.38
-11.69	29.31	40	-1.63	62.12	19.43	1115.85	0.83	0.64	0.54
-9.21	44.98	40	0.49	86.01	19.46	1500.30	0.77	0.58	0.50
1.70	71.80	40	12.12	127.15	25.75	2759.11	0.71	0.48	0.41
1.73	46.09	40	13.55	73.55	32.41	1566.04	0.89	0.72	0.63
2.83	28.31	40	13.13	50.18	33.39	1026.26	0.88	0.68	0.59
12.50	71.34	40	22.92	105.44	40.74	2722.49	0.80	0.62	0.53
12.51	64.02	40	22.98	95.23	41.03	2387.92	0.80	0.63	0.54
12.54	60.03	40	22.93	89.78	41.23	2276.38	0.80	0.63	0.54

Tevap [°C]	Tcond [°C]	Speed [rps]	Tsuc [°C]	Tdisch [°C]	M_refr [g/s]	Wc + Winv [W]	Vol. Eff. [-]	Isestr. Eff. [-]	Compr. Eff. [-]
12.62	38.22	40	22.69	57.62	46.12	1254.13	0.90	0.71	0.62
22.86	74.70	40	33.30	104.54	56.08	3069.35	0.81	0.63	0.54
23.26	56.20	40	33.34	78.95	57.55	2045.19	0.82	0.65	0.56
23.38	81.33	40	33.45	118.33	55.07	3681.39	0.78	0.55	0.49
23.38	66.15	40	33.37	91.26	57.62	2498.69	0.81	0.66	0.57
24.01	38.37	40	33.98	53.80	65.61	985.71	0.91	0.68	0.61
29.28	43.65	40	39.25	59.33	74.80	1107.22	0.89	0.65	0.59
32.52	54.85	40	42.44	71.70	82.45	1650.00	0.90	0.72	0.65
32.53	64.07	40	42.55	83.22	81.97	2218.54	0.89	0.74	0.66
38.39	54.89	40	48.80	71.09	96.68	1457.05	0.90	0.67	0.62
38.94	74.18	40	48.90	98.22	86.01	3050.87	0.79	0.61	0.53
43.61	62.72	40	53.59	79.28	111.31	1862.67	0.90	0.67	0.62
34.10	81.32	48	44.71	110.70	90.97	4355.97	0.80	0.61	0.53
34.17	85.02	48	44.24	116.74	90.82	4794.96	0.79	0.59	0.52
-14.70	52.79	60	-4.71	119.25	21.15	2611.05	0.67	0.46	0.39
-11.78	29.28	60	-1.56	64.36	29.29	1739.35	0.84	0.61	0.52

Tevap [°C]	Tcond [°C]	Speed [rps]	Tsuc [°C]	Tdisch [°C]	M_refr [g/s]	Wc + Winv [W]	Vol. Eff. [-]	Iseentr. Eff. [-]	Compr. Eff. [-]
-9.22	44.92	60	0.77	88.04	29.28	2288.31	0.77	0.57	0.49
-9.19	61.71	60	0.97	121.78	28.08	3176.23	0.74	0.49	0.43
1.66	64.70	60	11.73	106.47	42.52	3409.28	0.78	0.57	0.50
1.69	68.44	60	12.17	116.01	41.41	3761.65	0.76	0.53	0.47
1.70	71.88	60	11.86	122.32	40.87	3977.71	0.75	0.52	0.45
1.71	65.17	60	11.73	108.16	42.30	3484.85	0.77	0.56	0.49
2.16	46.10	60	13.26	73.43	49.85	2400.47	0.90	0.71	0.62
2.93	35.67	60	11.78	58.98	50.28	1975.52	0.88	0.67	0.58
12.51	39.93	60	22.95	60.82	69.22	2073.84	0.90	0.69	0.61
12.53	64.08	60	22.50	94.71	62.04	3525.30	0.81	0.63	0.56
12.53	59.34	60	22.51	88.32	62.38	3238.65	0.81	0.64	0.56
12.53	50.65	60	22.87	73.65	69.15	2662.57	0.90	0.72	0.63
12.58	82.08	60	23.10	125.97	60.06	5028.63	0.78	0.55	0.49
12.90	71.33	60	22.52	105.73	61.74	4062.09	0.79	0.60	0.53
23.37	76.02	60	33.39	105.19	86.38	4647.40	0.81	0.64	0.55
23.38	81.34	60	33.38	115.15	84.46	5202.81	0.80	0.60	0.53

Tevap [°C]	Tcond [°C]	Speed [rps]	Tsuc [°C]	Tdisch [°C]	M_refr [g/s]	Wc + Winv [W]	Vol. Eff. [-]	Isestr. Eff. [-]	Compr. Eff. [-]
23.41	66.15	60	33.39	90.60	87.05	3709.87	0.82	0.68	0.58
23.42	59.91	60	33.35	83.36	87.60	3332.11	0.82	0.65	0.57
23.42	66.17	60	33.46	92.14	86.42	3765.13	0.81	0.64	0.57
23.89	41.14	60	34.14	58.15	98.01	1867.89	0.91	0.66	0.57
29.60	43.66	60	39.41	59.18	113.91	1828.14	0.90	0.64	0.53
32.54	54.85	60	42.50	71.09	125.12	2609.67	0.91	0.75	0.62
33.12	64.07	60	42.63	81.15	127.26	3400.18	0.91	0.81	0.65
34.17	81.38	60	44.38	107.32	115.43	5654.36	0.80	0.69	0.52
34.19	74.34	60	44.64	95.47	113.45	4549.00	0.79	0.77	0.55
38.36	55.28	60	48.46	70.13	147.70	2383.50	0.92	0.75	0.59
39.05	81.32	60	49.57	105.79	130.11	5677.49	0.79	0.70	0.51
43.68	64.06	60	53.69	78.16	169.78	3111.47	0.91	0.91	0.60
-11.77	28.66	80	-1.46	67.01	39.12	2415.44	0.84	0.57	0.50
-9.23	44.93	80	0.77	90.44	39.13	3168.47	0.77	0.54	0.48
1.68	63.94	80	11.69	106.46	57.23	4605.94	0.78	0.56	0.50
1.68	68.90	80	13.43	118.15	55.28	5058.88	0.76	0.53	0.47

Tevap [°C]	Tcond [°C]	Speed [rps]	Tsuc [°C]	Tdisch [°C]	M_refr [g/s]	Wc + Winv [W]	Vol. Eff. [-]	Isentr. Eff. [-]	Compr. Eff. [-]
2.94	29.39	80	11.79	53.66	67.80	2495.19	0.88	0.59	0.51
12.50	63.97	80	22.57	94.44	83.32	4821.45	0.81	0.64	0.55
12.54	50.65	80	23.27	73.30	92.65	3769.13	0.91	0.74	0.60
12.54	39.03	80	22.80	59.66	92.44	2955.92	0.90	0.68	0.55
12.56	59.37	80	22.45	88.91	82.85	4501.55	0.81	0.62	0.54
12.60	71.34	80	23.03	105.71	82.63	5465.02	0.80	0.62	0.54
22.82	76.02	80	33.38	105.28	114.35	6355.92	0.82	0.66	0.55
23.28	81.33	80	33.46	113.14	113.20	7119.57	0.80	0.64	0.52
23.41	67.11	80	33.30	91.91	116.90	5222.56	0.82	0.67	0.57
30.76	81.40	80	43.66	101.45	138.99	7213.32	0.81	1.08	0.54
30.83	64.07	80	40.97	80.83	159.49	4849.53	0.91	0.88	0.62
32.76	55.50	80	42.54	69.88	169.27	3871.98	0.92	0.87	0.57
33.88	81.29	80	44.46	99.76	149.91	7340.06	0.79	1.04	0.52
34.29	79.25	80	44.12	96.38	155.75	6944.49	0.81	1.04	0.54
-11.72	29.23	100	-1.73	70.45	48.45	3244.00	0.83	0.54	0.46
-9.26	44.93	100	1.33	94.58	47.99	4136.25	0.76	0.52	0.45

Tevap [°C]	Tcond [°C]	Speed [rps]	Tsuc [°C]	Tdisch [°C]	M_refr [g/s]	Wc + Winv [W]	Vol. Eff. [-]	Iseentr. Eff. [-]	Compr. Eff. [-]
2.82	77.76	100	12.20	127.12	71.63	7681.28	0.75	0.53	0.43
12.52	63.65	100	22.48	93.62	103.84	6203.35	0.81	0.64	0.53
12.53	63.15	100	22.49	93.51	103.74	6216.36	0.81	0.63	0.52
12.53	71.32	100	22.36	104.00	103.71	7003.30	0.81	0.63	0.52
20.07	77.31	100	30.14	100.29	123.91	8378.69	0.77	0.84	0.49
20.08	71.84	100	30.30	92.95	125.39	7681.07	0.78	0.86	0.49
21.99	81.33	100	33.51	105.93	133.48	9044.26	0.79	0.86	0.50

Appendix 4:

Inverter Data

“Inverter A”

Tested Power	Tested Speed	Inv. Eff.	Carrier Freq.	Control mechanism	Tests
0.7-7 kW	15-110 Hz	0.87-0.96	6 kHz	Open Loop Control for PM	133

Speed [Hz]	Pin [W]	Pout [W]	Eff. Inv [-]	V_in [V]	I_in [A]	PF_in [-]	V_out [V]	I_out [A]
30	1331	1204	0.905	401.06	2.84	0.67	215.76	7.52
30	1595	1453	0.911	400.39	3.79	0.69	218.53	9.03
30	1947	1778	0.913	400.00	4.21	0.70	222.52	10.95
30	867	772	0.891	400.53	1.97	0.63	211.38	4.86
30	1118	1007	0.901	400.31	2.46	0.65	213.43	6.32
30	872	776	0.890	400.65	1.97	0.63	211.34	4.89
30	1064	955	0.897	399.92	2.36	0.64	212.78	6.00
30	1271	1147	0.903	399.58	2.74	0.66	214.57	7.19
30	1530	1386	0.906	400.07	3.81	0.69	217.41	8.65
30	1340	1213	0.905	399.97	2.87	0.67	215.49	7.58
30	1053	945	0.897	399.89	2.35	0.64	212.43	5.95
30	820	727	0.887	400.05	1.88	0.62	210.59	4.60
30	978	877	0.896	399.81	2.43	0.64	211.20	5.57
30	1272	1150	0.904	399.65	2.77	0.66	214.34	7.24
30	1627	1478	0.909	399.90	3.39	0.69	218.46	9.22
30	2055	1876	0.913	399.37	4.18	0.71	223.54	11.53
30	844	750	0.888	400.88	1.91	0.63	210.95	4.73

Speed [Hz]	Pin [W]	Pout [W]	Eff. Inv [-]	V_in [V]	I_in [A]	PF_in [-]	V_out [V]	I_out [A]
30	996	893	0.896	401.39	2.21	0.64	212.14	5.63
30	1174	1058	0.901	400.80	2.78	0.66	213.68	6.66
30	1403	1272	0.906	399.49	2.95	0.68	215.35	8.00
30	903	804	0.891	400.05	2.03	0.64	210.37	5.11
30	674	588	0.872	400.12	1.59	0.61	209.90	3.71
30	704	616	0.874	400.33	1.65	0.61	210.03	3.89
30	1736	1572	0.906	400.45	3.57	0.70	218.99	9.85
30	1291	1164	0.902	400.72	2.75	0.67	213.86	7.39
30	1057	948	0.896	399.81	2.32	0.65	211.46	6.02
50	2053	1912	0.932	398.98	4.21	0.70	271.49	7.43
50	2419	2260	0.934	398.86	5.10	0.72	273.17	8.79
50	1397	1292	0.925	399.76	2.99	0.67	269.07	5.01
50	1703	1582	0.929	399.56	3.54	0.69	270.09	6.14
50	2864	2677	0.935	398.25	5.61	0.74	275.95	10.40
50	1405	1300	0.925	399.77	3.21	0.68	269.02	5.04
50	1672	1553	0.928	398.83	3.50	0.69	269.75	6.02
50	1996	1861	0.933	400.90	4.07	0.70	271.62	7.23

Speed [Hz]	Pin [W]	Pout [W]	Eff. Inv [-]	V_in [V]	I_in [A]	PF_in [-]	V_out [V]	I_out [A]
50	2278	2127	0.934	399.35	4.80	0.72	272.54	8.28
50	2116	1973	0.932	399.03	4.31	0.71	271.14	7.72
50	1388	1282	0.924	400.28	3.16	0.68	269.21	4.97
50	1607	1491	0.928	400.88	3.36	0.68	269.73	5.80
50	1406	1301	0.925	398.94	3.20	0.68	268.36	5.06
50	1720	1599	0.929	400.51	3.57	0.69	270.23	6.22
50	2104	1961	0.932	399.69	4.24	0.71	271.74	7.63
50	2558	2388	0.934	398.90	5.05	0.73	274.06	9.29
50	1685	1566	0.929	398.89	3.53	0.69	268.25	6.16
50	1466	1357	0.926	399.51	3.33	0.67	267.93	5.32
50	1965	1828	0.930	399.69	4.03	0.70	269.02	7.25
50	1694	1574	0.929	398.12	3.55	0.69	268.46	6.17
50	2069	1929	0.932	398.86	4.23	0.70	270.83	7.55
50	2542	2376	0.935	399.67	5.28	0.73	273.97	9.29
50	3122	2923	0.936	399.33	6.61	0.75	278.30	11.36
50	1859	1731	0.931	400.31	3.87	0.69	270.40	6.75
50	2539	2372	0.934	399.56	5.06	0.72	272.94	9.33

Speed [Hz]	P _{in} [W]	P _{out} [W]	Eff. Inv [-]	V _{in} [V]	I _{in} [A]	PF _{in} [-]	V _{out} [V]	I _{out} [A]
50	1166	1069	0.917	399.71	2.54	0.66	267.91	4.14
50	1173	1076	0.918	400.26	2.55	0.66	268.09	4.17
70	2930	2775	0.947	400.35	6.22	0.74	317.48	7.88
70	3423	3243	0.947	399.80	7.01	0.75	318.93	9.24
70	4002	3789	0.947	400.55	7.59	0.76	322.25	10.81
70	2462	2324	0.944	399.92	4.95	0.71	315.74	6.59
70	2062	1942	0.942	400.36	4.22	0.70	315.28	5.49
70	2041	1922	0.942	400.31	4.21	0.70	315.33	5.43
70	2404	2269	0.944	400.32	4.83	0.72	315.69	6.43
70	2791	2643	0.947	400.71	5.47	0.73	316.48	7.52
70	3246	3072	0.946	399.58	6.46	0.75	317.30	8.77
70	2960	2801	0.946	400.47	5.98	0.74	316.14	8.02
70	2596	2452	0.944	400.56	5.11	0.73	315.28	6.99
70	1963	1849	0.942	399.79	3.98	0.71	314.13	5.24
70	2261	2133	0.943	401.23	4.54	0.71	315.11	6.07
70	2089	1970	0.943	400.53	4.28	0.70	315.16	5.59
70	2476	2340	0.945	400.13	4.98	0.71	315.88	6.65

Speed [Hz]	Pin [W]	Pout [W]	Eff. Inv [-]	V_in [V]	I_in [A]	PF_in [-]	V_out [V]	I_out [A]
70	2985	2824	0.946	401.27	5.82	0.73	317.62	8.04
70	3549	3362	0.947	400.49	7.00	0.76	319.63	9.59
70	2079	1957	0.942	401.08	4.23	0.70	314.19	5.59
70	2355	2223	0.944	400.35	4.72	0.72	313.82	6.39
70	2673	2525	0.945	400.40	5.28	0.73	314.31	7.30
70	3410	3227	0.946	400.33	6.74	0.75	317.63	9.30
70	2545	2402	0.944	400.50	5.04	0.73	315.01	6.88
70	2995	2831	0.945	400.88	5.84	0.74	316.91	8.11
70	3571	3383	0.947	400.19	6.82	0.75	319.10	9.69
70	4337	4097	0.945	400.64	7.98	0.78	323.93	11.74
70	1751	1644	0.938	400.47	3.63	0.69	314.77	4.64
70	1678	1572	0.937	399.90	3.49	0.69	314.03	4.45
90	3805	3628	0.953	398.95	6.74	0.78	354.36	8.20
90	4421	4218	0.954	397.66	7.84	0.79	355.72	9.57
90	5069	4838	0.954	399.72	9.13	0.80	359.63	10.99
90	2750	2615	0.951	399.85	5.21	0.76	352.86	5.88
90	3248	3094	0.953	399.96	6.07	0.77	353.48	6.97

Speed [Hz]	Pin [W]	Pout [W]	Eff. Inv [-]	V_in [V]	I_in [A]	PF_in [-]	V_out [V]	I_out [A]
90	3174	3022	0.952	400.34	5.94	0.76	353.19	6.82
90	3641	3470	0.953	400.12	6.71	0.78	353.73	7.85
90	2715	2580	0.950	400.19	5.13	0.76	353.07	5.80
90	4188	3992	0.953	400.75	7.79	0.77	355.41	9.06
90	3298	3139	0.952	399.75	6.16	0.77	352.90	7.09
90	3874	3692	0.953	399.87	7.09	0.78	354.10	8.35
90	4580	4367	0.953	400.48	8.30	0.79	357.43	9.89
90	2892	2750	0.951	401.91	5.48	0.75	353.97	6.20
90	2694	2556	0.949	400.05	5.08	0.76	351.77	5.79
90	2978	2832	0.951	400.36	5.58	0.76	352.60	6.40
90	2701	2565	0.949	400.72	5.04	0.77	350.79	5.84
90	3037	2887	0.950	401.01	5.66	0.77	350.91	6.61
90	3441	3273	0.951	399.49	6.38	0.77	350.15	7.55
90	3367	3205	0.952	401.10	6.22	0.77	352.98	7.27
90	3819	3637	0.952	400.45	6.97	0.78	353.08	8.30
90	4367	4161	0.953	401.19	7.87	0.79	354.71	9.56
90	4065	3873	0.953	400.46	7.43	0.78	354.43	8.82

Speed [Hz]	Pin [W]	Pout [W]	Eff. Inv [-]	V_in [V]	I_in [A]	PF_in [-]	V_out [V]	I_out [A]
90	4708	4488	0.953	400.29	8.49	0.79	357.45	10.22
90	5491	5235	0.953	400.12	9.81	0.80	362.51	11.90
90	3569	3398	0.952	400.13	6.58	0.78	352.78	7.73
90	2403	2281	0.950	2.52	2.56	91.39	352.65	5.12
90	2243	2125	0.948	399.69	4.46	0.72	352.59	4.77
110	4840	4644	0.959	400.82	8.87	0.78	388.02	8.77
110	5552	5331	0.960	400.42	10.09	0.79	390.58	10.08
110	6344	6108	0.963	401.46	11.45	0.79	396.34	11.54
110	4164	3989	0.958	400.70	7.88	0.76	387.26	7.51
110	4023	3854	0.958	401.15	7.59	0.76	387.29	7.26
110	3484	3332	0.956	400.60	6.68	0.75	386.43	6.26
110	3599	3443	0.957	401.39	6.88	0.75	386.96	6.47
110	4297	4115	0.958	400.93	8.04	0.77	387.00	7.77
110	4959	4757	0.959	400.27	9.16	0.78	387.71	8.99
110	5828	5600	0.961	401.79	10.56	0.79	393.01	10.59
110	4604	4410	0.958	400.86	8.52	0.78	387.31	8.33
110	3300	3155	0.956	399.91	6.37	0.75	385.49	5.95

Speed [Hz]	Pin [W]	Pout [W]	Eff. Inv [-]	V_in [V]	I_in [A]	PF_in [-]	V_out [V]	I_out [A]
110	3772	3608	0.956	400.59	7.08	0.76	385.17	6.82
110	4244	4062	0.957	399.72	7.87	0.78	384.52	7.72
110	3388	3239	0.956	399.56	6.43	0.76	382.20	6.19
110	3785	3622	0.957	400.10	7.15	0.76	381.71	6.98
110	4775	4572	0.957	400.34	8.75	0.78	385.39	8.74
110	5217	4996	0.958	400.09	9.47	0.79	388.00	9.48
110	5269	5063	0.961	400.78	9.67	0.78	388.82	9.63
110	6010	5774	0.961	401.42	10.89	0.79	393.54	10.96
110	6939	6663	0.960	400.26	12.44	0.80	401.13	12.53
110	2901	2768	0.954	400.56	5.60	0.74	386.51	5.19
110	4737	4535	0.957	400.06	8.80	0.77	386.54	8.63
110	5378	5144	0.957	401.54	9.68	0.80	388.39	9.86
110	4271	4085	0.956	400.74	7.96	0.77	383.01	7.88
110	3802	3638	0.957	399.54	7.27	0.75	386.19	6.86

Appendix 5:

Inverter Data

“Inverter B”

Tested Power	Tested Speed	Inv. Eff.	Carrier Freq.	Control mechanism	Tests
0.7-5 kW	15-110 Hz	0.91-0.94	6.6 kHz	Open Loop Control for PM	35

Speed [Hz]	Pin [W]	Pout [W]	Eff. Inv [-]	V_in [V]	I_in [A]	PF_in [-]	V_out [V]	I_out [A]
15	704	643	0.913	230.56	1.70	1.05	185.20	7.66
15	776	713	0.919	230.58	1.54	0.68	185.00	7.70
15	567	510	0.900	231.71	2.20	1.83	186.10	7.63
30	1601	1534	0.958	230.69	2.96	0.75	245.46	7.28
30	1155	1108	0.960	231.33	2.25	0.72	246.37	5.27
30	1305	1253	0.960	230.49	2.86	1.73	245.19	5.92
30	1834	1756	0.958	229.87	3.30	0.76	246.10	8.25
30	947	904	0.954	230.80	1.87	0.70	251.94	5.25
50	2988	2896	0.969	232.33	4.99	0.82	314.50	8.37
50	2222	2141	0.963	232.26	3.80	0.80	313.00	6.21
60	2610	2537	0.972	232.03	4.46	0.80	340.20	6.24
60	3049	2965	0.973	233.26	5.01	0.82	342.20	7.25
60	3110	3025	0.973	232.83	5.17	0.82	342.50	7.37
60	2567	2497	0.973	231.66	4.41	0.80	341.60	6.09
60	3112	3026	0.972	232.45	5.25	0.81	342.30	7.37
60	2384	2324	0.975	231.81	4.13	0.79	339.50	5.67
60	3572	3473	0.972	233.45	5.79	0.84	344.80	8.41

Speed [Hz]	Pin [W]	Pout [W]	Eff. Inv [-]	V_in [V]	I_in [A]	PF_in [-]	V_out [V]	I_out [A]
60	2673	2601	0.973	232.50	4.49	0.80	342.80	6.32
60	3231	3143	0.973	233.32	5.25	0.83	343.90	7.62
60	3364	3261	0.969	232.74	5.59	0.82	343.55	7.91
60	2800	2714	0.969	231.77	4.73	0.80	342.30	6.60
60	3359	3256	0.969	233.14	5.55	0.83	343.80	7.90
60	3747	3646	0.973	231.82	6.00	0.85	343.70	8.83
60	3951	3841	0.972	232.65	6.24	0.86	344.60	9.30
80	4228	4133	0.978	232.69	6.50	0.86	394.60	7.64
80	4903	4793	0.978	233.05	7.50	0.88	396.30	8.82
80	5148	5027	0.977	233.24	7.74	0.89	397.20	9.23
80	5443	5319	0.977	232.82	8.04	0.89	398.10	9.75
90	3611	3536	0.979	232.63	5.83	0.85	416.40	5.91
100	4323	4244	0.982	232.99	6.76	0.86	433.50	6.41
100	4106	4030	0.982	232.34	6.54	0.87	431.30	6.13
100	5494	5394	0.982	232.90	8.36	0.89	432.10	8.14
100	6422	6297	0.980	235.56	9.63	0.91	435.00	9.45
100	6735	6607	0.981	233.41	10.17	0.91	431.20	9.99

Speed [Hz]	Pin [W]	Pout [W]	Eff. Inv [-]	V_in [V]	I_in [A]	PF_in [-]	V_out [V]	I_out [A]
100	7060	6926	0.981	233.21	10.68	0.91	430.20	10.46

Appendix 6:

Inverter Data

“Inverter C”

Tested Power	Tested Speed	Inv. Eff.	Carrier Freq.	Control mechanism	Tests
0.6-7 kW	15-100 Hz	0.90-0.98	5 kHz	Open Loop Control for PM	17

fc [Hz]	Pin [W]	Pout [W]	Eff. Inv [-]	V_in [V]	I_in [A]	PF_in [-]	V_out [V]	I_out [A]
30	1584	1463	0.924	229.11	6.94	1.00	172.32	9.98
30	1696	1566	0.923	231.00	7.36	1.00	173.22	10.64
30	683	623	0.912	230.16	3.06	0.97	165.13	4.45
30	659	600	0.910	230.41	2.96	0.97	164.97	4.31
50	2930	2743	0.936	230.29	12.73	1.00	218.72	11.62
50	1267	1188	0.938	231.55	5.52	0.99	210.26	5.27
70	4036	3797	0.941	232.11	17.41	1.00	254.18	11.87
70	3637	3424	0.941	229.60	15.86	1.00	250.38	10.87
88.3	5120	4814	0.940	229.44	22.39	1.00	283.64	12.19
90	3891	3676	0.945	231.86	16.80	1.00	275.79	9.45
90	4774	4499	0.942	230.48	20.77	1.00	281.75	11.37
90	2438	2313	0.949	227.53	10.72	1.00	273.53	6.16
95	5113	4813	0.941	230.23	22.28	1.00	284.58	11.95
106.6	5106	4811	0.942	231.97	22.08	1.00	284.43	11.76
110	5020	4730	0.942	230.97	21.80	1.00	284.41	11.49
110	3850	3646	0.947	230.01	16.76	1.00	284.78	8.80
110	3182	3019	0.949	230.02	13.84	1.00	285.55	7.46

Appendix 7:

OCR measurements

Oil Separator	T evap [°C]	Tcond [°C]	SH [K]	SC [K]	speed [rpm]	M_coriolis [g/s]	± U (k=2)	M_evap [g/s]	± U (k=2)2	M_oil [g/s]	± U (k=2)3	OCR [%]	± U (k=2)4
✓	-30	50	10	4	1800	4.09	0.02	3.78	0.43	0.31	0.43	7.5%	10.6%
✗	-30	50	10	4	1800	4.27	0.02	4.08	0.41	0.19	0.41	4.4%	9.5%
✓	-20	50	10	4	1800	6.15	0.06	5.93	0.31	0.22	0.32	3.6%	5.2%
✗	-20	50	10	4	1800	6.47	0.02	6.28	0.44	0.20	0.45	3.0%	6.9%
✓	-10	50	10	4	1800	8.99	0.01	9.15	0.22	-0.16	0.22	-1.8%	2.5%
✗	-10	50	10	4	1800	9.24	0.01	9.22	0.24	0.01	0.24	0.1%	2.6%
✓	0	50	10	4	1800	12.63	0.07	12.77	0.14	-0.14	0.16	-1.1%	1.2%
✗	0	50	10	4	1800	12.88	0.07	12.83	0.18	0.05	0.19	0.4%	1.5%
✓	10	50	10	4	1800	17.00	0.01	17.44	0.08	-0.44	0.08	-2.6%	0.5%
✗	10	50	10	4	1800	17.46	0.01	17.52	0.08	-0.06	0.08	-0.3%	0.5%
✓	25	50	10	4	1800	26.20	0.01	26.75	0.23	-0.54	0.23	-2.1%	0.9%
✗	25	50	10	4	1800	26.41	0.01	26.73	0.31	-0.32	0.31	-1.2%	1.2%
✓	-30	50	10	4	3600	8.60	0.07	8.89	0.50	-0.29	0.51	-3.3%	5.9%
✗	-30	50	10	4	3600	8.96	0.08	8.32	0.43	0.63	0.44	7.1%	4.9%
✓	-20	50	10	4	3600	13.05	0.07	12.67	0.31	0.39	0.31	3.0%	2.4%
✗	-20	50	10	4	3600	13.73	0.07	12.59	0.31	1.14	0.31	8.3%	2.3%

Oil Separator	T evap [°C]	Tcond [°C]	SH [K]	SC [K]	speed [rpm]	M_coriolis [g/s]	± U (k=2)	M_evap [g/s]	± U (k=2)2	M_oil [g/s]	± U (k=2)3	OCR [%]	± U (k=2)4
✓	-10	50	10	4	3600	18.87	0.02	18.95	0.24	-0.08	0.24	-0.4%	1.3%
✗	-10	50	10	4	3600	19.47	0.03	18.62	0.27	0.85	0.27	4.4%	1.4%
✓	0	50	10	4	3600	26.16	0.02	26.54	0.13	-0.37	0.13	-1.4%	0.5%
✗	0	50	10	4	3600	27.04	0.02	26.14	0.37	0.90	0.37	3.3%	1.4%
✓	10	50	10	4	3600	35.39	0.01	35.83	0.27	-0.44	0.27	-1.3%	0.8%
✗	10	50	10	4	3600	36.52	0.01	35.81	0.25	0.71	0.25	1.9%	0.7%
✓	25	50	10	4	3600	53.58	0.09	54.20	0.28	-0.62	0.29	-1.2%	0.5%
✗	25	50	10	4	3600	54.60	0.10	54.23	0.34	0.38	0.36	0.7%	0.7%
✓	-30	50	10	4	6600	16.04	0.09	15.61	0.39	0.43	0.40	2.7%	2.5%
✗	-30	50	10	4	6600	16.31	0.09	15.30	0.44	1.01	0.45	6.2%	2.8%
✓	-20	50	10	4	6600	24.02	0.11	23.88	0.34	0.14	0.35	0.6%	1.5%
✗	-20	50	10	4	6600	24.96	0.11	23.21	0.37	1.75	0.38	7.0%	1.6%
✓	-10	50	10	4	6600	34.51	0.07	34.73	0.31	-0.22	0.32	-0.6%	0.9%
✗	-10	50	10	4	6600	36.20	0.07	33.96	0.45	2.23	0.46	6.2%	1.3%
✓	0	50	10	4	6600	48.49	0.15	48.12	0.30	0.36	0.33	0.7%	0.7%
✗	0	50	10	4	6600	49.94	0.15	47.50	0.41	2.44	0.44	4.9%	0.9%

Oil Separator	T evap [°C]	Tcond [°C]	SH [K]	SC [K]	speed [rpm]	M_coriolis [g/s]	± U (k=2)	M_evap [g/s]	± U (k=2)2	M_oil [g/s]	± U (k=2)3	OCR [%]	± U (k=2)4
✓	10	50	10	4	6600	65.30	0.06	65.26	0.26	0.04	0.27	0.1%	0.4%
✗	10	50	10	4	6600	67.49	0.06	65.04	0.24	2.45	0.25	3.6%	0.4%
✓	25	50	10	4	6600	99.49	0.07	98.55	0.37	0.93	0.38	0.9%	0.4%
✗	25	50	10	4	6600	101.69	0.08	97.62	0.47	4.07	0.48	4.0%	0.5%
✓	-20	50	10	4	5100	18.69	0.08	18.63	0.29	0.06	0.30	0.3%	1.6%
✗	-20	50	10	4	5100	19.41	0.08	18.47	0.28	0.94	0.29	4.9%	1.5%
✓	-10	50	10	4	5100	26.72	0.02	27.09	0.20	-0.37	0.20	-1.4%	0.7%
✗	-10	50	10	4	5100	27.99	0.03	26.98	0.19	1.01	0.19	3.6%	0.7%
✓	0	50	10	4	5100	37.19	0.07	37.71	0.14	-0.52	0.16	-1.4%	0.4%
✗	0	50	10	4	5100	38.37	0.07	37.27	0.13	1.10	0.15	2.9%	0.4%
✓	10	50	10	4	5100	50.25	0.09	50.97	0.23	-0.72	0.25	-1.4%	0.5%
✗	10	50	10	4	5100	51.91	0.09	50.73	0.23	1.18	0.25	2.3%	0.5%
✓	25	50	10	4	5100	76.31	0.12	76.95	0.25	-0.64	0.28	-0.8%	0.4%
✗	25	50	10	4	5100	78.07	0.12	76.81	0.25	1.26	0.28	1.6%	0.4%
✓	-20	50	10	4	2700	9.62	0.03	9.31	0.29	0.31	0.29	3.2%	3.1%

Oil Separator	T evap [°C]	Tcond [°C]	SH [K]	SC [K]	speed [rpm]	M_coriolis [g/s]	± U (k=2)	M_evap [g/s]	± U (k=2)2	M_oil [g/s]	± U (k=2)3	OCR [%]	± U (k=2)4
X	-20	50	10	4	2700	10.08	0.03	9.35	0.29	0.74	0.29	7.3%	2.9%
✓	-10	50	10	4	2700	13.90	0.02	13.87	0.19	0.02	0.20	0.2%	1.4%
X	-10	50	10	4	2700	14.39	0.02	13.96	0.19	0.43	0.19	3.0%	1.3%
✓	0	50	10	4	2700	19.45	0.07	19.78	0.13	-0.33	0.15	-1.7%	0.8%
X	0	50	10	4	2700	19.96	0.07	19.52	0.12	0.44	0.14	2.2%	0.7%
✓	10	50	10	4	2700	26.38	0.08	26.84	0.08	-0.46	0.11	-1.8%	0.4%
X	10	50	10	4	2700	26.94	0.08	26.85	0.08	0.09	0.11	0.3%	0.4%
✓	25	50	10	4	2700	39.88	0.01	40.49	0.23	-0.61	0.23	-1.5%	0.6%
X	25	50	10	4	2700	40.60	0.02	40.43	0.23	0.17	0.23	0.4%	0.6%
✓	-20	50	10	4	7200	26.16	0.11	26.42	0.28	-0.26	0.31	-1.0%	1.2%
X	-20	50	10	4	7200	27.07	0.11	25.28	0.28	1.80	0.30	6.6%	1.2%
✓	-10	50	10	4	7200	37.54	0.10	38.00	0.20	-0.46	0.23	-1.2%	0.6%
X	-10	50	10	4	7200	39.20	0.09	37.40	0.19	1.80	0.21	4.6%	0.6%
✓	0	50	10	4	7200	52.09	0.07	52.99	0.16	-0.89	0.17	-1.7%	0.3%
X	0	50	10	4	7200	54.18	0.07	52.46	0.14	1.72	0.16	3.2%	0.3%
✓	10	50	10	4	7200	70.75	0.08	71.09	0.25	-0.34	0.26	-0.5%	0.4%

Oil Separator	T evap [°C]	Tcond [°C]	SH [K]	SC [K]	speed [rpm]	M_coriolis [g/s]	± U (k=2)	M_evap [g/s]	± U (k=2)2	M_oil [g/s]	± U (k=2)3	OCR [%]	± U (k=2)4
X	10	50	10	4	7200	73.26	0.08	70.69	0.24	2.57	0.26	3.5%	0.4%
✓	25	50	10	4	7200	107.60	0.18	107.17	0.29	0.43	0.34	0.4%	0.3%
X	25	50	10	4	7200	111.03	0.16	106.49	0.30	4.54	0.34	4.1%	0.3%

